Energy Systems in Electrical Engineering

Ravindra Munje
Balasaheb Patre
Akhilanand Tiwari

Investigation of Spatial Control Strategies with Application to Advanced Heavy Water Reactor

Springer

Energy Systems in Electrical Engineering

Series editor

Muhammad H. Rashid, Lakeland, USA

More information about this series at http://www.springer.com/series/13509

Ravindra Munje · Balasaheb Patre
Akhilanand Tiwari

Investigation of Spatial Control Strategies with Application to Advanced Heavy Water Reactor

Springer

Ravindra Munje
Department of Electrical Engineering
K. K. Wagh Institute of Engineering
Education and Research
Nashik, Maharashtra
India

Balasaheb Patre
Shri Guru Gobind Singhji Institute
of Engineering and Technology
Nanded, Maharashtra
India

Akhilanand Tiwari
Bhabha Atomic Research Centre
Mumbai, Maharashtra
India

ISSN 2199-8582 ISSN 2199-8590 (electronic)
Energy Systems in Electrical Engineering
ISBN 978-981-10-3013-0 ISBN 978-981-10-3014-7 (eBook)
https://doi.org/10.1007/978-981-10-3014-7

Library of Congress Control Number: 2017947715

Printed on acid-free paper

This Springer imprint is published by Springer Nature
The registered company is Springer Nature Singapore Pte Ltd.
The registered company address is: 152 Beach Road, #21-01/04 Gateway East, Singapore 189721, Singapore

OM SAHANA VAVATU SAHANAU
BHUNAKTU
SAHA VIRYAM KARAWAVAHAI
TEJASVINAVADI TAMASTU MA
VIDVISHAVAHAI
OM SHANTI SHANTI SHANTI OM

(Together may we be protected,
Together may we be nourished,
Together may we work with great energy,
May our journey together be brilliant and effective,
May there be no bad feelings between us,
Peace, peace, peace.)

Kato Upanishad

To our Parents and Teachers, who made us what we are now.

Foreword

About five decades ago, India started its nuclear power programme with the launch of Boiling Water Reactor units at Tarapur. Now, it has more than 20 nuclear power reactor units in operation, several more are under different phases of construction, commissioning and planning.

A wide variety of nuclear reactor designs constitute the three-stage Indian nuclear power programme. The pressurized heavy water reactor technology is the one which has matured in India and such reactors are likely to remain as the mainstay of the first stage of the programme. Advanced heavy water reactor design, which uses slightly enriched uranium or plutonium along with thorium as fuel, heavy water as moderator and boiling light water as coolant, has been conceived to enhance the safety performance, consistent with the expectations from the next-generation reactor systems through innovative configuration of the best features of pressurized heavy water reactor designs and the light-water reactor designs besides extracting significant energy from thorium.

Design of control systems and the control algorithms for the core and plant control have always been challenging and more so in case of nuclear reactors in which xenon-induced spatial oscillations too require control. Hence, in the past four decades, spatial reactor control has attracted attention of several researchers. Thus, besides conventional controllers which just attempt to achieve stability of the closed-loop system, numerous modern control algorithms capable of achieving stability along with optimum performance, have been evolved to address complexities and nonlinearities of the system.

This monograph introduces most recent concepts of state and output feedback with application to core control of advanced heavy water reactor. It presents knowledge in structured manner and in lucid language. Mathematical equations governing the reactor have been introduced in the initial portion of the monograph. Subsequently, it goes on suggesting the application of different control techniques. Simulation steps have been elaborated using block diagrams depicting the control flow and results have been depicted by graphs making it easy to comprehend. At the end, the monograph brings out comparison of the effectiveness of the different techniques.

My compliments to authors for putting together this valuable contribution in the form of a monograph which would be of interest and use to graduate students and researchers alike.

August 2017

Anil Kakodkar
Former Chairman, Atomic Energy Commission, India,
President, National Academy of Sciences, India,
Chairman, Rajiv Gandhi Science & Technology Commission, India,
Chairman, Technology Information,
Forecasting & Assessment Council, India

Preface

In India, Advanced Heavy Water Reactor (AHWR), a heavy water moderated and boiling light water cooled thermal reactor, has been designed. Its design aims at large-scale commercial utilization of thorium and integrated technological demonstration of thorium cycle. Control and operation of AHWR pose several challenges. In this monograph, different spatial control techniques namely, static output feedback, state feedback control, sliding mode control, fast output sampling feedback, periodic output feedback, and discrete-time sliding mode control are examined for regulation of spatial power distribution in AHWR. AHWR core is considered to be divided into 17 relatively large nodes. The nodal core model has been obtained based on finite difference approximation of the two group neutron diffusion equations and the associated equations for an effective single group of delayed neutron precursors', xenon and iodine concentrations. Further, nonlinear model characterizing important thermal hydraulics parameters of AHWR has been integrated with the neutronics model to obtain a coupled neutronics–thermal hydraulics model of AHWR. From these nonlinear equations of AHWR system, a vectorized nonlinear model of AHWR has been developed and is implemented in MATLAB/Simulink environment. The model of the reactor is then linearized at the rated power and put into standard state variable form. It is characterized by 90 states, 5 inputs, and 18 outputs. Viability of achieving control over total power and spatial power distribution of AHWR through static output feedback has been investigated and a strategy utilizing conventional concepts for control of global (total) power as well as spatial power distribution is evolved.

As is the case with several large-scale physical systems, the model of the AHWR is seen to possess the simultaneous presence of slow, medium, and fast varying dynamic modes, thereby exhibiting a multi-time-scale property. Hence, in this monograph further, innovative techniques based on singular perturbation are developed for decomposition of the original multi-time-scale system into smaller order subsystems. Four control techniques based on two-time-scale decomposition and two on three-time-scale decomposition are explored for AHWR.

Finally, all the spatial control strategies are compared in terms of their computational intensiveness, sensitivity, robustness, and response under the same

representative transients. Various time-domain specifications and error performance indices are calculated for each transient and the most appropriate control technique is identified for spatial control of AHWR. Although the mathematical model of reactor core, controller design and simulation methodologies have been proposed for AHWR, they can be easily adopted to other types of nuclear reactors.

This monograph can be beneficial to mathematicians, scientists, as well as researchers working on nonlinear modeling and control for a better fundamental understanding of numerically ill-conditioned large-scale systems. The authors acknowledge IEEE and Elsevier for granting the permission to reuse materials copyrighted by these publishers in this monograph. The authors express sincere thanks to Board of Research in Nuclear Sciences, Department of Atomic Energy, Government of India for funding the project entitled "Comparison of Controllers for Advanced Heavy Water Reactor" under the grant 2009/36/102-BRNS/3284. The authors would like to express their deep sense of gratitude to their parents and teachers who have made them competent enough to write this monograph. The authors wish to thank many individuals who had helped them directly or indirectly in completing this monograph particularly Dr. S.R. Shimjith and Mr. P.S. Londhe. Finally, authors wish to acknowledge the support, patience, and love of their spouses and children during the preparation of this monograph.

Nashik, India
August 2017

Ravindra Munje
Balasaheb Patre
Akhilanand Tiwari

Contents

About the Authors

Ravindra Munje was born in Mangrulpir, India, in 1983. He received his B.E. degree in Electrical Engineering from Mumbai University in 2005, his M.E. degree in Electrical Engineering from Pune University in 2009, and his Ph.D. in Electrical Engineering from Swami Ramanand Teerth Marathwada University, Nanded in 2015. He has published around 30 papers in national and international conferences and journals. He is a life member of ISTE and the Institution of Engineers (India), and a member of the IEEE and IET. His areas of interest include modeling of large-scale systems and design of controllers based on modern control techniques such as multirate output feedback (like fast output sampling and periodic output feedback), singular perturbation techniques, and sliding mode control. At present, he is working as an associate professor at the Electrical Engineering Department of K.K. Wagh Institute of Engineering Education and Research, Nashik. He also received the Promising Engineer Award by Institution of Engineers (India) in 2016.

Balasaheb Patre received B.E. and M.E. degrees in Instrumentation and Control Engineering from Marathwada University, Aurangabad in 1986 and 1990, respectively and a Ph.D. in Systems and Control Engineering from the Indian Institute of Technology Bombay in 1998. He has published around 160 papers in international journals and conferences. He has presented his research work at Cambridge University, UK, and in Germany. He is a life member of ISTE and the Instrument Society of India, a member of IETE, and a senior member of the IEEE and IET. He is a reviewer for several international Journals. His areas of interest include sliding mode control and its applications, robust control, large-scale systems, interval arithmetic applications, intelligent control, etc. At present, he is working as a Professor of Instrumentation Engineering at the SGGS Institute of Engineering and Technology, Nanded, India.

Akhilanand Tiwari joined Bhabha Atomic Research Centre (BARC) through the 28th batch of BARC training school in 1985. He completed his B.Sc. in Electrical Engineering from Aligarh Muslim University in 1984 and his Ph.D. in Systems and Control Engineering at Indian Institute of Technology (IIT) Bombay in 2000. During his early career at BARC, he worked on control analysis of the Dhruva

reactor and control system design of the Purnima-III U-233 fuelled reactor. From 1995–2002, he worked on the development of the Liquid Zone Control System for the 540 MWe PHWR. He was also responsible for the design of process control and instrumentation systems and control algorithms for AHWR. His research areas include time-scale and singular perturbation methods in control, multivariable control, and sliding mode control with application to nuclear reactors. He has guided a number of Ph.D. and M.Tech. students at Indian Institute of Technology Bombay and Homi Bhabha National Institute Mumbai and is actively involved in research in the area of modern control systems design for large reactors, namely PHWR and AHWR. He received the DAE Science and Technology Award in 2003 and Group Achievement Awards in 2006, 2012, and 2013 for his various activities. He also received the HBNI Distinguished Faculty Award in 2015.

Acronyms

AHWR	Advanced Heavy Water Reactor
CPPRRL	Constant Plus Proportional Rate Reaching Law
DSMC	Discrete-time Sliding Mode Control
FLC	Fuzzy Logic Control
FOS	Fast Output Sampling
IAE	Integral Absolute Error
ISE	Integral Square Error
ITAE	Integral Time Absolute Error
ITSE	Integral Time Square Error
LQR	Linear Quadratic Regulator
MROF	Multirate Output Feedback
MW	Mega Watt
MWe	Mega Watt Electrical
MWt	Mega Watt Thermal
PHWR	Pressurized Heavy Water Reactor
PID	Proportional Integral Derivative
POF	Periodic Output Feedback
PRRL	Power Rate Reaching Law
PWR	Pressurized Water Reactor
RR	Regulating Rod
SIFLC	Single Input Fuzzy Logic Control
SMC	Sliding Mode Control
SOFC	Static Output Feedback Control
VSC	Variable Structure Control
VSS	Variable Structure System

Symbols

General Notations and Operations

Matrix	Bold upper case
Vector	Bold lower case
$\mathbf{0}$	Zero vector or zero matrix
$\mathbf{E}_n$	Identity matrix of dimension n
$\mathbf{A} > 0$	Positive definite matrix $\mathbf{A}$
$\mathbf{A} \geq 0$	Positive semidefinite matrix $\mathbf{A}$
$\mathbf{A}^T$	Transpose of matrix $\mathbf{A}$
$\mathbf{A}^{-1}$	Inverse of square matrix $\mathbf{A}$
$\varphi(\mathbf{A})$	Eigenvalues of square matrix $\mathbf{A}$
$diag(\cdot)$	Diagonal elements of matrix
$max(\cdot)$	Maximum of function
$min(\cdot)$	Minimum of function
$rank(\cdot)$	Rank of matrix
$sgn(\cdot)$	Signum function
$sig(\cdot)$	Sigmoid function
$\Re^n$	Real space of dimension n
$x \in \Re^n$	x belongs to real space of dimension n
$\Re e\{\mathbf{x}\}$	Real part of $\mathbf{x}$
$\Im m\{\mathbf{x}\}$	Imaginary part of $\mathbf{x}$
$\|x\|$	Modulus of x
$\cdot$	Scalar multiplication
$\odot$	Element-wise multiplication
$*$	Array multiplication

Notations Used in AHWR Model Representation

C	Delayed neutron precursor concentration
E_{eff}	Average thermal energy liberated per fission, J
H	Position of regulating rod, % in

I	Iodine concentration
P	Drum pressure, MPa
Q	Fission power, W
V	Volume, m^3
X	Xenon concentration
h	Enthalpy, kJ/kg
q	Mass flow rate, kg/s
v	Control signal, Volts
x	Exit mass quality
α	Coupling coefficient
β	Delayed neutron fraction
γ	Fraction fission yield
λ	Decay constant
ℓ	Prompt neutron lifetime, s
ρ	Reactivity, k
σ_a	Microscopic absorption cross section, cm^2
$\sum_a$	Macroscopic absorption cross section, cm^{-1}
$\sum_f$	Macroscopic fission cross section, cm^{-1}
κ	Constant of regulating rod position
δ	Deviation parameter

Other Notations

$\mathbf{A}$	State matrix of a linear continuous-time system
$\mathbf{A}_{ij}$	Submatrices of state matrix
$\mathbf{B}$	Input matrix of a linear continuous-time system
$\mathbf{B}_i$	Submatrices of input matrix
$\mathbf{C}$	Hyperplane matrix
$\mathbf{F}$	Feedback gain matrix of discrete-time system
$\mathbf{G}$	Output injection matrix
J	Quadratic performance index
$\mathbf{K}$	Feedback gain matrix
$\mathbf{L}$	Fast output sampling gain matrix
$\mathbf{M}$	System output matrix
$\mathbf{M}_{ij}$	Submatrices of output matrix
N	Sampling interval
$\mathbf{T}$	Linear state transformation matrix
V	Lyapunov function
a	Positive scaler
j	Complex number
m	Number of inputs
n	Number of states or system order
p	Number of outputs
$\mathbf{s}$	Sliding surface

t	Time, s
$\mathbf{u}$	System input vector
$\mathbf{y}$	System output vector
$\mathbf{z}$	System state vector
$\dot{\mathbf{z}}$	Time derivative of $\mathbf{z}$
Φ_τ	State matrix of a linear discrete-time system when sampling is done at the rate of $\frac{1}{\tau}$
Φ_Δ	State matrix of a linear discrete-time system when sampling is done at the rate of $\frac{1}{\Delta}$
Γ_τ	Input matrix of a linear discrete-time system when sampling is done at the rate of $\frac{1}{\tau}$
Γ_Δ	Input matrix of a linear discrete-time system when sampling is done at the rate of $\frac{1}{\Delta}$
τ	Output sampling period
Δ	Input sampling period
μ	Observability index
ν	Controllability index
ξ, η	Positive scalars
ε	Perturbation parameter

Subscripts

C	Precursor
H	Position of regulating rod
I	Iodine
L	Left
Q	Power
R	Right
X	Xenon
c	Vaporization
gp	Global (total) power component
d	Downcomer
f	Fast or Feed water or Fission
$f1, f2$	Fast 1, Fast 2
i, j	Node number
k	Regulating rod number
s	Steam or Slow
sp	Spatial power component
w	Water
x	Exit quality

List of Figures

List of Tables

Chapter 1
Introduction

1.1 Introduction

Even though atoms are tiny, their nuclei together hold huge amount of energy. In 1904, the father of nuclear science, Ernest Rutherford wrote:

> If it were possible to control at will the rate of disintegration of the radio element, an enormous amount of energy could be obtained from a small amount of matter.

In 1934, physicist Enrico Fermi demonstrated splitting of many kinds of atoms using neutrons. In the fall of 1938, German scientists Otto Hahn and Fritz Strassmann revealed that bombarding neutrons on the nucleus of the uranium atom convert some of the uranium into barium. This Hahn's experiment of splitting the uranium atom was well acknowledged by Austrian physicist Lise Meitner and Otto R. Frisch in 1939, and named as nuclear fission process. The promising design for a uranium chain reaction was recommended by Fermi and his associate Leo Szilard in 1941. Early in 1942, a group of scientists guided by Fermi congregated at the University of Chicago for developing their theories. They all were prepared for construction to begin on the world's first nuclear reactor by November 1942. On the morning of December 2, 1942, they successfully established the first self-sustaining nuclear chain reaction at University of Chicago, Illinois and transformed scientific theory into technological realism [38]. Among the peaceful use of this form of energy, is the generation of electricity. A system used to transform nuclear energy into electrical energy is called nuclear power plant. The first commercial nuclear power plant started operation in 1950s. According to World Nuclear Association [8], there are around 440 commercial nuclear power plants operating in 31 countries with over 380,000 MWe (Mega Watt Electrical) of total capacity. About 65 more reactors are under construction. They provide about 11.5% of world's electricity as continuous, reliable base load power, without carbon dioxide emission. Fifty-six countries operate a total of about 240 research reactors. Further, 180 nuclear reactors power some 140 ships and submarines.

R. Munje et al., *Investigation of Spatial Control Strategies with Application to Advanced Heavy Water Reactor*, Energy Systems in Electrical Engineering, https://doi.org/10.1007/978-981-10-3014-7_1

In India, nuclear power is the fourth largest source of electricity after thermal, hydroelectric, and renewable sources of electricity. According to Nuclear Power Corporation of India Limited [7] as of 2016, India has 21 nuclear reactors in operation in 7 nuclear power plants, generating 5780 MWe while 3 other reactors are under construction and are expected to generate an additional 3800 MWe. Except for two units at Tarapur which have Boiling Water Reactors and one unit at Kudankulam which has Pressurized Water Reactor (PWR), all nuclear power plants in India employ Pressurized Heavy Water Reactor (PHWR) concepts in which natural uranium is used as fuel and heavy water as moderator. India has been operating and developing improved versions of its current generation PHWR on the basis of operating experience, international trends and indigenous research and development inputs as a first stage of nuclear power program. In the second stage, Fast Breeder Reactor programs were launched with the Fast Breeder Test Reactor, which operates with a uranium-plutonium mixed carbide fuel. Considering the large thorium reserves in India, thorium utilization for large-scale energy production has been an important goal of the third stage of nuclear power program [29–31]. For the timely development of thorium-based technologies for the entire thorium fuel cycle, the Advanced Heavy Water Reactor (AHWR) has been designed.

1.2 An Overview of Advanced Heavy Water Reactor

The active core of AHWR is 3.5 m long and is divided into 513 lattice locations as shown in Fig. 1.1. Out of these lattice locations, 452 house fuel assemblies and the 24 host reactivity control devices which include Absorber, Shim, and Regulating Rods (RRs) each 8. Absorber Rods are usually fully inside and Shim Rods are fully out of the reactor core whereas; RRs are partially inside the reactor core under normal operating conditions for fine regulation of reactor power. Again, out of the eight RRs, four are controlled automatically and the remaining 4 are controlled manually. The rest 37 lattice locations are engaged by Shut-Off Rods of the shutdown system-1. Out-of-core ion chambers as well as in-core detectors are used to measure neutron flux. The total power of the reactor is inferred from ion chambers in low power range and from in-core detectors in power range. In-core detectors, however, are provided primarily for monitoring of spatial flux distribution in the core [23, 26–28, 30]. 452 coolant channels in the reactor core, the same number of tail pipes and inlet feeders, 16 downcomers, 4 horizontal cylindrical steam drums, and an inlet header form main heat transport system. For illustrating the structure, main heat transport system with a coolant channel, a tail pipe, an inlet feeder, a downcomer, a steam drum, and an inlet header is depicted in Fig. 1.2 (for simplicity only one steam drum is shown). On absorbing the fission heat, boiling of coolant in the reactor core takes place. Coolant channels associated with each quadrant of the reactor core are joined to separate steam drums through individual tail pipes. The coolant flow is driven by natural convection through tail pipes to steam drum at 7 MPa. Within steam drums, separation of steam–water phase and mixing of feed water occur. This steam is then

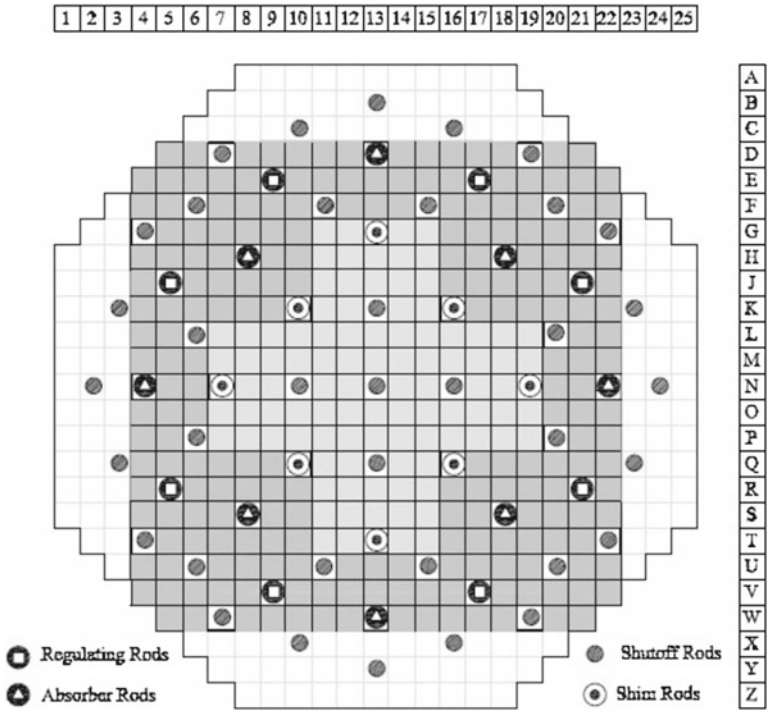

Fig. 1.1 AHWR Core map [27]

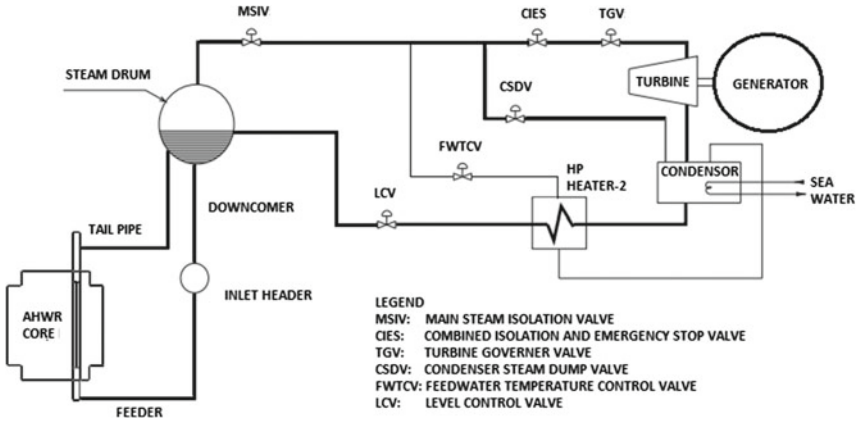

Fig. 1.2 AHWR main heat transport system

fed to the turbine whereas, the subcooled water flows back to the coolant channels through the four downcomer pipes to a common inlet header. Individual coolant channels of the core are fed from this common header through individual feeder pipes [5, 23, 26, 30].

The operation and control of nuclear power plants, like AHWR, represent a difficult problem due to the possibility of accidents or sabotage. Therefore, a number of safety and control aspects are taken into consideration while designing power plant and operational policies are incorporated to circumvent accidental release of radioactivity to the general population. Further, the severity of the problem increases with increase in the size of nuclear reactor.

1.3 Spatial Control Problem

Fission reactions taking place in the reactor core give birth to numerous nuclear species. One of the isotopes is xenon (^{135}Xe), which requires attention, due to the large cross section of thermal neutron absorption. A small portion of ^{135}Xe is created directly in fission but the major part results from the radioactive decay of iodine (^{135}I). Furthermore, it decays at a comparatively slower rate than ^{135}I does. Therefore, an abrupt increase in neutron flux in the reactor core decreases the concentration of ^{135}Xe, which further increases neutron flux. This persists for few hours and then an opposite action takes place, in which the increased neutron flux results into formation of more xenon which in turn reduces the neutron flux. In this way, oscillations of the neutron flux are initiated by ^{135}Xe [4, 6]. In small nuclear reactors, these oscillations can be effectively controlled by appropriate control rod algorithm and hence do not pose serious concern in operation and control. However, in 'large' nuclear reactors where physical size is quite a lot of times the neutron migration length, spatial oscillations are significantly important. If these oscillations in the spatial power are not controlled, the power density and the rate of change of power at some positions in the core may go beyond their respective thermal limits, and may result in fuel failure. Therefore, in large thermal nuclear reactors, it becomes essential to utilize automatic power distribution control system, apart from the control of the total power of the reactor. The main intention is to maintain the core power distribution close to a preferred shape.

The foremost problem encountered in control analysis and design of a large reactor is the development of mathematical model. Nuclear reactors of small core size are adequately represented by the well-known point kinetics model which depicts the dynamics of the core averaged neutron flux/power and the associated delayed neutron precursor groups. For large reactors, however, this model will not suffice since the flux shape in large reactor undergoes variations which the point kinetics model is unable to capture [4]. Therefore, for large nuclear reactors, it is essential to adopt more detailed space-time kinetics models for analysis. Thus, it becomes essential to develop a suitable mathematical model which captures all the essential properties of the reactor core and then to develop and implement a computer code in the form of an offline computer algorithm to regulate the behavior of system in various proposed transient situations.

As far as the power distribution control in a nuclear reactor is concerned, it is important to note that the model of a nuclear reactor belongs to a special class of systems called singularly perturbed systems. The simultaneous presence of both the slow as well as the fast varying dynamical modes could cause ill-conditioning of the problem. Fortunately, the rich literature on singular perturbations and control makes it feasible to analyze such systems and design the controller. Using these techniques, model of the nuclear reactor can be transformed into a proper form whereby stiffness is completely removed. Once, this has been done, numerous approaches are available for carrying out the design of spatial power distribution control systems.

Feedback of total power (or core averaged power) is normally sufficient for control of small or medium size nuclear reactors, whereas large reactors may necessitate feedback of spatial power distribution along with the total power feedback for efficient spatial control. However, a major limitation of the static output feedback is that it may not guarantee arbitrary pole placement. Hence, static output feedback is not preferable as it may not meet all the performance specifications. Employing dynamic output feedback may be feasible but it again leads to sophisticated feedback system. Therefore, spatial control using state feedback would have been a better option for arbitrary pole placement. Again, practical implementation of such a controller would require a state observer which will increase the complexity. A better candidate would be the use of output information through modern control techniques such as fast output sampling or periodic output feedback. However, in such applications, the intricacies associated with multi-time-scale properties of the model need to be handled carefully.

1.4 Nuclear Reactor Control: A Review

Application of modern control techniques for spatial control of large nuclear reactors, like Pressurized Heavy Water Reactor and Advanced Heavy Water Reactor, becomes difficult because of interacting dynamic phenomena of widely different speeds, giving rise to widely separated groups of eigenvalues. In this situation, singular perturbation techniques prove to be superior. Application of singular perturbation approach to a different type of reactor control problem is given by Reddy and Sannuti [16]. Further, in [36], numerically ill-conditioned model of PHWR is decoupled into two subsystems based on singular perturbation technique. Subsystem regulator problems are designed separately and then they are combined to obtain the near-optimum composite control, for original model, for the regulation of spatial power distribution in the reactor core. As an extension to this, simultaneous decomposition of singularly perturbed three-time-scale system of AHWR into three subsystems is achieved in [24]. These singular perturbation techniques eliminate numerical ill-conditioning issues associated with PHWR and AHWR. However, these methods require all the states for feedback. Several mechanisms for detection of neutron flux or power are known but there is not any instrument for measuring delayed neutron precursor, xenon, and iodine concentrations in the reactor. As a consequence of this, it is diffi-

cult to implement the control laws based upon modern concepts characterized by state variable feedback. To overcome this problem, a deterministic, linear, and reduced order observer has been designed in [34] for estimation of an average delayed neutron precursor, xenon, and iodine concentrations in different regions of the PHWR core. However, observer-based design results in complex structured closed-loop system requiring expensive hardware and processing network which increase the implementation cost and reduces the reliability of control system. Hence, it is desirable to go for an output feedback design. Spatial control strategy based on static output feedback control (SOFC) has been attempted in [26] and it is shown that spatial stabilization of AHWR is possible with the feedback of total power and spatial power distribution signals. This technique is easy to implement. However, complete pole assignment and guaranteed closed-loop stability are still not obtained by using SOFC [32]. The dynamic output feedback controller involves more dynamics and is more complex to design.

Recently, multirate output feedback (MROF) has drawn much interest of many researchers and the application to nuclear reactor for spatial control is successfully demonstrated. In contrast to observer-based design in which accuracy of estimation of states improves after long time, exact computation of states in just one sampling period is feasible if MROF is employed. In MROF, sampling rates of input and output are different. In one type of MROF technique called periodic output feedback (POF), the input is sampled at faster rate than the output. In the other type of MROF called fast output sampling (FOS) feedback, output is sampled faster than the input. Application of periodic output feedback control for PHWR is reported in [33, 37]. In [37] using linear transformation of state variables, the singularly perturbed model of PHWR is converted into a block triangular form in which the fast subsystem is decoupled. Then, an output injection gain matrix stabilizing the slow subsystem is obtained. The periodic output feedback gain is subsequently calculated only for the slow subsystem and the same for the fast subsystem is set equal to zero. Finally, the POF gain for the composite system is obtained using the POF gains computed separately for the slow and fast subsystems. A decentralized periodic output feedback is proposed for PHWR in [33], which proves to be simpler for practical implementation. Fast output sampling technique for PHWR and AHWR is suggested in [17, 18, 25]. A robust controller for uncertain systems using FOS technique is examined for PHWR in [18]. The FOS control allows the realization of the robust state feedback gain simultaneously for family of linear models. The issues of noise sensitivity and error dynamics are overcome by posing the problem as linear matrix inequality problem. In [17], the discrete system of PHWR is transformed into block diagonal form in which slow and fast subsystems are decoupled. State feedback control is designed for the slow subsystem while the state feedback for fast subsystem is taken as zero. Then, composite state feedback controller is obtained and it is realized by fast output sampling feedback gain. The technique presented in [18] is extended for three-time-scale system and has been successfully applied to AHWR in [25]. However, these methods lack robustness. Also, these control techniques may not work satisfactorily in the presence of disturbances, parameter variations and perturbations in the operating conditions. Robust control techniques could be useful in such situations.

In recent years, one of the robust control techniques named, sliding mode control (SMC) has attracted the attention of many researchers. Sliding mode spatial control of PHWR is documented in [12–15]. In [14], sliding mode observer is proposed to estimate the states of PHWR. Further in [12, 13, 15], MROF-based sliding mode control is proposed for PHWR. These methods do not require state information of the system for feedback purpose and hence may be easier to implement. Sometimes, it is required to design a closed-loop system which is fault tolerant in the sense that the stability is not lost even if sensors or control actuators have failed. Incorporating such a consideration in the design leads to multi-model plant description for which usual design methods are not tractable. Fault-tolerant spatial control systems for PHWR are presented in [19, 35]. Approach presented in [35] is based on POF whereas in [19] it is based on FOS. Spatial control means to suppress xenon oscillations from growing. A modified method based on the concept of three axial offsets has been presented in [20] for controlling xenon oscillations in large PWR. This method gives continuous information of oscillations in reactor to operator, which helps the operator to understand the situation rather clearly. As an extension to this, concept of monitoring and control of radial xenon oscillations in PWR has been suggested in [21], which utilizes feedback of not only axial offsets but also uses information of power reactor distribution in respective core regions. Further, similar kind of approach based on characteristics ellipse trajectory drawn by three axial offsets is proposed in [22].

In recent years, fuzzy logic controllers (FLCs) are very promising for nuclear reactor applications [9–11]. They provide a high degree of robustness and immunity to external disturbances. Furthermore, they can be configured to be self-learning and adaptive. A fuzzy model predictive control method [11] is used to design an automatic controller for thermal power control in PWRs. In this, the future reactor power is predicted by using fuzzy model identified by a subtractive clustering method of a fast and robust algorithm. The objectives of the presented fuzzy model predictive control law are to minimize both the difference between the predicted reactor power and the desired one, and the variation of the control rod positions. These objectives are subject to maximum and minimum control rod positions and maximum control rod speed. The genetic algorithm, useful to accomplish multiple objectives, is used to optimize the fuzzy model predictive controller. Recently, Londhe et al. [9] have proposed spatial control of AHWR using single-input fuzzy logic controller (SIFLC). The SIFLC reduces the conventional two-input fuzzy logic controller to a single-input FLC. It is shown that the SIFLC offers a significant reduction in rule inferences and simplifies the tuning of control parameters. Also, SIFLC requires less execution time compared to conventional two-input fuzzy logic controller for the control of spatial oscillations in AHWR. Further in [10], a simplified fuzzy like proportional derivative controller is proposed for spatial control of AHWR. Some other control techniques, based on discrete Proportional–Integral–Derivative (PID) and fractional order PID, are recommended in [1–3].

In the subsequent chapters of this monograph, systematic investigation of applicability of multivariable spatial control techniques for power regulation of AHWR has been accomplished. More specifically, comparison of these spatial control techniques is presented.

1.5 Overview of Monograph

The remaining chapters of this monograph are organized as follows:

- Chapter 2 discusses the mathematical model of AHWR, its representation in the standard state-space form, vectorization of modeling equations, and spatial control based on static output feedback.
- Chapter 3 recommends a state feedback technique based on two-stage decomposition for AHWR nonlinear system for spatial control.
- Chapter 4 presents application of spatial control technique based on two-time-scale decomposition using quasi-steady-state method to nonlinear model of AHWR.
- Chapter 5 illustrates application of robust sliding mode controller for AHWR system, based on two-stage decomposition. Since, fast subsystem is found to be stable, SMC is designed using slow subsystem alone. This is then applied to vectorized nonlinear model of AHWR and simulation results are discussed.
- Chapter 6 demonstrates the application of fast output sampling control strategy to AHWR system and nonlinear simulations carried out under different transient conditions.
- Chapter 7 suggests a novel periodic output feedback control technique for three-time-scale system and its application to AHWR for spatial stabilization.
- Chapter 8 investigates discrete-time sliding mode control technique with two different reaching conditions, based on three-time-scale decomposition. These techniques are applied to AHWR and spatial control is achieved.
- Chapter 9 compares all the controllers under the same representative transients.

References

1. Bhase, S.S., Patre, B.M.: Robust FOPI controller design for power control of PHWR under step-back condition. Nucl. Eng. Design **274**, 20–29 (2014)
2. Das, S., Das, S., Gupta, A.: Fractional order modeling of a PHWR under step-back condition and control of its global power with a robust $PI^{\lambda}D^{\mu}$ controller. IEEE Trans. Nucl. Sci. **58**(5), 2431–2441 (2011)
3. Dasgupta, S., Routh, A., et al.: Networked control of a large PHWR with discrete proportional-integral-derivative controllers. IEEE Trans. Nucl. Sci. **60**(5), 3879–3888 (2013)
4. Duderstadt, J.J., Hamilton, L.J.: Nuclear Reactor Analysis. Wiley, New York (1976)
5. Gaikwad, A.J., Vijayan, P.K., Iyer, K., Bhartiya, S., Kumar, R., Lele, H.G., Ghosh, A.K., Kushwaha, H.S., Sinha, R.K.: Effect of loop configuration on steam drum level control for multiple drum interconnected loops pressure tube type boiling water reactor. IEEE Trans. Nucl. Sci. **56**(6), 3712–3725 (2009)
6. Glasstone, S., Sesonske, A.: Nuclear Reactor Engineering. Springer, Heidelberg (1994)
7. https://www.npcil.nic.in/main/AllProjectOperationDisplay.aspx
8. https://www.world-nuclear.org/information-library/current-and-future-generation/nuclear-power-in-the-world-today.aspx
9. Londhe, P.S., Patre, B.M., Tiwari, A.P.: Design of single-input fuzzy logic controller for spatial control of advanced heavy water reactor. IEEE Trans. Nucl. Sci. **61**, 901–911 (2014)
10. Londhe, P.S., Patre, B.M., Tiwari, A.P.: Fuzzy like PD controller for spatial control of advanced heavy water reactor. Nucl. Eng. Design **274**, 77–89 (2014)

11. Man, G.N., In, J.H., Yoon, J.L.: Design of a fuzzy model predictive power controller for pressurized water reactors. IEEE Trans. Nucl. Sci. **53**(3), 1504–1514 (2006)
12. Reddy G.D., Bandyopadhyay B., Tiwari A.P.: Spatial control of a large pressurize heavy water reactor by multirate output feedback based sliding mode control. Proc. IEEE Int. Conf. Ind. Technol., 1925–1930 (2006)
13. Reddy, G.D., Bandyopadhyay, B., Tiwari, A.P.: Multirate output feedback based sliding mode spatial control for a large pressurize heavy water reactor. IEEE Trans. Nucl. Sci. **54**, 2677–2686 (2007)
14. Reddy, G.D., Bandyopadhyay, B., Tiwari, A.P., Fernando, T.: Spatial control of a large pressurize heavy water reactor using sliding mode observer and control. Proc. IEEE Int. Conf. Control Autom. Rob. Vis. **53**(6), 2142–2147 (2008)
15. Reddy, G.D., Park, Y., Bandyopadhyay, B., Tiwari, A.P.: Discrete-time output feedback sliding mode control for spatial control of a large pressurize heavy water reactor. Automatica **45**, 2159–2163 (2009)
16. Reddy, P.B., Sannuti, P.: Optimal control of a coupled-core nuclear reactor by a singular perturbation method. IEEE Trans. Autom. Control **20**(6), 766–769 (1975)
17. Sharma, G.L., Bandyopadhyay, B.: Robust controller design for a pressurized heavy water reactor by fast output sampling technique. Proc. IEEE Int. Conf. Ind. Technol. **1**, 301–306 (2000)
18. Sharma, G.L., Bandyopadhyay, B., Tiwari, A.P.: Spatial control of a large pressurized heavy water reactor by fast output sampling technique. IEEE Trans. Nucl. Sci. **50**, 1740–1751 (2003)
19. Sharma, G.L., Bandyopadhyay, B., Tiwari, A.P.: Fault tolerance spatial control of a large PHWR by fast output sampling technique. Proc. IEE Control Theory Appl. **151**(1), 117–124 (2004)
20. Shimazu, Y.: Continuous guidance procedure for xenon oscillation control. J. Nucl. Sci. Technol. **32**(2), 95–100 (1995)
21. Shimazu, Y., Takeda, K.: Monitoring and control of radial xenon oscillation in PWRs by a three-radial-offset concept. J. Nucl. Sci. Technol. **44**(2), 155–162 (2007)
22. Shimazu, Y., Takeda, K.: Xenon oscillation control in large PWRs using a characteristic ellipse trajectory drawn by three axial offsets. J. Nucl. Sci. Technol. **45**(4), 257–262 (2008)
23. Shimjith, S.R., Tiwari, A.P., Bandyopadhyay, B.: Coupled neutronics thermal hydraulics model of advanced heavy water reactor for control system studies. Proc. Annual IEEE India Conf. **1**, 126–131 (2008)
24. Shimjith, S.R., Tiwari, A.P., Bandyopadhyay, B.: A three-time-scale approach for design of linear state regulator for spatial control of advanced heavy water reactor. IEEE Trans. Nucl. Sci. **58**(3), 1264–1276 (2011)
25. Shimjith, S.R., Tiwari, A.P., Bandyopadhyay, B.: Design of fast output sampling controller for three-time-scale systems: application to spatial control of advanced heavy water reactor. IEEE Trans. Nucl. Sci. **58**(6), 3305–3316 (2011)
26. Shimjith, S.R., Tiwari, A.P., Bandyopadhyay, B., Patil, R.K.: Spatial stabilization of advanced heavy water reactor. Ann. Nucl. Energy **38**(7), 1545–1558 (2011)
27. Shimjith, S.R., Tiwari, A.P., Bandyopadhyay, B.: Modeling and Control of Large Nuclear Reactor: A Three Time Scale Approach. Lecture Notes in Control and Information Sciences, vol. 431. Springer, Berlin (2013)
28. Shimjith, S.R., Tiwari, A.P., Naskar, M., Bandyopadhyay, B.: Space-time kinetics modeling of advanced heavy water reactor for control studies. Ann. Nucl. Energy **37**(3), 310–324 (2010)
29. Sinha, R.K., Kakodkar, A.: The road map for a future Indian nuclear energy system. In: Proceedings of the International Conference on Innovative Technologies for Nuclear Fuel Cycles and Nuclear Power, Vienna (2003)
30. Sinha, R.K., Kakodkar, A.: Design and development of the AHWR-the Indian thorium fuelled innovative nuclear reactor. Nucl. Eng. Des. **236**, 683–700 (2006)
31. Sinha, R.K., Kushwaha, H.S.: Design and development of AHWR-the Indian thorium fuelled innovative nuclear reactor. In: Proceedings of the Annual Conference of Indian Nuclear Society, Mumbai (2000)

32. Syrmos, V.L., Abdallah, C.T., Dorato, P., Grigoriadis, K.: Static output feedback-a survey. Automatica **33**, 125–137 (1997)
33. Talange, D.B., Bandyopadhyay, B., Tiwari, A.P.: Spatial control of a large pressurize heavy water reactor by decentralized periodic output feedback and model reduction techniques. IEEE Trans. Nucl. Sci. **53**, 2308–2317 (2006)
34. Tiwari, A.P., Bandyopadhyay, B.: Control of xenon induced spatial oscillations in a large pressurized heavy water reactor. Proc. IEEE Int. Conf. Global Connect. Energy Comput. Commun. Control **1**, 178–181 (1998)
35. Tiwari, A.P., Bandyopadhyay, B.: An approach to the design of fault tolerant spatial control system for large pressurize heavy water reactor. Proc. IEEE Int. Conf. Ind. Technol. **1**, 747–752 (2000)
36. Tiwari, A.P., Bandyopadhyay, B., Govindarajan, G.: Spatial control of large pressurized heavy water reactor. IEEE Trans. Nucl. Sci. **43**, 2440–2453 (1996)
37. Tiwari, A.P., Bandyopadhyay, B., Werner, H.: Spatial control of a large pressurize heavy water reactor by piecewise constant periodic output feedback. IEEE Trans. Nucl. Sci. **47**, 389–402 (2000)
38. United States, Office of the Assistant Secretary for Nuclear Energy and United States, Department of Energy, History Division: The History of Nuclear Energy. U.S. Department of Energy (1985). https://books.google.co.in/books?id=vKIlGQAACAAJ

Chapter 2
Modeling of AHWR and Control by Static Output Feedback

2.1 Introduction

The physical dimensions of Advanced Heavy Water Reactor (AHWR) are comparatively larger than the neutron migration length in the reactor core. As a result, a severe condition called flux tilt may take place in AHWR. Additionally, circumstances such as online refueling might cause momentary variations in flux shape from the equilibrium flux shape. For analysis of such conditions, it is required to develop an appropriate space-time kinetics model of AHWR. Moreover, the models used for detailed core physics calculations, thermal hydraulics analysis or burnup optimization are usually of very large order and are not readily suited to control studies. A simplified model for representing the space-time kinetics phenomena in a Pressurized Heavy Water Reactor has been derived in [15] based on finite difference approximation of multigroup diffusion equations. In a similar manner, mathematical model of AHWR is obtained in [11, 12, 14] and the same has been used for the study carried out in this monograph.

Designing a robust spatial control technique for a nuclear reactor heavily depends on thorough understanding of system/plant dynamics. These dynamics are nothing but the interactions among the various state variables. To explore reactor dynamics and investigate spatial control strategies, a suitable reactor model, capturing important features and reasonable in its complexity, is required. So, simulation studies can be carried out in the form of offline computer programs to study the performance of nuclear reactor in various predicted accident conditions [1, 7, 10, 16].

This chapter provides mathematical modeling of AHWR. This includes modeling of core neutronics and thermal hydraulics behaviors along with internal reactivity feedbacks. Subsequently, model is linearized and design of static output feedback control (SOFC) is investigated. This chapter also serves as basis for subsequent chapters in this monograph.

R. Munje et al., *Investigation of Spatial Control Strategies with Application to Advanced Heavy Water Reactor*, Energy Systems in Electrical Engineering, https://doi.org/10.1007/978-981-10-3014-7_2

2.2 Mathematical Modeling of AHWR

Complete AHWR model is developed by combining models of core neutronics behavior and thermal hydraulics of main heat transport system.

2.2.1 Core Neutronics Modeling

The simplified core neutronics model is obtained by the nodal approach, based on finite difference approximation of the two group neutron diffusion equations and the associated equation for an effective single group of delayed neutron precursor's concentration. In this, for decoupling the space and time dependence, the AHWR core is divided into 17 nodes as depicted in Fig. 2.1. This 17 nodes division is obtained by considering a central region (node 1) in the core and concentric radial regions. The inner radial region consists of nodes 2–9 which also contain individual regulating rods (RRs). The outer radial region consists of nodes 10–17. The top and bottom reflector regions are divided into 17 nodes in an identical pattern, whereas the side reflector region is divided into 8 nodes. Within each node in the reactor core, the neutron fluxes and other neutronic parameters are represented by the respective average values integrated over its volume. The nodes 2, 4, 6, and 8 contain RRs under

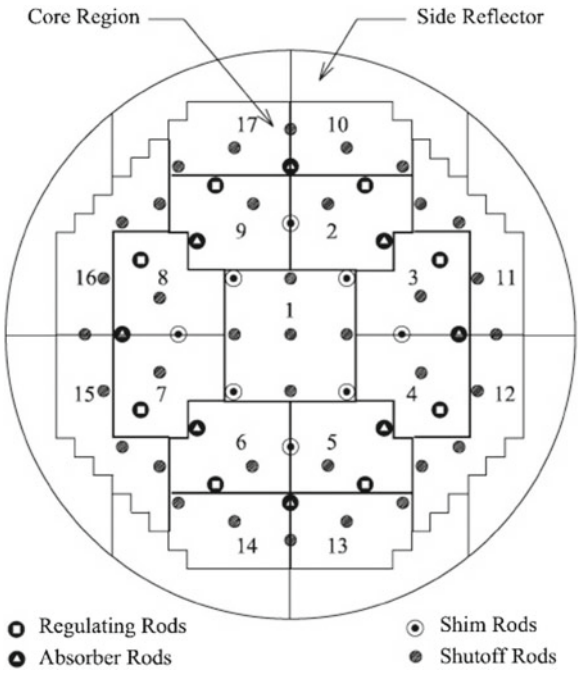

Fig. 2.1 17 nodes AHWR scheme

automatic control [13]. For convenience, the RRs under automatic control are numbered according to the nodes containing them as RR2, RR4, RR6, and RR8. These nodes are considered as 17 small cores, each of which is coupled to its neighboring nodes through neutron diffusion. The following nonlinear equations constitute the neutronics model of the reactor core without internal reactivity feedback.

$$\frac{dQ_i}{dt} = (\rho_i - \alpha_{ii} - \beta)\frac{Q_i}{\ell} + \sum_{j=1}^{17} \alpha_{ji}\frac{Q_j}{\ell} + \lambda C_i, \tag{2.1}$$

$$\frac{dC_i}{dt} = \frac{\beta}{\ell} Q_i - \lambda C_i, \qquad i = 1, 2, ..., 17, \tag{2.2}$$

where α_{ji} and α_{ii} denote the coupling coefficients between jth and ith nodes and self-coupling coefficients of ith node, respectively, β and λ, respectively, are effective one group delayed neutron yield and decay constant, ℓ is the neutron lifetime. Q_i and C_i are the nodal power level and the effective one group delayed neutron precursor concentration of ith node, respectively.

The most important fission product poison is xenon because of its exceptionally large capture cross section for thermal neutrons and half-life of 9.2 h. Main proportion of this isotope in a reactor originates from radioactive decay of iodine with half-life of 6.7 h [4, 5]. To formulate xenon reactivity feedback, iodine and xenon dynamics in each node are represented as

$$\frac{dI_i}{dt} = \gamma_I \Sigma_{f_i} Q_i - \lambda_I I_i, \tag{2.3}$$

$$\frac{dX_i}{dt} = \gamma_X \Sigma_{f_i} Q_i + \lambda_I I_i - (\lambda_X + \bar{\sigma}_{X_i} Q_i) X_i, \tag{2.4}$$

where γ_I and γ_X are fission yields of iodine and xenon respectively, λ_I and λ_X are, respectively, decay constants of iodine and xenon and $\bar{\sigma}_{X_i} = \sigma_{X_i}/E_{eff}\Sigma_{f_i}V_i$; I_i denotes iodine concentration and X_i the xenon concentration of ith node. Also, E_{eff} is energy liberated in each fission, V_i is the node volume, and Σ_{f_i} is thermal neutron fission cross section of ith node.

Regulating rods are driven by the respective reversible variable speed-type three-phase induction motor and static frequency converter. The speed of RR is directly proportional to the voltage applied to the drive motor and it is given by

$$\frac{dH_k}{dt} = \kappa v_k, \qquad k = 2, 4, 6, 8; \tag{2.5}$$

where v_k is control signal applied to the RR drives in the range of ± 1 volt, κ is a constant having value 0.56, and H_k is '% in' position of RR of kth node. Differential equations (2.1)–(2.5) characterize the nodal model of AHWR core neutronics. The neutronic parameters, coupling coefficients, nodal volumes, and cross sections are given in Tables 2.1, 2.2, and 2.3, respectively.

Table 2.1 Neutronic parameters

Parameter	Corresponding value
β	2.643×10^{-3}
λ	$6.4568 \times 10^{-2}\,\mathrm{s}^{-1}$
ℓ	$3.6694 \times 10^{-4}\mathrm{s}$
λ_I	$2.878 \times 10^{-5}\,\mathrm{s}^{-1}$
λ_X	$2.1 \times 10^{-5}\,\mathrm{s}^{-1}$
γ_I	5.7×10^{-2}
γ_X	1.1×10^{-2}
σ_X	$1.8 \times 10^{-22}\,\mathrm{cm}^{-1}$
E_{eff}	$3.2 \times 10^{-11}\,\mathrm{J}$

Table 2.2 Coupling coefficients for the AHWR model

$\alpha_{1,1} = 3.1567 \times 10^{-2}$
$\alpha_{2,2} = \alpha_{5,5} = \alpha_{6,6} = \alpha_{9,9} = 5.4918 \times 10^{-2}$
$\alpha_{3,3} = \alpha_{4,4} = \alpha_{7,7} = \alpha_{8,8} = 6.2052 \times 10^{-2}$
$\alpha_{10,10} = \alpha_{13,13} = \alpha_{14,14} = \alpha_{17,17} = 3.8351 \times 10^{-2}$
$\alpha_{11,11} = \alpha_{12,12} = \alpha_{15,15} = \alpha_{16,16} = 4.3567 \times 10^{-2}$
$\alpha_{1,2} = \alpha_{1,5} = \alpha_{1,6} = \alpha_{1,9} = 6.5746 \times 10^{-3}$
$\alpha_{1,3} = \alpha_{1,4} = \alpha_{1,7} = \alpha_{1,8} = 6.5204 \times 10^{-3}$
$\alpha_{2,1} = \alpha_{5,1} = \alpha_{6,1} = \alpha_{9,1} = 4.5833 \times 10^{-3}$
$\alpha_{3,1} = \alpha_{4,1} = \alpha_{7,1} = \alpha_{8,1} = 4.3309 \times 10^{-3}$
$\alpha_{2,3} = \alpha_{5,4} = \alpha_{6,7} = \alpha_{9,8} = 1.3044 \times 10^{-2}$
$\alpha_{3,2} = \alpha_{4,5} = \alpha_{7,6} = \alpha_{8,9} = 1.2428 \times 10^{-2}$
$\alpha_{3,4} = \alpha_{4,3} = \alpha_{7,8} = \alpha_{8,7} = 1.6097 \times 10^{-2}$
$\alpha_{2,9} = \alpha_{5,6} = \alpha_{6,5} = \alpha_{9,2} = 1.0445 \times 10^{-2}$
$\alpha_{2,10} = \alpha_{5,13} = \alpha_{6,14} = \alpha_{9,17} = 2.3481 \times 10^{-2}$
$\alpha_{3,11} = \alpha_{4,12} = \alpha_{7,15} = \alpha_{8,16} = 2.7555 \times 10^{-2}$
$\alpha_{10,2} = \alpha_{13,5} = \alpha_{14,6} = \alpha_{17,9} = 1.9198 \times 10^{-2}$
$\alpha_{11,2} = \alpha_{12,5} = \alpha_{15,6} = \alpha_{16,9} = 5.6901 \times 10^{-3}$
$\alpha_{2,11} = \alpha_{5,12} = \alpha_{6,15} = \alpha_{9,16} = 5.4963 \times 10^{-3}$
$\alpha_{11,3} = \alpha_{12,4} = \alpha_{15,7} = \alpha_{16,8} = 2.9941 \times 10^{-2}$
$\alpha_{10,17} = \alpha_{17,10} = \alpha_{11,12} = \alpha_{12,11} = \alpha_{13,14} = \alpha_{14,13} = \alpha_{15,16} = \alpha_{16,15} = 9.9912 \times 10^{-3}$
Rest all $\alpha_{i,j} = 0$

2.2.2 Thermal Hydraulics Model

Thermal hydraulics model of main heat transport system of AHWR has been developed by evolving separate models for reactor core thermal hydraulics and for the steam drums, and afterwards clubbing them together [2, 12] as given below.

Table 2.3 Nodal volumes and cross sections

Node No.	Volume (m^3)	Σ_f (cm^{-1})	Σ_a (cm^{-1})
1	8.6822	2.6657×10^{-3}	6.9514×10^{-3}
2, 5, 6, 9	5.4042	2.3898×10^{-3}	6.6828×10^{-3}
3, 4, 7, 8	5.1384	2.5325×10^{-3}	6.7898×10^{-3}
10, 13, 14, 17	4.4297	2.5665×10^{-3}	6.8991×10^{-3}
11, 12, 15, 16	5.5814	2.5665×10^{-3}	6.8991×10^{-3}

2.2.2.1 Core Thermal Hydraulics

A thermal hydraulics model of the reactor core is obtained assuming an equivalent coolant channel for each node, ignoring the pressure drops in downcomers, feeders and tail pipes, and taking uniform distribution of nodal power along the flow axis. Also, the steam quality is considered to be uniformly increasing along the axial length in the channels after the point of onset of boiling. Now, applying mass and energy balance equations to the boiling section and solving them together, the core thermal hydraulics model is written as

$$e_{vp_i} \frac{dP}{dt} + e_{vx_i} \frac{dx_i}{dt} = Q_i - q_{d_i}(h_w - h_d) - x_i h_c q_{d_i}, \tag{2.6}$$

where P is drum pressure, h_w, h_d and h_c are water, downcomer, and condensation enthalpies, respectively, x_i is the nodal average exit quality, q_{d_i} is flow rate of the coolant entering the ith node through downcomer and e_{vp_i} and e_{vx_i} are constants of ith node.

2.2.2.2 Steam Drums

A simple lumped model of the steam drums is developed assuming (1) insignificant carry over and carry under effects; (2) a mixture of saturated water and steam enters the steam drum and subcooled water leaves steam drum into the reactor core; and (3) average values of density and enthalpy of the water in the steam drum. Mass and energy balance equations of the steam drums are respectively represented by

$$e_{pv} \frac{dV_w}{dt} + e_{pp} \frac{dP}{dt} = -\sum_{i=1}^{17} (q_{d_i} - q_{r_i}) + q_f - q_s, \tag{2.7}$$

$$e_{xv} \frac{dV_w}{dt} + e_{xp} \frac{dP}{dt} = q_f h_f + x q_r h_s + (1 - x) q_r h_w - q_d h_d - q_s h_s, \tag{2.8}$$

where q_f, q_s, q_r, and q_d are average values of feed water, steam, saturated steam, and subcooled water flow rates, respectively, and V_w is the volume of water in the

Table 2.4 Constant coefficients of thermal hydraulics model

Node No.	e_{vx_i}
1	2.4406
2, 5, 6, 9	1.0909
3, 4, 7, 8	1.2160
10, 13, 14, 17	1.9861
11, 12, 15, 16	1.1677
e_{x_i}	0.5114

steam drum. Finally applying energy balance equation to water volume in steam drum yields

$$e_{p_i}\frac{dP}{dt} + e_{v_i}\frac{dV_w}{dt} + e_{x_i}\frac{dh_d}{dt} = q_f h_f + (1-x)q_r h_w - q_d h_d. \tag{2.9}$$

Complete thermal hydraulics model is given by set of equations (2.6)–(2.9). Further, drum pressure and water volume are being regulated at respective set points by plant control system. Hence, derivatives of P and V_w vanish from Eqs. (2.6) to (2.9). The above equations, therefore, reduce to

$$e_{vx_i}\frac{dx_i}{dt} = Q_i - q_{d_i}(h_w - h_d) - q_{d_i}x_i h_c, \tag{2.10}$$

$$e_{x_i}\frac{dh_d}{dt} = q_f(\hat{k}_2 h_f - \hat{k}_1) - q_d(\hat{k}_2 h_d - \hat{k}_1), \tag{2.11}$$

where $\hat{k}_2 = \frac{h_s}{h_c}$ and $\hat{k}_1 = h_w\hat{k}_2$. Values of e_{vx_i} and e_{x_i} are listed in Table 2.4. The coolant flow rate through the channels is the function of normalized nodal powers, and is given as

$$q_{d_i} = \left\{k_1\left[\frac{Q_i}{Q_{i_0}}\right]^3 + k_2\left[\frac{Q_i}{Q_{i_0}}\right]^2 + k_3\left[\frac{Q_i}{Q_{i_0}}\right] + k_4\right\} q_{d_{i_0}} \tag{2.12}$$

where $k_1 = 0.2156, k_2 = -0.5989, k_3 = 0.48538$, and $k_4 = 0.8988$. Q_{i_0} denotes the power produced by ith node under full power operation and $q_{d_{i_0}}$ is the corresponding coolant flow rate.

2.2.3 Reactivity Feedbacks

The reactivity term ρ_i in (2.1) is expressed as

$$\rho_i = \rho_{i_u} + \rho_{i_X} + \rho_{i_\alpha}, \tag{2.13}$$

where ρ_{i_u} is the reactivity introduced by the control rods, ρ_{i_X} is the reactivity feedback due to xenon, and ρ_{i_α} is the reactivity feedback due to coolant void fraction. The reactivity contributed by the movement of the RRs is expressed as

$$\rho_{i_u} = \begin{cases} (-10.234 H_i + 676.203) \times 10^{-6}, & \text{if } i = 2, 4, 6, 8. \\ 0 & \text{elsewhere.} \end{cases} \tag{2.14}$$

The xenon reactivity feedback in node i can be expressed as

$$\rho_{i_X} = \frac{\bar{\sigma}_{X_i} X_i}{\Sigma_{a_i}}. \tag{2.15}$$

The reactivity contribution by the coolant void fraction is

$$\begin{aligned} \rho_{i_\alpha} = &- 5 \times 10^{-3} (9.2832 x_i^5 - 27.7192 x_i^4 + 31.7643 x_i^3 \\ &- 17.7389 x_i^2 + 5.2308 x_i + 0.0792). \end{aligned} \tag{2.16}$$

The reactivity contributed by the coolant, fuel, and moderator temperature feedbacks are neglected due to their lesser significance. Equations (2.1)–(2.5), (2.10), and (2.11) constitute complete coupled neutronics–thermal hydraulics model of AHWR. Seventeen equations each of power, delayed neutron precursor, xenon, iodine concentrations, and exit quality, four equations of RR positions, and one equation of downcomer enthalpy result into 90 nonlinear first-order differential equations. Four control signals to RRs and feed flow rate are input variables with 17 nodal powers and total power as output variables. The nodal powers and coolant flow rates are constants as given in Table 2.5 under steady-state full power operation. The equilibrium positions of all RRs are 66.1% inside the core. Coolant enters the core at a temperature of 260 °C and feed water enters the steam drum at 130 °C. The operating pressure of the main heat transport system is 7 MPa. Equilibrium values of other variables like delayed neutron precursor, iodine and xenon concentrations, exit quality, and feed flow rate can easily be computed from the steady-state forms of respective equations.

2.3 Linearization and State-Space Representation

The set of nonlinear equations given by (2.1)–(2.5), (2.10), and (2.11) can be linearized around steady-state operating conditions (H_{k_0}, X_{i_0}, I_{i_0}, h_{d_0}, C_{i_0}, x_{i_0}, Q_{i_0}) and the linear equations, so obtained, can be represented in standard state-space form. For this, define the state vector as

$$\mathbf{z} = \left[\mathbf{z}_H^T \ \mathbf{z}_X^T \ \mathbf{z}_I^T \ \delta h_d \ \mathbf{z}_C^T \ \mathbf{z}_x^T \ \mathbf{z}_Q^T \right]^T, \tag{2.17}$$

Table 2.5 Nodal powers and coolant flow rates under full power operation

Node No.	Steady-state values of	
	Power (MWt)	Coolant flow rate (kg/s)
1	91.8743	187.32
2, 5, 6, 9	54.9991	130.20
3, 4, 7, 8	55.7410	125.38
10, 13, 14, 17	42.6967	97.06
11, 12, 15, 16	53.7146	125.78
Total	920.480	2101.0

where $\mathbf{z}_H = \left[\, \delta H_2 \;\; \delta H_4 \;\; \delta H_6 \;\; \delta H_8 \,\right]^T$ and the rest $\mathbf{z}_\xi = \left[\, (\delta\xi_1/\xi_{1_0}) \;\cdots\; (\delta\xi_{17}/\xi_{17_0}) \,\right]^T$, $\xi = X, I, C, x, Q$, in which δ denotes the deviation from respective steady-state value of the variable. Likewise, define the input vector as

$$\mathbf{u} = \left[\, \delta v_2 \;\; \delta v_4 \;\; \delta v_6 \;\; \delta v_8 \,\right]^T \tag{2.18}$$

and output vector as

$$\mathbf{y} = \left[\, y_T \;\; y_1 \;\cdots\; y_{17} \,\right]^T, \tag{2.19}$$

where $y_T = \sum_{i=1}^{17} \frac{\delta Q_i}{\sum_{j=1}^{17} Q_{j_0}}$ and $y_i = \frac{\delta Q_i}{Q_{i_0}}$ correspond to normalized total reactor power and nodal powers, respectively. Then, the system given by (2.1)–(2.5), (2.10) and (2.11) can be expressed in standard linear state-space form as

$$\dot{\mathbf{z}} = \mathbf{A}\mathbf{z} + \mathbf{B}\mathbf{u} + \mathbf{B}_{fw}\delta q_{fw}, \tag{2.20}$$

$$\mathbf{y} = \mathbf{M}\mathbf{z}, \tag{2.21}$$

where q_{fw} is feed water flow rate. The characteristic matrix $\mathbf{A}$ is of 90th order, expressed as

$$\mathbf{A} = \begin{bmatrix} \mathbf{0} & \mathbf{0} & \mathbf{0} & \mathbf{0} & \mathbf{0} & \mathbf{0} & \mathbf{0} \\ \mathbf{0} & \mathbf{A}_{XX} & \mathbf{A}_{XI} & \mathbf{0} & \mathbf{0} & \mathbf{0} & \mathbf{A}_{XQ} \\ \mathbf{0} & \mathbf{0} & \mathbf{A}_{II} & \mathbf{0} & \mathbf{0} & \mathbf{0} & \mathbf{A}_{IQ} \\ \mathbf{0} & \mathbf{0} & \mathbf{0} & \mathbf{A}_{hh} & \mathbf{0} & \mathbf{0} & \mathbf{A}_{hQ} \\ \mathbf{0} & \mathbf{0} & \mathbf{0} & \mathbf{0} & \mathbf{A}_{CC} & \mathbf{0} & \mathbf{A}_{CQ} \\ \mathbf{0} & \mathbf{0} & \mathbf{0} & \mathbf{A}_{xh} & \mathbf{0} & \mathbf{A}_{xx} & \mathbf{A}_{xQ} \\ \mathbf{A}_{QH} & \mathbf{A}_{QX} & \mathbf{0} & \mathbf{0} & \mathbf{A}_{QC} & \mathbf{A}_{Qx} & \mathbf{A}_{QQ} \end{bmatrix} \tag{2.22}$$

where the first row corresponds to four rows of zeros and $\mathbf{0}$ stands for null matrix of appropriate dimensions. Remaining submatrices are given as follows.

$$\mathbf{A}_{QC} = \frac{\beta}{\ell}\mathbf{E}_{17};$$

$$\mathbf{A}_{QQ}(i,j) = \begin{cases} \frac{1}{\ell}\left(-\Sigma_{k=1}^{17}\alpha_{ki}\frac{Q_{k_0}}{Q_{i_0}} - \beta\right) & \text{if } i = j \\ \frac{1}{\ell}\alpha_{ji}\frac{Q_{j_0}}{Q_{i_0}} & \text{if } i \neq j \end{cases}$$

$$\mathbf{A}_{QX} = diag\left[\, a_{qx1}\ a_{qx2}\ \cdots\ a_{qx17}\,\right],\ \text{where } a_{qxi} = -\frac{1}{\ell}\left(\frac{\bar{\sigma}_{Xi}X_{i_0}}{\Sigma_{ai}}\right);$$

$$\mathbf{A}_{Qx} = \frac{1}{\ell}\,diag\left[\, k_{\alpha_1}Q_{1_0}\ k_{\alpha_2}Q_{2_0}\ \cdots\ k_{\alpha_{17}}Q_{17_0}\,\right];$$

$$\text{where } k_{\alpha_i} = -5\times10^{-3}\left(46.416x_{i_0}^4 - 110.8787x_{i_0}^3 + 95.229x_{i_0}^2 - 35.4779x_{i_0} + 5.2308\right);$$

$$\mathbf{A}_{CQ} = \lambda\mathbf{E}_{17};$$

$$\mathbf{A}_{CC} = -\mathbf{A}_{CQ};$$

$$\mathbf{A}_{IQ} = \lambda_I\mathbf{E}_{17};$$

$$\mathbf{A}_{II} = -\mathbf{A}_{IQ};$$

$$\mathbf{A}_{XQ} = \lambda_X\mathbf{E}_{17} - diag\left[\,\lambda_I\frac{I_{1_0}}{X_{1_0}}\ \cdots\ \lambda_I\frac{I_{17_0}}{X_{17_0}}\,\right];$$

$$\mathbf{A}_{XX} = -diag\left[\,\lambda_X + \bar{\sigma}_{X_1}Q_{1_0}\ \lambda_X + \bar{\sigma}_{X_2}Q_{2_0}\ \cdots\ \lambda_X + \bar{\sigma}_{X_{17}}Q_{17_0}\,\right];$$

$$\mathbf{A}_{XI} = \lambda_I\,diag\left[\,\frac{I_{1_0}}{X_{1_0}}\ \cdots\ \frac{I_{17_0}}{X_{17_0}}\,\right];$$

$$\mathbf{A}_{hh} = -\hat{k}_1\frac{q_{d_0}}{e_{xh}h_w};$$

$$\mathbf{A}_{hQ} = \frac{\hat{k}_1}{e_{xh}}(3k_1 + 2k_2 + k_3)\left(\frac{1}{h_{d_0}} - \frac{1}{h_w}\right)\left[\,q_{d_{1_0}}\ q_{d_{2_0}}\ \cdots\ q_{d_{17_0}}\,\right];$$

$$\mathbf{A}_{xh} = \left[\,\frac{q_{d_{1_0}}h_{d_0}}{e_{vx_1}x_{1_0}}\ \frac{q_{d_{2_0}}h_{d_0}}{e_{vx_2}x_{2_0}}\ \cdots\ \frac{q_{d_{17_0}}h_{d_0}}{e_{vx_{17}}x_{17_0}}\,\right]^T;$$

$$\mathbf{A}_{xx} = -h_c\,diag\left[\,\frac{q_{d_{1_0}}}{e_{vx_1}}\ \frac{q_{d_{2_0}}}{e_{vx_2}}\ \cdots\ \frac{q_{d_{17_0}}}{e_{vx_{17}}}\,\right];$$

$$\mathbf{A}_{xQ} = diag\left[\, a_{xq1}\ a_{xq2}\ \cdots\ a_{xq17}\,\right];$$

$$\text{where } a_{xqi} = \frac{1}{e_{vx_i}x_{i_0}}\left(\, Q_{i_0} - (h_w - h_{d_0} + x_{i_0}h_c)q_{di_0}(3k_1 + 2k_2 + k_3)\,\right);$$

$$\mathbf{A}_{QH}(i,j) = \begin{cases} \frac{-10.23\times10^{-6}Q_{i_0}}{\ell} & \text{for } i = 2,4,6,8;\ \ j = i/2, \\ 0 & \text{elsewhere.} \end{cases}$$

Matrix $\mathbf{B}$ of dimension (90×4) is as follows

$$\mathbf{B} = \left[\,\mathbf{B}_H^T\ \mathbf{0}\ \mathbf{0}\ \mathbf{0}\ \mathbf{0}\ \mathbf{0}\ \mathbf{0}\,\right]^T \tag{2.23}$$

where $\mathbf{B}_H$ is a diagonal matrix of dimensional (4×4), with κ as diagonal entries and all other submatrices are zero. Matrix $\mathbf{B}_{fw}$ is of dimension (90×1) with $b_2 = \hat{k}_1 q_{f_0}\left(\frac{h_{f_0}-1}{e_{x_i}h_{d0}}\right)$ on the 39th row and remaining all entries zero.

The normalized total reactor power and the nodal powers are measured and they constitute the output vector $\mathbf{y}$. Hence, in (2.21), matrix $\mathbf{M}$ is of dimension (18×90), given by

$$\mathbf{M} = \begin{bmatrix} \mathbf{M}_1 & \mathbf{M}_2 \end{bmatrix} \tag{2.24}$$

where $\mathbf{M}_1$ is a null matrix of dimension (18×73) and

$$\mathbf{M}_2 = \begin{bmatrix} \frac{Q_{1_0}}{\Sigma_{j=1}^{17} Q_{j_0}} & \frac{Q_{2_0}}{\Sigma_{j=1}^{17} Q_{j_0}} & \cdots & \frac{Q_{17_0}}{\Sigma_{j=1}^{17} Q_{j_0}} \\ 1 & 0 & \cdots & 0 \\ 0 & 1 & \cdots & 0 \\ \vdots & \vdots & \ddots & \vdots \\ 0 & 0 & \cdots & 1 \end{bmatrix}. \tag{2.25}$$

2.4 Linear System Properties

2.4.1 Stability

The linear system (2.20) is said to be asymptotically stable if

$$\Re e\{\varphi_i(\mathbf{A})\} < 0, \qquad \forall i,$$

where $\varphi_i(\mathbf{A})$ is an eigenvalue of $\mathbf{A}$. Unstable modes of the system are those φ_i's such that $\Re e\{\varphi_i(\mathbf{A})\} \geq 0$ [3]. Hence, stability can be assessed by checking the eigenvalues of the corresponding open-loop linear system matrix $\mathbf{A}$ defined by (2.22). The eigenvalues of system matrix $\mathbf{A}$ are given in Table 2.6. It can be observed that the system has six eigenvalues with positive real parts (eigenvalues 1–6) besides the four eigenvalues at the origin (eigenvalues 7–10), which indicates instability. The unstable eigenvalues are represented by shaded region in Table 2.6. Hence, it is necessary to devise a closed-loop control that effectively maintains the total power of the reactor while the xenon-induced oscillations are being controlled.

2.4.2 Controllability

The linear system (2.20) with order n is said to be controllable, if and only if

$$rank\left\{\begin{bmatrix} \mathbf{A} - \varphi_i \mathbf{E}_n & \mathbf{B} \end{bmatrix}\right\} = n, \qquad \forall i,$$

where φ_i is ith eigenvalue of $\mathbf{A}$ and $\mathbf{E}_n$ is an identity matrix of dimension n. If this is satisfied, then it is commonly mentioned that $(\mathbf{A}, \mathbf{B})$ pair is controllable. Uncontrollable modes of the system are those φ_i's for which $rank\left\{\begin{bmatrix} \mathbf{A} - \varphi_i \mathbf{E}_n & \mathbf{B} \end{bmatrix}\right\} \neq n$.

Table 2.6 Open-loop eigenvalues with thermal hydraulics feedback

Sr. No.	Eigenvalues	Sr. No.	Eigenvalues	Sr. No.	Eigenvalues
1	7.4551×10^{-3}	39	-1.2514×10^{-2}	66	-1.6316×10^{-1}
2–3	$(8.8268\pm j1.8656)\times10^{-5}$	40	-1.6108×10^{-2}	67	-1.6325×10^{-1}
4–5	$(8.0470\pm j2.4129)\times10^{-5}$	41	-5.0954×10^{-2}	68	-1.6405×10^{-1}
6	3.9654×10^{-6}	42	-5.1159×10^{-2}	69	-1.6576×10^{-1}
7–10	0	43	-5.7730×10^{-2}	70	-1.8037×10^{-1}
11–12	$(-3.5182 \pm j7.7577)\times10^{-5}$	44	-5.7893×10^{-2}	71	-1.8049×10^{-1}
13	-3.7781×10^{-5}	45	-5.9707×10^{-2}	72	-1.8122×10^{-1}
14–15	$(-3.7785 \pm j7.6475)\times10^{-5}$	46	-5.9723×10^{-2}	73	-1.8395×10^{-1}
16	-3.7993×10^{-5}	47	-6.0344×10^{-2}	74	-7.2516
17	-4.0124×10^{-5}	48	-6.0642×10^{-2}	75	-3.2844×10^{1}
18	-4.1520×10^{-5}	49	-6.1848×10^{-2}	76	-3.3372×10^{1}
19	-4.2245×10^{-5}	50	-6.1942×10^{-2}	77	-6.6599×10^{1}
20	-4.4204×10^{-5}	51	-6.2200×10^{-2}	78	-6.8323×10^{1}
21	-4.7476×10^{-5}	52	-6.2380×10^{-2}	79	-9.3653×10^{1}
22	-4.8866×10^{-5}	53	-6.2458×10^{-2}	80	-9.4612×10^{1}
23–24	$(-6.4855 \pm j5.3109) \times 10^{-5}$	54	-6.2608×10^{-2}	81	-1.0868×10^{2}
25–26	$(-6.5890 \pm j5.4696) \times 10^{-5}$	55	-6.2865×10^{-2}	82	-1.1705×10^{2}
27–28	$(-7.3359 \pm j3.9319) \times 10^{-5}$	56	-6.2893×10^{-2}	83	-1.6967×10^{2}
29–30	$(-7.7407 \pm j2.9929) \times 10^{-5}$	57	-1.1714×10^{-1}	84	-1.7568×10^{2}
31	-1.4107×10^{-4}	58	-1.4712×10^{-1}	85	-1.9497×10^{2}
32	-1.4624×10^{-4}	59	-1.4713×10^{-1}	86	-2.1110×10^{2}
33	-1.5717×10^{-4}	60	-1.4809×10^{-1}	87	-2.1904×10^{2}
34	-1.6524×10^{-4}	61	-1.4849×10^{-1}	88	-2.3591×10^{2}
35	-1.6720×10^{-4}	62	-1.5580×10^{-1}	89	-2.7163×10^{2}
36	-1.7308×10^{-4}	63	-1.5585×10^{-1}	90	-2.7626×10^{2}
37	-1.8807×10^{-4}	64	-1.5662×10^{-1}		
38	-1.8870×10^{-4}	65	-1.5759×10^{-1}		

The condition of controllability governs the existence of a complete solution to the control system design problem [6]. Designing a controller to stabilize an unstable system and to achieve any specified transient response characteristics may not be possible if the system is uncontrollable. In case of AHWR, with matrices $\mathbf{A}$ and $\mathbf{B}$ given by equations (2.22) and (2.23) respectively, test has been performed, which results that the pair ($\mathbf{A}$, $\mathbf{B}$) is controllable, i.e., $rank\left\{\left[\mathbf{A} - \varphi_i \mathbf{E}_n \ \mathbf{B}\right]\right\} = n, \forall i$, where $n = 90$.

2.4.3 Observability

The linear system (2.20)–(2.21) of order n is said to be observable, if and only if

$$rank\left\{\begin{bmatrix}\mathbf{A}-\varphi_i\mathbf{E}_n\\ \mathbf{M}\end{bmatrix}\right\}=n,\qquad \forall i.$$

If this is satisfied, then it is commonly mentioned that $(\mathbf{A},\mathbf{M})$ pair is observable. Unobservable modes of the system are those φ_i's for which $rank\left\{\begin{bmatrix}\mathbf{A}-\varphi_i\mathbf{E}_n\\ \mathbf{M}\end{bmatrix}\right\}\neq n$. Observability denotes whether every state can be determined from the observation of the outputs over a finite interval of time [6]. The concept of observability thus helps in solving the problem of reconstructing unmeasured state variables from the measured variables. This plays a significant role in control system design, since the information of all the state variables is many a times essential for designing a suitable controller. The observability test of AHWR model has been carried out using pair $(\mathbf{A},\mathbf{M})$ given by (2.22) and (2.24) and it is found that $rank\left\{\begin{bmatrix}\mathbf{A}-\varphi_i\mathbf{E}_n\\ \mathbf{M}\end{bmatrix}\right\}=n,\forall i$. This concludes that system given by (2.20)–(2.21) is observable.

2.5 Vectorization of AHWR Model

For brevity, the equations governing the coupled neutronics–thermal hydraulics model of AHWR are revisited here:

$$\frac{dQ_i}{dt}=(\rho_i-\alpha_{ii}-\beta)\frac{Q_i}{\ell}+\sum_{j=1}^{17}\alpha_{ji}\frac{Q_j}{\ell}+\lambda C_i, \tag{2.26}$$

$$\frac{dC_i}{dt}=\frac{\beta}{\ell}Q_i-\lambda C_i, \tag{2.27}$$

$$\frac{dI_i}{dt}=\gamma_I\Sigma_{f_i}Q_i-\lambda_I I_i, \tag{2.28}$$

$$\frac{dX_i}{dt}=\gamma_X\Sigma_{f_i}Q_i+\lambda_I I_i-(\lambda_X+\bar{\sigma}_{X_i}Q_i)X_i, \tag{2.29}$$

$$\frac{dH_k}{dt}=\kappa v_k, \tag{2.30}$$

$$e_{vx_i}\frac{dx_i}{dt} = Q_i - q_{d_i}(h_w - h_d) - q_{d_i}x_i h_c, \tag{2.31}$$

$$e_{x_i}\frac{dh_d}{dt} = q_f(\hat{k}_2 h_f - \hat{k}_1) - q_d(\hat{k}_2 h_d - \hat{k}_1), \tag{2.32}$$

where $i = 1, 2, \ldots, 17$; $k = 2, 4, 6, 8$; and

$$q_{d_i} = \left\{ k_1\left[\frac{Q_i}{Q_{i_0}}\right]^3 + k_2\left[\frac{Q_i}{Q_{i_0}}\right]^2 + k_3\left[\frac{Q_i}{Q_{i_0}}\right] + k_4 \right\} q_{d_{i_0}}, \tag{2.33}$$

$$\rho_i = \rho_{i_u} + \rho_{i_X} + \rho_{i_\alpha}, \tag{2.34}$$

$$\rho_{i_u} = \begin{cases} (-10.234H_i + 676.203) \times 10^{-6}, & \text{if } i = 2, 4, 6, 8 \\ 0 & \text{elsewhere,} \end{cases} \tag{2.35}$$

$$\rho_{i_X} = \frac{\bar{\sigma}_{X_i} X_i}{\Sigma_{a_i}}, \tag{2.36}$$

$$\rho_{i_\alpha} = -5 \times 10^{-3}(9.2832x_i^5 - 27.7192x_i^4 + 31.7643x_i^3 - 17.7389x_i^2 + 5.2308x_i + 0.0792). \tag{2.37}$$

The dynamic equations (2.26)–(2.37) can be written in vector/matrix form to implement in MATLAB/Simulink environment [8]. For that rearrange Eq. (2.26) of nodal powers as

$$\frac{dQ_i}{dt} = \frac{1}{\ell}\left[\rho_i Q_i - \alpha_{ii} Q_i - \beta Q_i + \sum_{j=1}^{17} \alpha_{ji} Q_j + \lambda \ell C_i\right]. \tag{2.38}$$

In the above equation ℓ, β are constants, ρ_i, α_{ii}, C_i, and Q_i are column vectors and α_{ji} is a matrix. However, the terms $\rho_i Q_i$, $\alpha_{ii} Q_i$, βQ_i, $\sum_{j=1}^{17} \alpha_{ji} Q_j$ and $\lambda \ell C_i$ are all column vectors of the same dimensions. If scalar multiplication is denoted by '$\cdot$', element-wise multiplication is denoted by '$\odot$', and array multiplication is denoted by '$*$' then (2.38) can be rewritten as

$$\frac{dQ_i}{dt} = \frac{1}{\ell} \cdot \left[\rho_i \odot Q_i - \alpha_{ii} \odot Q_i - \beta \cdot Q_i + \sum_{j=1}^{17} \alpha_{ji} Q_j + (\lambda \ell) \cdot C_i\right]. \tag{2.39}$$

Above equation is implemented using only one integrator, instead of 17 different integrators. Simulink of MATLAB automatically expands the equation to appropriate size as shown in Fig. 2.2. Initial values of nodal powers can be inserted in the integrator in vector form by double clicking 'integrator' block.

Similarly, the delayed neutron precursor, iodine, xenon concentrations, and rod position dynamics can be structured in vector/matrix form as

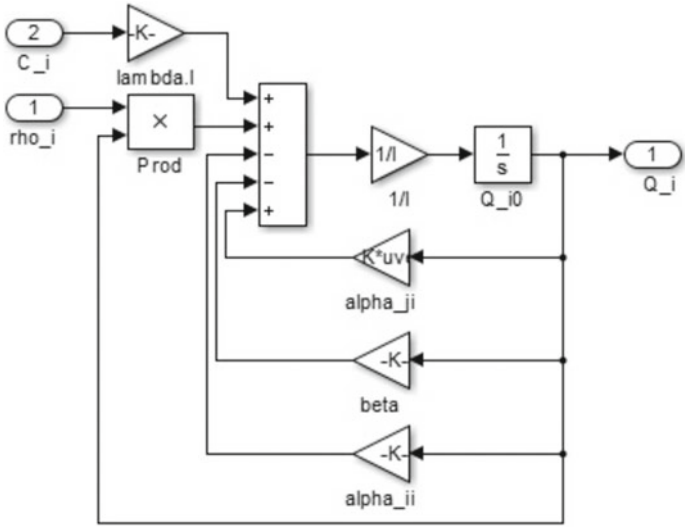

Fig. 2.2 Implementation of nodal powers

$$\frac{dC_i}{dt} = \frac{\beta}{\ell} \cdot Q_i - \lambda \cdot C_i, \tag{2.40}$$

$$\frac{dI_i}{dt} = (\gamma_I \cdot \Sigma_{f_i}) \odot Q_i - \lambda_I \cdot I_i, \tag{2.41}$$

$$\frac{dX_i}{dt} = (\gamma_X \cdot \Sigma_{fi}) \odot Q_i + \lambda_I \cdot I_i - (\lambda_X + \bar{\sigma}_{Xi} \odot Q_i) \odot X_i, \tag{2.42}$$

$$\frac{dH_k}{dt} = \kappa \cdot v_k, \quad k = 2, 4, 6, 8; \quad i = 1, 2, ..., 17. \tag{2.43}$$

After defining vector gains, above Eqs. (2.40)–(2.43) can be easily realized in Simulink as a core neutronics model subsystem block, as depicted in Fig. 2.3. In the similar manner, the thermal hydraulics model involving dynamics of exit quality and downcomer enthalpy, given by (2.31) and (2.32), is represented in vectorized form as

$$\frac{dx_i}{dt} = \frac{1}{e_{vx_i}} \odot \left[Q_i - q_{d_i} \cdot (h_w - h_d) - (q_{d_i} \odot x_i) \cdot h_c \right], \tag{2.44}$$

$$\frac{dh_d}{dt} = \frac{1}{e_{x_i}} \odot \left[q_f \cdot (\hat{k}_2 h_f - \hat{k}_1) - q_d \cdot (\hat{k}_2 h_d - \hat{k}_1) \right] \tag{2.45}$$

and employed in Simulink as given in Fig. 2.4. The instantaneous coolant flow rate through the channels can be evaluated as per (2.33) and is represented in Fig. 2.4 as 'coolant flowrate' subsystem block. Reactivity on account of RR movements is the function of its position, as defined by (2.30) and (2.35). These two equations can be collectively implemented as represented in Fig. 2.5. All these equations can be

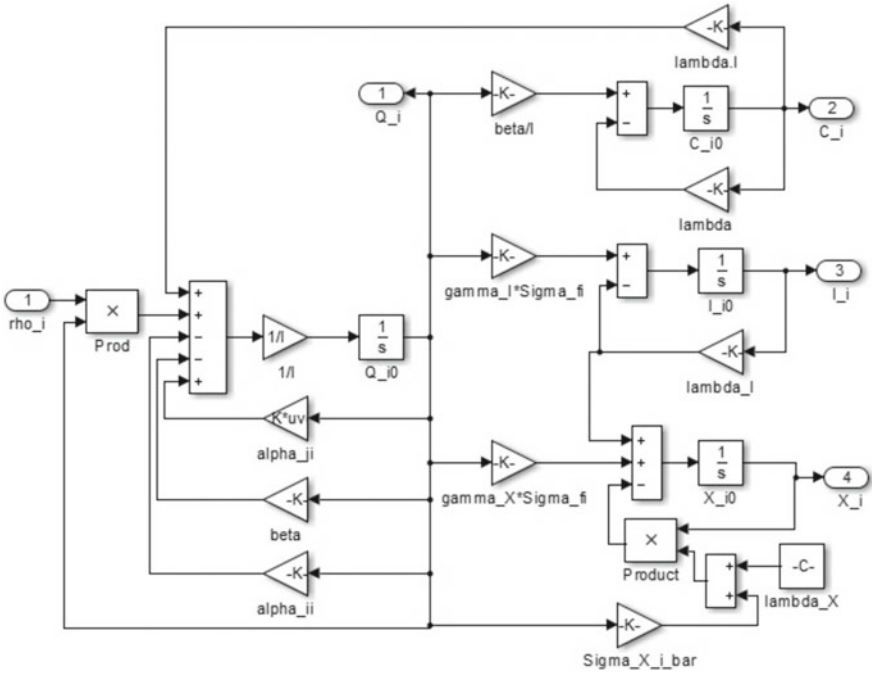

Fig. 2.3 Block of core neutronics model

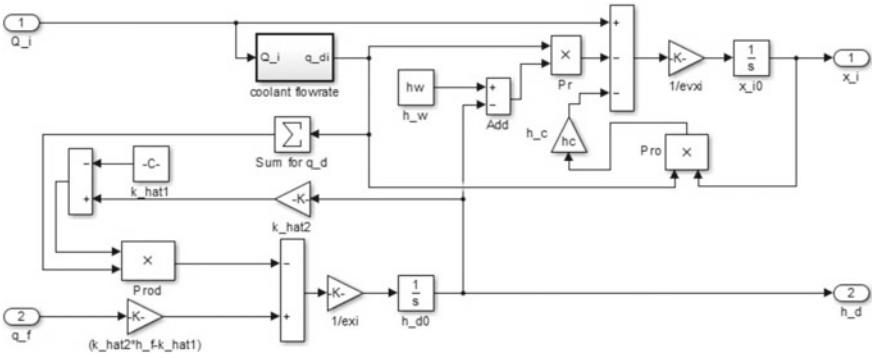

Fig. 2.4 Block of thermal hydraulics model

combined together, in the form of different subsystems, considering proper relationship between different variables and reactivity feedbacks, to form complete AHWR model. This complete model, shown in Fig. 2.6, eventually leads to an automatic program that solves nonlinear equations (2.26)–(2.32). Advantages of this type of model constructed in Simulink are:

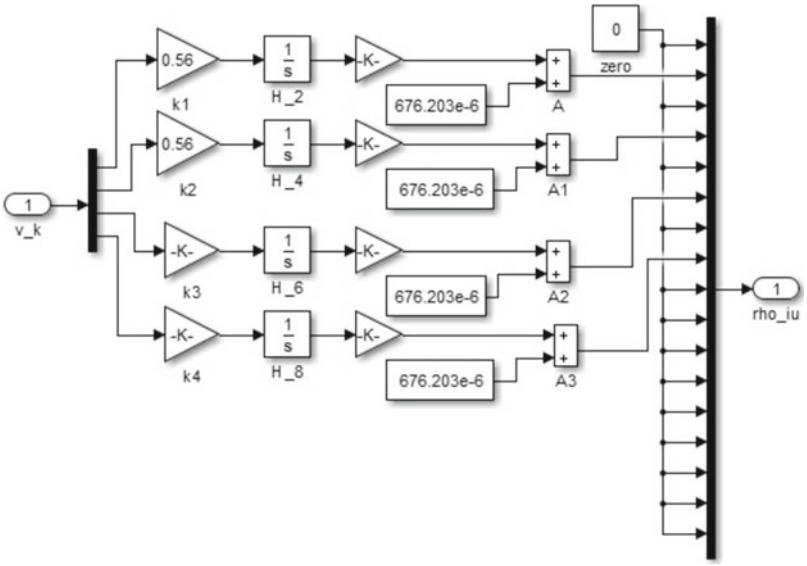

Fig. 2.5 Block of reactivity due to control rod positions

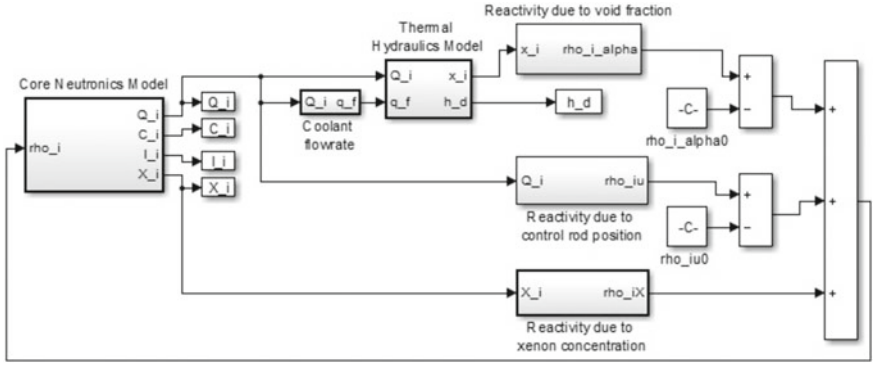

Fig. 2.6 Complete AHWR model

1. It can be used for different types of reactors with different number of nodes, provided that the coupling coefficients matrix and reactivity feedbacks are modeled properly,
2. Variations of any variable with respect to time or any other variable can be studied by applying 'scope' block across that variable,
3. Visualization of calculations and their recording for further applications is possible,

4. Different methods of solving nonlinear differential equations with different time steps can be studied, and
5. The computations are performed in much less time compared to the transient duration.

2.6 Static Output Feedback Control for AHWR

As mentioned in Sect. 2.4.1, the existence of multiple eigenvalues at the origin and eigenvalues with positive real part depicts instabilities in the AHWR. Hence, it is necessary to devise a closed-loop control that efficiently maintains the total power of the reactor core while the xenon-induced oscillations are being controlled.

Generally feedback of total power is sufficient to control small and medium size nuclear reactors, however, large reactors, like AHWR, require feedback of spatial power distribution along with the total power feedback for effective spatial control. Based on these considerations, let us consider the input $\mathbf{u}$ in (2.20) of the form

$$\mathbf{u} = -\mathbf{K}\mathbf{y} = -\mathbf{K} * \mathbf{y}, \tag{2.46}$$

where $\mathbf{K}$ is a (4×18) matrix. With the above control and (2.21), the system (2.20) becomes

$$\dot{\mathbf{z}} = (\mathbf{A} - \mathbf{BKM})\mathbf{z} + \mathbf{B}_{fw}\delta q_{fw} = \hat{\mathbf{A}}\mathbf{z} + \mathbf{B}_{fw}\delta q_{fw}, \tag{2.47}$$

where $\hat{\mathbf{A}} = (\mathbf{A} - \mathbf{BKM})$.

2.6.1 Total Power Feedback

First consider that

$$\mathbf{K} = \left[\bar{\mathbf{K}}_T \ \mathbf{0} \cdots \mathbf{0}\right] \tag{2.48}$$

in which $\mathbf{0}$ represents vectors of (4×1) dimension and $\bar{\mathbf{K}}_T = \left[K_T \ K_T \ K_T \ K_T\right]^T$ such that the feedback gain corresponding to total power is K_T for all RRs and is zero corresponding to nodal powers. The total power feedback control scheme is depicted in Fig. 2.7. The stability characteristic of the system (2.47) is investigated by varying the value of K_T and for $K_T = 12.5$, the gross behavior of the system seems stable though the system can show spatial instability. To reveal this, a transient involving a spatial power disturbance was simulated using vectorized nonlinear model of the reactor obtained from Eqs. (2.26)–(2.37) developed in MATLAB/Simulink. It was assumed that the reactor was operating initially at full power, with control signal

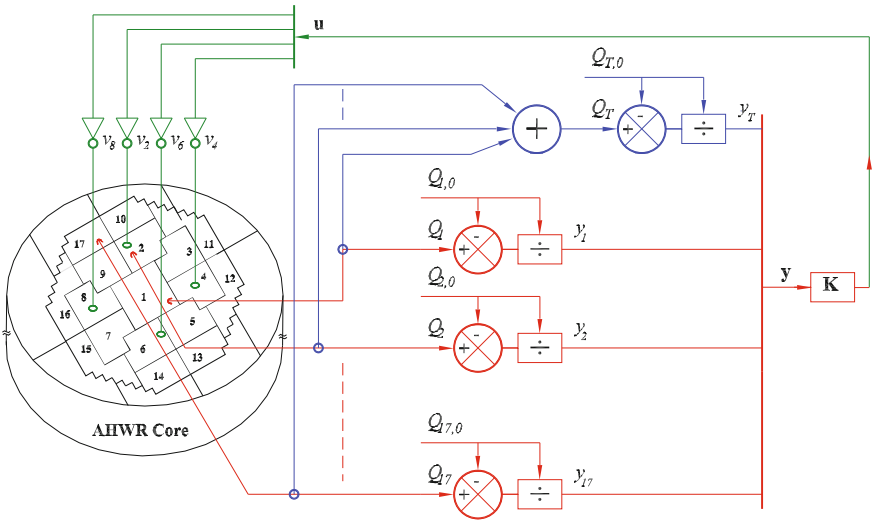

Fig. 2.7 Output feedback control scheme for AHWR ($Q_{T,0}$ and Q_T are respectively steady-state and instantaneous values of total reactor power)

generated by (2.46). The RR2 which was initially at its equilibrium position was driven out by about 1% by giving proper control signal. Immediately after that RR2 was driven back to its original position and thereafter left under the influence of controller. The response of the model to this disturbance was investigated in terms of variations in total reactor power and tilts in the first and second azimuthal modes defined as

$$\text{First azimuthal tilt} = \frac{Q_L - Q_R}{\sum_{i=1}^{17} \frac{Q_i}{2}} \times 100\% \tag{2.49}$$

$$\text{where } Q_L = \frac{1}{2}Q_1 + \sum_{i=6}^{9} Q_i + \sum_{i=14}^{17} Q_i,$$

$$Q_R = \frac{1}{2}Q_1 + \sum_{i=2}^{5} Q_i + \sum_{i=10}^{13} Q_i;$$

$$\text{Second azimuthal tilt} = \frac{Q_{p1} - Q_{p2}}{\sum_{i=1}^{17} \frac{Q_i}{2}} \times 100\% \tag{2.50}$$

$$\text{where } Q_{p1} = \frac{1}{2}Q_1 + Q_2 + Q_3 + Q_6 + Q_7 + Q_{10} + Q_{11} + Q_{14} + Q_{15},$$

$$Q_{p2} = \frac{1}{2}Q_1 + Q_4 + Q_5 + Q_8 + Q_9 + Q_{12} + Q_{13} + Q_{16} + Q_{17}.$$

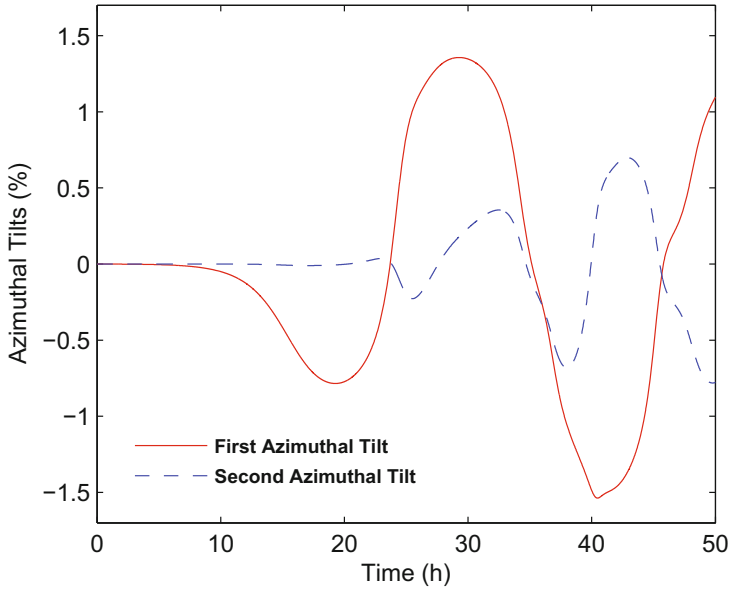

Fig. 2.8 Unstable modes of spatial instability

From simulation results, it was noticed that although the total power is being regulated at steady state, the power distribution in the core experiences oscillations. In 38 h, the first and second azimuthal tilts raise to the amplitudes of the order of 1.4 and 0.75% respectively as shown in Fig. 2.8. The period of the oscillations for first and second azimuthal modes are observed to be 20 and 12 h, respectively. If coolant void fraction reactivity feedback is not modeled, the amplitudes of first and second azimuthal tilts are observed to be markedly higher than as given in Fig. 2.8. Whereas, if xenon reactivity feedback is removed, then no oscillations were observed in power distribution, signifying that these are certainly xenon-induced spatial oscillations. These spatial oscillations and following local overpowers pose a potential threat to the fuel integrity of any nuclear reactor and hence necessitate control. Therefore, it is needed to devise an appropriate spatial power controller for AHWR.

2.6.2 Spatial Power Feedback

As observed in the Sect. 2.6.1, the AHWR system is showing spatial instability even with total power feedback. This is because the system (2.47) has still four eigenvalues with positive real parts and three eigenvalues at the origin. Hence, in addition to total power feedback, feedback of spatial power is required. Here, spatial stabilization of AHWR system is achieved with the feedback of nodal powers, in which RRs are placed along with total power feedback. Thus, in (2.48), **K** that was restricted

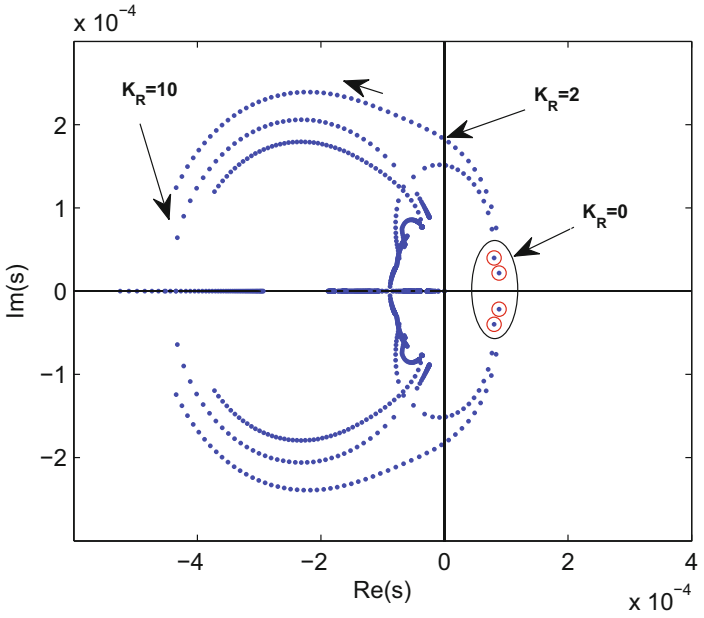

Fig. 2.9 Effect of feedback of nodal powers wherein RRs are located on location of unstable eigenvalues

to contain nonzero values only in the first column, will now be allowed to have nonzero values in other locations. This can be realized in such way that feedback gain corresponding to total power is K_T and feedback gain to power in nodes 2, 4, 6, and 8 is K_R, that is

$$\mathbf{K} = \begin{bmatrix} K_T & 0 & K_R & 0 & 0 & 0 & 0 & 0 & 0 & 0\,0\,0\,0\,0\,0\,0\,0\,0 \\ K_T & 0 & 0 & 0 & K_R & 0 & 0 & 0 & 0 & 0\,0\,0\,0\,0\,0\,0\,0\,0 \\ K_T & 0 & 0 & 0 & 0 & 0 & K_R & 0 & 0 & 0\,0\,0\,0\,0\,0\,0\,0\,0 \\ K_T & 0 & 0 & 0 & 0 & 0 & 0 & 0 & K_R & 0\,0\,0\,0\,0\,0\,0\,0\,0 \end{bmatrix}. \tag{2.51}$$

Figure 2.9 shows the locus of both stable and unstable eigenvalues near origin when K_R was increased progressively from zero. It is observed that all the unstable eigenvalues are stabilized for $K_R \geq 2$, which proves that the feedback of nodal powers in which RRs are placed can be effectively used to stabilize the system. Most of the eigenvalues near to the origin are found to have settled at their respective new locations for $K_R \approx 10$. With this consideration value of K_R is selected as 10. Closed-loop eigenvalues with $K_R = 10$ and $K_T = 12.5$ are found to be in the left half of s-plane, as listed in Table 2.7. This shows that the control law (2.46) stabilizes the system (2.47) with $\mathbf{K}$ given by (2.51). Spatial power feedback control scheme can be implemented with the same Fig. 2.7, where $\mathbf{K}$ is given by (2.51) [9].

Table 2.7 Closed-loop eigenvalues of AHWR model

Sr. No.	Eigenvalues	Sr. No.	Eigenvalues	Sr. No.	Eigenvalues
1	-2.8773×10^{-5}	37	-5.8834×10^{-2}	69	-1.751×10^{-1}
2	-2.8773×10^{-5}	38	-5.9364×10^{-2}	70	-1.8053×10^{-1}
3	-2.8773×10^{-5}	39	-5.966×10^{-2}	71	-1.8078×10^{-1}
4	-2.8773×10^{-5}	40	-5.9845×10^{-2}	72	-1.8221×10^{-1}
5	-4.0085×10^{-5}	41	-6.1191×10^{-2}	73	-2.6345×10^{-1}
6	-4.0237×10^{-5}	42	-6.1316×10^{-2}	74	-6.9796
7	-4.3283×10^{-5}	43–44	$(-5.9085 \pm j1.6901) \times 10^{-2}$	75	-3.2787×10^{1}
8	-4.3593×10^{-5}	45	-6.1803×10^{-2}	76	-3.3327×10^{1}
9	-6.755×10^{-5}	46	-6.1872×10^{-2}	77	-6.6584×10^{1}
10	-7.1457×10^{-5}	47	-6.235×10^{-2}	78	-6.8302×10^{1}
11–12	$(-7.6810 \pm j3.0862) \times 10^{-5}$	48	-6.2387×10^{-2}	79	-9.3652×10^{1}
13–14	$(-7.6926 \pm j3.0637) \times 10^{-5}$	49	-6.2702×10^{-2}	80	-9.4604×10^{1}
15–16	$(-2.0967 \pm j8.2771) \times 10^{-5}$	50	-6.2723×10^{-2}	81	-1.0867×10^{2}
17–18	$(-3.7556 \pm j7.6706) \times 10^{-5}$	51–52	$(-6.5120 \pm j2.2626) \times 10^{-2}$	82	-1.1704×10^{2}
19–20	$(-6.4610 \pm j5.6114) \times 10^{-5}$	53–54	$(-6.8026 \pm j2.3457) \times 10^{-2}$	83	-1.6966×10^{2}
21–22	$(-3.5386 \pm j7.7973) \times 10^{-5}$	55	-8.4982×10^{-2}	84	-1.7567×10^{2}
23–24	$(-5.6889 \pm j0.8659) \times 10^{-6}$	56	-1.1257×10^{-1}	85	-1.9496×10^{2}
25	-9.4731×10^{-5}	57	-1.3375×10^{-1}	86	-2.1109×10^{2}
26	-1.0049×10^{-4}	58	-1.4715×10^{-1}	87	-2.1903×10^{2}
27	-1.5741×10^{-4}	59	-1.4718×10^{-1}	88	-2.359×10^{2}
28	-1.5881×10^{-4}	60	-1.4844×10^{-1}	89	-2.7162×10^{2}
29	-1.7621×10^{-4}	61	-1.5045×10^{-1}	90	-2.7625×10^{2}
30	-1.7705×10^{-4}	62	-1.5592×10^{-1}		
31	-2.3573×10^{-4}	63	-1.5602×10^{-1}		
32	-2.3586×10^{-4}	64	-1.5749×10^{-1}		
33	-2.4991×10^{-4}	65	-1.6038×10^{-1}		
34	-2.5026×10^{-4}	66	-1.6324×10^{-1}		
35	-1.5734×10^{-4}	67	-1.6339×10^{-1}		
36	-5.7761×10^{-2}	68	-1.6499×10^{-1}		

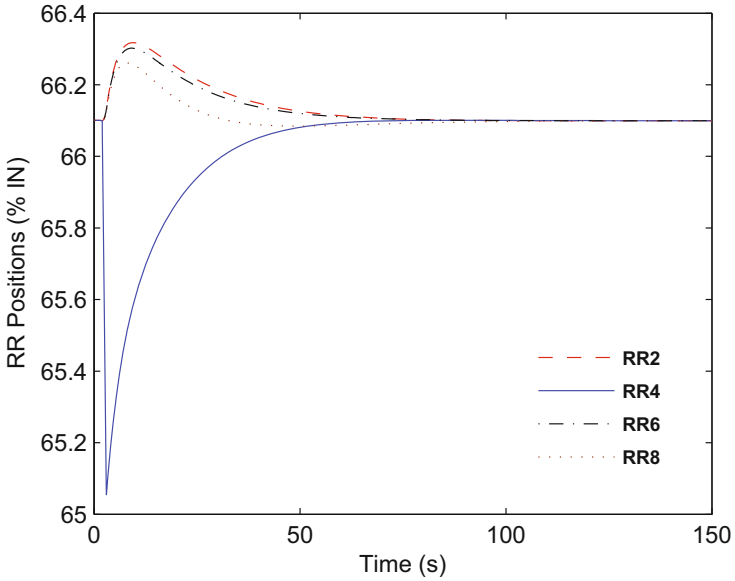

Fig. 2.10 Effect of RR disturbance on regulating rod positions

2.6.3 Transient Simulations

The controller performance was examined by simulating the nonlinear system of AHWR. Assuming that the reactor is operating at full power steady-state condition, with control signal generated by (2.46) and **K** given by (2.51), shortly, RR4, initially under auto control was driven out by almost 1% manually by giving proper control signal after 2 s and left under the influence of automatic control thereafter. As shown in the Fig. 2.7, deviations in nodal powers from their respective equilibrium values are given as input to the feedback gain **K**. This gain is designed such that it utilizes only the deviations of nodal powers in which RRs are placed, along with total power deviation. From the transient simulation, it was noticed that the RRs are driven back to their equilibrium position, as shown in Fig. 2.10. As a result of the controller action, disturbance in total power and spatial powers are suppressed in around 80 s. The variation in total power is depicted in Fig. 2.11 and variations in nodal powers, measured in terms of azimuthal tilts, are shown in Fig. 2.12. Since the transient is of very short duration, amplitudes of first and second azimuthal tilts are, respectively, 0.0128 and 0.0048%.

In one more transient, the reactor is assumed to be operating at steady-state full power condition, i.e., at 920.48 MW[1] with nodal powers as given in Table 2.5. Concentrations of iodine, xenon, and delayed neutron precursor are also in equilibrium with the respective nodal powers. Now, the demand power is decreased uniformly

[1] MW is used to represent Mega Watt Thermal.

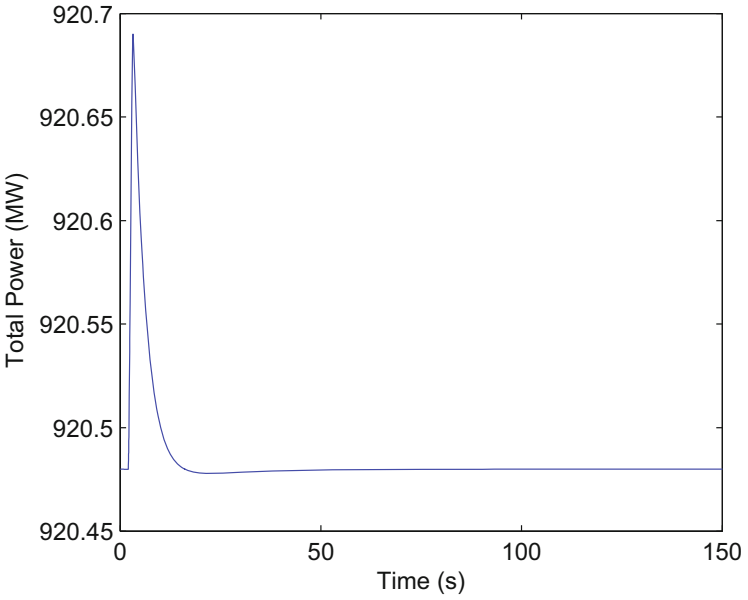

Fig. 2.11 Effect of RR disturbance on total reactor power

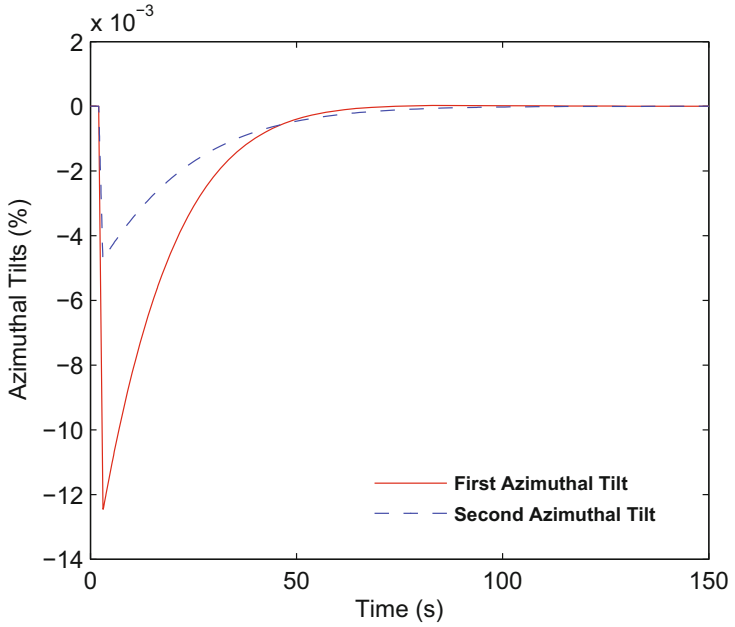

Fig. 2.12 Effect of RR disturbance on azimuthal tilts

at the rate of 1.5 MW/s to 828.43 MW, in around 61 s and thereafter held steady. Figures 2.13, 2.14, 2.15, 2.16, and 2.17 represent respective variations in total power, nodal powers, nodal xenon, and delayed neutron precursor concentrations during the transient period. From Fig. 2.13 it is noticed that the total power is maintained close to the demand power. The total power variation during initial 0.06 h (216 s) is shown in Fig. 2.14. The total power is near about 822.42 MW at 0.02 h (72 s) and it settles within $\pm 0.12\%$ of new demand power approximately in next 90 s. The nodal powers achieve new steady-state values within about 90 s as represented in Fig. 2.15 and do not show any variation during the remaining prolonged simulation. The xenon concentrations become stable at their respective new steady-state values in about 50 h. The delayed neutron precursor concentrations take only 90 s to achieve new steady state (Fig. 2.17). Though the change in stabilization time for delayed neutron precursor and xenon concentrations is several hours, this does not create any intricacy in simulation, which is achieved in Simulink proficiently using suggested vectorization of modeling equation.

Finally, to test the performance of controller under disturbance condition, nonlinear model was once again simulated. Apart from four voltage signals to RRs, feed flow is the fifth input of the AHWR system. Change in the feed flow rate is nothing but the disturbance for the system. When reactor was operating at equilibrium condition, a 5% positive step change was introduced in feed flow as shown in Fig. 2.18 after 100 s. Due to this, the downcomer enthalpy is decreased by 0.64% as shown in Fig. 2.19 and total power experienced variations as depicted in Fig. 2.20. The total power rises from 920.48 to 920.70 MW and becomes stable at its original value in about next 100 s. It is evident from the Fig. 2.21, that in order to maintain total power at equilibrium level, all the RRs are moved inside almost by 1%. Since the variation in total power is observed to be very small, i.e., 0.02% (Fig. 2.20), variations in delayed neutron precursor and xenon concentrations are also found to be very small, as indicated in Figs. 2.22 and 2.23. Again in spite of huge difference in time constants for delayed neutron precursor and xenon concentrations, the simulations are carried out without any difficulty. This shows the efficacy of the controller.

2.7 Conclusion

Analysis of nuclear reactor system and design of suitable control require a mathematical model. In this chapter, a simplified coupled core neutronics–thermal hydraulics model of AHWR system is presented. The final model equations are represented into standard state-space form for control system studies and stability, controllability, and observability properties of the AHWR system are examined. Thereafter, nonlinear model of AHWR is developed in MATLAB/Simulink environment by vectorization and steady state is achieved by giving feedback of total power. When this model is simulated for transient condition, it is observed that total power remains constant

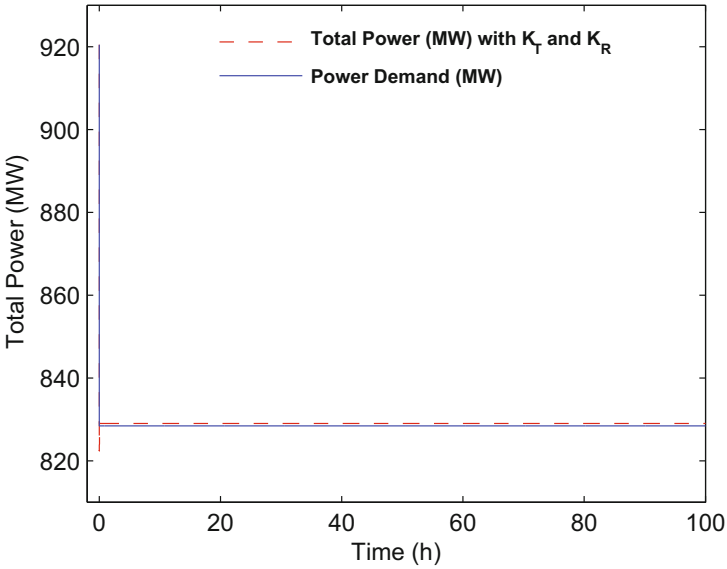

Fig. 2.13 Effect of power maneuvering on total power

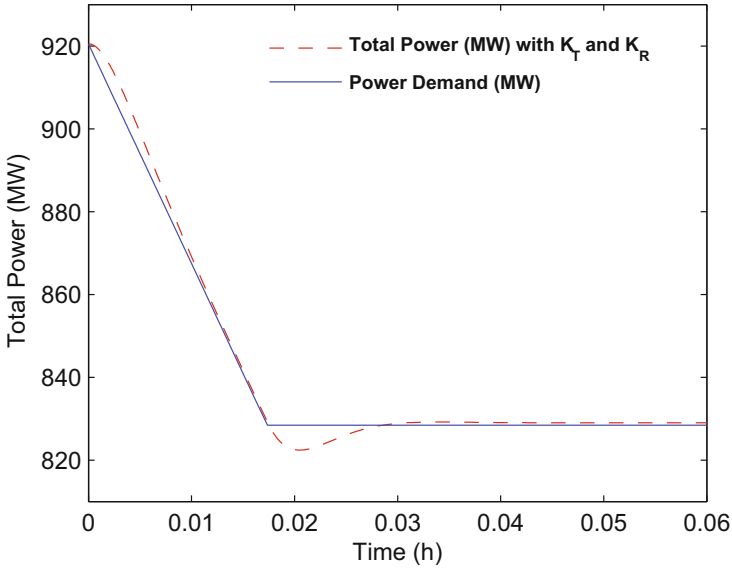

Fig. 2.14 Effect of power maneuvering on total power for initial 0.06 h (216 s)

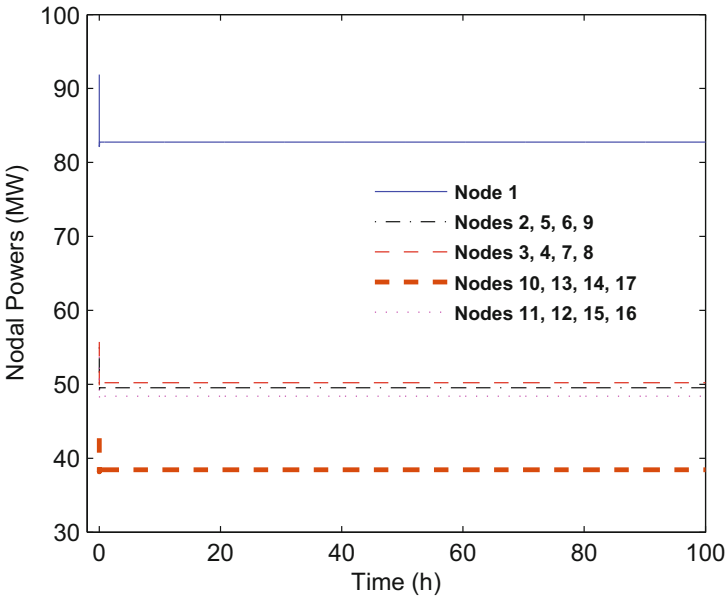

Fig. 2.15 Effect of power maneuvering on nodal powers

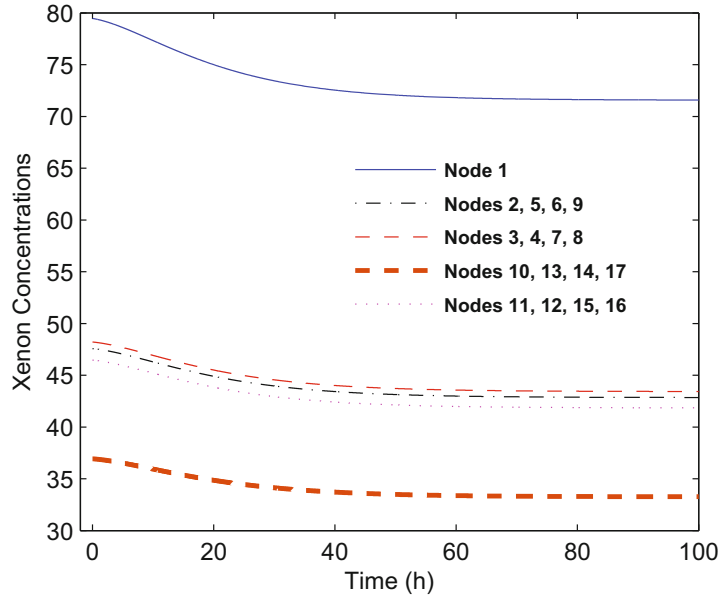

Fig. 2.16 Effect of power maneuvering on xenon concentrations

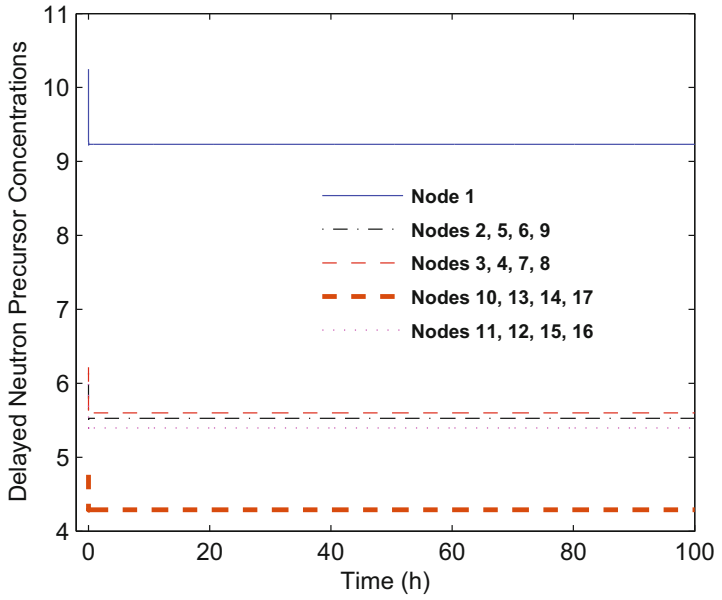

Fig. 2.17 Effect of power maneuvering on delayed neutron precursor concentrations

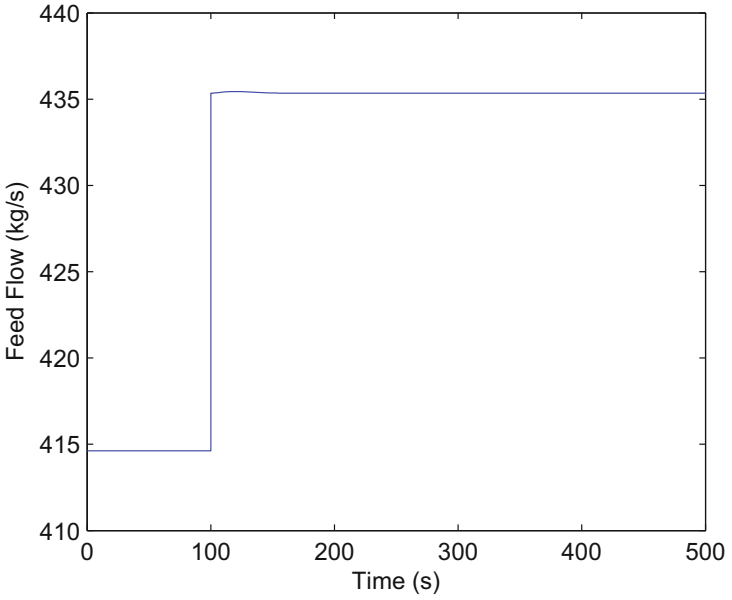

Fig. 2.18 Step change of 5% in the feed flow

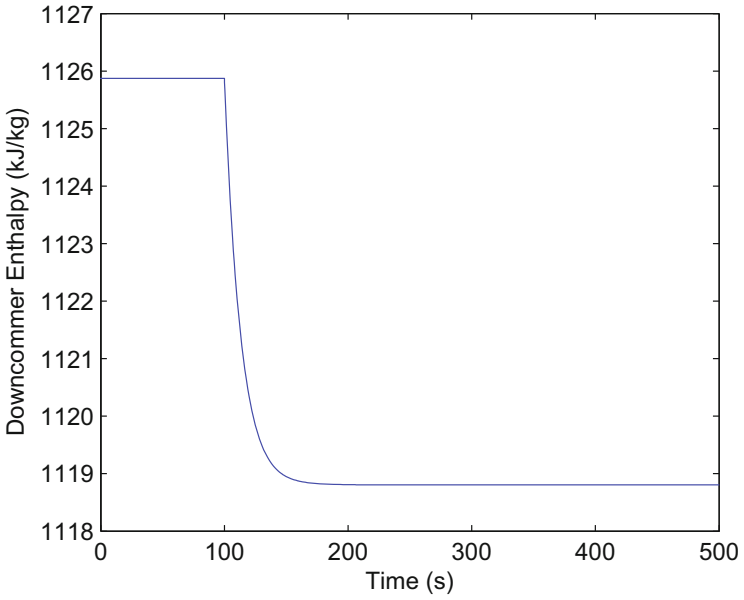

Fig. 2.19 Effect of step change in feed flow on downcomer enthalpy

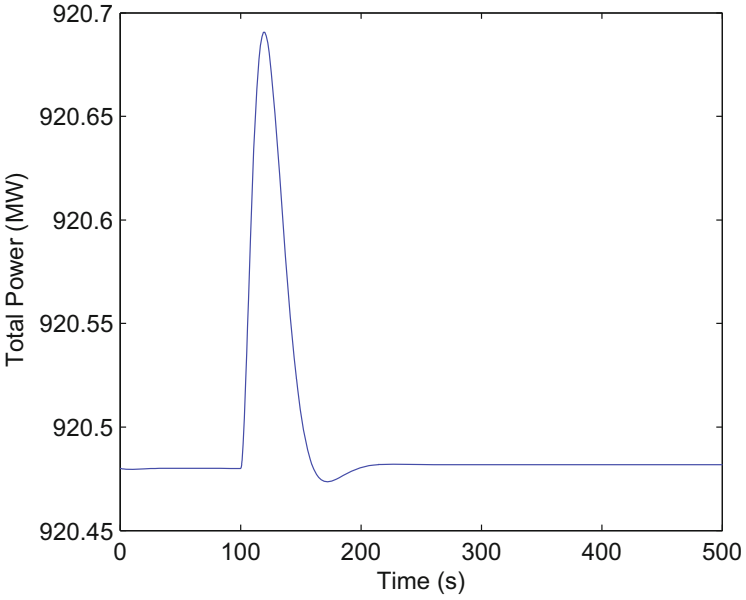

Fig. 2.20 Effect of step change in feed flow on total power

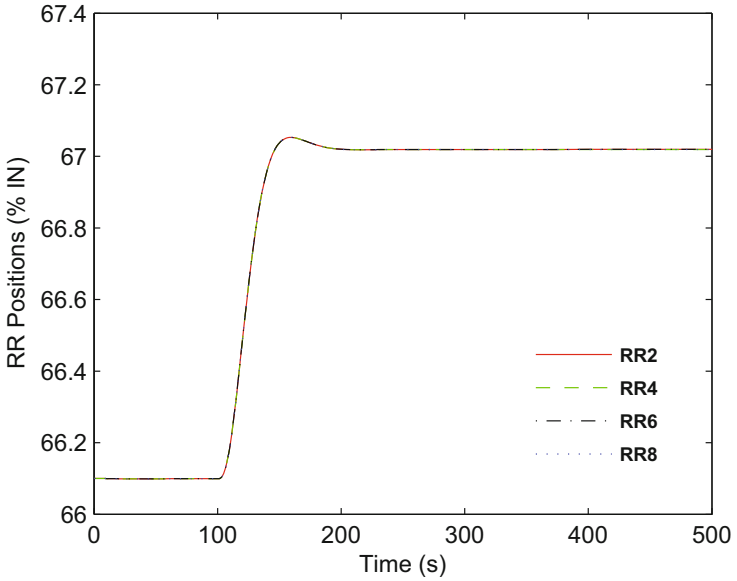

Fig. 2.21 Effect of step change in feed flow on RR positions

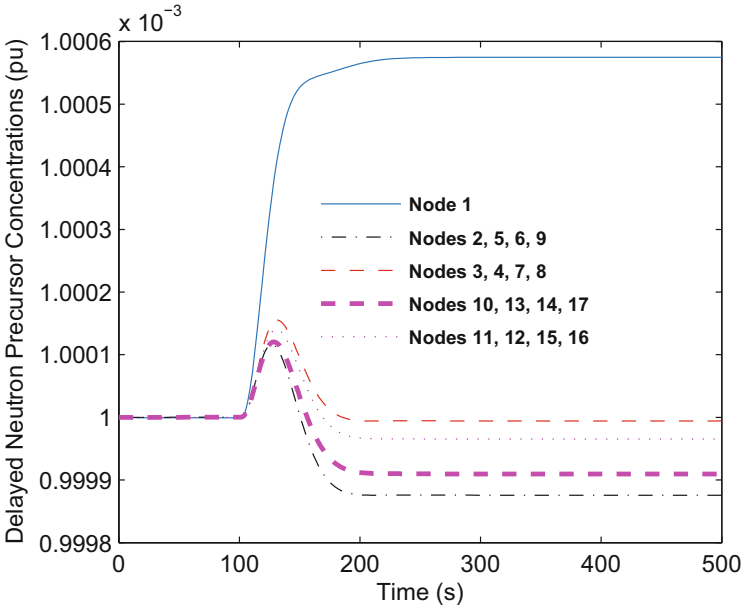

Fig. 2.22 Effect of step change in feed flow on nodal delayed neutron precursor concentrations

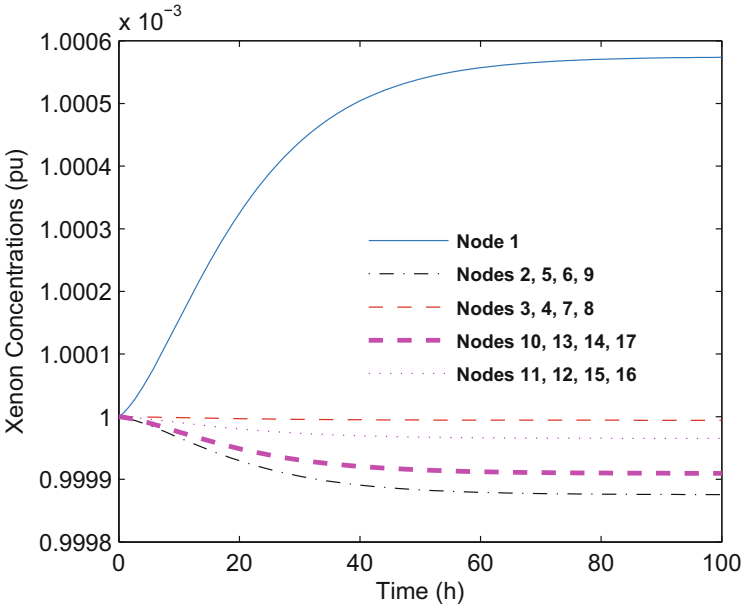

Fig. 2.23 Effect of step change in feed flow on nodal xenon concentrations

but the power in opposite regions of the core undergoes oscillations. Therefore, the feedback of nodal powers where RRs are placed is given in addition to total power feedback. Effectiveness of this static output feedback control is justified by testing the performance under different transient conditions.

References

1. Arda, S.E., Holbert, K.E.: Nonlinear dynamic modeling and simulation of a passively cooled small modular reactor. Prog. Nucl. Energy **91**, 116–131 (2016)
2. Astrom, K.J., Bell, R.D.: Drum-boiler dynamics. Automatica **36**(3), 363–378 (2000)
3. Chen, C.-T.: Linear System Theory and Design. Oxford University Press, New York (1999)
4. Duderstadt, J.J., Hamilton, L.J.: Nuclear Reactor Analysis. Wiley, New York (1976)
5. Glasstone, S., Sesonske, A.: Nuclear Reactor Engineering. Springer, Heidelberg (1994)
6. Hautus, M.L.J.: Stabilization controllability and observability of linear autonomous systems. Nederl. Akad. Wetensch. Proc. Ser. **73**, 448–455 (1970)
7. Javidnia, H., Jiang, J., Borairi, M.: Modeling and simulation of a CANDU reactor for control system design and analysis. Nucl. Technol. **165**, 174–189 (2009)
8. MATLAB/Simulink Control Design Toolbox User Manual (2012)
9. Munje, R.K., Patre, B.M., Tiwari, A.P.: Nonlinear simulation and control of xenon induced oscillations in advanced heavy water reactor. Ann. Nucl. Energy **64**, 191–200 (2014)
10. Seyed, A.M.S.: The simulation of a model by SIMULINK of MATLAB for determining the best ranges for velocity and delay time of control rod movement in LWR reactors. Prog. Nucl. Energy **54**, 64–67 (2012)

11. Shimjith, S.R., Tiwari, A.P., Bandyopadhyay, B.: Modeling and Control of Large Nuclear Reactor: A Three Time Scale Approach. Lecture Notes in Control and Information Sciences, vol. 431. Springer, Berlin (2013)
12. Shimjith, S.R., Tiwari, A.P., Bandyopadhyay, B.: Coupled neutronics thermal hydraulics model of advanced heavy water reactor for control system studies. Proc. Ann. IEEE India Conf. **1**, 126–131 (2008)
13. Shimjith, S.R., Tiwari, A.P., Bandyopadhyay, B., Patil, R.K.: Spatial stabilization of advanced heavy water reactor. Ann. Nucl. Energy **38**(7), 1545–1558 (2011)
14. Shimjith, S.R., Tiwari, A.P., Naskar, M., Bandyopadhyay, B.: Space-time kinetics modeling of advanced heavy water reactor for control studies. Ann. Nucl. Energy **37**(3), 310–324 (2010)
15. Tiwari, A.P., Bandyopadhyay, B., Govindarajan, G.: Spatial control of large pressurized heavy water reactor. IEEE Trans. Nucl. Sci. **43**, 2440–2453 (1996)
16. Xia, L., Jiang, J., Javidnia, H., Luxat, J.C.: Performance evaluation of 3-D kinetic model of CANDU reactors in a closed-loop environment. Nucl. Eng. Des. **243**, 76–86 (2012)

Chapter 3
State Feedback Control Using Pole Placement

3.1 Introduction

Singularly perturbed systems are the systems that possess small time constants or similar 'parasitic' parameters which usually are neglected in simplified modeling. When those small quantities are taken into consideration, the order of the model is increased and the computation needed for control design can be time-consuming and even ill-conditioned. Singular perturbation methods have been developed for years to address the stability and robustness of those systems. Singularly perturbed systems, more generally multi-time-scale systems, often occur naturally in mathematical models due to the presence of small time constants, masses, large feedback gains, weak coupling [3, 6], etc. It was recognized long ago that the singular perturbations are present in most classical and modern control schemes based on reduced order models, and it led to the development of time-scale methods for a variety of applications including state feedback, output feedback, filter, and observer design [9, 12]. Controllers for the large-scale system are effectively designed by splitting the original system into slow and fast subsystems using singular perturbation techniques [3]. The system decoupling, achieved either by quasi-steady-state method [2] or by direct block diagonalization [4, 6, 7], results in reduction in order. For quite a small perturbation parameter ε, the quasi-steady-state is an efficient technique for decoupling. On the other hand, for systems like nuclear reactor, the perturbation parameter is not zero. Consequently, the eigenvalues of the slow and fast subsystems are no longer in the same position as the eigenvalues of the full-order system, when quasi-steady-state method is used. For that reason, block diagonalization process [6, 7] can be utilized. In this technique, accurate decoupling is accomplished. Control law synthesis for such systems may be carried out for each individual subsystem and then outcomes are merged to get a composite feedback control for the original system. The state feedback control cases are discussed in [1, 7, 8, 11]. In [1]; the technique for singularly perturbed linear system is developed using linear quadratic

R. Munje et al., *Investigation of Spatial Control Strategies with Application to Advanced Heavy Water Reactor*, Energy Systems in Electrical Engineering, https://doi.org/10.1007/978-981-10-3014-7_3

optimal design, in which a cost functional of the subsystems is taken out from the cost functional for the full-order system. Further, it is shown that a composite controller is stabilizing and is near-optimal with the optimal cost. Suzuki [11] has revealed that controllability and stabilizability features of the slow subsystem are invariant about the feedback from fast subsystem. This feature is again investigated in [8]. Furthermore, two-stage eigenvalue placement via two-stage decomposition is presented in [7].

In Chap. 2, mathematical model of Advanced Heavy Water Reactor (AHWR) was discussed and was represented into standard state-space form. Thereafter, nonlinear model was implemented in MATLAB/Simulink by vectorization of modeling equations and control strategy based on feedback of total power and nodal powers in which regulating rods (RRs) are located was presented for spatial control. However, it would be more interesting to investigate the other spatial control strategies for better transient performance and robustness characteristics than those obtained with static output feedback. Also, closed-loop stability is not guaranteed in static output feedback in general [13].

In this chapter, specifically speaking, model of AHWR is represented into the singularly perturbed two-time-scale form. It is then decoupled into a slow subsystem of 73rd order and fast subsystem of 17th order, using the technique presented in [7] and a composite controller is formulated. Contrary to the previous work of [10], in which quasi-steady-state approach was used to get three subsystems, this two-stage decomposition approach offers higher degree of accuracy.

3.2 Singular Perturbation Model

Consider a linear time-invariant controllable and observable continuous-time system of order n, as

$$\dot{\mathbf{z}} = \mathbf{A}\mathbf{z} + \mathbf{B}\mathbf{u}, \tag{3.1}$$

$$\mathbf{y} = \mathbf{M}\mathbf{z}, \tag{3.2}$$

where $\mathbf{z} \in \Re^n$ is the system state, $\mathbf{u} \in \Re^m$ is the control input, and $\mathbf{y} \in \Re^p$ is the system output. The matrices $\mathbf{A}$, $\mathbf{B}$, and $\mathbf{M}$ are constants of appropriate dimensions. Now, the system (3.1)–(3.2) is represented into standard singularly perturbed two-time-scale form as

$$\dot{\mathbf{z}_1} = \mathbf{A}_{11}\mathbf{z}_1 + \mathbf{A}_{12}\mathbf{z}_2 + \mathbf{B}_1\mathbf{u}; \quad \mathbf{z}_1(t_0) = \mathbf{z}_{1_0}, \tag{3.3}$$

$$\varepsilon\dot{\mathbf{z}_2} = \mathbf{A}_{21}\mathbf{z}_1 + \mathbf{A}_{22}\mathbf{z}_2 + \mathbf{B}_2\mathbf{u}; \quad \mathbf{z}_2(t_0) = \mathbf{z}_{2_0}, \tag{3.4}$$

$$\mathbf{y} = \mathbf{M}_1\mathbf{z}_1 + \mathbf{M}_2\mathbf{z}_2, \tag{3.5}$$

where $\mathbf{z}_1 \in \Re^{n_1}$ and $\mathbf{z}_2 \in \Re^{n_2}$ represent states such that $n_1 + n_2 = n$, the matrices $\mathbf{A}_{ij}$, $\mathbf{B}_i$ and $\mathbf{M}_i$ are of suitable dimensionality, and parameter $\varepsilon > 0$ is a scalar denoting the speed ratio of the slow versus fast phenomena. When ε approaches

zero, the solution behaves nonuniformly, producing so-called singularly perturbed stiff problem. The scalar ε represents all the small parameters to be neglected. The parameter ε can be picked up on the basis of knowledge of the process/system and components. Suppose $\varphi(\mathbf{A})$ be the eigenvalues of matrix $\mathbf{A}$ arranged in increasing order of absolute values as

$$\varphi(\mathbf{A}) = \left\{ \varphi_1, \varphi_2, ..., \varphi_{n_1}, \varphi_{n_1+1}, ..., \varphi_n \right\},$$

where

$$0 \leq |\varphi_1| < |\varphi_2| < ... < |\varphi_{n_1}| \ll |\varphi_{n_1+1}| < ... < |\varphi_n|.$$

Thus the system (3.1) has n_1 dominant (slow) modes and n_2 nondominant (fast) modes. The system (3.3)–(3.4) can also be rewritten in the matrix form as

$$\begin{bmatrix} \dot{\mathbf{z}}_1 \\ \dot{\mathbf{z}}_2 \end{bmatrix} = \begin{bmatrix} \mathbf{A}_{11} & \mathbf{A}_{12} \\ \frac{\mathbf{A}_{21}}{\varepsilon} & \frac{\mathbf{A}_{22}}{\varepsilon} \end{bmatrix} \begin{bmatrix} \mathbf{z}_1 \\ \mathbf{z}_2 \end{bmatrix} + \begin{bmatrix} \mathbf{B}_1 \\ \frac{\mathbf{B}_2}{\varepsilon} \end{bmatrix} \mathbf{u} \tag{3.6}$$

and recall that

$$\mathbf{A} = \begin{bmatrix} \mathbf{A}_{11} & \mathbf{A}_{12} \\ \frac{\mathbf{A}_{21}}{\varepsilon} & \frac{\mathbf{A}_{22}}{\varepsilon} \end{bmatrix}, \mathbf{B} = \begin{bmatrix} \mathbf{B}_1 \\ \frac{\mathbf{B}_2}{\varepsilon} \end{bmatrix}, \mathbf{z} = \begin{bmatrix} \mathbf{z}_1 \\ \mathbf{z}_2 \end{bmatrix}. \tag{3.7}$$

3.3 Design of Controller

Design of state feedback controller using eigenvalue placement for singularly perturbed two-time-scale system is done by decoupling higher order system into two lower order subsystems by direct block diagonalization. In doing this, controllability and observability properties of individual subsystems, of an original higher order controllable and observable system, are retained. Thereafter, controllers are designed for individual subsystems and then they are combined to formulate a composite controller.

3.3.1 Two-Stage Decomposition

The main purpose of employing two-stage decomposition technique in obtaining reduced order models is to decouple the nondominant modes from dominant modes. This is achieved by two-stage linear transformation. The first stage includes applying change of variables

$$\begin{bmatrix} \mathbf{z}_1 \\ \mathbf{z}_f \end{bmatrix} = \begin{bmatrix} \mathbf{E}_{n_1} & \mathbf{0} \\ \mathbf{L} & \mathbf{E}_{n_2} \end{bmatrix} \begin{bmatrix} \mathbf{z}_1 \\ \mathbf{z}_2 \end{bmatrix} = \mathbf{T}_1 \begin{bmatrix} \mathbf{z}_1 \\ \mathbf{z}_2 \end{bmatrix} \tag{3.8}$$

to system (3.6). Here $\mathbf{E}_{n_1}$ and $\mathbf{E}_{n_2}$ are, respectively, n_1 and n_2 identity matrices and $(n_2 \times n_1)$ matrix $\mathbf{L}$ satisfies

$$\varepsilon \mathbf{L}\mathbf{A}_{11} + \mathbf{A}_{21} - \varepsilon \mathbf{L}\mathbf{A}_{12}\mathbf{L} - \mathbf{A}_{22}\mathbf{L} = \mathbf{0}. \tag{3.9}$$

Then system (3.6) transforms into

$$\begin{bmatrix} \dot{\mathbf{z}_1} \\ \dot{\mathbf{z}_f} \end{bmatrix} = \begin{bmatrix} \mathbf{A}_s & \mathbf{A}_{12} \\ \mathbf{0} & \frac{\mathbf{A}_f}{\varepsilon} \end{bmatrix} \begin{bmatrix} \mathbf{z}_1 \\ \mathbf{z}_f \end{bmatrix} + \begin{bmatrix} \mathbf{B}_1 \\ \frac{\mathbf{B}_f}{\varepsilon} \end{bmatrix} \mathbf{u}, \tag{3.10}$$

where $\mathbf{A}_s = \mathbf{A}_{11} - \mathbf{A}_{12}\mathbf{L}$, $\mathbf{A}_f = \mathbf{A}_{22} + \varepsilon \mathbf{L}\mathbf{A}_{12}$, and $\mathbf{B}_f = \mathbf{B}_2 + \varepsilon \mathbf{L}\mathbf{B}_1$. If $\mathbf{A}_{22}$ is invertible, unique solution of $\mathbf{L}$ in (3.9) can be determined by iterative procedure. Now the second linear transformation is applied as

$$\begin{bmatrix} \mathbf{z}_s \\ \mathbf{z}_f \end{bmatrix} = \begin{bmatrix} \mathbf{E}_{n_1} & -\varepsilon \mathbf{N} \\ \mathbf{0} & \mathbf{E}_{n_2} \end{bmatrix} \begin{bmatrix} \mathbf{z}_1 \\ \mathbf{z}_f \end{bmatrix} = \mathbf{T}_2 \begin{bmatrix} \mathbf{z}_1 \\ \mathbf{z}_f \end{bmatrix} \tag{3.11}$$

to system (3.10) and choose $(n_1 \times n_2)$ matrix $\mathbf{N}$ such that

$$\mathbf{A}_{12} - \mathbf{N}\mathbf{A}_{22} - \varepsilon \mathbf{N}\mathbf{L}\mathbf{A}_{12} + \varepsilon(\mathbf{A}_{11} - \mathbf{A}_{12}\mathbf{L})\mathbf{N} = \mathbf{0}. \tag{3.12}$$

Then system (3.10) is transformed into

$$\begin{bmatrix} \dot{\mathbf{z}_s} \\ \dot{\mathbf{z}_f} \end{bmatrix} = \begin{bmatrix} \mathbf{A}_s & \mathbf{0} \\ \mathbf{0} & \frac{\mathbf{A}_f}{\varepsilon} \end{bmatrix} \begin{bmatrix} \mathbf{z}_s \\ \mathbf{z}_f \end{bmatrix} + \begin{bmatrix} \mathbf{B}_s \\ \frac{\mathbf{B}_f}{\varepsilon} \end{bmatrix} \mathbf{u}, \tag{3.13}$$

where $\mathbf{B}_s = \mathbf{B}_1 - \mathbf{N}\mathbf{B}_f$. Thus, the system (3.6) is decoupled into separate slow and fast subsystems in (3.13) by the application of two-stage linear transformation from where the slow and fast variables, $\mathbf{z}_s$ and $\mathbf{z}_f$, respectively, can be solved independently. Moreover, the magnitude of the smallest eigenvalue of $\frac{\mathbf{A}_f}{\varepsilon}$ is much larger than the magnitude of the largest eigenvalue of $\mathbf{A}_s$, i.e., $max|\varphi(\mathbf{A}_s)| \ll min|\varphi\left(\frac{\mathbf{A}_f}{\varepsilon}\right)|$. The transformations (3.8) and (3.11) relate the slow and fast variables $\mathbf{z}_s$ and $\mathbf{z}_f$ with the original variables $\mathbf{z}_1$ and $\mathbf{z}_2$ as

$$\mathbf{z}_d = \mathbf{T}\mathbf{z} \tag{3.14}$$

where $\mathbf{z}_d = \begin{bmatrix} \mathbf{z}_s^T & \mathbf{z}_f^T \end{bmatrix}^T$, $\mathbf{z} = \begin{bmatrix} \mathbf{z}_1^T & \mathbf{z}_2^T \end{bmatrix}^T$ and $\mathbf{T} = \mathbf{T}_2\mathbf{T}_1$.

3.3.2 *Design of Composite Controller*

The complete controllability of (3.6) means the same for the individual subsystems in (3.13), i.e., for the pairs $(\mathbf{A}_s, \mathbf{B}_s)$ and $(\mathbf{A}_f, \mathbf{B}_f)$. Now, so as to devise the state

feedback for system (3.6), a two-step process is exercised. The input $\mathbf{u}$ is written as $\mathbf{u} = \mathbf{u}_s + \mathbf{u}_f$. The input $\mathbf{u}_s$ is calculated as

$$\mathbf{u}_s = \begin{bmatrix} \mathbf{K}_s & \mathbf{0} \end{bmatrix} \begin{bmatrix} \mathbf{z}_s \\ \mathbf{z}_f \end{bmatrix}, \tag{3.15}$$

where $\mathbf{K}_s$ is $(m \times n_1)$ feedback matrix to place eigenvalues of $(\mathbf{A}_s + \mathbf{B}_s\mathbf{K}_s)$ at n_1 desired locations. Substituting the value of $\mathbf{u}_s$ from (3.15) into (3.13) yields

$$\begin{bmatrix} \dot{\mathbf{z}_s} \\ \dot{\mathbf{z}_f} \end{bmatrix} = \begin{bmatrix} \mathbf{A}_s + \mathbf{B}_s\mathbf{K}_s & \mathbf{0} \\ \frac{\mathbf{B}_f\mathbf{K}_s}{\varepsilon} & \frac{\mathbf{A}_f}{\varepsilon} \end{bmatrix} \begin{bmatrix} \mathbf{z}_s \\ \mathbf{z}_f \end{bmatrix} + \begin{bmatrix} \mathbf{B}_s \\ \frac{\mathbf{B}_f}{\varepsilon} \end{bmatrix} \mathbf{u}_f. \tag{3.16}$$

Now using transformation

$$\begin{bmatrix} \mathbf{z}_s \\ \mathbf{g}_f \end{bmatrix} = \begin{bmatrix} \mathbf{E}_{n_1} & \mathbf{0} \\ \mathbf{U} & \mathbf{E}_{n_2} \end{bmatrix} \begin{bmatrix} \mathbf{z}_s \\ \mathbf{z}_f \end{bmatrix} = \mathbf{T}_3 \begin{bmatrix} \mathbf{z}_s \\ \mathbf{z}_f \end{bmatrix} \tag{3.17}$$

system (3.16) is changed to

$$\begin{bmatrix} \dot{\mathbf{z}_s} \\ \dot{\mathbf{g}_f} \end{bmatrix} = \begin{bmatrix} \mathbf{A}_s + \mathbf{B}_s\mathbf{K}_s & \mathbf{0} \\ \mathbf{0} & \frac{\mathbf{A}_f}{\varepsilon} \end{bmatrix} \begin{bmatrix} \mathbf{z}_s \\ \mathbf{g}_f \end{bmatrix} + \begin{bmatrix} \mathbf{B}_s \\ \frac{\bar{\mathbf{B}}_f}{\varepsilon} \end{bmatrix} \mathbf{u}_f, \tag{3.18}$$

where $\bar{\mathbf{B}}_f = \mathbf{B}_f + \varepsilon\mathbf{U}\mathbf{B}_s$ and $(n_2 \times n_1)$ matrix $\mathbf{U}$ satisfies

$$\varepsilon\mathbf{U}(\mathbf{A}_s + \mathbf{B}_s\mathbf{K}_s) - \mathbf{A}_f\mathbf{U} + \mathbf{B}_f\mathbf{K}_s = \mathbf{0}. \tag{3.19}$$

As systems (3.16) and (3.18) are related via linear transformation (3.17), pair $(\mathbf{A}_f, \bar{\mathbf{B}}_f)$ is also controllable. Therefore, the second input $\mathbf{u}_f$ is selected as

$$\mathbf{u}_f = \begin{bmatrix} \mathbf{0} & \mathbf{K}_f \end{bmatrix} \begin{bmatrix} \mathbf{z}_s \\ \mathbf{g}_f \end{bmatrix}, \tag{3.20}$$

where $\mathbf{K}_f$ is $(m \times n_2)$ feedback matrix to place eigenvalues of $(\frac{\mathbf{A}_f + \bar{\mathbf{B}}_f\mathbf{K}_f}{\varepsilon})$ at n_2 desired locations. Closed-loop system, obtained after application of $\mathbf{u}_f$ to (3.18), is given by

$$\begin{bmatrix} \dot{\mathbf{z}_s} \\ \dot{\mathbf{g}_f} \end{bmatrix} = \begin{bmatrix} \mathbf{A}_s + \mathbf{B}_s\mathbf{K}_s & \mathbf{B}_s\mathbf{K}_f \\ \mathbf{0} & \frac{\mathbf{A}_f + \bar{\mathbf{B}}_f\mathbf{K}_f}{\varepsilon} \end{bmatrix} \begin{bmatrix} \mathbf{z}_s \\ \mathbf{g}_f \end{bmatrix}. \tag{3.21}$$

Thus, the control input $\mathbf{u} = \mathbf{u}_s + \mathbf{u}_f$ can be expressed as

$$\begin{aligned} \mathbf{u} &= \begin{bmatrix} \mathbf{K}_s & \mathbf{0} \end{bmatrix} \begin{bmatrix} \mathbf{z}_s \\ \mathbf{z}_f \end{bmatrix} + \begin{bmatrix} \mathbf{0} & \mathbf{K}_f \end{bmatrix} \begin{bmatrix} \mathbf{z}_s \\ \mathbf{g}_f \end{bmatrix}, \\ &= \left(\begin{bmatrix} \mathbf{K}_s & \mathbf{0} \end{bmatrix} + \begin{bmatrix} \mathbf{0} & \mathbf{K}_f \end{bmatrix} \mathbf{T}_3 \right) \mathbf{T}\mathbf{z}. \end{aligned} \tag{3.22}$$

Consequently, composite state feedback gain for the system (3.13) is given by

$$\mathbf{K}_d = \begin{bmatrix} \mathbf{K}_s + \mathbf{K}_f \mathbf{U} & \mathbf{K}_f \end{bmatrix}, \tag{3.23}$$

from which state feedback gain matrix for (3.6) is obtained as

$$\mathbf{K} = \mathbf{K}_d \mathbf{T}. \tag{3.24}$$

Applying linear control $\mathbf{u} = \mathbf{K}\mathbf{z}$ to (3.1), one can get closed-loop system as

$$\dot{\mathbf{z}} = (\mathbf{A} + \mathbf{B}\mathbf{K})\mathbf{z} \tag{3.25}$$

which is stable, i.e., $(\mathbf{A} + \mathbf{B}\mathbf{K})$ has all the eigenvalues in the left half of the s-plane.

Lemma 3.1 *If the fast subsystem is asymptotically stable, i.e.,* $\varphi\left(\frac{\mathbf{A}_f}{\varepsilon}\right) < 0$ *then state feedback designed for the slow subsystem alone can stabilize the system (3.6).*

Proof State feedback control designed for the slow subsystem is given by (3.15). Closed-loop system obtained by applying this control to the system (3.13) is given by

$$\begin{bmatrix} \dot{\mathbf{z}_s} \\ \dot{\mathbf{z}_f} \end{bmatrix} = \begin{bmatrix} \mathbf{A}_s + \mathbf{B}_s \mathbf{K}_s & \mathbf{0} \\ \frac{\mathbf{B}_f \mathbf{K}_s}{\varepsilon} & \frac{\mathbf{A}_f}{\varepsilon} \end{bmatrix} \begin{bmatrix} \mathbf{z}_s \\ \mathbf{z}_f \end{bmatrix}. \tag{3.26}$$

As $(\mathbf{A}_s + \mathbf{B}_s \mathbf{K}_s)$ is stable by design and $\frac{\mathbf{A}_f}{\varepsilon}$ is assumed to be stable, system (3.26) is stable. Further, system formulation (3.13) is related to its original form (3.6) via linear transformation (3.14). Therefore, system (3.6) will also be stabilized with state feedback designed for slow subsystem alone.

Remark 3.1 If $\varphi\left(\frac{\mathbf{A}_f}{\varepsilon}\right) < 0$, then one can assume $\mathbf{K}_f = 0$ in (3.23), which yields reduced order approximation to $\mathbf{K}_d$ as $\bar{\mathbf{K}}_d = \begin{bmatrix} \mathbf{K}_s & \mathbf{0} \end{bmatrix}$.

3.4 Application to AHWR System

The model of 920.48 MW Advanced Heavy Water Reactor was discussed in Chap. 2. This complex nonlinear model was linearized around steady-state operating values and represented by (2.20)–(2.21). The same is rewritten here for convenience as

$$\dot{\mathbf{z}} = \mathbf{A}\mathbf{z} + \mathbf{B}\mathbf{u} + \mathbf{B}_{fw}\delta q_{fw}, \tag{3.27}$$

$$\mathbf{y} = \mathbf{M}\mathbf{z}. \tag{3.28}$$

Important characteristics of the model such as stability, controllability, and observability were also investigated. Further, vectorized nonlinear model of AHWR was developed and a spatial control technique based on static output feedback was presented. In this section, eigenvalue placement by state feedback control is examined for AHWR. For that, consider the input $\mathbf{u}$ in (3.27) of the form

$$\mathbf{u} = \mathbf{u}_{gp} + \mathbf{u}_{sp}, \tag{3.29}$$

where $\mathbf{u}_{gp}$ is global (total) power feedback component and $\mathbf{u}_{sp}$ is spatial power feedback component. Total power feedback was discussed in detail in Chap. 2 and it was given by

$$\mathbf{u} = \mathbf{u}_{gp} = -\mathbf{K}_G\mathbf{y} \tag{3.30}$$

where $\mathbf{K}_G$[1] is (4×18) matrix given by $\left[\bar{\mathbf{K}}_T\ \mathbf{0} \cdots \mathbf{0}\right]$ and $\bar{\mathbf{K}}_T = \left[K_T\ K_T\ K_T\ K_T\right]^T$ such that the feedback gain corresponding to total power is K_T for all RRs and is zero corresponding to nodal powers. Using (3.30) the state equation (3.27) becomes

$$\dot{\mathbf{z}} = \hat{\mathbf{A}}\mathbf{z} + \mathbf{B}\mathbf{u}_{sp} + \mathbf{B}_{fw}\delta q_{fw}, \tag{3.31}$$

where $\hat{\mathbf{A}} = \mathbf{A} - \mathbf{B}\mathbf{K}_G\mathbf{M}$ has eigenvalues falling in three different clusters. First cluster of 38 eigenvalues is ranging from 6.2899×10^{-3} to $(8.8268 \pm j1.8656) \times 10^{-5}$, second cluster of 35 eigenvalues ranges from -1.8396×10^{-1} to -1.1779×10^{-2}, and the third one of 17 eigenvalues ranges from -2.7626×10^{2} to -7.2513. This shows that the system of AHWR has 38 slow modes, 35 fast modes, and 17 very fast modes, as depicted in Fig. 3.1. Feedback control design for systems containing interaction of slow, fast, and very fast modes often suffers from ill-conditioning. In singular perturbation approach to feedback control design, the interaction of slow, fast, and very fast phenomena is taken advantage of by decomposing the original ill-conditioned system into lower order subsystems representing the slow, fast, and very fast phenomena. Feedback design may then proceed for each subsystem and results are combined to yield a composite feedback control for original system. Here, state feedback control employing two-stage decomposition is designed for AHWR model. For that, slow and fast modes, represented in Fig. 3.1a and b, respectively, are grouped to form slow subsystem of order 73 and very fast modes, illustrated in Fig. 3.1c, are considered as fast subsystem of order 17.

[1] Notation of total power feedback is changed from $\mathbf{K}$ in (2.48) to $\mathbf{K}_G$, in order to avoid repeatability of symbol.

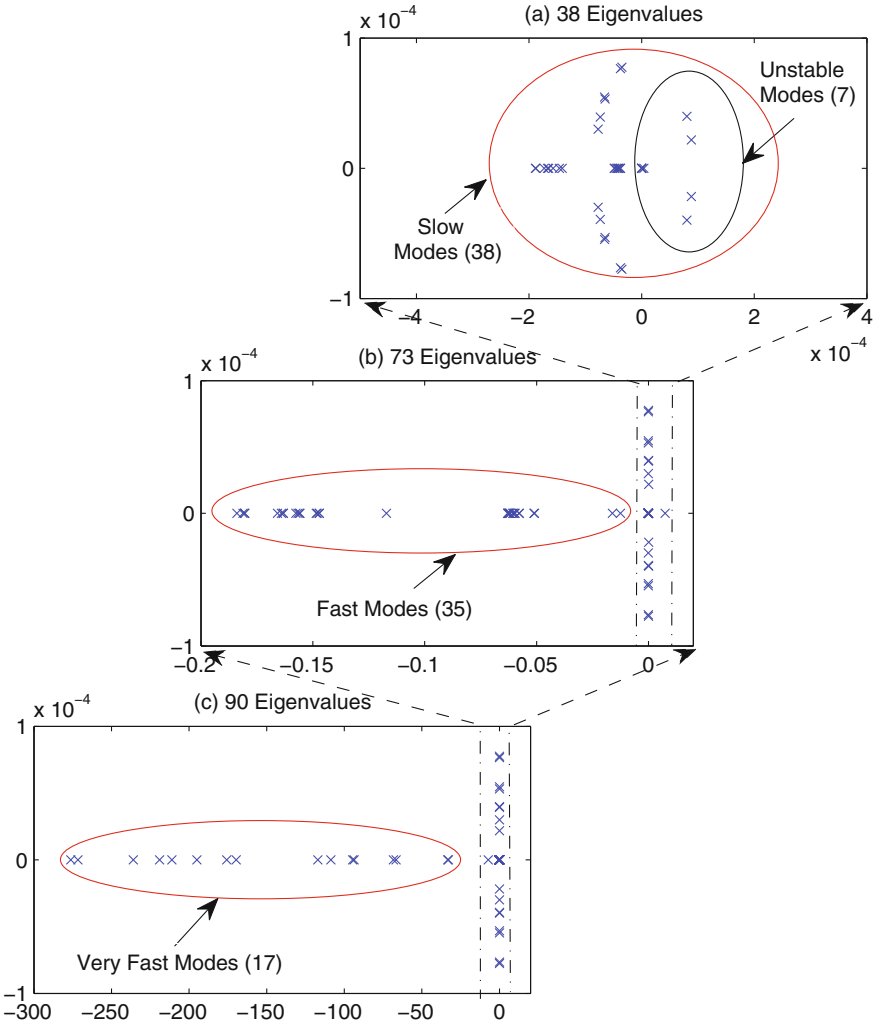

Fig. 3.1 Eigenvalues of $\hat{\mathbf{A}}$ in s-plane: **a** merely those eigenvalues which are very near to imaginary axis, **b** those eigenvalues which are not very far to the left of imaginary axis in addition to those shown in **a**, and **c** all eigenvalues

3.4.1 Singularly Perturbed Form of AHWR Model

In case of AHWR, after linearization of set of equations given by (2.1)–(2.5), (2.10) and (2.11), it is indeed observed that coefficients in the 17 equations for nodal powers, contain ℓ in their denominator. Its value is 3.6694×10^{-4} s. This parameter can be picked up as ε. Therefore, the states of system defined by (2.17) are grouped into slow and fast ones as

$$\mathbf{z}_1 = \left[\, \mathbf{z}_H^T \; \mathbf{z}_X^T \; \mathbf{z}_I^T \; \delta h_d \; \mathbf{z}_C^T \; \mathbf{z}_x^T \,\right]^T , \tag{3.32}$$

$$\mathbf{z}_2 = \mathbf{z}_Q . \tag{3.33}$$

Now, the AHWR model is transformed into standard singularly perturbed two-time-scale form, given by (3.6), where $n_1 = 73$ and $n_2 = 17$. Submatrices $\mathbf{A}_{11}$, $\mathbf{A}_{12}$, $\frac{\mathbf{A}_{21}}{\varepsilon}$, $\frac{\mathbf{A}_{22}}{\varepsilon}$, $\mathbf{B}_1$, and $\frac{\mathbf{B}_2}{\varepsilon}$ are, respectively, of dimensions (73×73), (73×17), (17×73), (17×17), (73×4), and (17×4). This grouping of states also justifies the selection of modes of AHWR system, given in Fig. 3.1, for two-time-scale representation.

3.4.2 Controller Design

Singularly perturbed model of AHWR, discussed in Sect. 3.4.1, is decoupled into slow and fast subsystems of orders 73 and 17, respectively, by using the procedure described in Sect. 3.3.1. In this case, compared to quasi-steady-state method, exact decoupling of subsystems into slow and fast is achieved. This is evident from slow subsystem eigenvalues, given in Table 3.1, in which the unstable eigenvalues are shown highlighted. Here unstable eigenvalues 1–3 are zero which are exactly same as those of original system matrix $\hat{\mathbf{A}}$. Further, from Table 3.2 it can be observed that the eigenvalues of fast subsystem are asymptotically stable, i.e., $\varphi\left(\frac{\mathbf{A}_f}{\varepsilon}\right) < 0$. Hence, composite control law can be constructed using the slow subsystem alone, as proved in Lemma 3.1 and Remark 3.1. For that, the state feedback gain matrix $\mathbf{K}_s$ is obtained for the slow subsystem, so as to place slow subsystem eigenvalues between -4.5×10^{-6} and -1.9×10^{-1}. The state feedback gain matrix $\mathbf{K}_s$ is given by

$$\mathbf{K}_s = \begin{bmatrix} 1.4607 & 0.0328 & 0.0267 & 0.0321 & 6.4861 & 57.8428 & -13.0624 & 2.1041 & 0.3645 \\ 0.0328 & 1.4634 & 0.0321 & 0.0299 & 3.0597 & 1.7011 & -15.6783 & 57.2228 & -31.1424 \\ 0.0267 & 0.0321 & 1.4607 & 0.0328 & 6.4861 & 1.3260 & 1.5459 & 1.9882 & -18.6444 \\ 0.0321 & 0.0299 & 0.0328 & 1.4634 & 3.0597 & 1.6699 & 0.3899 & 1.5436 & -1.3853 \end{bmatrix}$$

$$\begin{matrix} 1.3260 & 1.5459 & 1.9882 & -18.6444 & -31.1100 & -26.8332 & 0.7897 & -0.3391 & 0.2953 \\ 1.6699 & 0.3899 & 1.5436 & -1.3853 & -1.6230 & -28.1566 & -40.1151 & -27.9088 & -5.5588 \\ 57.8428 & -13.0624 & 2.1041 & 0.3645 & 0.2953 & 0.7270 & -1.3270 & -26.9278 & -31.1100 \\ 1.7011 & -15.6783 & 57.2228 & -31.1424 & -5.5588 & -0.1955 & 0.7869 & -1.8258 & -1.6230 \end{matrix}$$

$$\begin{matrix} 0.7270 & -1.3270 & -26.9278 & -3.0499 & 0.9599 & -7.3877 & -0.2164 & 0.0736 & -0.0198 \\ -0.1955 & 0.7869 & -1.8258 & -4.2472 & -0.1843 & -9.5829 & 0.9768 & -11.5154 & -0.1619 \\ -26.8332 & 0.7897 & -0.3391 & -3.0499 & -0.0198 & -0.0538 & -0.1929 & -6.6967 & 0.9599 \\ -28.1566 & -40.1151 & -27.9088 & -4.2472 & -0.1619 & -0.26526 & -0.0442 & -0.2186 & -0.1843 \end{matrix}$$

$$\begin{matrix} -0.0538 & -0.1929 & -6.6967 & -13.5515 & -6.7902 & 0.0250 & 0.0973 & 0.0310 & 0.0159 \\ -0.2652 & -0.0442 & -0.2186 & -0.2721 & -5.2128 & -21.8045 & -4.4168 & -0.6406 & -0.1009 \\ -7.3877 & -0.2164 & 0.0736 & 0.0310 & 0.0159 & -0.5022 & -4.2451 & -13.5515 & -6.7902 \\ -9.5829 & 0.9768 & -11.5154 & -0.6406 & -0.1009 & -0.0208 & -0.0373 & -0.2721 & -5.2128 \end{matrix}$$

$$
\begin{bmatrix}
-0.5022 & -4.2451 & -0.0492 & -1.9240 & -1.7899 & -1.3715 & -0.9872 & -0.7566 & -0.7035 \\
-0.0208 & -0.0373 & -0.0491 & -2.0298 & -0.9759 & -1.4135 & -1.8874 & -1.3658 & -0.9419 \\
0.0250 & 0.0973 & -0.0492 & -1.9240 & -0.7035 & -0.8069 & -0.9528 & -1.2057 & -1.7899 \\
-21.8045 & -4.4168 & -0.0491 & -2.0298 & -0.9419 & -0.8622 & -0.8152 & -0.7881 & -0.9759
\end{bmatrix}
$$

$$
\begin{bmatrix}
-0.8069 & -0.9528 & -1.2057 & -1.2583 & -1.2295 & -0.7882 & -0.5017 & -0.4749 & -0.6426 \\
-0.8622 & -0.8152 & -0.7881 & -0.6495 & -1.1594 & -1.5988 & -0.9468 & -0.7073 & -0.7093 \\
-1.3715 & -0.9872 & -0.7566 & -0.4749 & -0.6426 & -0.8145 & -0.9545 & -1.2583 & -1.2295 \\
-1.4135 & -1.8874 & -1.3658 & -0.7073 & -0.7093 & -0.6557 & -0.5517 & -0.6495 & -1.1594
\end{bmatrix}
$$

$$
\begin{bmatrix}
-0.8145 & -0.9545 & -0.0019 & -2.5479 & -0.3134 & 0.0693 & 0.0041 & 0.0107 & 0.0134 & 0.0603 \\
-0.6557 & -0.5517 & -0.0511 & -0.0064 & -0.4038 & -2.4207 & -0.5067 & 0.0037 & -0.0010 & 0.0157 \\
-0.7882 & -0.5017 & -0.0019 & 0.0107 & 0.0134 & 0.0603 & -0.3248 & -2.5479 & -0.3134 & 0.0693 \\
-1.5988 & -0.9468 & -0.0511 & 0.0037 & -0.0010 & 0.0157 & -0.0149 & -0.0064 & -0.4038 & -2.4207
\end{bmatrix}
$$

$$
\begin{bmatrix}
-0.3248 & -0.6753 & -0.3514 & 0.0131 & -0.0019 & 0.0026 & 0.0056 & -0.0084 & -0.2686 \\
-0.0149 & -0.0172 & -0.2778 & -0.9070 & -0.2751 & -0.0491 & -0.0026 & 0.0061 & -0.0150 \\
0.0041 & 0.0026 & 0.0056 & -0.0084 & -0.2686 & -0.6753 & -0.3514 & 0.0131 & -0.0019 \\
-0.5067 & -0.0491 & -0.0026 & 0.0061 & -0.0150 & -0.0172 & -0.2778 & -0.9070 & -0.2751
\end{bmatrix}. \tag{3.34}
$$

No state feedback is designed for fast subsystem; hence, these eigenvalues are left unaltered. However, for controller implementation, reduced order approximation of $\mathbf{K}_d$, designed for decoupled system (3.13), is represented into original states using relation (3.24). This is the feedback gain for original system (3.6). Hence, it should be noted that, although composite controller is obtained from slow subsystem alone, feedback of all the states is required for implementation purpose. Desired closed-loop eigenvalue locations are selected such that the system is stable as well as the closed-loop system maintains two-time-scale structure. Closed-loop eigenvalues of the system with composite control law are given in Table 3.3 [5].

3.4.3 Transient Simulations

The closed-loop response of the system with a composite controller is assessed by nonlinear simulations using a vectorized AHWR model. The component in the RR control signals corresponding to the total power feedback was generated and applied in each time step. The spatial control component using a composite controller was generated and superimposed on the total power control signal. The system was initially assumed to be at full power steady-state condition, with all RRs at their equilibrium positions. RR2, which was originally under automatic control, was suddenly moved out by around 1% by giving appropriate manual control signal after 2 s. Subsequently, it is left on automatic control as shown in Fig. 3.2. All other RRs (RR4, RR6, and RR8) moved in under the influence of the controller so as to bring the total reactor power at steady-state value back. Following the time period during which the manual control signal was imposed on RR2, all RRs were being moved by the controller to their initial steady-state positions in 120 s. However, the response was observed to be underdamped. Variations in spatial power measured in terms of first

Table 3.1 Eigenvalues of slow subsystem ($\mathbf{A}_s$) obtained by two-stage decomposition

Sr. No.	Eigenvalues	Sr. No.	Eigenvalues	Sr. No.	Eigenvalues
1–3	0	33	-1.5717×10^{-4}	54	-6.2608×10^{-2}
4	-2.6799×10^{-5}	34	-1.6524×10^{-4}	55	-6.2865×10^{-2}
5	-3.7781×10^{-5}	35	-1.6653×10^{-4}	56	-6.2893×10^{-1}
6	-3.7993×10^{-5}	36	-1.7308×10^{-4}	57	-1.1715×10^{-1}
7	-4.0124×10^{-5}	37	-1.8807×10^{-4}	58	-1.4712×10^{-1}
8	-4.152×10^{-5}	38	-1.8870×10^{-2}	59	-1.4713×10^{-1}
9	-4.2044×10^{-5}	39	-5.2501×10^{-2}	60	-1.4809×10^{-1}
10	-4.4204×10^{-5}	40	-1.5867×10^{-2}	61	-1.485×10^{-1}
11	-4.7371×10^{-5}	41	-5.0954×10^{-2}	62	-1.5580×10^{-1}
12	-4.8866×10^{-5}	42	-5.1159×10^{-2}	63	-1.5585×10^{-1}
13–14	$(-7.7407 \pm j2.9929) \times 10^{-5}$	43	-5.773×10^{-2}	64	-1.5662×10^{-1}
15–16	$(-7.3359 \pm j3.9319) \times 10^{-5}$	44	-5.7893×10^{-2}	65	-1.5585×10^{-1}
17–18	$(-6.5952 \pm j5.4785) \times 10^{-5}$	45	-5.9707×10^{-2}	66	-1.5662×10^{-1}
19–20	$(-6.4855 \pm j5.3109) \times 10^{-5}$	46	-5.9723×10^{-2}	67	-1.5761×10^{-1}
21–22	$(-3.9003 \pm j8.9009) \times 10^{-5}$	47	-6.0344×10^{-2}	68	-1.6325×10^{-1}
23–24	$(-3.7785 \pm j7.6475) \times 10^{-5}$	48	-6.0642×10^{-2}	69	-1.6405×10^{-1}
25–26	$(-3.5380 \pm j7.7343) \times 10^{-5}$	49	-6.1848×10^{-2}	70	-1.8037×10^{-1}
27–28	$(8.8268 \pm j2.1800) \times 10^{-5}$	50	-6.1942×10^{-2}	71	-1.8049×10^{-1}
29–30	$(8.0470 \pm j3.9864) \times 10^{-5}$	51	-6.22×10^{-2}	72	-1.8122×10^{-1}
31	-1.4107×10^{-4}	52	-6.238×10^{-2}	73	-1.8402×10^{-1}
32	-1.4532×10^{-4}	53	-6.2458×10^{-2}		

Table 3.2 Eigenvalues of fast subsystem ($\mathbf{A}_f$) obtained by two-stage decomposition

Sr. No.	Eigenvalues	Sr. No.	Eigenvalues
1	-7.2484	10	-1.6967×10^{2}
2	-3.2844×10^{1}	11	-1.7568×10^{2}
3	-3.3372×10^{1}	12	-1.9497×10^{2}
4	-6.6599×10^{1}	13	-2.111×10^{2}
5	-6.8323×10^{1}	14	-2.1904×10^{2}
6	-9.3653×10^{1}	15	-2.3591×10^{2}
7	-9.4612×10^{1}	16	-2.7163×10^{2}
8	-1.0868×10^{2}	17	-2.7626×10^{2}
9	-1.1705×10^{2}		

Table 3.3 Closed-loop eigenvalues of the AHWR model

Sr. No.	Eigenvalues	Sr. No.	Eigenvalues	Sr. No.	Eigenvalues
1	-4.5625×10^{-6}	36	-7.9531×10^{-3}	64	-1.5662×10^{-1}
2–3	$(-3.5399 \pm j\ 7.7474) \times 10^{-5}$	37	-7.9591×10^{-3}	65	-1.5761×10^{-1}
4	-3.7779×10^{-5}	38–39	$(-9.7370 \pm j\ 0.11351) \times 10^{-3}$	66	-1.6316×10^{-1}
5	-3.7991×10^{-5}	40	-1.5769×10^{-2}	67	-1.6324×10^{-1}
6–7	$(-3.8092 \pm j7.6314) \times 10^{-5}$	41	-5.0952×10^{-2}	68	-1.6405×10^{-1}
8–9	$(-6.4915 \pm j5.2981) \times 10^{-5}$	42	-5.1157×10^{-2}	69	-1.6579×10^{-1}
10–11	$(-6.5894 \pm j5.4694) \times 10^{-5}$	43	-5.7730×10^{-2}	70	-1.8037×10^{-1}
12–13	$(-7.3379 \pm j3.9266) \times 10^{-5}$	44	-5.7892×10^{-2}	71	-1.8049×10^{-1}
14–15	$(-7.7423 \pm j2.9886) \times 10^{-5}$	45	-5.9707×10^{-2}	72	-1.8122×10^{-1}
16–17	$(-8.1067 \pm j3.8606) \times 10^{-5}$	46	-5.9723×10^{-2}	73	-1.8401×10^{-1}
18–19	$(-8.8817 \pm j1.8965) \times 10^{-5}$	47	-6.0344×10^{-2}	74	-7.2484
20	-4.0122×10^{-5}	48	-6.0642×10^{-2}	75	-3.2844×10^{1}
21	-4.1518×10^{-5}	49	-6.1848×10^{-2}	76	-3.3372×10^{1}
22	-4.2241×10^{-5}	50	-6.1942×10^{-2}	77	-6.6599×10^{1}
23	-4.4224×10^{-5}	51	-6.2200×10^{-2}	78	-6.8323×10^{1}
24	-4.7464×10^{-5}	52	-6.2380×10^{-2}	79	-9.3653×10^{1}
25	-4.8903×10^{-5}	53	-6.2458×10^{-2}	80	-9.4612×10^{1}
26	-1.4098×10^{-4}	54	-6.2608×10^{-2}	81	-1.0868×10^{2}
27	-1.4626×10^{-4}	55	-6.2865×10^{-2}	82	-1.1705×10^{2}
28	-1.5720×10^{-4}	56	-6.2893×10^{-2}	83	-1.6967×10^{2}
29	-1.6526×10^{-4}	57	-1.1715×10^{-1}	84	-1.7568×10^{2}
30	-1.6722×10^{-4}	58	-1.4712×10^{-1}	85	-1.9497×10^{2}
31	-1.7311×10^{-4}	59	-1.4713×10^{-1}	86	-2.1110×10^{2}
32	-1.8809×10^{-4}	60	-1.4809×10^{-1}	87	-2.1904×10^{2}
33	-1.8871×10^{-4}	61	-1.4850×10^{-1}	88	-2.3591×10^{2}
34	-3.3851×10^{-3}	62	-1.5580×10^{-1}	89	-2.7163×10^{2}
35	-7.9331×10^{-3}	63	-1.5585×10^{-1}	90	-2.7626×10^{2}

and second azimuthal tilts, and total power are, respectively, shown in Figs. 3.3 and 3.4. The azimuthal tilts were also observed to be oscillatory in nature with decreasing amplitude and completely suppressed after 120 s. First and second azimuthal tilts attended steady-state value after approximately 10 and 5 cycles of oscillation, whereas no significant oscillations were observed in total power.

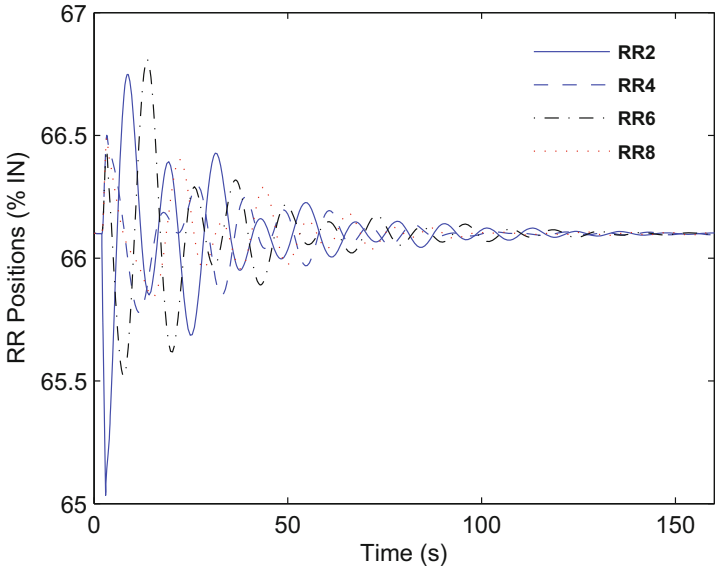

Fig. 3.2 Variations in RR positions subsequent to withdrawal of RR2

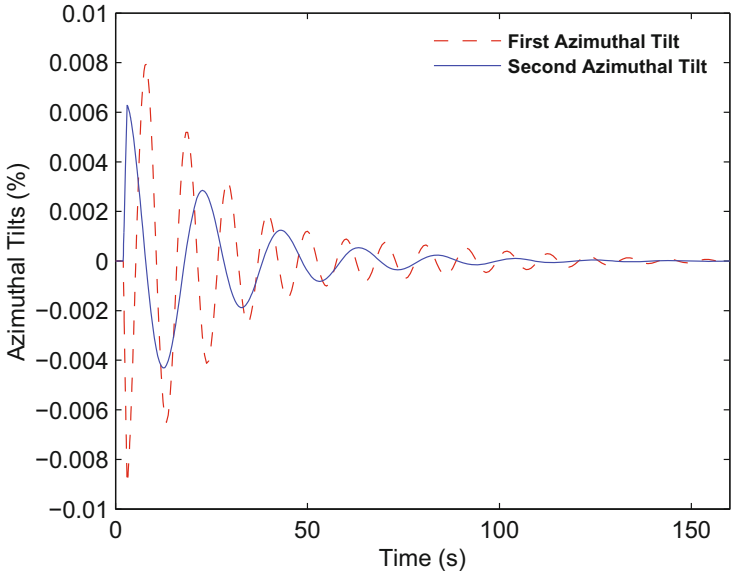

Fig. 3.3 Variations in azimuthal tilts subsequent to withdrawal of RR2

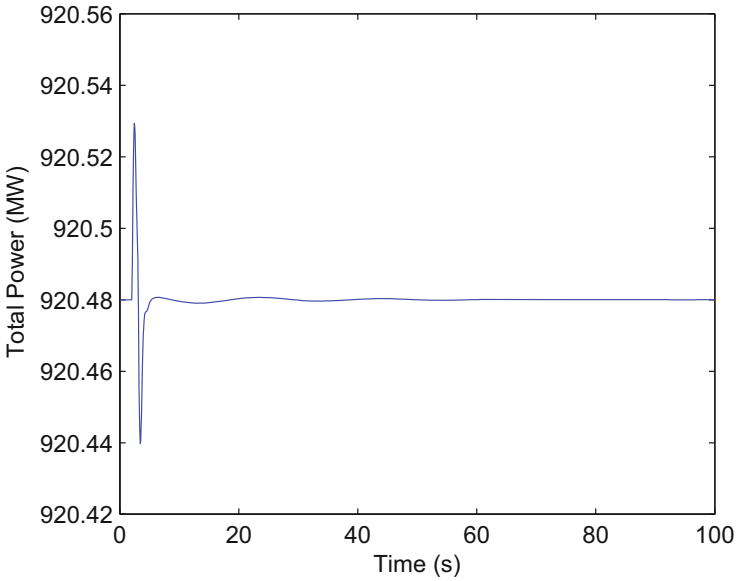

Fig. 3.4 Variations in total power subsequent to withdrawal of RR2

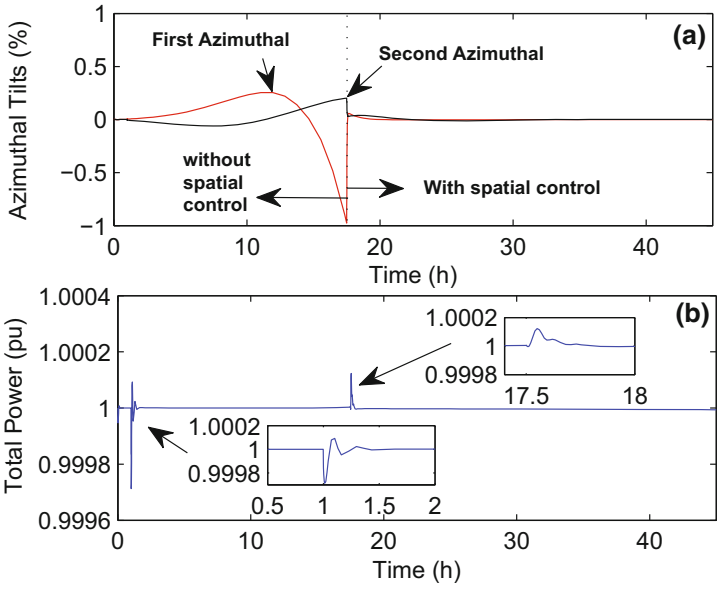

Fig. 3.5 Effect of spatial power feedback: **a** Variations in azimuthal tilts with and without spatial control and **b** Corresponding variations in total power

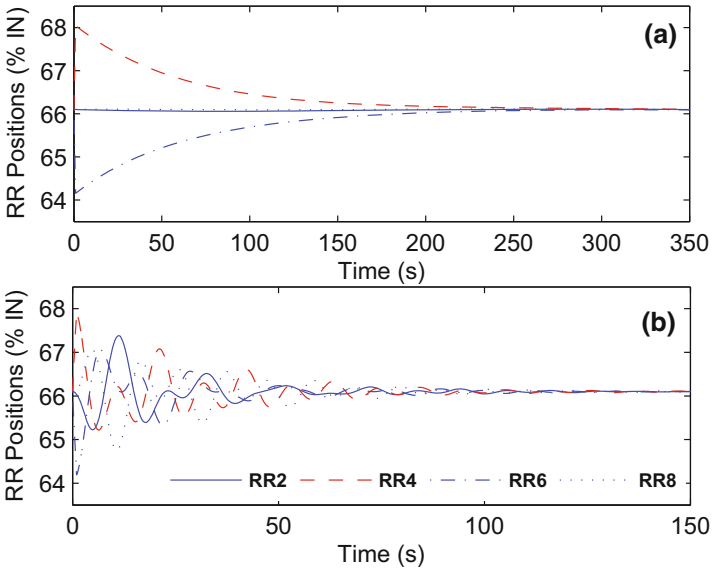

Fig. 3.6 Comparison of controllers: **a** Response due to three-time-scale approach [10] and **b** Response due to two-stage decomposition

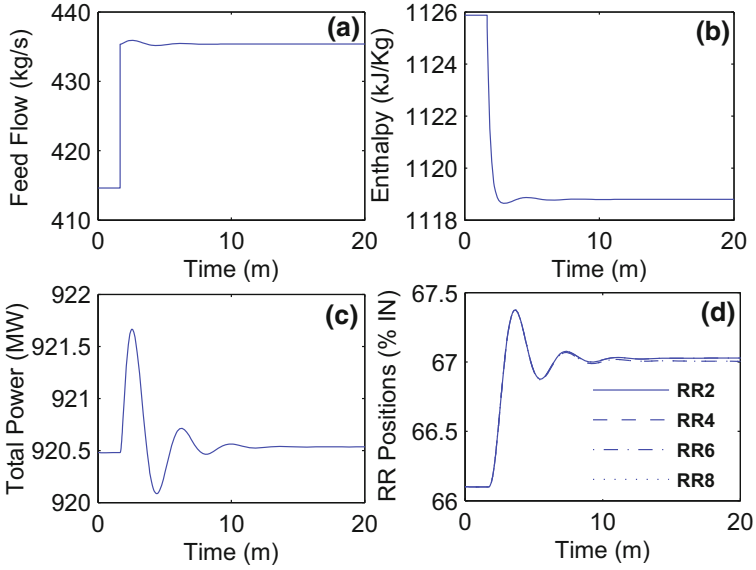

Fig. 3.7 Response due to change in the feed flow: **a** 5 % positive step change in feed flow, **b** Downcomer enthalpy, **c** Total power and **d** RR positions

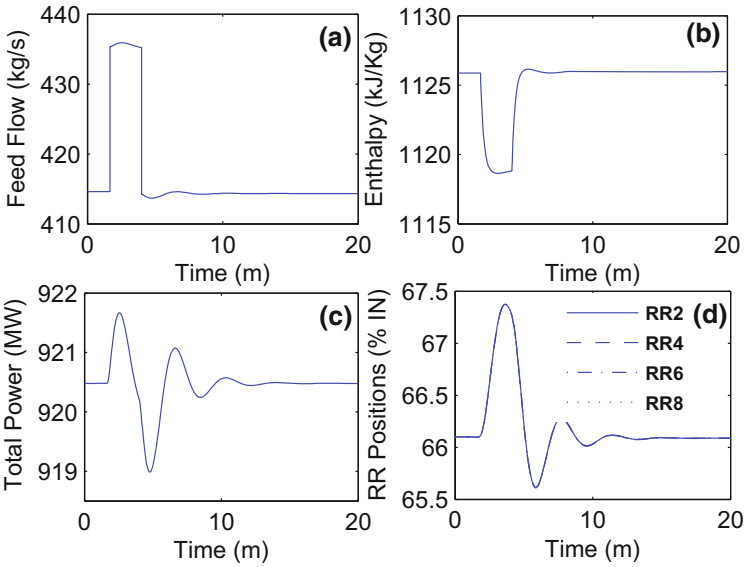

Fig. 3.8 Response due to temporary change in the feed flow: **a** Change in feed flow, **b** Downcomer enthalpy, **c** Total power and **d** RR positions

Closed-loop response of the AHWR system in one more transient, generated by the abrupt disturbance in the position of RR2, is shown in Fig. 3.5. It was observed that the reactor was originally working at full power steady state with the control obtained only by total power feedback. The RR2, which was originally at its equilibrium state, was moved in by 1.5% and at once moved out to its earlier position. As a result of this disturbance, it was noticed that the first and second azimuthal tilts started picking up as illustrated in Fig. 3.5a. The spatial power control signal was introduced in the existing control signal after about 17.5 h. As a result, magnitudes of the tilts are reduced in about 5 min and are completely controlled in 1.5 h. The tilts stay suppressed afterward during the remaining extended simulation. Figure 3.5b depicts the variations in the total power. It shows variation only at the time of initiation of transient and introduction of spatial power component. Total power remains steady at other time instants.

Furthermore, the performance of suggested controller is compared with the controller presented in [10]. In this, positions of two RRs are simultaneously changed by giving suitable manual control signal. RR6 was moved out and RR4 was moved in by 2%. Instantaneously after that RRs were moved back to their earlier positions. Simulation results are obtained for variations in control rod positions for both the controllers using the nonlinear model of AHWR as shown in Fig. 3.6. It is noticed that, with both the controllers, RRs are moved back to their steady-state positions but time needed to do so is significantly less in the presented controller.

So as to evaluate the reaction of the AHWR system to disturbance in feed flow, the nonlinear model was again simulated when 5% positive step change was initiated in the feed flow as depicted in Fig. 3.7a. As a consequence of this, the incoming coolant enthalpy decreased by about 0.64% (Fig. 3.7b). The total power was observed to be stabilizing at its steady-state value due to the controller action (Fig. 3.7c). Nevertheless, RRs are moved in by 0.9% (Fig. 3.7d). For the short-term disturbance in feed flow the total power is found to be stabilizing back at their initial value and RRs also came back to their steady positions as shown in Fig. 3.8.

3.5 Conclusion

In this chapter, using two-stage decomposition, model of advanced heavy water reactor is decoupled into slow and fast subsystems of orders 73 and 17, respectively. Out of the two subsystems, fast subsystem is found to be asymptotically stable. Hence, stabilizing state feedback control is designed only for slow subsystem. It is then represented into original states by linear transformation and composite state feedback control for full-order system is derived. This composite controller is found to be stabilizing the linear AHWR system. It is then applied to the nonlinear model of AHWR system to test the performance under various transient conditions. From the simulation results, it is noticed that the response of controller under representative transients is satisfactory. It is also compared with the three-time-scale controller to show the effectiveness.

References

1. Chow, J.H., Kokotovic, P.V.: A decomposition of near-optimum regulators for systems with slow and fast modes. IEEE Trans. Autom. Ctrl. **21**(5), 701–705 (1976)
2. Gajic, Z., Lim, M.-T.: Optimal Control of Singularly Perturbed Linear Systems and Applications: High Accuracy Techniques. Marcel Dekker, New York (2001)
3. Kokotovic, P.V., O'Malley, R.E., Sannuti, P.: Singular perturbation and order reduction in control theory-an overview. Automatica **12**, 123–132 (1976)
4. Ladde, G.S., Siljak, D.D.: Multiparameter singular perturbations of linear systems with multiple time scales. Automatica **19**, 385–394 (1983)
5. Munje, R.K., Parkhe, J.G., Patre, B.M.: Spatial control of advanced heavy water reactor via two stage decomposition. Ann. Nucl. Energy **77**, 326–334 (2015)
6. Naidu, D.S.: Singular Perturbation Methodology in Control Systems. Peter Peregrinus Ltd., London (1988)
7. Phillips, R.G.: A two-stage design of linear feedback controls. IEEE Trans. Autom. Control **25**, 1220–1223 (1980)
8. Saberi, A., Khalil, H.: Stabilization and regulation of nonlinear singularly perturbed systems-composite control. IEEE Trans. Autom. Control **30**, 739–747 (1985)
9. Saksena, V.R., O'Reilly, J., Kokotovic, P.V.: Singular perturbation and time-scale methods in control theory: survey 1976–1983. Automatica **20**, 273–293 (1984)

10. Shimjith, S.R., Tiwari, A.P., Bandyopadhyay, B.: A three-time-scale approach for design of linear state regulator for spatial control of advanced heavy water reactor. IEEE Trans. Nucl. Sci. **58**(3), 1264–1276 (2011)
11. Suzuki, M.: Composite controls for singularly perturbed systems. IEEE Trans. Autom. Control **26**, 505–507 (1981)
12. Syrcos, G., Sannuti, P.: Singular perturbation modeling of continuous and discrete physical systems. Int. J. Control **37**, 1007–1022 (1983)
13. Syrmos, V.L., Abdallah, C.T., Dorato, P., Grigoriadis, K.: Static output feedback-a survey. Automatica **33**, 125–137 (1997)

Chapter 4
State Feedback Control Using Linear Quadratic Regulator

4.1 Introduction

Higher order and interacting dynamics of widely different speeds complicate the analysis and control of large-scale systems. These types of systems are comprehensively studied by singular perturbations and time-scale methods. Over the period of time, excellent overviews and surveys have been published for the periods up to 1976 [7], 1976–1983 [14], 1984–2001 [11] and 2002–2012 [21]. Survey on modeling of physical systems using singular perturbation and time-scale is also documented in [19]. Singular perturbation approach has proven to be an effective tool for control design.

Singular perturbation methods are also useful for model order reduction. The order reduction procedure and its validation for both linear and nonlinear systems can be found in [7]. The approach makes use of the standard singularly perturbed form representation of dynamic systems in which the derivatives of some state variables are multiplied with a small positive scalar, ε. Recall that this type of representation was discussed in Chap. 3 in context to two-time-scale explicit decomposition. Here, the model reduction is achieved by setting $\varepsilon = 0$ and substituting the solution of states, whose derivatives are multiplied with ε, in terms of the other state variables [6]. In application, models of physical systems are put in the standard singularly perturbed form by expressing small time constants, small masses, large gains, etc., in terms of ε. In power system models ε can represent machine reactance or transients in voltage regulators, in industrial control systems it may represent time constants of drives and actuators, and in nuclear reactor models it is due to prompt neutrons.

The two-time-scale behavior of singularly perturbed systems suggests that a transformation may separate the slow and fast subsystems. Such a transformation for linear systems is constructed by Chang [1]. Optimal control of nonlinear as well as linear singularly perturbed systems is extensively studied in the control literature and the most actively investigated optimal control problem in the case of singularly perturbed systems is the linear quadratic regulator (LQR) problem. A key point in studying the

R. Munje et al., *Investigation of Spatial Control Strategies with Application to Advanced Heavy Water Reactor*, Energy Systems in Electrical Engineering, https://doi.org/10.1007/978-981-10-3014-7_4

asymptotic behavior of the Riccati equation, as $\varepsilon \to 0$, is seeking the solution of a particular form,

$$\mathbf{S} = \begin{bmatrix} \mathbf{S}_{11} & \varepsilon \mathbf{S}_{12} \\ \varepsilon \mathbf{S}_{12}^T & \varepsilon \mathbf{S}_{22} \end{bmatrix}, \tag{4.1}$$

which was first done by Sannuti and Kokotovic [15]. With this, the Riccati equation for the full singularly perturbed system is partitioned into three equations, which are solved independently. Such a formulation results into the decomposition of the original higher order problem into two lower order problems. Feedback designs for systems containing interaction of slow and fast phenomena often suffer from ill-conditioning. In the singular perturbation approach to feedback design, the interaction of slow and fast phenomena is taken advantage of by decomposing the original ill-conditioned system into two lower order subsystems. Design of feedback controller may then proceed for each subsystem independently and the results are combined to yield a composite feedback control for the original system. The design procedure usually starts by neglecting the fast dynamics, equivalently setting $\varepsilon = 0$, to get the slow subsystem model. A state feedback control is designed such that the closed-loop slow subsystem is stable and meets other design criteria. Next, with the slow subsystem state fixed at the equilibrium point, a control is designed for the fast subsystem such that the closed-loop fast subsystem is stable and meets other design criteria. Finally, the composite control for the original system is obtained as the sum of the slow and fast subsystem state feedback controllers. Several papers justify this design approach for various cases. The advantages of this method are not limited to the computational ones. The method, in fact, provides a systematic approach for designing a feedback control strategy that matches the time-scale configuration of the open-loop system, which if executed properly can lead to better designs and/or efficient implementations. In many control problems, the design criteria for the slow dynamics of a system are more strict than those for the fast dynamics; on the other hand, fast dynamics are less accurately modeled than the slow dynamics. Decomposing the design problem, into subproblems for slow and fast subsystems, provides the designer with the opportunity of making different compromises for the slow and fast parts of a system depending upon the design criteria and model inaccuracies for each part. On the implementation side, it is seen that the design procedure leads naturally to a hierarchical structure which could be very efficient when factors like cost of communication and multirate sampling are taken into consideration. The cases of state feedback are treated in [3, 5, 10, 12, 13, 16, 18]. In [3], conditions are formulated for exact separation of slow and fast subsystem regulator designs and a near-optimum state regulator combining two subsystem regulator, is developed. Suzuki [18] has proved that controllability and stabilizability properties of the slow subsystem are invariant with respect to the feedback from fast subsystem state variables. This property is again investigated in [13]. Furthermore, in [17], a two-stage design procedure of the two-time-scale system to decompose the original higher order system into three subsystems is considered. Another technique of direct decoupling of a higher order multi-time-scale singularly perturbed linear system with multiparameters is given by

Ladde et al. [8]. Also, they formulated a threefold version of Chang's transformation [2]. However, the study is restricted only to autonomous systems, i.e., aspects of controller design are not discussed. Comparable results in three-time-scale decomposition of autonomous systems, with more extensive mathematical background, can also be found in [4]. As an extension, simultaneous decomposition of a nonautonomous singularly perturbed system into three subsystems is described in [16]. In addition to this, composite controller design in terms of the individual subsystem controllers is obtained and the decomposition of the optimal control problem of the original system into three lower order optimal control problems is explained.

Preceding chapters were devoted to modeling of Advanced Heavy Water Reactor (AHWR), output feedback design, and state feedback design using pole placement. In this chapter, again the controller obtained is based on state feedback; however, the design approach is LQR. AHWR model is decoupled into slow and fast subsystems by quasi-steady-state method and separate linear regulators are designed for subsystems. Finally they are combined to construct composite control law.

4.2 Linear Quadratic Regulator Design for Two-Time-Scale System

For brevity let us rewrite the general linear time-invariant controllable and observable two-time-scale system (3.3)–(3.5) of order n, as

$$\dot{\mathbf{z}_1} = \mathbf{A}_{11}\mathbf{z}_1 + \mathbf{A}_{12}\mathbf{z}_2 + \mathbf{B}_1\mathbf{u}; \quad \mathbf{z}_1(t_0) = \mathbf{z}_{1_0}, \tag{4.2}$$

$$\varepsilon\dot{\mathbf{z}_2} = \mathbf{A}_{21}\mathbf{z}_1 + \mathbf{A}_{22}\mathbf{z}_2 + \mathbf{B}_2\mathbf{u}; \quad \mathbf{z}_2(t_0) = \mathbf{z}_{2_0}, \tag{4.3}$$

$$\mathbf{y} = \mathbf{M}_1\mathbf{z}_1 + \mathbf{M}_2\mathbf{z}_2, \tag{4.4}$$

where $\mathbf{z}_1 \in \Re^{n_1}$ and $\mathbf{z}_2 \in \Re^{n_2}$ denote states such that $n_1 + n_2 = n$, the matrices $\mathbf{A}_{ij}$, $\mathbf{B}_i$, and $\mathbf{M}_i$ are of appropriate dimensions, and parameter $\varepsilon > 0$ is perturbation parameter. It must be noted that the system is having n_1 slow and n_2 fast modes.

Among the slow and fast modes in the system given by (4.2)–(4.4), the fast modes are important only during a short initial period. After that period they are negligible and the behavior of the system can be described by its slow modes. The model with the fast modes neglected is called quasi-steady-state model [3]. Neglecting fast modes is equivalent to assuming that they are infinitely fast, i.e., letting $\varepsilon \to 0$ in (4.2)–(4.3). When $\varepsilon = 0$, the order of the system in (4.2)–(4.3) reduces from $(n_1 + n_2)$ to n_1, because the differential equation (4.3) degenerates into algebraic equation

$$\mathbf{0} = \mathbf{A}_{21}\bar{\mathbf{z}}_1 + \mathbf{A}_{22}\bar{\mathbf{z}}_2 + \mathbf{B}_2\bar{\mathbf{u}}, \tag{4.5}$$

where the bar is used to indicate that the variables belong to a system with $\varepsilon = 0$. The model (4.2)–(4.3) is in standard form if and only if (4.5) has a unique solution or a finite number of distinct solutions in the domain of interest. If $\mathbf{A}_{22}^{-1}$ exists, then

the solution $\bar{\mathbf{z}}_2$ is obtained as

$$\bar{\mathbf{z}}_2 = -\mathbf{A}_{22}^{-1}\mathbf{A}_{21}\bar{\mathbf{z}}_1 - \mathbf{A}_{22}^{-1}\mathbf{B}_2\bar{\mathbf{u}}. \tag{4.6}$$

Substituting the solution of $\bar{\mathbf{z}}_2$ from (4.6) in (4.2) and (4.4), slow subsystem model is obtained as

$$\dot{\mathbf{z}}_s = \mathbf{A}_s\mathbf{z}_s + \mathbf{B}_s\mathbf{u}_s, \tag{4.7}$$
$$\mathbf{y}_s = \mathbf{M}_s\mathbf{z}_s + \mathbf{N}_s\mathbf{u}_s, \tag{4.8}$$

where $\mathbf{z}_s = \bar{\mathbf{z}}_1$, $\mathbf{u}_s = \bar{\mathbf{u}}$, $\mathbf{A}_s = \mathbf{A}_{11} - \mathbf{A}_{12}\mathbf{A}_{22}^{-1}\mathbf{A}_{21}$, $\mathbf{B}_s = \mathbf{B}_1 - \mathbf{A}_{12}\mathbf{A}_{22}^{-1}\mathbf{B}_2$, $\mathbf{M}_s = \mathbf{M}_1 - \mathbf{M}_2\mathbf{A}_{22}^{-1}\mathbf{A}_{21}$, and $\mathbf{N}_s = -\mathbf{M}_2\mathbf{A}_{22}^{-1}\mathbf{B}_2$. In order to derive fast subsystem, slow variables are assumed constant during fast transients. The fast subsystem model is given as

$$\varepsilon\dot{\mathbf{z}}_f = \mathbf{A}_f\mathbf{z}_f + \mathbf{B}_f\mathbf{u}_f, \tag{4.9}$$
$$\mathbf{y}_f = \mathbf{M}_f\mathbf{z}_f, \tag{4.10}$$

where $\mathbf{z}_f = \mathbf{z}_2 - \bar{\mathbf{z}}_2$, $\mathbf{u}_f = \mathbf{u} - \bar{\mathbf{u}}$, $\mathbf{A}_f = \mathbf{A}_{22}$, $\mathbf{B}_f = \mathbf{B}_2$, and $\mathbf{M}_f = \mathbf{M}_2$. Thus the original higher order system described by (4.2)–(4.4) is decomposed into n_1-dimensional slow subsystem given by (4.7)–(4.8) and n_2-dimensional fast subsystem given by (4.9)–(4.10).

4.2.1 Linear State Feedback Control

For convenience, system (4.2)–(4.4) is again given in the following form:

$$\dot{\mathbf{z}} = \mathbf{A}\mathbf{z} + \mathbf{B}\mathbf{u}, \tag{4.11}$$
$$\mathbf{y} = \mathbf{M}\mathbf{z}, \tag{4.12}$$

where $\mathbf{z} = \begin{bmatrix} \mathbf{z}_1^T & \mathbf{z}_2^T \end{bmatrix}^T$ is the $n_1 + n_2 = n$ dimensional state vector and recall that

$$\mathbf{A} = \begin{bmatrix} \mathbf{A}_{11} & \mathbf{A}_{12} \\ \underline{\mathbf{A}_{21}} & \underline{\mathbf{A}_{22}} \\ \varepsilon & \varepsilon \end{bmatrix}, \mathbf{B} = \begin{bmatrix} \mathbf{B}_1 \\ \underline{\mathbf{B}_2} \\ \varepsilon \end{bmatrix}, \mathbf{M} = \begin{bmatrix} \mathbf{M}_1 & \mathbf{M}_2 \end{bmatrix}.$$

In particular, it is considered to minimize the quadratic performance index

$$J = \int_0^\infty \left[\mathbf{z}^T\mathbf{Q}\mathbf{z} + \mathbf{u}^T\mathbf{R}\mathbf{u} \right] dt, \tag{4.13}$$

where $\mathbf{Q} \geq 0$ and $\mathbf{R} > 0$ are, respectively, $(n \times n)$ and $(m \times m)$ matrices. The solution to the problem (4.13) is the optimal linear feedback

$$\mathbf{u} = -\mathbf{R}^{-1}\mathbf{B}^T\mathbf{S}\left[\mathbf{z}_1^T \ \mathbf{z}_2^T\right]^T = \mathbf{K}_{opt}\left[\mathbf{z}_1^T \ \mathbf{z}_2^T\right]^T \tag{4.14}$$

where $(n \times n)$ matrix $\mathbf{S}$ in (4.14) can be obtained by solving the Riccati equation

$$\mathbf{SA} + \mathbf{A}^T\mathbf{S} - \mathbf{SBR}^{-1}\mathbf{B}^T\mathbf{S} + \mathbf{Q} = \mathbf{0}. \tag{4.15}$$

The simultaneous presence of the slow and fast phenomena in the system results in ill-conditioning of the system so that it becomes difficult to solve (4.15) for finding $\mathbf{S}$. However, by application of singular perturbation approach, the original higher order ill-condition system is decomposed in two subsystems and the linear regulator design is carried out for two separate subsystems individually. Finally, separately designed regulators are combined to obtain control given by (4.14). For design purpose, the matrices $\mathbf{Q}$ and $\mathbf{S}$ are assumed to be partitioned as

$$\mathbf{Q} = \begin{bmatrix} \mathbf{Q}_{11} & \mathbf{Q}_{12} \\ \mathbf{Q}_{12}^T & \mathbf{Q}_{22} \end{bmatrix} \text{ and } \mathbf{S} = \begin{bmatrix} \mathbf{S}_{11} & \varepsilon\mathbf{S}_{12} \\ \varepsilon\mathbf{S}_{12}^T & \varepsilon\mathbf{S}_{22} \end{bmatrix}. \tag{4.16}$$

Now, for fast subsystem (4.9), optimal control [3, 20] is given by

$$\mathbf{u}_f = -\mathbf{R}^{-1}\mathbf{B}_f^T\mathbf{S}_{22}\mathbf{z}_f = \mathbf{K}_2\mathbf{z}_f, \tag{4.17}$$

where

$$\mathbf{S}_{22}\mathbf{A}_f + \mathbf{A}_f^T\mathbf{S}_{22} - \mathbf{S}_{22}\mathbf{B}_f\mathbf{R}^{-1}\mathbf{B}_f^T\mathbf{S}_{22} + \mathbf{Q}_f = \mathbf{0} \tag{4.18}$$

with $\mathbf{Q}_f = \mathbf{Q}_{22} \geq 0$ and $\mathbf{R} > 0$. A unique solution of $\mathbf{S}_{22}$ exists if the fast subsystem pair $(\mathbf{A}_f, \mathbf{B}_f)$ is controllable. The optimal control [3, 20] for (4.7) is given by

$$\mathbf{u}_s = -\mathbf{R}_0^{-1}\left(\mathbf{H}_0 + \mathbf{B}_0^T\mathbf{S}_0\right)\mathbf{z}_s = \mathbf{K}_0\mathbf{z}_s, \tag{4.19}$$

where $\mathbf{S}_0$ is obtained by solving

$$\mathbf{S}_0\mathbf{A}_0 + \mathbf{A}_0^T\mathbf{S}_0 - \mathbf{S}_0\mathbf{B}_0\mathbf{R}_0^{-1}\mathbf{B}_0^T\mathbf{S}_0 + \mathbf{Q}_0 = \mathbf{0}, \tag{4.20}$$

in which

$$\begin{aligned} \mathbf{A}_0 &= \mathbf{A}_s - \mathbf{B}_s\mathbf{R}_0^{-1}\mathbf{H}_0, \\ \mathbf{B}_0 &= \mathbf{B}_s, \\ \mathbf{R}_0 &= \mathbf{R} + \left(\mathbf{A}_{22}^{-1}\mathbf{B}_f\right)^T\mathbf{Q}_{22}\mathbf{A}_{22}^{-1}\mathbf{B}_f, \\ \mathbf{Q}_0 &= \bar{\mathbf{Q}}_0 - \mathbf{H}_0^T\mathbf{R}_0^{-1}\mathbf{H}_0, \end{aligned}$$

where

$$\mathbf{H}_0 = -\left(\mathbf{A}_{22}^{-1}\mathbf{B}_f\right)^T\left[\mathbf{Q}_{12}^T - \mathbf{Q}_{22}\mathbf{A}_{22}^{-1}\mathbf{A}_{21}\right],$$
$$\bar{\mathbf{Q}}_0 = \mathbf{Q}_{11} - \mathbf{Q}_{12}\mathbf{A}_{22}^{-1}\mathbf{A}_{21} - \left(\mathbf{A}_{22}^{-1}\mathbf{A}_{21}\right)^T\left[\mathbf{Q}_{12}^T - \mathbf{Q}_{22}\mathbf{A}_{22}^{-1}\mathbf{A}_{21}\right].$$

4.2.2 Composite Controller Design

Separately designed optimal controllers (4.17) and (4.19) should ensure the stability of subsystems, i.e.,

$$\Re e\{\varphi(\mathbf{A}_f + \mathbf{B}_f\mathbf{K}_2)\} < 0 \quad \text{and} \quad \Re e\{\varphi(\mathbf{A}_s + \mathbf{B}_s\mathbf{K}_0)\} < 0. \tag{4.21}$$

As a result, an asymptotically stable closed-loop behavior can be obtained if composite control

$$\mathbf{u} = \mathbf{K}_0\mathbf{z}_s + \mathbf{K}_2\mathbf{z}_f \tag{4.22}$$

is applied to the system (4.2)–(4.3). In terms of states $\mathbf{z}_1$ and $\mathbf{z}_2$, one can write

$$\begin{aligned}\mathbf{u} &= \left[(\mathbf{E}_m + \mathbf{K}_2\mathbf{A}_{22}^{-1}\mathbf{B}_2)\mathbf{K}_0 + \mathbf{K}_2\mathbf{A}_{22}^{-1}\mathbf{A}_{21}\right]\mathbf{z}_1 + \mathbf{K}_2\mathbf{z}_2 \\ &= [\mathbf{K}_1\mathbf{K}_2]\left[\mathbf{z}_1^T\mathbf{z}_2^T\right]^T,\end{aligned} \tag{4.23}$$

where $\mathbf{K}_1 = (\mathbf{E}_m + \mathbf{K}_2\mathbf{A}_{22}^{-1}\mathbf{B}_2)\mathbf{K}_0 + \mathbf{K}_2\mathbf{A}_{22}^{-1}\mathbf{A}_{21}$, in which $\mathbf{E}_m$ is $(m \times m)$ identity matrix. Further (4.23) can be written as

$$\mathbf{u} = \mathbf{K}_{opt}\mathbf{z}, \tag{4.24}$$

where $\mathbf{K}_{opt} = [\mathbf{K}_1\ \mathbf{K}_2]$. This composite control serves as a near-optimum control for the actual higher order system.

Remark 4.1 If the system is having stable fast modes, then $\mathbf{K}_2$ can be taken as null matrix of $(m \times n_2)$ dimension. This yields reduced two-time-scale approximation to $\mathbf{K}_{opt}$ as $\bar{\mathbf{K}}_{opt} = [\mathbf{K}_0\ \mathbf{0}]$.

4.3 Application to AHWR Model

Singularly perturbed model of AHWR, discussed in Sect. 3.4.1, is decoupled into slow and fast subsystems of orders 73 and 17, respectively, by using (4.7)–(4.10). The eigenvalues of matrices $\mathbf{A}_s$ and $\mathbf{A}_f$ are given in Tables 4.1 and 4.2, respectively. It is seen that the eigenvalues of the fast subsystem matrix $\mathbf{A}_f$ are in excellent agreement

Table 4.1 Eigenvalues of slow subsystem ($\mathbf{A}_s$) obtained using quasi-steady-state method

Sr. No.	Eigenvalues	Sr. No.	Eigenvalues	Sr. No.	Eigenvalues
1	2.4139×10^{-17}	31	-1.5717×10^{-4}	53	-6.2865×10^{-2}
2	6.1105×10^{-17}	32	-1.6524×10^{-4}	54	-6.2894×10^{-2}
3	-2.2396×10^{-17}	33	-1.6573×10^{-4}	55	-9.7168×10^{-2}
4	-2.8757×10^{-5}	34	-1.7308×10^{-4}	56	-1.0708×10^{-1}
5	-3.7781×10^{-5}	35	-1.8807×10^{-4}	57	-1.3169×10^{-1}
6	-3.7993×10^{-5}	36	-1.8870×10^{-4}	58	-1.4712×10^{-1}
7	-4.0124×10^{-5}	37	-2.4408×10^{-4}	59	-1.4713×10^{-1}
8	-4.1520×10^{-5}	38	-1.5738×10^{-2}	60	-1.4808×10^{-1}
9	-4.1968×10^{-5}	39	-5.0954×10^{-2}	61	-1.5063×10^{-1}
10	-4.4204×10^{-5}	40	-5.1179×10^{-2}	62	-1.5580×10^{-1}
11	-4.7338×10^{-5}	41	-5.7743×10^{-2}	63	-1.5585×10^{-1}
12	-4.8866×10^{-5}	42	-5.7898×10^{-2}	64	-1.5662×10^{-1}
13–14	$(-7.7407\pm j2.9929)\times10^{-5}$	43	-5.9709×10^{-2}	65	-1.6019×10^{-1}
15–16	$(-7.3360\pm j3.9319)\times10^{-5}$	44	-5.9727×10^{-2}	66	-1.6316×10^{-1}
17–18	$(-6.4855\pm j5.3109)\times10^{-5}$	45	-6.0346×10^{-2}	67	-1.6324×10^{-1}
19–20	$(-3.5444\pm j7.7360)\times10^{-5}$	46	-6.0644×10^{-2}	68	-1.6404×10^{-1}
21–22	$(-3.7785\pm j7.6475)\times10^{-5}$	47	-6.1849×10^{-2}	69	-1.7531×10^{-1}
23–24	$(-6.5949\pm j5.4819)\times10^{-5}$	48	-6.1946×10^{-2}	70	-1.8031×10^{-1}
25–26	$(8.0471\pm j3.9863)\times10^{-5}$	49	-6.2200×10^{-2}	71	-1.8049×10^{-1}
27–28	$(8.8268\pm j2.1800)\times10^{-5}$	50	-6.2385×10^{-2}	72	-1.8122×10^{-1}
29	-1.4107×10^{-4}	51	-6.2458×10^{-2}	73	-2.7823×10^{-1}
30	-1.4441×10^{-4}	52	-6.2608×10^{-2}		

Table 4.2 Eigenvalues of fast subsystem ($\mathbf{A}_f$) obtained using quasi-steady-state method

Sr. No.	Eigenvalues	Sr. No.	Eigenvalues	Sr. No.	Eigenvalues
1	-7.2028	7	-9.4608×10^{1}	13	-2.1110×10^{2}
2	-3.2833×10^{1}	8	-1.0868×10^{2}	14	-2.1904×10^{2}
3	-3.3361×10^{1}	9	-1.1704×10^{2}	15	-2.3591×10^{2}
4	-6.6593×10^{1}	10	-1.6967×10^{2}	16	-2.7163×10^{2}
5	-6.8317×10^{1}	11	-1.7568×10^{2}	17	-2.7626×10^{2}
6	-9.3649×10^{1}	12	-1.9497×10^{2}		

with the last 17 eigenvalues of matrix $\hat{\mathbf{A}}$. Similarly, the slow subsystem eigenvalues compare well with remaining 73 eigenvalues of matrix $\hat{\mathbf{A}}$. Hence, it can be concluded that the singularly perturbed form of model (3.31), discussed in Sect. 3.4.1, is valid in case of AHWR. Slow subsystem contains the eigenvalues which are unstable along with those near the origin, whereas fast subsystem contains stable eigenvalues. Observe the unstable eigenvalues (1–3 and 25–28) in slow subsystem, as shown in

Table 4.1. It is important to note that the unstable eigenvalues 1–3 are zero in original system matrix $\hat{\mathbf{A}}$. However, there is no much change in remaining 70 eigenvalues of slow subsystem. It may further be noticed that the submatrix $\mathbf{B}_2$ of the input matrix is null matrix, thereby leading to $\mathbf{B}_f = 0$. In other words, the fast subsystem is uncontrollable. However, it can be verified that the slow subsystem is controllable and hence only $\mathbf{K}_0$ needs to be designed for slow subsystem as

$$\mathbf{u}_{sp} = \mathbf{K}_0 \mathbf{z}_1. \tag{4.25}$$

The regulator design is carried out using equations described in Sect. 4.2.1 with $\mathbf{R}$ as a (4×4) identity matrix and the matrix $\mathbf{Q}$, given in [16], as

$$\mathbf{Q} = diag\left[\mathbf{Q}_H\, \mathbf{Q}_X\, \mathbf{Q}_I\, Q_h\, \mathbf{Q}_C\, \mathbf{Q}_x\, \mathbf{Q}_Q\right] \times 10^{-3}, \tag{4.26}$$

where $\mathbf{Q}_H = 0.2 \times \mathbf{E}_4$, $\mathbf{Q}_X = 0.1 \times \mathbf{E}_{17}$, $\mathbf{Q}_I = 0.1 \times \mathbf{E}_{17}$, $Q_h = 1.0$, $\mathbf{Q}_C = 0.2 \times \mathbf{E}_{17}$, $\mathbf{Q}_x = 1.0 \times \mathbf{E}_{17}$, and $\mathbf{Q}_Q = 10 \times \mathbf{E}_{17}$. The matrix $\mathbf{S}_0$ is evaluated by solving (4.20) and the optimal control gain $\mathbf{K}_0$ for the slow subsystem is determined from (4.19). Finally, the composite gain matrix $\mathbf{K}_{opt}$ is determined from (4.23) and is given by

$$\mathbf{K}_{opt} = -\left[\mathbf{K}_H\, \mathbf{K}_X\, \mathbf{K}_I\, \mathbf{K}_h\, \mathbf{K}_C\, \mathbf{K}_x\, \mathbf{0}\right], \tag{4.27}$$

where $\mathbf{0}$ denotes a null matrix of (4×17) order and $\mathbf{K}_H$, $\mathbf{K}_X$, $\mathbf{K}_I$, $\mathbf{K}_h$, $\mathbf{K}_C$, and $\mathbf{K}_x$ are feedback gains corresponding to regulating rod (RR) positions, xenon, iodine concentrations, enthalpy, delayed neutron precursor concentration, and exit quality, respectively, given by

$$\mathbf{K}_H = \begin{bmatrix} -19.9545 & -5.7393 & -4.9452 & -5.6978 \\ -5.7393 & -20.7841 & -5.6978 & -5.7178 \\ -4.9452 & -5.6978 & -19.9545 & -5.7393 \\ -5.6978 & -5.7178 & -5.7393 & -20.7841 \end{bmatrix} \times 10^{-3}, \tag{4.28}$$

$$\mathbf{K}_X = \begin{bmatrix} -10.7345 & -8.3090 & -8.0272 & -5.9800 & -3.7218 & -2.8063 & -3.9180 \\ -11.4554 & -5.8965 & -8.3055 & -9.2395 & -7.9956 & -5.7743 & -4.4195 \\ -10.7345 & -2.8063 & -3.9180 & -5.8549 & -7.3040 & -8.3090 & -8.0272 \\ -11.4554 & -5.7743 & -4.4195 & -3.5621 & -3.7827 & -5.8965 & -8.3055 \\ -5.8549 & -7.3040 & -6.8392 & -7.4296 & -4.7889 & -1.9474 & -1.3720 \\ -3.5621 & -3.7827 & -3.8666 & -7.2293 & -8.4341 & -6.1019 & -4.6704 \\ -5.9800 & -3.7218 & -1.3720 & -2.7189 & -5.2149 & -6.1906 & -6.8392 \\ -9.2395 & -7.9956 & -4.6704 & -3.5452 & -2.4453 & -2.5284 & -3.8666 \\ -2.7189 & -5.2149 & -6.1906 \\ -3.5452 & -2.4453 & -2.5284 \\ -7.4296 & -4.7889 & -1.9474 \\ -7.2293 & -8.4341 & -6.1019 \end{bmatrix} \times 10^{-1}, \tag{4.29}$$

$$\mathbf{K}_I = \begin{bmatrix} 2.6987 & 2.8876 & 2.0075 & 1.5505 & 0.5708 & 0.0338 & 0.9088 \\ 2.8489 & 1.6278 & 2.2559 & 2.4676 & 2.7771 & 1.4134 & 0.8170 \\ 2.6987 & 0.0338 & 0.9088 & 1.3398 & 2.3417 & 2.8876 & 2.0075 \\ 2.8489 & 1.4134 & 0.8170 & 0.5847 & 0.3009 & 1.6278 & 2.2559 \end{bmatrix}$$

$$\begin{bmatrix} 1.3398 & 2.3417 & 3.2291 & 3.2090 & 1.3042 & -0.4368 & -0.9069 \\ 0.5847 & 0.3009 & 0.8915 & 3.0851 & 3.9466 & 2.6712 & 1.4555 \\ 1.5505 & 0.5708 & -0.9069 & -0.3615 & 1.4543 & 2.7375 & 3.2291 \\ 2.4676 & 2.7771 & 1.4555 & -0.0985 & -0.9381 & -0.2702 & 0.8915 \end{bmatrix}$$

$$\begin{bmatrix} -0.3615 & 1.4543 & 2.7375 \\ -0.0985 & -0.9381 & -0.2702 \\ 3.2090 & 1.3042 & -0.4368 \\ 3.0851 & 3.9466 & 2.6712 \end{bmatrix} \times 10^{-2}, \tag{4.30}$$

$$\mathbf{K}_h = \begin{bmatrix} -6.4051 \\ -6.9423 \\ -6.4051 \\ -6.9423 \end{bmatrix} \times 10^{-2}, \tag{4.31}$$

$$\mathbf{K}_C = \begin{bmatrix} 14.0427 & 7.6659 & 8.0974 & 7.8364 & 7.0751 & 6.9674 & 7.5856 \\ 15.0907 & 7.8229 & 8.6745 & 8.8328 & 8.0833 & 7.7858 & 8.1696 \\ 14.0427 & 6.9674 & 7.5856 & 7.7988 & 7.4837 & 7.6659 & 8.0974 \\ 15.0907 & 7.7858 & 8.1696 & 8.0781 & 7.5728 & 7.8229 & 8.6745 \end{bmatrix}$$

$$\begin{bmatrix} 7.7988 & 7.4837 & 5.7549 & 6.9890 & 6.6659 & 5.1516 & 5.0851 \\ 8.0781 & 7.5728 & 5.7310 & 7.4248 & 7.6125 & 5.9913 & 5.8023 \\ 7.8364 & 7.0751 & 5.0851 & 6.4267 & 6.6905 & 5.6319 & 5.7549 \\ 8.8328 & 8.0833 & 5.8023 & 6.9652 & 6.8531 & 5.5769 & 5.7310 \end{bmatrix}$$

$$\begin{bmatrix} 6.4267 & 6.6905 & 5.6319 \\ 6.9652 & 6.8531 & 5.5769 \\ 6.9890 & 6.6659 & 5.1516 \\ 7.4248 & 7.6125 & 5.9913 \end{bmatrix} \times 10^{-3}, \tag{4.32}$$

$$\mathbf{K}_x = \begin{bmatrix} -6.8688 & -1.1302 & -1.9942 & -2.0213 & -1.3383 & -1.3331 & -1.9952 \\ -7.3973 & -1.4558 & -2.1455 & -1.9598 & -1.4153 & -1.4642 & -2.1597 \\ -6.8688 & -1.3331 & -1.9952 & -2.0278 & -1.3277 & -1.1302 & -1.9942 \\ -7.3973 & -1.4642 & -2.1597 & -2.1471 & -1.4462 & -1.4558 & -2.1455 \end{bmatrix}$$

$$\begin{bmatrix} -2.0278 & -1.3277 & -1.1880 & -1.3670 & -1.4090 & -1.3058 & -1.3009 \\ -2.1471 & -1.4462 & -1.4287 & -1.4971 & -1.3839 & -1.4077 & -1.4420 \\ -2.0213 & -1.3383 & -1.3009 & -1.3943 & -1.4180 & -1.2997 & -1.1880 \\ -1.9598 & -1.4153 & -1.4420 & -1.5168 & -1.5035 & -1.4205 & -1.4287 \end{bmatrix}$$

$$\begin{bmatrix} -1.3943 & -1.4180 & -1.2997 \\ -1.5168 & -1.5035 & -1.4205 \\ -1.3670 & -1.4090 & -1.3058 \\ -1.4971 & -1.3839 & -1.4077 \end{bmatrix} \times 10^{-4}. \tag{4.33}$$

Table 4.3 Closed-loop eigenvalues of the AHWR model with $\mathbf{K}_{opt}$

Sr. No.	Eigenvalues	Sr. No.	Eigenvalues	Sr. No.	Eigenvalues
1	-2.8369×10^{-5}	35	-7.9732×10^{-3}	63	-1.5662×10^{-1}
2–3	$(-3.6054\pm j7.7099)\times10^{-5}$	36	-8.0749×10^{-3}	64	-1.6022×10^{-1}
4–5	$(-3.9491\pm j7.5495)\times10^{-5}$	37	-8.1030×10^{-3}	65	-1.6316×10^{-1}
6	-3.7779×10^{-5}	38	-5.7736×10^{-2}	66	-1.6324×10^{-1}
7	-3.7985×10^{-5}	39	-5.7892×10^{-2}	67	-1.6405×10^{-1}
8	-4.1515×10^{-5}	40	-5.9706×10^{-2}	68	-1.7542×10^{-1}
9	-4.1942×10^{-5}	41	-5.9723×10^{-2}	69	-1.8037×10^{-1}
10	-4.0111×10^{-5}	42	-6.0344×10^{-2}	70	-1.8049×10^{-1}
11	-4.4291×10^{-5}	43	-6.0642×10^{-2}	71	-1.8122×10^{-1}
12	-4.7331×10^{-5}	44	-6.1848×10^{-2}	72	-2.8889×10^{-1}
13	-4.9080×10^{-5}	45	-6.1945×10^{-2}	73	-1.0800×10^{-1}
14–15	$(-6.5115\pm j5.2628)\times10^{-5}$	46	-6.2200×10^{-2}	74	-6.9171×10^{0}
16–17	$(-6.5926\pm j5.4855)\times10^{-5}$	47	-6.2384×10^{-2}	75	-3.2844×10^{1}
18–19	$(-7.3405\pm j3.9069)\times10^{-5}$	48	-6.2458×10^{-2}	76	-3.3372×10^{1}
20–21	$(-7.7414\pm j2.9910)\times10^{-5}$	49	-6.2608×10^{-2}	77	-6.6599×10^{1}
22–23	$(-8.3203\pm j3.3684)\times10^{-5}$	50	-6.2865×10^{-2}	78	-6.8323×10^{1}
24	-8.4318×10^{-5}	51	-6.2893×10^{-2}	79	-9.4612×10^{1}
25	-9.6873×10^{-5}	52	-5.0944×10^{-2}	80	-9.3653×10^{1}
26	-1.4048×10^{-4}	53	-5.1151×10^{-2}	81	-1.0868×10^{2}
27	-1.4459×10^{-4}	54	-1.5738×10^{-2}	82	-1.1705×10^{2}
28	-1.5742×10^{-4}	55	-9.6913×10^{-2}	83	-1.6967×10^{2}
29	-1.6516×10^{-4}	56	-1.3225×10^{-1}	84	-1.7568×10^{2}
30	-1.6590×10^{-4}	57	-1.4712×10^{-1}	85	-1.9497×10^{2}
31	-1.7323×10^{-4}	58	-1.4713×10^{-1}	86	-2.1110×10^{2}
32	-1.8816×10^{-4}	59	-1.4809×10^{-1}	87	-2.1904×10^{2}
33	-1.8871×10^{-4}	60	-1.5068×10^{-1}	88	-2.3591×10^{2}
34	-2.4746×10^{-4}	61	-1.5580×10^{-1}	89	-2.7163×10^{2}
		62	-1.5585×10^{-1}	90	-2.7626×10^{2}

It can be observed that the feedback gains corresponding to xenon concentration are large and that of exit quality are small. The diagonal dominance of $\mathbf{K}_H$ can also be noticed. Using total power feedback (3.30) and spatial power feedback (4.25) with gain (4.27), the overall control input (3.29) becomes

$$\mathbf{u} = -\mathbf{K}_G\mathbf{y} - \mathbf{K}_H\mathbf{z}_H - \mathbf{K}_X\mathbf{z}_X - \mathbf{K}_I\mathbf{z}_I - \mathbf{K}_h\mathbf{z}_h - \mathbf{K}_C\mathbf{z}_C - \mathbf{K}_x\mathbf{z}_x. \tag{4.34}$$

Table 4.3 lists the closed-loop eigenvalues of (3.27) with control input (4.34). From (4.34) it is evident that controller demands feedbacks of RR positions, enthalpy, xenon, iodine, and delayed neutron precursor concentrations and hence, only a reduced order observer would be sufficient for the controller implementation [9].

4.3.1 Transient Simulations

Performance of the control technique was examined by simulating the nonlinear system of AHWR, given by (2.26)–(2.32), for the transient involving a disturbance in the spatial power distribution. Initially, the reactor was observed to be working at full power steady-state condition. Suddenly, RR2, initially under automatic control signal, was moved out using manual control by about 1% by giving suitable control signal after 2 s and afterward left on automatic control as depicted in Fig. 4.1. All other RRs were driven in under the influence of control action so as to regulate the total power of reactor. Following the time period when the manual control signal was applied to RR2, all RRs were being moved by the controller to their initial positions in about 135 s. Variations in spatial power, measured in terms of first and second azimuthal tilts and defined by (2.49)–(2.50), quadrant powers, and total power are, respectively, shown in Figs. 4.2, 4.3, and 4.4.

With the purpose of testing the performance of controller to the disturbance in feed flow, the nonlinear model was again simulated when positive step change of 5% was initiated in the feed flow. As a consequence of this, the incoming coolant enthalpy decreased by around 0.64%. However, due to controller action the total power was observed to be stabilizing at its steady-state value (Fig. 4.5a). This is compensated by moving the RRs inside the reactor by 0.9% (Fig. 4.5b). When the temporary disturbance was initiated in the feed flow the total reactor power was

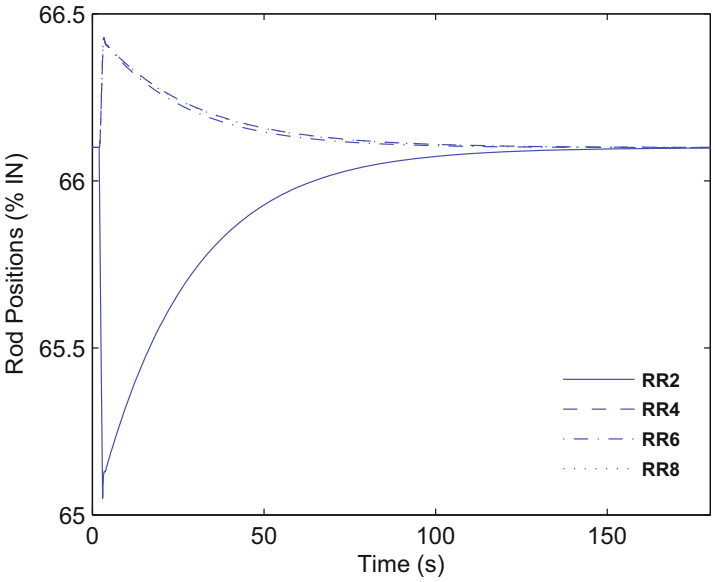

Fig. 4.1 Deviations in regulating rod positions during the transient

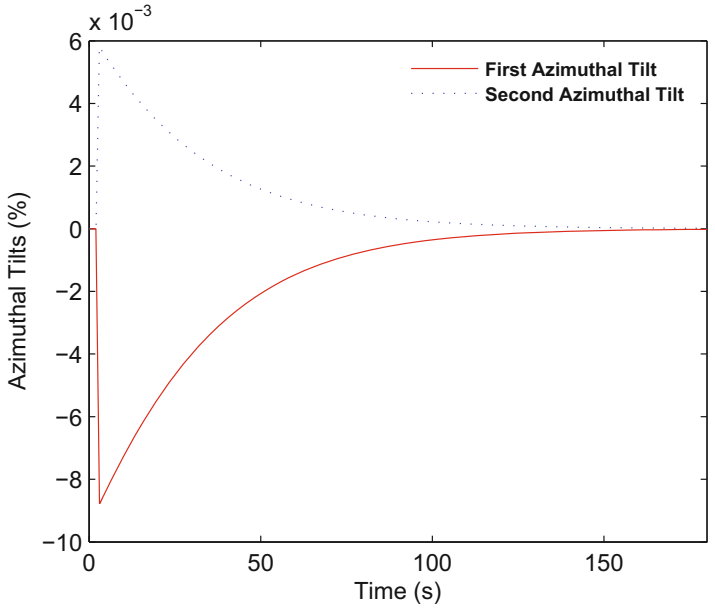

Fig. 4.2 Suppression of azimuthal tilts initiated by change in RR2 position

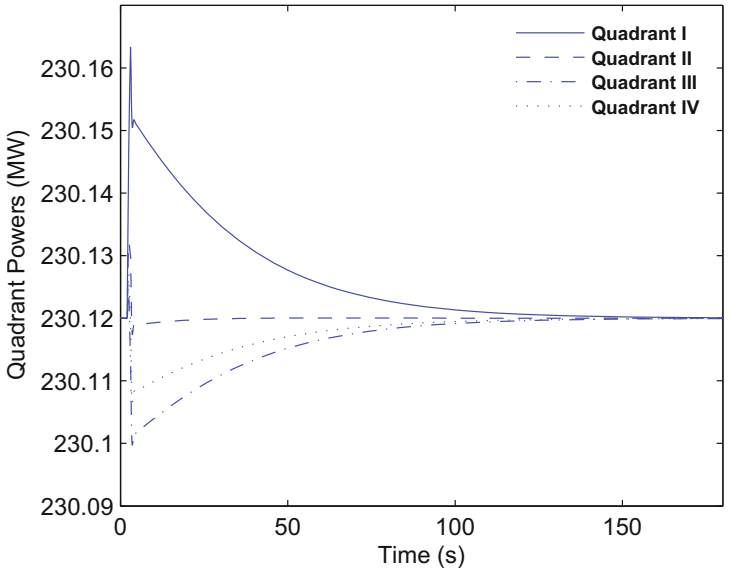

Fig. 4.3 Deviations in quadrant powers during the transient

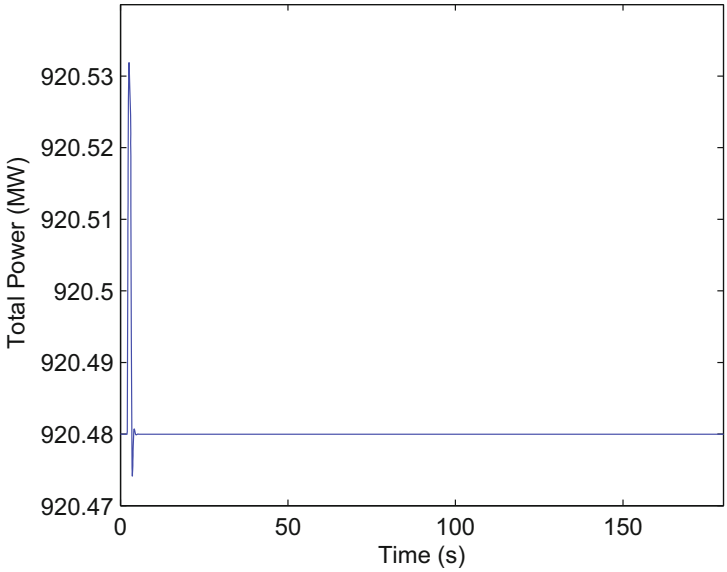

Fig. 4.4 Variations in total power during the transient

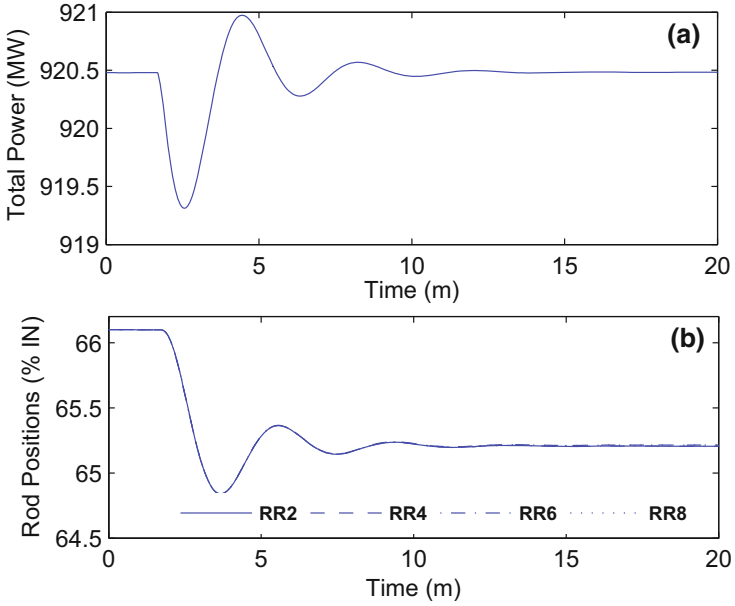

Fig. 4.5 Effect of 5% positive step change in the feed flow on **a** Total power and **b** Regulating rod positions

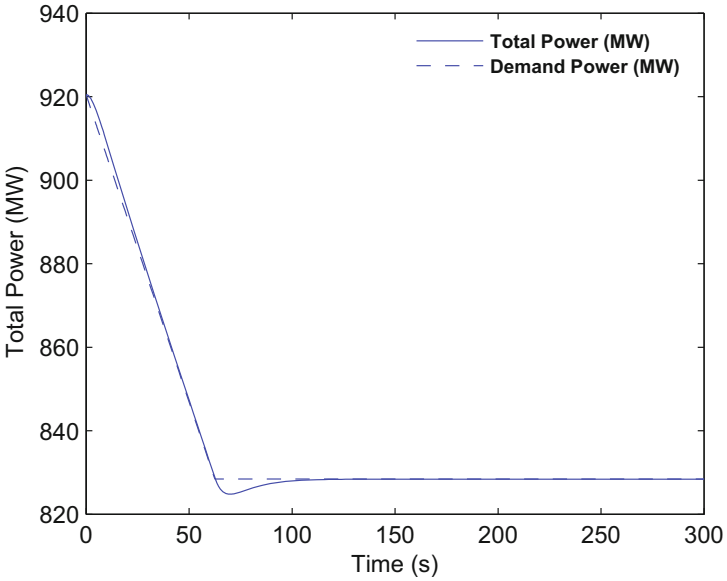

Fig. 4.6 Variations in total power during power maneuvering from 920.48 to 828.43 MW

found to be stabilizing back at its original value and all RRs also came back to their steady-state positions.

In one more transient, originally, the reactor is under equilibrium condition and is observed to be working at 920.48 MW with nodal power distribution as given in Table 2.5. Now, the demand power is decreased uniformly at the rate of 1.5 MW/s to 828.43 MW, in 61 s and maintained constant subsequently. Throughout the transient, it is found that the total power is tracking the demand power as indicated in Fig. 4.6 and settles after 90 s. It is observed that the feed flow decreases at the rate of 0.66 kg/s/s (Fig. 4.7a), whereas downcomer enthalpy increases at the rate of 0.28 kJ/kg/s (Fig. 4.7b) and attains new steady states in 90 s. However, the nodal xenon concentrations reach to their respective new equilibrium values in about 50 h.

Furthermore, the performance of controller is compared with the controller suggested in [16]. In this case, RR6 was moved out by manual control signal by 2% by giving suitable control signal and at the same time RR4 was moved in by same amount, instantly after that RRs were moved back to their initial positions. Simulation results are generated for variations in RR positions using both the controllers as depicted in Fig. 4.8. It is noticed that, with both the controllers, RRs are moved back to their equilibrium positions but time required to do so is significantly less in case of the present controller. For this transient quadrant power variations are illustrated in Fig. 4.9.

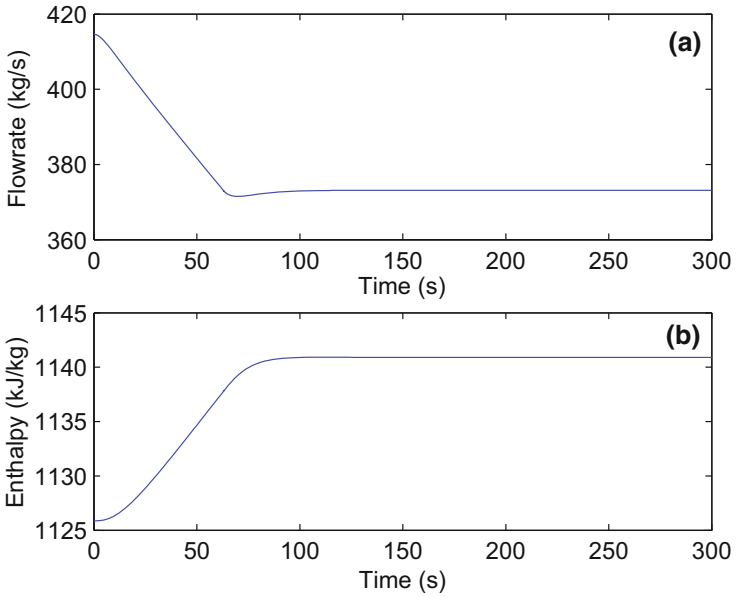

Fig. 4.7 Effect of power maneuvering on **a** Feed flow rate and **b** Downcomer enthalpy

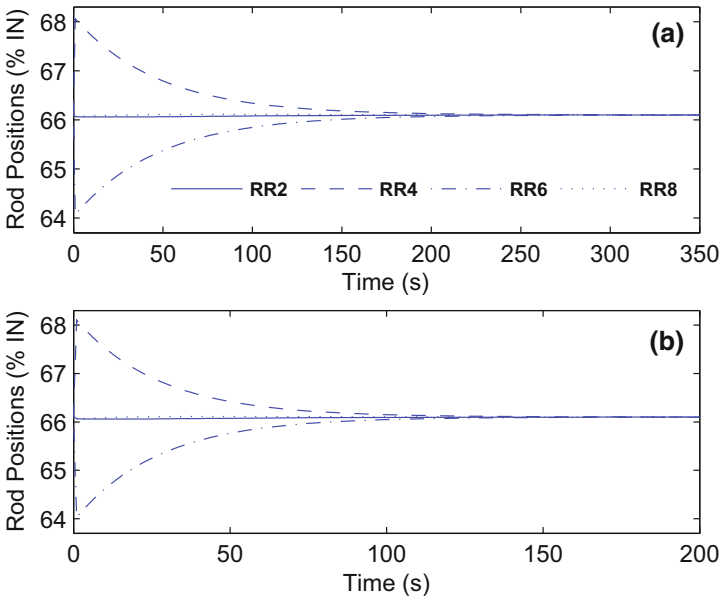

Fig. 4.8 Comparison of controllers: **a** Response due to three-time-scale [16] approach and **b** Response due to two-time-scale method

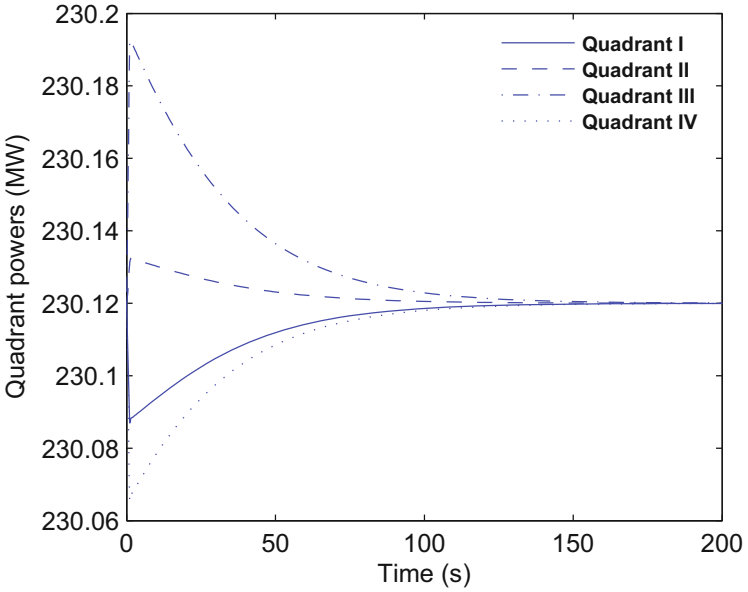

Fig. 4.9 Quadrant power variations during the transient

4.4 Conclusion

The numerically ill-conditioned 90th order linear system of AHWR is decoupled into two lower order subsystems by quasi-steady-state method. After that, linear quadratic regulators are designed for the slow and fast subsystems separately and a composite controller for original system is derived. An asymptotic approximation to the closed-loop system is achieved and at the same time ill-conditioning issues linked with AHWR system are eliminated after application of composite controller. Performance of the presented controller is tested through simulations carried out under various transient conditions. Also, the performance of controller is compared with three-time-scale composite controller for the same transient condition. It is noticed that the performance of the suggested controller is superior to three-time-scale composite controller.

References

1. Chang, K.W.: Singular perturbations of a general boundary value problem. SIAM J. Math. Anal. **3**(3), 520–526 (1972)
2. Chang, K.W.: Diagonalization method for a vector boundary problem of singular perturbation type. J. Math. Anal. Appl. **48**(3), 652–665 (1974)

3. Chow, J.H., Kokotovic, P.V.: A decomposition of near-optimum regulators for systems with slow and fast modes. IEEE Trans. Autom. Control **21**(5), 701–705 (1976)
4. Gaitsgory, V., Nguyen, M.T.: Averaging of three time scale singularly perturbed control systems. Syst. Control Lett. **42**(5), 395–403 (2001)
5. Gajic, Z., Lim, M.-T.: Optimal Control of Singularly Perturbed Linear Systems and Applications: High Accuracy Techniques. Marcel Dekker Inc., New York (2001)
6. Kokotovic, P.V., Khalil, H.K., Reilly, J.O.: Singular Perturbation Methods in Control, Analysis and Design. Academic, New York (1986)
7. Kokotovic, P.V., O'Malley, R.E., Sannuti, P.: Singular perturbation and order reduction in control theory - an overview. Automatica **12**, 123–132 (1976)
8. Ladde, G.S., Rajalakshmi, S.G.: Diagonalization and stability of multi-time-scale singularly perturbed linear systems. Appl. Math. Comput. **16**(2), 115–140 (1985)
9. Munje, R.K., Patre, B.M.: Spatial power control of singularly perturbed nuclear reactor. Control Eng. Appl. Inform. **18**(3), 22–29 (2016)
10. Naidu, D.S.: Singular Perturbation Methodology in Control Systems. Peter Peregrinus Ltd., London (1988)
11. Naidu, D.S.: Singular perturbations and time scales in control theory and applications: overview. Dyn. Contin. Discrete Impuls. Syst. **9**, 233–278 (2002)
12. Phillips, R.G.: A two stage design of linear feedback controls. IEEE Trans. Autom. Control **25**, 1220–1223 (1980)
13. Saberi, A., Khalil, H.: Stabilization and regulation of nonlinear singularly perturbed systems-composite control. IEEE Trans. Autom. Cotrol **30**, 739–747 (1985)
14. Saksena, V.R., O'Reilly, J., Kokotovic, P.V.: Singular perturbation and time-scale methods in control theory: survey 1976–1983. Automatica **20**, 273–293 (1984)
15. Sannuti, P., Kokotovic, P.V.: Near optimum design of linear systems by a singular perturbation method. IEEE Trans. Autom. Control **14**(1), 15–22 (1969)
16. Shimjith, S.R., Tiwari, A.P., Bandyopadhyay, B.: A three-time-scale approach for design of linear state regulator for spatial control of advanced heavy water reactor. IEEE Trans. Nucl. Sci. **58**(3), 1264–1276 (2011)
17. Singh, N.P., Singh, Y.P., Ahson, S.I.: An iterative approach to reduced-order modeling of synchronous machines using singular perturbation. Proc. IEEE **74**, 892–893 (1986)
18. Suzuki, M.: Composite controls for singularly perturbed systems. Proc. IEEE Int. Conf. Control Appl. **26**(2), 123–124 (1981)
19. Syrcos, G., Sannuti, P.: Singular perturbation modeling of continuous and discrete physical systems. Int. J. Control **37**, 1007–1022 (1983)
20. Tiwari, A.P., Bandyopadhyay, B., Werner, H.: Spatial control of a large pressurize heavy water reactor by piecewise constant periodic output feedback. IEEE Trans. Nucl. Sci. **47**, 389–402 (2000)
21. Yan, Z., Naidu, D.S., Cai, C., Zou, Y.: Singular perturbations and time scales in control theories and applications: an overview 2002–2012. Int. J. Inf. Syst. Sci. **9**, 1–36 (2012)

Chapter 5
Sliding Mode Control

5.1 Introduction

Variable structure control (VSC) with sliding mode control (SMC) was first proposed and elaborated in the early 1950s in the Soviet Union by Emelyanov and several coresearchers [6, 10]. Thereafter, a considerable interest was generated on variable structure system (VSS) and SMC in the research community exploring control applications. In VSS, the control is permitted to alter its structure by changing to another member of a set of possible continuous function of states. The VSS then may have new features which individual controls may not hold. It is possible to design control which drives the system to predefined manifold, known as sliding manifold. Once the system motion is confined to the sliding manifold, it asymptotically moves towards the origin. Thus, designing a sliding mode control is a two-step method. First, a stable sliding manifold is designed and second a control law is designed which forces the system states to the sliding manifold in finite time. Afterwards, it keeps the states on the manifold at all instant. This peculiar system characteristics is claimed to result in superb system performance which includes insensitivity to parameter variations and complete rejection of disturbances [6, 22]. Fast control action is needed to maintain the states on the predefined manifold [5].

System imperfections, for example, delays and hysteresis, are notorious to create high-frequency oscillations, i.e., chattering. Chattering is characterized by the states, continually crossing the sliding surface, rather than remaining on it. This type of motion is highly undesirable and results in damage to the actuator components [21]. To avoid this, discontinuous control action is modified, in which instead of forcing the states to rest on the sliding surface, they are forced to stay within an arbitrarily small boundary layer close to it [19]. In the literature it is often referred to as a pseudo-sliding motion. In this case, the total invariance property associated with ideal sliding will be lost. Nevertheless, an arbitrarily close approximation to ideal sliding can be achieved.

R. Munje et al., *Investigation of Spatial Control Strategies with Application to Advanced Heavy Water Reactor*, Energy Systems in Electrical Engineering, https://doi.org/10.1007/978-981-10-3014-7_5

Designing a sliding mode control for multi-time-scale (singularly perturbed) system is difficult due to interactions of slow, fast, and very fast dynamical modes of the system and discontinuous nature of control law. Over the period of time, variety of techniques discussing application of SMC to singularly perturbed systems are published in the literature [1, 4, 9, 11–14, 16, 17, 23]. For stabilizing a class of linear time-invariant system composite SMC is derived from the individual subsystem SMCs [9]. A similar kind of approach is studied by Li et al. [12, 13], in which the upper bound problem of singular perturbation parameter in such a control system is also determined. Global stability of closed-loop system decoupled into lower order subsystems using singular perturbation approach with small perturbation parameter is discussed in [11]. Nevertheless, the effect of external disturbances is not considered in above methods. Yue and Xu [23] suggested SMC design for a singularly perturbed system with external disturbances and parameter uncertainties, but it is complicated to calculate some parameters for the control law design. SMC design using merely slow subsystem states for the full-order system is examined in [1]. In recent times, Nguyen et al. [16] claimed a method where a state feedback control is initially designed to stabilize either slow or fast dynamics and then an SMC is worked out for remaining dynamics to guarantee stability and rejection of disturbance. Furthermore, in [17] SMC scheme for singularly perturbed systems in the presence of matched bounded external disturbance is elaborated. In [4], SMC is designed by means of reduced model approach, where higher order system is decoupled by direct block diagonallization into slow and fast subsystems. In addition, it is demonstrated that the SMC designed for only slow subsystem can result in sliding mode motion for the original full-order system. All the SMC techniques discussed above use two-time-scale decomposition of singularly perturbed system, i.e., either quasi-steady-state method or direct block diagonalization. Recently, Munje et al. [14] have designed SMC for three-time-scale system, in which singularly perturbed system is decomposed into three subsystems, namely, slow, fast 1, and fast 2 by quasi-steady-state method. Composite controller is then designed and applied to point kinetics model of nuclear reactor. Few other applications of sliding mode control for nuclear reactor are presented in [2, 3, 7]. All these are based on point kinetics model of nuclear reactor, which is of lower order.

The basic philosophy of the variable structure control is that the structure of the system varies under certain conditions, from one to another member of a set of admissible continuous-time functions. A variable structure system can inherit combined useful properties from the structures. In addition, it can be endowed with special properties which are not present in any of the structures [6, 20]. In this chapter, sliding mode control technique is explored for Advanced Heavy Water Reactor (AHWR). Implementation of SMC requires state feedback, as was the case of pole placement and linear quadratic regulator designs presented in earlier chapters. Two-time-scale structure built in the Chap. 3 has been utilized in this chapter for SMC design via two-time-scale formulation.

5.2 Sliding Mode Control

Sliding mode control is a type of variable structure control, where sliding surfaces or manifolds are designed such that system trajectories exhibit desirable properties as confined to these manifolds. A system using an SMC strategy can display a robust performance against parametric uncertainties and exogenous disturbances [8]. This property is of extreme importance in practice where most of the plants are heavily affected by parametric and external disturbances.

The SMC design includes design of a switching surface $\mathbf{s} = 0$ to represent the desired dynamics of system, which is of reduced order than the original system and then design of an appropriate control, such that any system state outside the switching surface is moved toward the surface in finite time.

Consider a linear time-invariant controllable and observable continuous-time system of order n, as

$$\dot{\mathbf{z}} = \mathbf{A}\mathbf{z} + \mathbf{B}\mathbf{u}, \tag{5.1}$$

$$\mathbf{y} = \mathbf{M}\mathbf{z}, \tag{5.2}$$

where $\mathbf{z} \in \Re^n$ is the system state, $\mathbf{u} \in \Re^m$ is the control input, and $\mathbf{y} \in \Re^p$ is the system output with $1 \leq m \leq n$. The matrices $\mathbf{A}$, $\mathbf{B}$, and $\mathbf{M}$ are constants of appropriate dimensions. As (5.1) is completely controllable there exists a transformation matrix $\mathbf{T}_r \in \Re^{n \times n}$ such that

$$\mathbf{T}_r\mathbf{B} = \begin{bmatrix} \mathbf{0} \\ \mathbf{B}_0 \end{bmatrix}, \tag{5.3}$$

where $\mathbf{B}_0 \in \Re^{m \times m}$ and is nonsingular. Under this transformation, system (5.1) is transformed into regular form given as

$$\begin{bmatrix} \dot{\bar{\mathbf{z}}}_1 \\ \dot{\bar{\mathbf{z}}}_2 \end{bmatrix} = \begin{bmatrix} \bar{\mathbf{A}}_{11} & \bar{\mathbf{A}}_{12} \\ \bar{\mathbf{A}}_{21} & \bar{\mathbf{A}}_{22} \end{bmatrix} \begin{bmatrix} \bar{\mathbf{z}}_1 \\ \bar{\mathbf{z}}_2 \end{bmatrix} + \begin{bmatrix} \mathbf{0} \\ \mathbf{B}_0 \end{bmatrix} \mathbf{u}, \tag{5.4}$$

where $\bar{\mathbf{z}}_1$ and $\bar{\mathbf{z}}_2$ are of orders $(n - m)$ and m, respectively, and

$$\bar{\mathbf{z}} = \begin{bmatrix} \bar{\mathbf{z}}_1 \\ \bar{\mathbf{z}}_2 \end{bmatrix} = \mathbf{T}_r\mathbf{z}. \tag{5.5}$$

5.2.1 Sliding Surface Design

Consider the sliding surface [6, 10] of form $\bar{\mathbf{C}}^T\bar{\mathbf{z}} = 0$ with sliding function parameter of the form

$$\bar{\mathbf{C}}^T = \begin{bmatrix} \mathbf{K} & \mathbf{E}_m \end{bmatrix}. \tag{5.6}$$

The normal form (5.4), when restricted on sliding surface $\bar{\mathbf{C}}^T \bar{\mathbf{z}} = 0$, would obey the relationship

$$\bar{\mathbf{z}}_2 = -\mathbf{K}\bar{\mathbf{z}}_1. \tag{5.7}$$

Thus, the dynamics of $\bar{\mathbf{z}}_1$ can be represented as

$$\begin{aligned} \dot{\bar{\mathbf{z}}}_1 &= \bar{\mathbf{A}}_{11}\bar{\mathbf{z}}_1 - \bar{\mathbf{A}}_{12}\mathbf{K}\bar{\mathbf{z}}_1, \\ &= (\bar{\mathbf{A}}_{11} - \bar{\mathbf{A}}_{12}\mathbf{K})\bar{\mathbf{z}}_1. \end{aligned} \tag{5.8}$$

From (5.4), variable $\bar{\mathbf{z}}_2$ should be regarded as a control input to the dynamic equation of $\bar{\mathbf{z}}_1$. The controllability of $(\mathbf{A}, \mathbf{B})$ implies controllability of $(\bar{\mathbf{A}}_{11}, \bar{\mathbf{A}}_{12})$. As a result, from (5.8) if $\mathbf{K}$ is selected such that eigenvalues of $(\bar{\mathbf{A}}_{11} - \bar{\mathbf{A}}_{12}\mathbf{K})$ are assigned in desired locations, then $\bar{\mathbf{z}}_1$ is stabilized when confined to sliding surface. Consequently, due to algebraic relationship (5.7), $\bar{\mathbf{z}}_2$ is also stable and confined to sliding surface. Thus, stability requirement of the sliding surface is satisfied and it can be expressed in terms of original state coordinates as

$$\mathbf{s} = \bar{\mathbf{C}}^T \bar{\mathbf{z}} = \bar{\mathbf{C}}^{\mathbf{T}} \mathbf{T}_r \mathbf{z} = \mathbf{C}^T \mathbf{z}. \tag{5.9}$$

5.2.2 *Control Law Design*

When sliding surface (5.9) is designed, it is essential that for all initial conditions, the system states converge towards the switching surface. In other words, if $\mathbf{s} < 0$ then $\dot{\mathbf{s}} > 0$ and, if $\mathbf{s} > 0$ then $\dot{\mathbf{s}} < 0$. This may be combined to yield

$$\dot{\mathbf{s}}\mathbf{s} < 0. \tag{5.10}$$

This is the existence condition for sliding mode motion. And, when sliding motion takes place after finite time t_s, $\mathbf{s} = \mathbf{C}^T\mathbf{z} = 0$ and $\dot{\mathbf{s}} = \mathbf{C}^T\dot{\mathbf{z}} = 0$ for all $t \geq t_s$. Substituting for $\dot{\mathbf{z}}$ from (5.1) gives equivalent sliding mode control [6] as

$$\mathbf{u}_{eq} = -(\mathbf{C}^T\mathbf{B})^{-1}\mathbf{C}^T\mathbf{A}\mathbf{z}. \tag{5.11}$$

The control law (5.11) satisfies only the sliding condition. One must add a regulating control force $\mathbf{u}_{dis}$ (also called as discontinuous control law) in order to satisfy the reaching condition. Thus, define

$$\mathbf{u} = \mathbf{u}_{eq} + \mathbf{u}_{dis}, \tag{5.12}$$

where $\mathbf{u}_{dis}$ can be designed by using sigmoid function [13] so that chattering is eliminated and is implemented as

$$\mathbf{u}_{dis} = -(\mathbf{C}^T\mathbf{B})^{-1}\xi sig(\mathbf{C}^T\mathbf{z})sgn(\mathbf{C}^T\mathbf{z}), \tag{5.13}$$

where ξ is a positive scalar and

$$sig(\mathbf{C}^T\mathbf{z}) = \frac{1 - e^{-|\mathbf{C}^T\mathbf{z}|}}{1 + e^{-|\mathbf{C}^T\mathbf{z}|}} \geq 0, \tag{5.14}$$
$$sgn(\mathbf{C}^T\mathbf{z}) = \begin{cases} 1 & \text{for } \mathbf{C}^T\mathbf{z} > 0 \\ -1 & \text{for } \mathbf{C}^T\mathbf{z} < 0. \end{cases}$$

The system (5.1) is asymptotically stable in sliding mode on sliding surface (5.9) [13].

5.3 Sliding Mode Control Design for Two-Time-Scale System

It is complex and difficult to devise a sliding mode control for numerically ill-conditioned two-time-scale system (3.6) because of different time-scales and the discontinuous nature of control action. Therefore, the higher order system is decoupled into slow and fast subsystems as given by (3.13). Assuming fast subsystem as asymptotically stable, i.e., $\varphi\left(\frac{\mathbf{A}_f}{\varepsilon}\right) < 0$, SMC is formulated by using only slow subsystem states. For that, from (3.13) slow subsystem can be written as

$$\dot{\mathbf{z}_s} = \mathbf{A}_s\mathbf{z}_s + \mathbf{B}_s\mathbf{u}. \tag{5.15}$$

The relationship between the slow subsystem states (5.15) and states of system (3.13) is given as

$$\mathbf{z}_s = \begin{bmatrix} \mathbf{E}_{n_1} & \mathbf{0} \end{bmatrix} \begin{bmatrix} \mathbf{z}_s \\ \mathbf{z}_f \end{bmatrix} = \mathbf{T}_z\mathbf{z}_d, \tag{5.16}$$

where transformation matrix $\mathbf{T}_z \in \Re^{n_1 \times n}$. Let $\mathbf{s}_s = \mathbf{C}^T\mathbf{z}_s$ be a stable sliding surface for slow subsystem (5.15). Hence, the motion around $\mathbf{s}_s$ can be obtained by setting $\dot{\mathbf{s}}_s = 0$. Therefore, equivalent sliding mode control is

$$\mathbf{u}_{eq} = -(\mathbf{C}^T\mathbf{B}_s)^{-1}\mathbf{C}^T\mathbf{A}_s\mathbf{z}_s. \tag{5.17}$$

Thus, motion along $\mathbf{s}_s$ is given by

$$\begin{aligned}\dot{\mathbf{z}}_s &= \mathbf{A}_s\mathbf{z}_s - \mathbf{B}_s(\mathbf{C}^T\mathbf{B}_s)^{-1}\mathbf{C}^T\mathbf{A}_s\mathbf{z}_s,\\ &= (\mathbf{A}_s - \mathbf{B}_s(\mathbf{C}^T\mathbf{B}_s)^{-1}\mathbf{C}^T\mathbf{A}_s)\mathbf{z}_s.\end{aligned} \tag{5.18}$$

As the system (5.18) is stable by design, eigenvalues of $(\mathbf{A}_s - \mathbf{B}_s(\mathbf{C}^T\mathbf{B}_s)^{-1}\mathbf{C}^T\mathbf{A}_s)$ will be stable.

Lemma 5.1 *If motion around* $\mathbf{s}_s = \mathbf{C}^T\mathbf{z}_s$ *for system (5.15) is stable then the motion around*

$$\mathbf{s} = \mathbf{C}^T\mathbf{T}_z\mathbf{T}\mathbf{z} \tag{5.19}$$

for system (3.6) is also stable.

Proof Since, $\mathbf{s}_s = \mathbf{C}^T\mathbf{z}_s$ is a stable sliding surface for system (5.15), from (5.16) sliding surface for system (3.13) can be written as

$$\mathbf{s}_d = \mathbf{C}^T\mathbf{T}_z\mathbf{z}_d. \tag{5.20}$$

Sliding motion around $\mathbf{s}_d$ for system (3.13) can be obtained by setting $\dot{\mathbf{s}}_d = 0$. As a result equivalent control becomes

$$\mathbf{u}_{eq} = -(\mathbf{C}^T\mathbf{B}_s)^{-1}\mathbf{C}^T\begin{bmatrix}\mathbf{A}_s & \mathbf{0}\end{bmatrix}\mathbf{z}_d. \tag{5.21}$$

Thus, motion around switching surface $\mathbf{s}_d$ is

$$\dot{\mathbf{z}}_d = \begin{bmatrix}\mathbf{A}_s - \mathbf{B}_s(\mathbf{C}^T\mathbf{B}_s)^{-1}\mathbf{C}^T\mathbf{A}_s & 0\\ \frac{-\mathbf{B}_f(\mathbf{C}^T\mathbf{B}_s)^{-1}\mathbf{C}^T\mathbf{A}_s}{\varepsilon} & \frac{\mathbf{A}_f}{\varepsilon}\end{bmatrix}\mathbf{z}_d, \tag{5.22}$$

which is obtained from (3.13) by replacing $\mathbf{u}$ with $\mathbf{u}_{eq}$. As $(\mathbf{A}_s - \mathbf{B}_s(\mathbf{C}^T\mathbf{B}_s)^{-1}\mathbf{C}^T\mathbf{A}_s)$ is stable by design and $\frac{\mathbf{A}_f}{\varepsilon}$ is assumed to be stable, the sliding motion of (3.13) is stable. System formulation (3.13) is related to its original form (3.6) via linear transformation (3.14). Therefore, $\mathbf{s} = \mathbf{C}^T\mathbf{T}_z\mathbf{T}\mathbf{z}$ is also stable sliding surface for (3.6).

Now setting $\dot{\mathbf{s}} = 0$, equivalent control for system (3.6) can be obtained from (5.21) as

$$\mathbf{u}_{eq} = -(\mathbf{C}^T\mathbf{B}_s)^{-1}\mathbf{C}^T\begin{bmatrix}\mathbf{A}_s(\mathbf{E}_{n_1} - \varepsilon\mathbf{N}\mathbf{L}) & -\varepsilon\mathbf{A}_s\mathbf{N}\end{bmatrix}\mathbf{z}. \tag{5.23}$$

The control (5.23) satisfies only sliding condition for system (3.6), as proved in Lemma 5.1; however, reaching condition is satisfied by (5.13), where total control law is given by (5.12).

Lemma 5.2 *Full-order system (3.6) is asymptotically stable in sliding mode on sliding surface (5.19).*

Proof From (3.14), (5.16) and (5.19) sliding surface for full-order system (3.6) can be written as

$$\mathbf{s} = \mathbf{C}^T \left[\mathbf{E}_{n_1} - \varepsilon \mathbf{N}\mathbf{L} \; -\varepsilon \mathbf{N} \right] \mathbf{z}.$$

Now, choosing Lyapunov function as

$$V(s) = \frac{1}{2}\mathbf{s}^T\mathbf{s}, \tag{5.24}$$

$$\dot{V}(s) = -(\xi \mathbf{s}) sig(\mathbf{s}) sgn(\mathbf{s}) < 0 \tag{5.25}$$

for all $\mathbf{z} \neq 0$. The reaching condition is thus satisfied.

5.4 Application of SMC to AHWR System

Singularly perturbed model of AHWR, given in Sect. 3.4.1, is decoupled into slow subsystem of order 73 and fast subsystem of order 17 by using two-stage decomposition, discussed in Sect. 3.3.1. Eigenvalues of slow and fast subsystems are given in Tables 3.1 and 3.2. Since the fast subsystem is asymptotically stable, sliding mode control law can be constructed using only slow subsystem. For that the stable sliding surface for slow subsystem is designed and equivalent control is obtained as given below:

$$\mathbf{u}_{eq} = \mathbf{K}_{s,smc}\mathbf{z}_s, \tag{5.26}$$

where $\mathbf{K}_{s,smc} = -(\mathbf{C}^T\mathbf{B}_s)^{-1}\mathbf{C}^T\mathbf{A}_s$ is (4×73) gain matrix of slow subsystem, given by

$$\mathbf{K}_{s,smc} = \begin{bmatrix} 0.0119 & 0.0116 & 0.0104 & 0.0116 & 1.0046 & 0.5612 & 0.5873 & 0.5659 & 0.5107 \\ 0.0117 & 0.0133 & 0.0116 & 0.0117 & 1.0701 & 0.5600 & 0.6234 & 0.6389 & 0.5813 \\ 0.0104 & 0.0116 & 0.0119 & 0.0116 & 1.0046 & 0.5030 & 0.5474 & 0.5620 & 0.5416 \\ 0.0116 & 0.0117 & 0.0117 & 0.0133 & 1.0701 & 0.5562 & 0.5841 & 0.5783 & 0.5416 \end{bmatrix}$$

$$\begin{matrix} 0.5030 & 0.5474 & 0.5620 & 0.5416 & 0.4200 & 0.5049 & 0.4783 & 0.3713 & 0.3667 \\ 0.5562 & 0.5841 & 0.5783 & 0.5416 & 0.4090 & 0.5305 & 0.5490 & 0.4288 & 0.4131 \\ 0.5612 & 0.5873 & 0.5659 & 0.5107 & 0.3667 & 0.4609 & 0.4790 & 0.4069 & 0.4200 \\ 0.5600 & 0.6234 & 0.6389 & 0.5813 & 0.4131 & 0.4946 & 0.4875 & 0.3979 & 0.4090 \end{matrix}$$

$$\begin{matrix} 0.4609 & 0.4790 & 0.4069 & 0.0154 & 0.0142 & 0.0139 & 0.0089 & 0.0034 & 0.0011 \\ 0.4946 & 0.4875 & 0.3979 & 0.0165 & 0.0083 & 0.0142 & 0.0165 & 0.0132 & 0.0080 \\ 0.5049 & 0.4783 & 0.3713 & 0.0154 & 0.0011 & 0.0036 & 0.0086 & 0.0119 & 0.0142 \\ 0.5305 & 0.5490 & 0.4288 & 0.0165 & 0.0080 & 0.0045 & 0.0022 & 0.0031 & 0.0083 \end{matrix}$$

$$
\begin{bmatrix}
0.0036 & 0.0086 & 0.0119 & 0.0116 & 0.0120 & 0.0062 & 0.0005 & -0.0008 & 0.0013 \\
0.0045 & 0.0022 & 0.0031 & 0.0047 & 0.0113 & 0.0139 & 0.0097 & 0.0066 & 0.0029 \\
0.0139 & 0.0089 & 0.0034 & -0.0008 & 0.0013 & 0.0071 & 0.0102 & 0.0116 & 0.0120 \\
0.0142 & 0.0165 & 0.0132 & 0.0066 & 0.0029 & 0.0003 & 0.0016 & 0.0047 & 0.0113
\end{bmatrix}
$$

$$
\begin{bmatrix}
0.0071 & 0.0102 & -0.6269 & -0.0294 & -0.0168 & -0.0174 & -0.0164 & -0.0147 & -0.0144 \\
0.0003 & 0.0016 & -0.6515 & -0.0315 & -0.0165 & -0.0185 & -0.0190 & -0.0175 & -0.0164 \\
0.0062 & 0.0005 & -0.6269 & -0.0294 & -0.0144 & -0.0156 & -0.0163 & -0.0161 & -0.0168 \\
0.0139 & 0.0097 & -0.6515 & -0.0315 & -0.0164 & -0.0168 & -0.0166 & -0.0157 & -0.0165
\end{bmatrix}
$$

$$
\begin{bmatrix}
-0.0156 & -0.0163 & -0.0161 & -0.0126 & -0.0151 & -0.0139 & -0.0105 & -0.0103 & -0.0131 \\
-0.0168 & -0.0166 & -0.0157 & -0.0119 & -0.0158 & -0.0167 & -0.0127 & -0.0120 & -0.0143 \\
-0.0174 & -0.0164 & -0.0147 & -0.0103 & -0.0131 & -0.0139 & -0.0120 & -0.0126 & -0.0151 \\
-0.0185 & -0.0190 & -0.0175 & -0.0120 & -0.0143 & -0.0140 & -0.0114 & -0.0119 & -0.0158
\end{bmatrix}
$$

$$
\begin{bmatrix}
-0.0139 & -0.0120 & 0.0113 & 0.0307 & 0.0169 & 0.0125 & 0.0124 & 0.0113 & 0.0105 & 0.0118 \\
-0.0140 & -0.0114 & 0.0121 & 0.0152 & 0.0179 & 0.0272 & 0.0207 & 0.0143 & 0.0111 & 0.0104 \\
-0.0139 & -0.0105 & 0.0113 & 0.0113 & 0.0105 & 0.0118 & 0.0180 & 0.0307 & 0.0169 & 0.0125 \\
-0.0167 & -0.0127 & 0.0121 & 0.0143 & 0.0111 & 0.0104 & 0.0127 & 0.0152 & 0.0179 & 0.0272
\end{bmatrix}
$$

$$
\begin{bmatrix}
0.0180 & 0.0206 & 0.0181 & 0.0125 & 0.0096 & 0.0090 & 0.0104 & 0.0124 & 0.0152 \\
0.0127 & 0.0117 & 0.0174 & 0.0245 & 0.0154 & 0.0120 & 0.0113 & 0.0105 & 0.0103 \\
0.0124 & 0.0090 & 0.0104 & 0.0124 & 0.0152 & 0.0206 & 0.0181 & 0.0125 & 0.0096 \\
0.0207 & 0.0120 & 0.0113 & 0.0105 & 0.0103 & 0.0117 & 0.0174 & 0.0245 & 0.0154
\end{bmatrix}. \tag{5.27}
$$

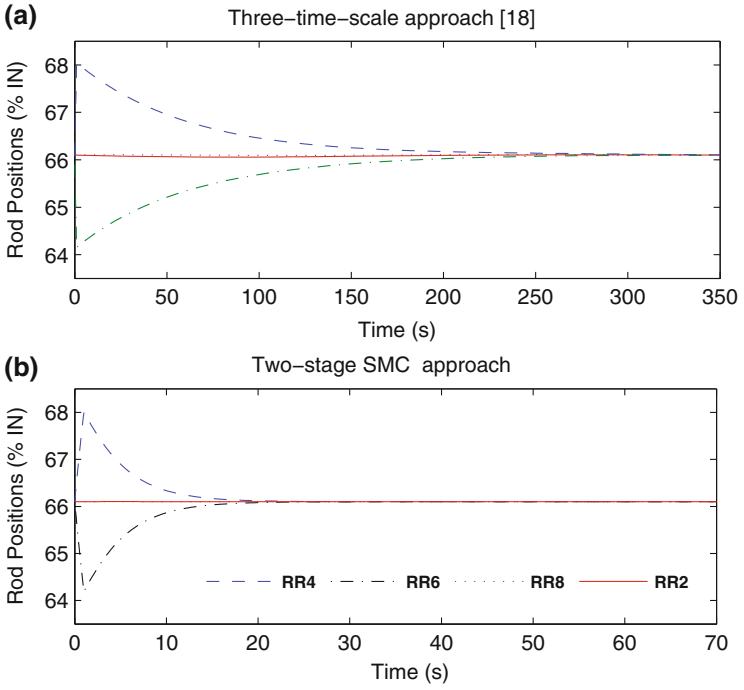

Fig. 5.1 Changes in regulating rod positions with three-time-scale [18] method and two-stage SMC approach

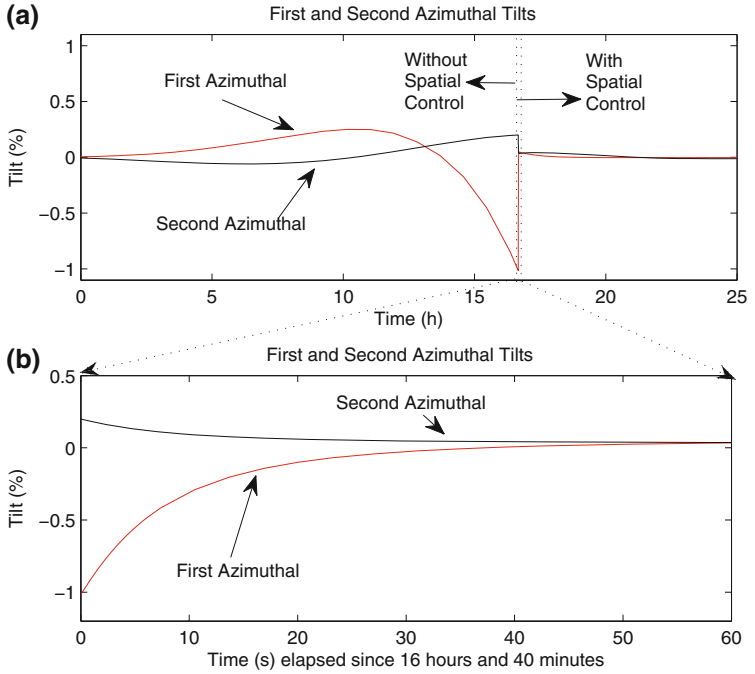

Fig. 5.2 Suppression of azimuthal tilts after introduction of spatial control

The maximum value of gain is observed to be 1.0701 and minimum value is −0.6515. This control is then represented into original states using (5.16) and (3.14). The equivalent control for original system of AHWR is then formulated as $\mathbf{K}_{smc}$. The reaching condition is given by (5.13). Combining these two, spatial control law is obtained as

$$\mathbf{u}_{sp} = \mathbf{K}_{smc} \begin{bmatrix} \mathbf{z}_1 \\ \mathbf{z}_2 \end{bmatrix} - (\mathbf{C}^T \mathbf{B}_s)^{-1} \xi sig(\mathbf{s}) sgn(\mathbf{s}), \tag{5.28}$$

where $\mathbf{K}_{smc} = -(\mathbf{C}^T \mathbf{B}_s)^{-1} \mathbf{C}^T \mathbf{A}_s \left[\mathbf{E}_{n_1} - \varepsilon \mathbf{NL} \; -\varepsilon \mathbf{N} \right]$ and $\mathbf{s}$ is the switching surface, given by

$$\mathbf{s} = \left[\mathbf{C}^T (\mathbf{E}_{n_1} - \varepsilon \mathbf{NL}) \right] \mathbf{z}_1 - \left(\varepsilon \mathbf{C}^T \mathbf{N} \right) \mathbf{z}_2.$$

In this case SMC is designed using merely slow subsystem states. For controller implementation this has been represented in terms of the original state variables using (5.28). Therefore, dimension of SMC gain matrix $\mathbf{K}_{smc}$ is obtained as (4×90), which indicates that the feedback of all the states is required for controller realization [15].

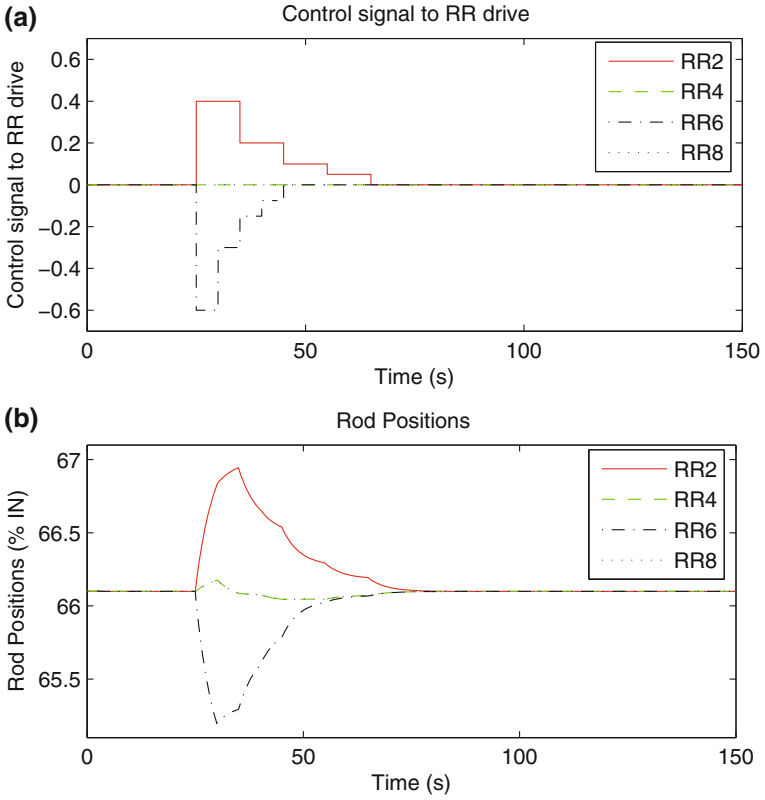

Fig. 5.3 Effect of change in control signal on regulating rod positions

5.4.1 Transient Simulations

The reactor was initially assumed to be working at full power steady-state condition. Suddenly, RR6, operating under automatic control, was moved out by about 2% by giving appropriate manual control signal and at the same time RR4 was moved in by 2%. Afterwards, these RRs were left at their new positions under the influence of automatic control. The control signals to RR drives were generated by combining (3.30) and (5.28). Vectorized nonlinear model of the AHWR developed from (2.26) to (2.32) is simulated for 10 ms step size. Simulation results generated are depicted in Fig. 5.1. As a result of controller action, RRs were driven back to their steady-state positions (Fig. 5.1b). Performance of the controller is compared with the three-time-scale composite controller [18] for the same transient. It is observed that both the controllers are forcing RRs back to their equilibrium positions but time needed to do so is relatively less in the recommended controller.

Figure 5.2 depicts response of closed-loop system when one more transient is initiated. In this case, RR2 was taken out and RR4 was moved in by 1% manually,

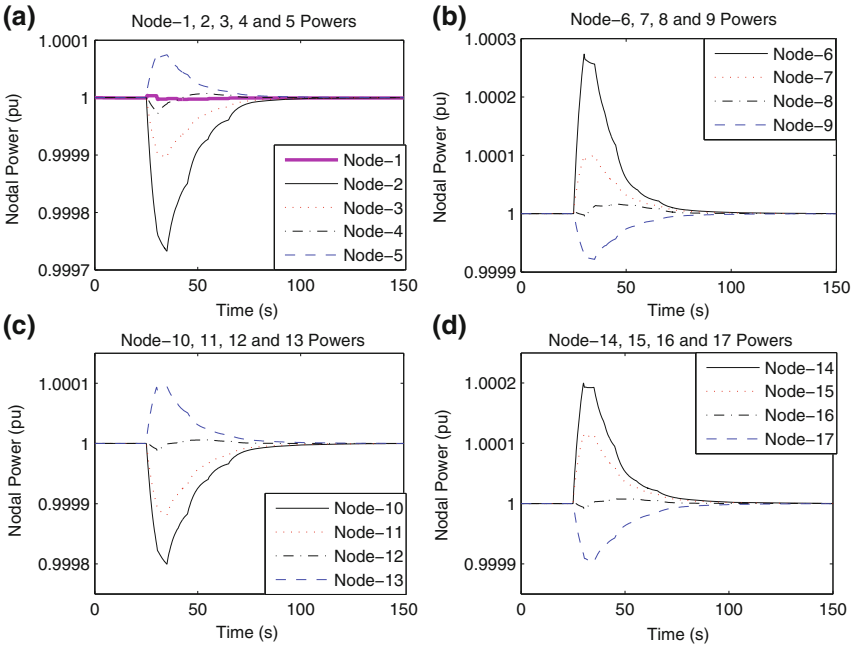

Fig. 5.4 Deviations in nodal powers due to changes in RR2 and RR6 positions

immediately after that these RRs were driven back to their initial positions respectively and transferred under the control action of (3.30), which is based on total power feedback alone. As a result of this transient and at the same time as the control is based on total power feedback alone, the azimuthal tilts started growing. The spatial power feedback control given by (5.28) was brought in the overall control after about 16 h and 40 min. Figure 5.2a illustrates the variations in first and second azimuthal tilts and Fig. 5.2b represents a zoomed version, highlighting the region near the introduction of spatial control. It was noticed that azimuthal tilts are suppressed within 50 s. Moreover, when control signal as given in Fig. 5.3a is applied to the RRs, the corresponding variations are seen to be as depicted in Fig. 5.3b. This action resulted into the perturbation in spatial power distribution, which was suppressed by the spatial controller in about 70 s, as shown in Fig. 5.4a–d.

5.5 Conclusion

In this chapter, spatial control of AHWR is achieved using sliding mode by two-stage decomposition. First of all AHWR system is decoupled into slow and fast subsystems and the SMC is devised using slow subsystem states. Afterwards, SMC for full-order system is constructed using linear transformation matrices. Efficacy

of the recommended controller is tested via simulations carried out under various transients with step time of 10 ms. It is noticed that the controller is stabilizing the spatial oscillations and nodal power variations instantly.

This control technique along with the technique discussed in previous Chap. 3 are based on two-stage decomposition. In both the methods controllers are designed using slow subsystem and represented into original states. Hence, these methods utilize the feedback of all the state variables.

References

1. Ahmed, A.E., Schwartz, H.M., Aitken, V.C.: Sliding mode control for singularly perturbed system. Proc. Asian Control Conf. **3**, 1946–1950 (2004)
2. Ansarifar, G.R., Rafiei, M.: Second-order sliding-mode control for a pressurized water nuclear reactor considering the xenon concentration feedback. Nucl. Eng. Technol. **47**, 94–101 (2015)
3. Ansarifar, G.R., Saadatzi, S.: Sliding mode control for pressurized-water nuclear reactors in load following operations with bounded xenon oscillations. Ann. Nucl. Energy **76**, 209–217 (2015)
4. Bandyopadhyay, B., G'Egziabher, A., Janardhanan, S., Victor, S.: Sliding mode control design via reduced order model approach. Int. J. Autom. Comput. **4**(4), 329–334 (2007)
5. Decarlo, R., Zak, S.H., Matthews, G.O.: Variable structure control of nonlinear multivariable systems: a tutorial. Proc. IEEE **76**(3), 212–232 (1988)
6. Edwards, C., Spurgeon, S.K.: Sliding Mode Control: Theory and Applications. Taylor & Francis, London (1998)
7. Eom, M., Chwa, D.: Adaptive integral sliding mode control for nuclear research reactor with system uncertainties and input perturbation. Electr. Lett. **52**, 272–274 (2016)
8. Furuta, K., Pan, Y.: Variable structure control with sliding sector. Automatica **36**, 211–228 (2000)
9. Heck, B.S.: Sliding mode for singularly perturbed systems. Int. J. Control **53**(4), 985–1001 (1991)
10. Hung, J.Y., Gao, W., Hung, J.C.: Variable structure control: a survey. IEEE Trans. Ind. Electron. **40**, 2–22 (1993)
11. Innocenti, M., Greco, L., Pollini, L.: Sliding mode control for two-time-scale systems: stability issues. Automatica **39**(2), 273–280 (2003)
12. Li, T.-H.S., Huang, J.-J.: Simplex sliding mode control of singular perturbation systems. Proc. IEEE Ind. Electron. Control Instrum. **2**, 742–747 (1995)
13. Li, T.-H.S., Lin, J.-L., Kung, F.-C.: Composite sliding mode control of singular perturbation systems. Proc. Am. Control Conf. **3**, 2248–2249 (1995)
14. Munje, R.K., Musmade, B.B., Parkhe, J.G., Patre, B.M.: Sliding mode control for three-time-scale system with matched disturbances. Proc. Ann. IEEE India Conf., pp. 421–434 (2012)
15. Munje, R.K., Patre, B.M., Shimjith, S.R., Tiwari, A.P.: Sliding mode control for spatial stabilization of advanced heavy water reactor. IEEE Trans. Nucl. Sci. **60**, 3040–3050 (2013)
16. Nguyen, T., Su, W-C., Gajic, Z.: Sliding mode control for singularly perturbed linear continuous time systems: composite control approaches. IEEE Int. Symp. Comput.-Aided Control Syst. Des., pp. 1946–1950 (2010)
17. Nguyen, T., Su, W.-C., Gajic, Z.: Variable structure control for singularly perturbed linear continuous systems with matched disturbance. IEEE Trans. Autom. Control **57**(3), 777–783 (2012)
18. Shimjith, S.R., Tiwari, A.P., Bandyopadhyay, B.: A three-time-scale approach for design of linear state regulator for spatial control of advanced heavy water reactor. IEEE Trans. Nucl. Sci. **58**(3), 1264–1276 (2011)

19. Slotin, J.: Sliding mode control design for nonlinear systems. Int. J. Control **40**, 421–434 (1984)
20. Utkin, V.I.: Variable structure systems with sliding modes. IEEE Trans. Autom. Control **22**, 212–222 (1977)
21. Utkin, V.I., Guldner, J., Shi, J.: Sliding Mode Control in Electromechanical Systems. Taylor & Francis, Bristol (1999)
22. Young, K.D., Utkin, V.I., Ozguner, U.: A control engineers guide to sliding mode control. IEEE Trans. Control Syst. Technol. **7**(3), 328–342 (1999)
23. Yue, D., Xu, S.: Sliding mode control of singular perturbation systems. Proc. IEEE Int. Conf. Syst. Man Cybern. **1**, 113–116 (1996)

Chapter 6
Fast Output Sampling Technique

6.1 Introduction

A standard result in control theory states that, the poles of a linear time-invariant controllable system can be assigned arbitrarily by state feedback. However, if all the states are not directly available for feedback, one usually resorts to dynamic output feedback provided the system is observable. Arbitrary pole assignment by static output feedback is still an open problem in control theory [8]. In [2], it is shown that, if a system is controllable and observable, then for almost all output sampling rates, any self-conjugate pole configuration can be assigned to the discrete-time closed loop system by piecewise constant output feedback, provided the number of gain changes is not less than the system's controllability index. Multirate Output Feedback (MROF) is the concept of sampling the system input and system output at different rates.

In the recent past, fast output sampling (FOS) control technique, a method which utilizes only the system output for feedback, has emerged as a promising candidate for control of sampled data control systems. In this method, the control signal is constrained to be a linear function of multirate output observation of the output signal. The control signal is kept constant over one discretizing interval and altered only at the input sampling intervals. The output is sampled at faster rate than the control input rate. The number of output sampling intervals is not less than observability index of system and input signal is constructed from these output observations. It was shown by Werner and Furuta [10] that if a system is controllable and observable, then for all sampling rates any self-conjugate pole configuration can be assigned to the closed loop system by non-dynamic multirate output feedback, provided the number of gain changes is not less than observability index. Since the feedback gains are piecewise constant, their method could be easily implemented and indicate a new possibility. Such a control law can stabilize much larger class of systems than static output feedback. Design of FOS-based controller for two-time-scale system is given in [6, 9]. Control technique presented in [9] is extended for three-time-scale system by Shimjith et al. [7]. In this, FOS control gain for a three-time-scale system is obtained by combining the solutions of the three subsystem problems, obtained separately. Since three smaller order subsystem problems are to be solved in lieu of

R. Munje et al., *Investigation of Spatial Control Strategies with Application to Advanced Heavy Water Reactor*, Energy Systems in Electrical Engineering, https://doi.org/10.1007/978-981-10-3014-7_6

one high order problem, numerical ill-conditioning is completely avoided.

In contrast to the preceding chapters in which treatise was based on continuous-time approach, in this and subsequent chapters attention is shifted to discrete-time system approach. Fast output sampling based controller is examined for Advanced Heavy Water Reactor (AHWR) using two-stage decomposition. By means of two-stage decomposition approach, the initial system of AHWR is first decoupled into slow and fast subsystems. After that state feedback gain is obtained for slow subsystem alone and is taken zero for fast subsystem. A composite controller is derived, which is then implemented using FOS feedback gain. Further the performance of the controller is compared with the controller recommended in [7].

6.2 Fast Output Sampling

In FOS, the system state information is calculated from the system output by multi-rate observations. The control input is maintained constant throughout the sampling interval τ [7, 10] as depicted in Fig. 6.1. When the system (3.1)–(3.2) is sampled at the rate of $1/\tau$, the corresponding discrete-time system is

$$\mathbf{z}_{k+1} = \Phi_\tau \mathbf{z}_k + \Gamma_\tau \mathbf{u}_k, \tag{6.1}$$

$$\mathbf{y}_k = \mathbf{M}\mathbf{z}_k \tag{6.2}$$

where $\Phi_\tau = e^{\mathbf{A}\tau}$ and $\Gamma_\tau = \int_0^\tau e^{\mathbf{A}s}\mathbf{B}ds$. Also let

$$\mathbf{z}_{k+1} = \Phi_\Delta \mathbf{z}_k + \Gamma_\Delta \mathbf{u}_k \tag{6.3}$$

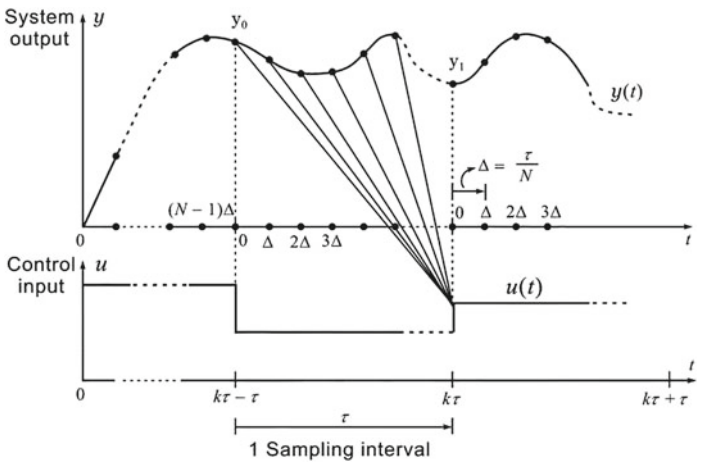

Fig. 6.1 Illustration of FOS feedback

be the discrete-time system equivalent to the system (3.1) sampled at the rate of $1/\Delta$, where $\Delta = \tau/N$. Let μ denote the observability index [1] of $(\Phi, \mathbf{M})$ and $N \geq \mu$. The system matrices of the τ system and Δ system have the relation

$$\Phi_\tau = \Phi_\Delta^N \text{ and } \Gamma_\tau = \sum_{i=0}^{N-1} \Phi_\Delta^i \Gamma_\Delta.$$

In FOS, output measurements are taken at time instants $t = l\Delta, l = 0, 1, \ldots, N-1$. The control input during the interval $k\tau < t \leq (k+1)\tau$ is formulated as a linear combination of the last N output observations. Let $\mathbf{F}$ be an original state feedback gain so that the closed loop system $(\Phi_\tau + \Gamma_\tau \mathbf{F})$ has no eigenvalues at the origin. In that case, one can characterize a fictitious measurement matrix as

$$\bar{\mathbf{M}} = (\mathbf{M_0} + \mathbf{D_0}\mathbf{F})(\Phi_\tau + \Gamma_\tau \mathbf{F})^{-1} \tag{6.4}$$

which satisfies the fictitious measurement equation $\mathbf{y}_k = \bar{\mathbf{M}}\mathbf{z}_k$, where $\mathbf{M_0}$ and $\mathbf{D_0}$ are given [9] as

$$\mathbf{M_0} = \begin{bmatrix} \mathbf{M} \\ \mathbf{M}\Phi_\Delta \\ \mathbf{M}\Phi_\Delta^2 \\ \vdots \\ \mathbf{M}\Phi_\Delta^{N-1} \end{bmatrix}, \qquad \mathbf{D_0} = \begin{bmatrix} \mathbf{0} \\ \mathbf{M}\Gamma_\Delta \\ \mathbf{M}\Phi_\Delta\Gamma_\Delta + \mathbf{M}\Gamma_\Delta \\ \vdots \\ \mathbf{M}\Sigma_{i=0}^{N-2}\Phi_\Delta^i\Gamma_\Delta \end{bmatrix}.$$

The structure of control law is

$$\mathbf{u}(t) = \mathbf{L}\mathbf{y}_k, \qquad k\tau < t \leq (k+1)\tau. \tag{6.5}$$

For $\mathbf{L}$ to realize the effect of $\mathbf{F}$, it must satisfy

$$\mathbf{z}_{k+1} = (\Phi_\tau + \Gamma_\tau \mathbf{F})\mathbf{z}_k = (\Phi_\tau + \Gamma_\tau \mathbf{L}\bar{\mathbf{M}})\mathbf{z}_k \tag{6.6}$$

that is,

$$\mathbf{L}\bar{\mathbf{M}} = \mathbf{F}. \tag{6.7}$$

For $N \geq \mu$, the matrix $\bar{\mathbf{M}}$ has full rank and that for $N = \mu$, $\mathbf{L}$ is uniquely calculated from (6.7). On the other hand, if $N > \mu$, $\mathbf{L}$ so found is not unique. Whatsoever is the condition, $\mathbf{L}$ found from (6.7) realizes the state feedback gain $\mathbf{F}$ [9].

At time $t = 0$, the control input $\mathbf{u}(t) = u_0$ for $0 < t \leq \tau$, cannot be calculated from (6.5) because the output measurements are unavailable for $t < 0$. But, u_0 can be arbitrarily chosen if the eigenvalues of $(\mathbf{L}\mathbf{D_0} - \mathbf{F}\Gamma_\tau)$ are in unit circle in z-plane as under this condition, the initial error in input will slowly disappear [7, 9].

6.3 Fast Output Sampling Controller for Two-Time-Scale System

The presence of slow and fast dynamics makes the system ill-conditioned. Designing $\mathbf{F}$ and later $\mathbf{L}$ from (6.7) for such systems is a tough task. However, the problem can be easily solved by singular perturbation approach. In this the original system is decoupled into slow and fast subsystems and controller design for original system is carried out by using subsystem controller designs. Now, for determining $\mathbf{L}$ for (3.6), the corresponding system is discretized with sampling period τ as

$$\begin{bmatrix} \mathbf{z}_{1,k+1} \\ \mathbf{z}_{2,k+1} \end{bmatrix} = \begin{bmatrix} \Phi_{11} & \Phi_{12} \\ \Phi_{21} & \Phi_{22} \end{bmatrix} \begin{bmatrix} \mathbf{z}_{1,k} \\ \mathbf{z}_{2,k} \end{bmatrix} + \begin{bmatrix} \Gamma_1 \\ \Gamma_2 \end{bmatrix} \mathbf{u}_k, \tag{6.8}$$

$$\mathbf{y}_k = \begin{bmatrix} \mathbf{M}_1 & \mathbf{M}_2 \end{bmatrix} \begin{bmatrix} \mathbf{z}_{1,k}^T & \mathbf{z}_{2,k}^T \end{bmatrix}^T \tag{6.9}$$

where

$$\begin{bmatrix} \Phi_{11} & \Phi_{12} \\ \Phi_{21} & \Phi_{22} \end{bmatrix} = e^{\mathbf{A}\tau} \text{ and } \begin{bmatrix} \Gamma_1 \\ \Gamma_2 \end{bmatrix} = \int_0^\tau e^{\mathbf{A}s} \mathbf{B} ds$$

and recall that

$$\mathbf{A} = \begin{bmatrix} \mathbf{A}_{11} & \mathbf{A}_{12} \\ \frac{\mathbf{A}_{21}}{\epsilon} & \frac{\mathbf{A}_{22}}{\epsilon} \end{bmatrix} \text{ and } \mathbf{B} = \begin{bmatrix} \mathbf{B}_1 \\ \frac{\mathbf{B}_2}{\epsilon} \end{bmatrix}.$$

System (6.8)–(6.9) is decoupled into slow and fast subsystems [4, 5] and represented as

$$\begin{bmatrix} \mathbf{z}_{s,k+1} \\ \mathbf{z}_{f,k+1} \end{bmatrix} = \begin{bmatrix} \Phi_{\tau s} & 0 \\ 0 & \Phi_{\tau f} \end{bmatrix} \begin{bmatrix} \mathbf{z}_{s,k} \\ \mathbf{z}_{f,k} \end{bmatrix} + \begin{bmatrix} \Gamma_{\tau s} \\ \Gamma_{\tau f} \end{bmatrix} \mathbf{u}_k, \tag{6.10}$$

$$\mathbf{y}_k = \begin{bmatrix} \mathbf{M}_s & \mathbf{M}_f \end{bmatrix} \begin{bmatrix} \mathbf{z}_{s,k}^T & \mathbf{z}_{f,k}^T \end{bmatrix}^T \tag{6.11}$$

where $\mathbf{z}_s \in \Re^{n_1}$ and $\mathbf{z}_f \in \Re^{n_2}$ denote the slow and fast states, respectively. Such decoupling of continuous-time system is discussed in Sect. 3.3.1. States $\mathbf{z}_{s,k}$ and $\mathbf{z}_{f,k}$ are related to $\mathbf{z}_{1,k}$ and $\mathbf{z}_{2,k}$ through transformation matrix $\mathbf{T} \in \Re^{n \times n}$, such that

$$\begin{bmatrix} \mathbf{z}_{s,k}^T & \mathbf{z}_{f,k}^T \end{bmatrix}^T = \mathbf{T} \begin{bmatrix} \mathbf{z}_{1,k}^T & \mathbf{z}_{2,k}^T \end{bmatrix}^T. \tag{6.12}$$

Likewise block diagonalized discrete-time system for the sampling interval Δ can be given by

$$\begin{bmatrix} \mathbf{z}_{s,k+1} \\ \mathbf{z}_{f,k+1} \end{bmatrix} = \begin{bmatrix} \Phi_{\Delta s} & 0 \\ 0 & \Phi_{\Delta f} \end{bmatrix} \begin{bmatrix} \mathbf{z}_{s,k} \\ \mathbf{z}_{f,k} \end{bmatrix} + \begin{bmatrix} \Gamma_{\Delta s} \\ \Gamma_{\Delta f} \end{bmatrix} \mathbf{u}_k. \tag{6.13}$$

Now the composite state feedback gain for (6.10) can be found by the method described in Appendix A, as

$$\mathbf{F} = \begin{bmatrix} \mathbf{F}_1 & \mathbf{F}_2 \end{bmatrix} = \begin{bmatrix} \mathbf{F}_s & \mathbf{F}_f \end{bmatrix} \mathbf{T}_3 \tag{6.14}$$

where $\mathbf{F}_s$ and $\mathbf{F}_f$ are the state feedback gains for slow and fast subsystems, respectively, and $\mathbf{T}_3$ is appropriate transformation matrix (see Appendix A, for details). From (6.13) the equations for $\mathbf{M_0}$, $\mathbf{D_0}$ can be obtained and $(\mathbf{M_0} + \mathbf{D_0F})$ and $\mathbf{L}$ can be represented as

$$\mathbf{M_0} + \mathbf{D_0F} = \begin{bmatrix} \mathbf{M}_{s1} & \mathbf{M}_{f1} \\ \mathbf{M}_{s2} & \mathbf{M}_{f2} \end{bmatrix}, \qquad \mathbf{L} = \begin{bmatrix} \mathbf{L_f} & \mathbf{L_s} \end{bmatrix} \tag{6.15}$$

where $\mathbf{M}_{s1}$, $\mathbf{M}_{s2}$, $\mathbf{M}_{f1}$, and $\mathbf{M}_{f2}$ are respectively $(\mu_f p \times n_1)$, $((N - \mu_f)p \times n_1)$, $(\mu_f p \times n_2)$ and $((N - \mu_f)p \times n_1)$ submatrics. Similarly, $\mathbf{L_f}$ and $\mathbf{L_s}$ are respectively $(m \times \mu_f p)$, and $(m \times (N - \mu_f)p)$ submatrics, where μ_s and μ_f are respectively the observability indices of the slow and fast subsystems. From (6.4) and (6.7)

$$\mathbf{L}(\mathbf{M_0} + \mathbf{D_0F}) = \mathbf{F}(\Phi_\tau + \Gamma_\tau \mathbf{F}) \tag{6.16}$$

which can be manipulated using (6.10), (6.14), and (6.15) to get the following slow and fast subsystems FOS gains:

$$\mathbf{L_s} = (\tilde{\mathbf{F}}_1 - \tilde{\mathbf{F}}_2 \mathbf{M}_{f1}^{-1} \mathbf{M}_{s1})(\mathbf{M}_{s2} - \mathbf{M}_{f2} \mathbf{M}_{f1}^{-1} \mathbf{M}_{s1})^{-1}, \tag{6.17}$$

$$\mathbf{L_f} = (\tilde{\mathbf{F}}_2 - \mathbf{L_s} \mathbf{M}_{f2}) \mathbf{M}_{f1}^{-1} \tag{6.18}$$

where

$$\tilde{\mathbf{F}}_1 = \mathbf{F}_1(\Phi_{\tau_s} + \Gamma_{\tau_s} \mathbf{F}_1) + \mathbf{F}_2 \Gamma_{\tau_f} \mathbf{F}_1, \tag{6.19}$$

$$\tilde{\mathbf{F}}_2 = \mathbf{F}_2(\Phi_{\tau_f} + \Gamma_{\tau_f} \mathbf{F}_2) + \mathbf{F}_1 \Gamma_{\tau_s} \mathbf{F}_2. \tag{6.20}$$

$\mathbf{L}$ is exact solution of (6.7), consequently for system (6.6) the control (6.5) gives the same performance as the state feedback gain $\mathbf{F}$ does to it [9]. As, output measurements are not available for $t < 0$, u_0 can be chosen arbitrarily if

$$|\varphi(\mathbf{L D_0} - \mathbf{F}_1 \Gamma_{\tau s} - \mathbf{F}_2 \Gamma_{\tau f})| < 1. \tag{6.21}$$

Then, any error in control input due to unknown initial conditions will slowly vanish [9].

Remark 6.1 Since, the eigenvalues of $\Phi_{\Delta f}$ are very small, $\Phi_{\Delta f}$, $\Phi_{\Delta f}^2, \ldots$ would be very small. Thus, $\mathbf{M}_{f2}$ can be made zero. Further, if the fast subsystem is stable, then FOS gains in (6.15) change to $\bar{\mathbf{L}} = \begin{bmatrix} \mathbf{0} & \bar{\mathbf{L}}_\mathbf{s} \end{bmatrix}$, where $\bar{\mathbf{L}}_\mathbf{s}$ is given by

$$\bar{\mathbf{L}}_\mathbf{s} = \mathbf{F}_s(\Phi_{\tau s} + \Gamma_{\tau s} \mathbf{F}_s) \mathbf{M}_{s2}^{-1}. \tag{6.22}$$

This is obtained by setting $\mathbf{F}_f = 0$ and hence $\mathbf{F}_2 = \mathbf{0}$. However, $\bar{\mathbf{L}}$ must also satisfy (6.21) with $\mathbf{F}_2 = \mathbf{0}$ for making error in control input to vanish slowly.

6.4 Application of FOS to AHWR Model

The model of AHWR given by (3.31) is discretized to get

$$\mathbf{z}_{k+1} = \Phi_\tau \mathbf{z}_k + \Gamma_\tau \mathbf{u}_k + \Gamma_{\tau fw} \delta q_{fwk} \tag{6.23}$$

where $\Phi_\tau = e^{\hat{\mathbf{A}}\tau}$, $\Gamma_\tau = \int_0^\tau e^{\hat{\mathbf{A}}s}\mathbf{B}ds$ and $\Gamma_{\tau fw} = \int_0^\tau e^{\hat{\mathbf{A}}s}\mathbf{B}_{fw}ds$. The discrete system (6.23) exhibits two-time-scale property for sampling period ≥ 9 s. Therefore, the Δ is selected as 9 s, and equivalent discrete-time model is partitioned into slow and fast subsystems with dimensions 73 and 17 respectively. Observability indices of slow and fast subsystems are respectively noted to be $\mu_s = 5$ and $\mu_f = 1$ and that of original system as 6. Thus N is chosen as 6 and τ as 54 s. The system (3.31) is discretized with τ sampling interval and resulting system too is decoupled into slow and fast subsystems. Fast subsystem eigenvalues are observed to be at origin, while the slow subsystem eigenvalues are mentioned in Table 6.1, with highlighted

Table 6.1 Eigenvalues of slow subsystem ($\Phi_{\tau s}$)

Sr. No.	Eigenvalues	Sr. No.	Eigenvalues	Sr. No.	Eigenvalues
1	6.0957×10^{-5}	25	3.5484×10^{-2}	50	9.9845×10^{-1}
2	6.1378×10^{-5}	26	3.7925×10^{-2}	51	9.9845×10^{-1}
3	6.1527×10^{-5}	27	3.8557×10^{-2}	52	9.9845×10^{-1}
4	6.1548×10^{-5}	28	3.9904×10^{-2}	53	9.9845×10^{-1}
5	1.5702×10^{-4}	29	4.0008×10^{-2}	54	9.9887×10^{-1}
6	1.5775×10^{-4}	30	4.4194×10^{-2}	55	9.9887×10^{-1}
7	1.5811×10^{-4}	31	4.4615×10^{-2}	56	9.9887×10^{-1}
8	1.5815×10^{-4}	32	6.4933×10^{-2}	57	9.9887×10^{-1}
9	2.2811×10^{-4}	33	6.5723×10^{-2}	58	9.9887×10^{-1}
10	2.2943×10^{-4}	34	4.2577×10^{-1}	59	9.9887×10^{-1}
11	2.3017×10^{-4}	35–36	$(6.5415 \pm j6.3142) \times 10^{-1}$	60	9.9887×10^{-1}
12	2.3021×10^{-4}	37	9.9845×10^{-1}	61	9.9887×10^{-1}
13	3.6970×10^{-4}	38	9.9845×10^{-1}	62	9.9887×10^{-1}
14	3.7071×10^{-4}	39	9.9845×10^{-1}	63	9.9887×10^{-1}
15	3.7197×10^{-4}	40	9.9845×10^{-1}	64	9.9887×10^{-1}
16	3.7200×10^{-4}	41	9.9845×10^{-1}	65	9.9887×10^{-1}
17	1.9509×10^{-3}	42	9.9845×10^{-1}	66	9.9887×10^{-1}
18	3.3515×10^{-2}	43	9.9845×10^{-1}	67	9.9887×10^{-1}
19	3.3567×10^{-2}	44	9.9845×10^{-1}	68	9.9887×10^{-1}
20	3.4040×10^{-2}	45	9.9845×10^{-1}	69	$1.0010 \pm j4.7915 \times 10^{-4}$
21	3.4320×10^{-2}	46	9.9845×10^{-1}	70	$1.0011 \pm j2.6259 \times 10^{-4}$
22	3.4468×10^{-2}	47	9.9845×10^{-1}	71	1.0000
23	3.4809×10^{-2}	48	9.9845×10^{-1}	72	1.0000
24	3.5305×10^{-2}	49	9.9845×10^{-1}	73	1.0000

unstable eigenvalues. Using the procedure discussed in the Appendix A, a composite state feedback gain matrix is calculated for (6.10) in order to place the slow subsystem eigenvalues at preferred locations. Since the fast subsystem eigenvalues are already at origin, state feedback is not devised for the same. The FOS gain matrices $\mathbf{L_f}$ and $\mathbf{L_s}$, respectively of dimensions (4×17) and (4×73), are calculated using these subsystem gains and the subsystem matrices corresponding to the system (6.3). $\mathbf{L_f}$ and $\mathbf{L_s}$ are respectively given by

$$\mathbf{L}_f = \begin{bmatrix} 0 \cdots 0 \\ 0 \cdots 0 \\ 0 \cdots 0 \\ 0 \cdots 0 \end{bmatrix}, \tag{6.24}$$

$$\mathbf{L}_s = \begin{bmatrix} 9.0179 & -1.7628 & 1.0299 & 2.8958 & -2.4612 & -0.5893 & 0.6912 & 2.9414 \\ 9.4174 & -0.8632 & 1.2608 & 1.8747 & -2.4210 & -0.8257 & 0.7085 & 3.2260 \\ 9.0179 & -0.5893 & 0.6912 & 2.9414 & -2.3920 & -1.7628 & 1.0299 & 2.8958 \\ 9.4174 & -0.8257 & 0.7085 & 3.2260 & -2.5613 & -0.8632 & 1.2608 & 1.8747 \end{bmatrix}$$

$$\begin{matrix} -2.3920 & 2.2120 & 0.3186 & -0.6533 & 1.4550 & 1.0898 & 0.0469 & -0.6340 \\ -2.5613 & 1.0569 & 0.1501 & 0.6421 & 1.8876 & 1.0715 & 0.0208 & -0.6362 \\ -2.4612 & 1.0898 & 0.0469 & -0.6340 & 1.6954 & 2.2120 & 0.3186 & -0.6533 \\ -2.4210 & 1.0715 & 0.0208 & -0.6362 & 1.4935 & 1.0569 & 0.1501 & 0.6421 \end{matrix}$$

$$\begin{matrix} 1.6954 & -31.7079 & -0.6961 & -6.2013 & -17.4552 & 4.9850 & -7.4895 & -4.3938 \\ 1.4935 & -33.0719 & -6.2783 & -7.5908 & -11.1347 & 3.5526 & -6.4262 & -4.5134 \\ 1.4550 & -31.7079 & -7.4895 & -4.3938 & -17.6005 & 3.9773 & -0.6961 & -6.2013 \\ 1.8876 & -33.0719 & -6.4262 & -4.5134 & -19.4147 & 5.2192 & -6.2783 & -7.5908 \end{matrix}$$

$$\begin{matrix} -17.6005 & 3.9773 & -10.0946 & -4.0485 & 1.7283 & -6.5549 & -4.0465 & -2.3089 \\ -19.4147 & 5.2192 & -3.7503 & -3.0667 & -6.1627 & -8.4800 & -3.8488 & -2.2204 \\ -17.4552 & 4.9850 & -4.0465 & -2.3089 & 1.6079 & -7.6143 & -10.0946 & -4.0485 \\ -11.1347 & 3.5526 & -3.8488 & -2.2204 & 1.5439 & -6.6996 & -3.7503 & -3.0667 \end{matrix}$$

$$\begin{matrix} 1.6079 & -7.6143 & 27.1815 & 13.8733 & 13.4419 & 25.5601 & 6.9274 & 21.3629 \\ 1.5439 & -6.6996 & 28.2744 & 20.4578 & 15.2662 & 18.9042 & 9.3666 & 20.6132 \\ 1.7283 & -6.5549 & 27.1815 & 21.3629 & 11.8021 & 25.6739 & 8.2620 & 13.8733 \\ -6.1627 & -8.4800 & 28.2744 & 20.6132 & 12.1440 & 27.9029 & 7.0790 & 20.4578 \end{matrix}$$

$$\begin{matrix} 11.8021 & 25.6739 & 8.2620 & 15.8863 & 12.4952 & 6.2797 & 12.8215 & 10.1640 \\ 12.1440 & 27.9029 & 7.0790 & 9.9636 & 11.7936 & 15.0631 & 14.6993 & 10.1063 \\ 13.4419 & 25.5601 & 6.9274 & 10.1640 & 10.7741 & 6.4258 & 13.5747 & 15.8863 \\ 15.2662 & 18.9042 & 9.3666 & 10.1063 & 10.9242 & 6.7574 & 13.1198 & 9.9636 \end{matrix}$$

$$\begin{matrix} 10.7741 & 6.4258 & 13.5747 & 7.0087 & -15.5062 & -13.6269 & -2.1135 & -21.4116 \\ 10.9242 & 6.7574 & 13.1198 & 7.3767 & -11.0564 & -13.1705 & -9.4905 & -20.4774 \\ 12.4952 & 6.2797 & 12.8215 & 7.0087 & -9.4751 & -15.6926 & -2.0954 & -20.1321 \\ 11.7936 & 15.0631 & 14.6993 & 7.3767 & -11.0461 & -16.1665 & -0.8352 & -22.1016 \end{matrix}$$

$$\begin{matrix} -9.4751 & -15.6926 & -2.0954 & -20.1321 & -10.5580 & -15.3444 & -20.8889 & -13.8505 \\ -11.0461 & -16.1665 & -0.8352 & -22.1016 & -18.0174 & -17.2686 & -13.9233 & -12.8942 \\ -15.5062 & -13.6269 & -2.1135 & -21.4116 & -17.1904 & -17.4828 & -20.8310 & -12.6845 \\ -11.0564 & -13.1705 & -9.4905 & -20.4774 & -18.0499 & -18.1411 & -21.3344 & -14.2694 \end{matrix}$$

$$
\begin{bmatrix}
-17.1904 & -17.4828 & -20.8310 & -12.6845 & -11.4877 & 4.0984 & 5.3639 & -8.8781 \\
-18.0499 & -18.1411 & -21.3344 & -14.2694 & -11.9842 & -2.2508 & 4.2417 & -0.1469 \\
-10.5580 & -15.3444 & -20.8889 & -13.8505 & -11.4877 & -3.8004 & 7.6001 & -8.9101 \\
-18.0174 & -17.2686 & -13.9233 & -12.8942 & -11.9842 & -2.3061 & 7.8344 & -10.8701 \\
11.9675 & -3.8004 & 7.6001 & -8.9101 & 10.2923 & 2.5595 & 6.5862 & 13.5410 \\
9.9866 & -2.3061 & 7.8344 & -10.8701 & 12.3717 & 10.7526 & 8.3986 & 4.3875 \\
10.2923 & 4.0984 & 5.3639 & -8.8781 & 11.9675 & 9.9885 & 8.9778 & 13.4383 \\
12.3717 & -2.2508 & 4.2417 & -0.1469 & 9.9866 & 10.7264 & 9.4237 & 13.6761 \\
6.1347 & 9.9885 & 8.9778 & 13.4383 & 5.0343 & & & \\
4.7928 & 10.7264 & 9.4237 & 13.6761 & 6.3615 & & & \\
5.0343 & 2.5595 & 6.5862 & 13.5410 & 6.1347 & & & \\
6.3615 & 10.7526 & 8.3986 & 4.3875 & 4.7928 & & &
\end{bmatrix}. \tag{6.25}
$$

From (6.24) and (6.25), it may be observed that the gains of fast subsystem are all zeros, and the maximum values of the gains for the slow subsystem is 28, which appears to be good enough for practical realization. The closed-loop eigenvalues, mentioned in Table 6.2, of the full-order system with these gains are exactly same to those with state feedback and are observed to be stable. It can also be confirmed that the eigenvalues of (6.21) are in the unit circle in the z-plane [3]. The control scheme can be implemented as illustrated in Fig. 6.2.

6.4.1 Transient Simulations

The controller performance is assessed by simulating the nonlinear model of AHWR under different transient conditions. For controlling the fast transients in the total power, control input (3.30) was applied on every time step, i.e., on continuous time basis. However, to control spatial power variations, input signal was generated using FOS technique. In this, nodal powers were sampled every $\Delta = 9$ s and matrix $\mathbf{y}$ was formulated. Thereafter new values of control signal were generated every $\tau = 54$ s and given to the regulating rods (RRs) along with (3.30). At time $t = 0$, the control signal $\mathbf{u}(t) = u_0$, for $0 < t \leq \tau$ was arbitrarily chosen as zero.

First of all, the case of state regulation is considered. The reactor was observed to be originally working at full power steady-state condition. Suddenly, RR2, initially under automatic control was moved out by around 1% by giving suitable manual control signal and maintained under the influence of automatic control afterwards. As a result of this, perturbations were created in total and spatial power distribution, which were effectively controlled by the FOS controller, as depicted in Fig. 6.3. From Fig. 6.3a it is noticed that the total power rises from 920.48 to 920.68 MW and then it achieves initial steady-state value in 70 s. Spatial power variations calculated in terms of first and second azimuthal tilts are controlled in about 200 s as depicted in Fig. 6.3b. The control input to the RRs generated by the controller is shown in Fig. 6.4a. Corresponding positions of RRs are shown in Fig. 6.4b. It is noticed that the RRs achieve their steady state in 200 s. Figure 6.5 shows the response of three-

Table 6.2 Eigenvalues of $(\Phi_\tau + \Gamma_\tau \mathbf{F})$

Sr. No.	Eigenvalues	Sr. No.	Eigenvalues	Sr. No.	Eigenvalues
1	6.1464×10^{-5}	25	3.4318×10^{-2}	50	9.9845×10^{-1}
2	6.1563×10^{-5}	26	3.4467×10^{-2}	51	9.9845×10^{-1}
3	6.1605×10^{-5}	27	3.4808×10^{-2}	52	9.9845×10^{-1}
4	6.3025×10^{-5}	28	3.5307×10^{-2}	53	9.9845×10^{-1}
5	1.5806×10^{-4}	29	3.5482×10^{-2}	54	9.9845×10^{-1}
6	1.5819×10^{-4}	30	3.7921×10^{-2}	55	9.9845×10^{-1}
7	1.5824×10^{-4}	31	3.8551×10^{-2}	56	9.9845×10^{-1}
8	1.6236×10^{-4}	32	3.9899×10^{-2}	57	9.9845×10^{-1}
9	2.3005×10^{-4}	33	4.0005×10^{-2}	58	9.9887×10^{-1}
10	2.3029×10^{-4}	34	4.4172×10^{-2}	59	9.9887×10^{-1}
11	2.3066×10^{-4}	35–36	$9.9843 \times 10^{-1} \pm j1.2088 \times 10^{-4}$	60	9.9887×10^{-1}
12	2.3936×10^{-4}	37	4.4613×10^{-2}	61	9.9887×10^{-1}
13	3.7190×10^{-4}	38	6.4797×10^{-2}	62	9.9887×10^{-1}
14	3.7211×10^{-4}	39	6.5560×10^{-2}	63	9.9887×10^{-1}
15	3.7270×10^{-4}	40	4.2281×10^{-1}	64	9.9887×10^{-1}
16	4.0102×10^{-4}	41	7.0510×10^{-1}	65	9.9887×10^{-1}
17	5.4325×10^{-4}	42	9.9845×10^{-1}	66	9.9887×10^{-1}
18	5.4371×10^{-4}	43	9.9845×10^{-1}	67	9.9887×10^{-1}
19	5.4558×10^{-4}	44	9.9845×10^{-1}	68	9.9887×10^{-1}
20	5.6903×10^{-4}	45	9.9845×10^{-1}	69	9.9887×10^{-1}
21	1.9462×10^{-3}	46	9.9845×10^{-1}	70	9.9887×10^{-1}
22	3.3513×10^{-2}	47	9.9845×10^{-1}	71	9.9887×10^{-1}
23	3.3565×10^{-2}	48	9.9845×10^{-1}	72	9.9887×10^{-1}
24	3.4038×10^{-2}	49	9.9845×10^{-1}	73	9.9887×10^{-1}
74–90	0				

time-scale controller, given in [7], for the same transient level. It is observed that in both the controllers RRs are attaining equilibrium values, but the time required in the suggested controller is comparatively less.

In another transient, trajectory tracking performance of the controller is tested, for which the reactor is again assumed to be working at steady-state full power of 920.48 MW with distribution of nodal powers as stated in Table 2.5. Iodine, xenon, and delayed neutron precursor concentrations are also in equilibrium with the corresponding nodal powers. Now, the demand power is decreased to 828.43 MW in 61 s uniformly at the rate of 1.5 MW/s and maintained constant afterwards. Throughout the transient, the variations in nodal powers and xenon concentrations occur respectively as shown in Figs. 6.6 and 6.7. Total power and control signal to regulating rod drives during first 300 s are shown in Fig. 6.8. The total power is about 822 MW at 66 s, and after that it settles at 828.43 MW within 100 s. It was noticed that throughout

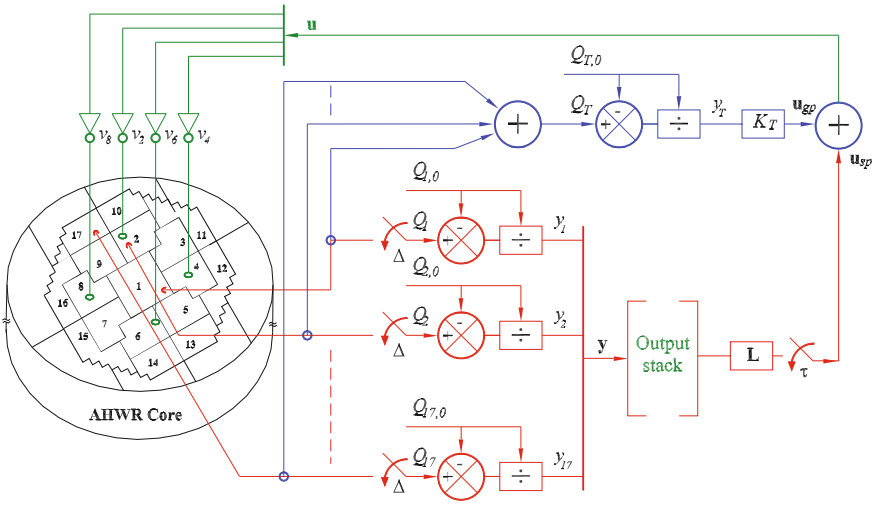

Fig. 6.2 Fast output sampling feedback control scheme for AHWR

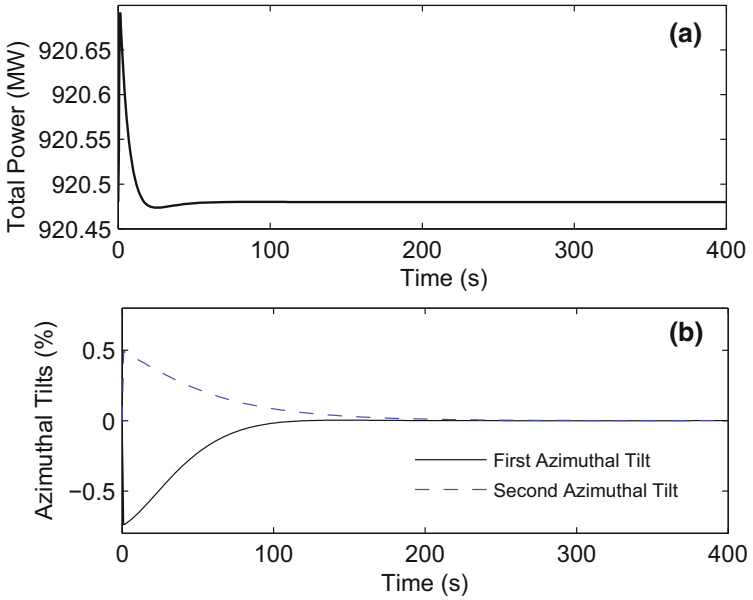

Fig. 6.3 Effect of regulating rod disturbance on **a** Total power and **b** Azimuthal tilts

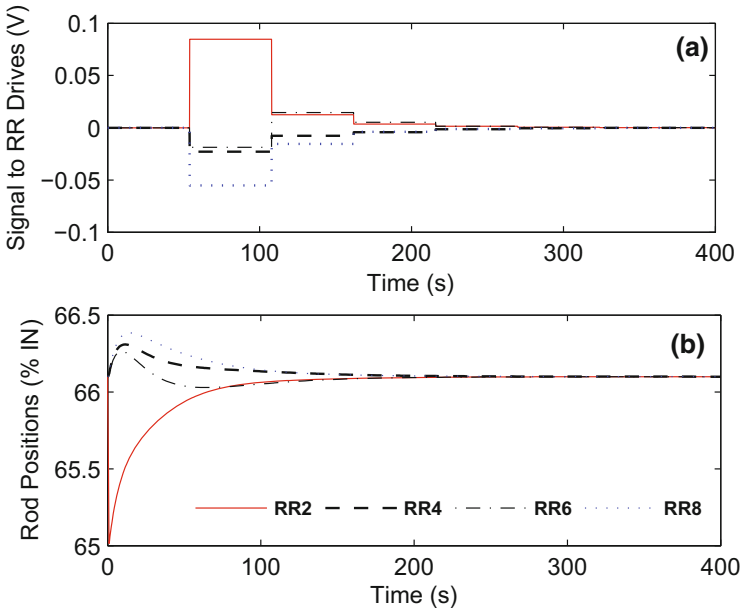

Fig. 6.4 Effect of regulating rod disturbance on **a** Control signal to RR drives and **b** Regulating rod positions

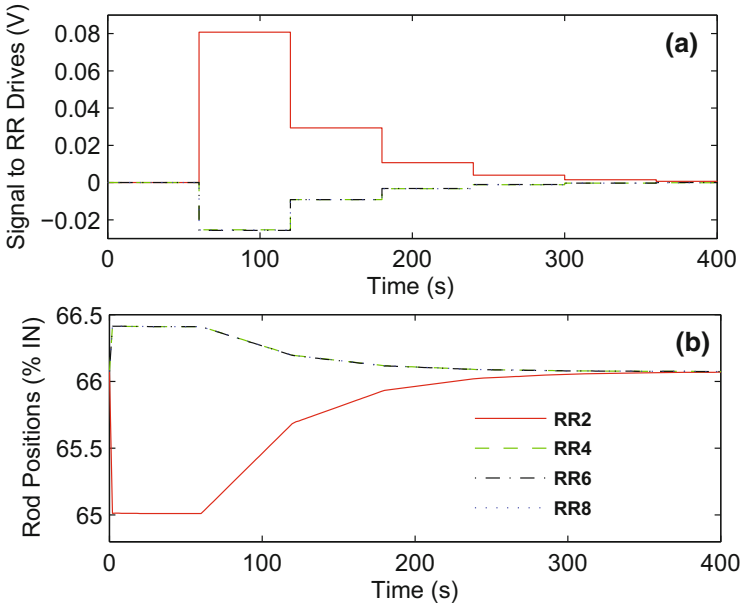

Fig. 6.5 Effect of regulating rod disturbance, with the controller of [7], on **a** Control signal to RR drives and **b** Regulating rod positions

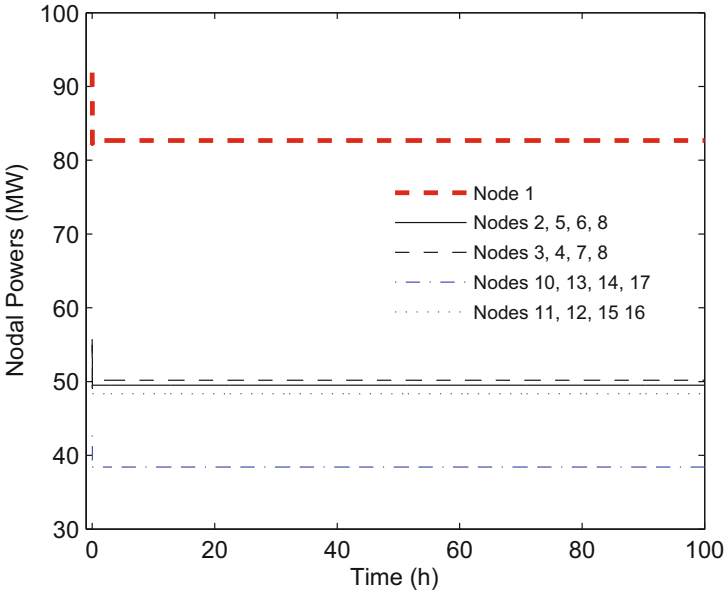

Fig. 6.6 Nodal power variations during power maneuvering

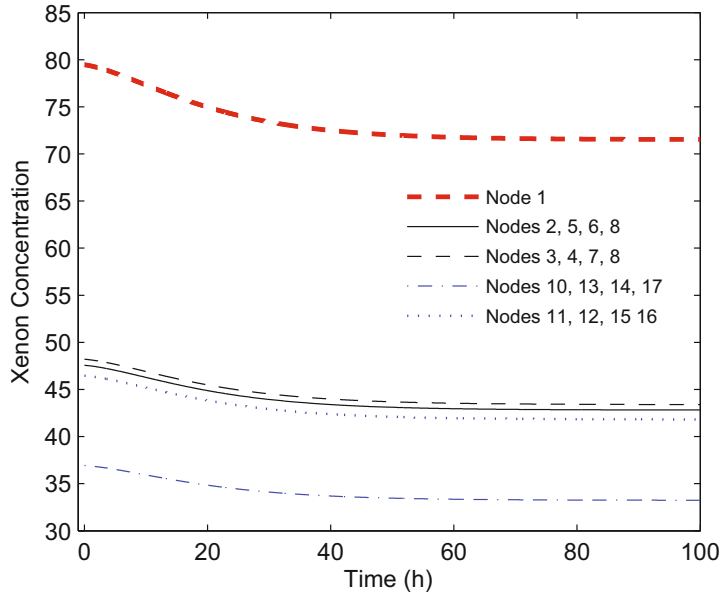

Fig. 6.7 Xenon concentration variations during power maneuvering

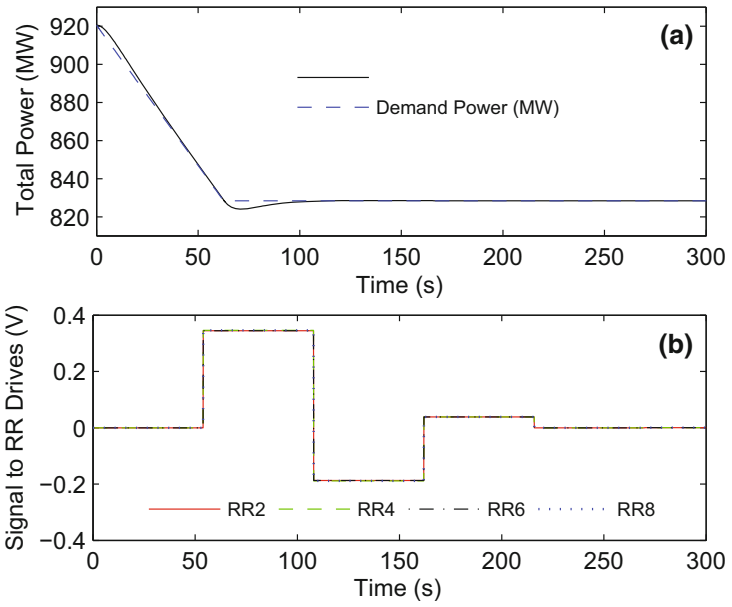

Fig. 6.8 Effect of power maneuvering (initial 300 s) from 920.48 to 828.43 MW on **a** Total power and **b** Control signal to RR drives

the transient, total power is tracking the demand power (Fig. 6.8a). The nodal powers achieve the new steady-state value in 100 s and xenon concentrations stabilize to their respective new equilibrium values in around 50 h.

6.5 Conclusion

In this chapter, fast output sampling control technique is designed for two-time-scale system. Initially the singularly perturbed discrete-time system is decoupled into two lower order subsystems, namely, slow subsystem and fast subsystem. State feedback controls are then designed for subsystems and composite state feedback control is obtained. This state feedback is realized by using FOS gain. The presented method is applied to AHWR for spatial control. At first, the discrete system of AHWR is block diagonalized to have separate slow and fast subsystems. As the fast subsystem is observed to be stable, state feedback control is then designed only for slow subsystem. Afterwards a composite state feedback controller is calculated which is implemented by FOS feedback gain. Its efficacy has been confirmed by simulations of nonlinear AHWR system. Overall performance of devised controller is observed to be satisfactory.

References

1. Chen, C.-T.: Linear System Theory and Design. Oxford University Press, New York (1999)
2. Chammas, A.B., Leondes, C.T.: Pole assignment by piecewise constant output feedback. Int. J. Control **29**(1), 31–38 (1979)
3. Munje, R.K., Londhe, P.S., Parkhe, J.G., Patre, B.M., Tiwari, A.P.: Spatial control of advanced heavy water reactor by fast output sampling technique. Proc. IEEE Int. Conf. Control Appl., 1212–1217 (2013)
4. Naidu, D.S.: Singular Perturbation Methodology in Control Systems. Peter Peregrinus Ltd., London (1988)
5. Phillips, R.G.: Reduced order modeling and control of two-time-scale discrete systems. Int. J. Control **31**, 765–780 (1980)
6. Sharma, G.L., Bandyopadhyay, B., Tiwari, A.P.: Spatial control of a large pressurized heavy water reactor by fast output sampling technique. IEEE Trans. Nucl. Sci. **50**, 1740–1751 (2003)
7. Shimjith, S.R., Tiwari, A.P., Bandyopadhyay, B.: Design of fast output sampling controller for three-time-scale systems: application to spatial control of advanced heavy water reactor. IEEE Trans. Nucl. Sci. **58**(6), 3305–3316 (2011)
8. Syrmos, V.L., Abdallah, C.T., Dorato, P., Grigoriadis, K.: Static output feedback-a survey. Automatica **33**, 125–137 (1997)
9. Tiwari, A.P., Reddy, G.D., Bandyopadhyay, B.: Design of periodic output feedback and fast output sampling based controllers for systems with slow and fast modes. Asian J. Control **14**(1), 271–277 (2012)
10. Werner, H., Furuta, K.: Simultaneous stabilization based on output measurement. Kybernetica **31**, 395–414 (1995)

Chapter 7
Periodic Output Feedback

7.1 Introduction

Periodic Output Feedback (POF) is the kind of multirate output feedback in which system output is sampled at slower rate than the input [16]. In POF, the value of input at a particular moment is derived from the value of the output at a prior moment. It is shown by Chammas and Leondes [2] that a controllable and observable plant is discrete-time pole assignable by periodically varying piecewise constant output feedback. The controller suggested by them consists solely of gain elements and does not include any dynamical element, such as an observer. It is only required to have provision for change of the input during an output sampling interval and the number of input changes is required to be greater than or equal to the controllability index. Later, it was shown by Hagiwara and Araki [4] that it is not a necessary condition that number of input changes be greater than the controllability index. It is seen in case of POF control that the behavior of closed-loop system at output sampling instants meets the desired specification but the states of the system undergo strong oscillation at instants when change of input occurs. Werner and Furuta [16] have discussed the problem and have suggested a methodology for determination of optimal gains whereby the behavior of the closed-loop system improves at the input sampling instants also. In the literature, POF is found extensively implemented to the variety of the systems [1, 5, 8, 15]. Formulation of POF for two-time-scale systems is reported in [9–11, 13, 14]. In [14], it is shown that, the POF controller for two-time-scale system can be readily obtained by combining the solutions of slow and fast subsystem problems, obtained separately. Thus, ill-conditioning is completely avoided and two lower order problems are required to be solved instead of one higher order problem.

In the previous chapter, the attention had been focused on the control of the 920.48 MW Advanced Heavy Water Reactor (AHWR) using fast output sampling technique. Recall that in FOS, control signal is generated as a linear combination of a number of output samples collected in one sampling interval, i.e., the input

R. Munje et al., *Investigation of Spatial Control Strategies with Application to Advanced Heavy Water Reactor*, Energy Systems in Electrical Engineering, https://doi.org/10.1007/978-981-10-3014-7_7

sampling time is larger compared to output sampling time. In this chapter, periodic output feedback control technique is presented for spatial control of AHWR. POF design is different from the FOS design in the sense that in POF input sampling rate is larger than the output sampling rate. This chapter begins with the brief introduction of POF controller. Thereafter design method of POF controller for three-time-scale system is discussed. This design method is then used for spatial control of AHWR and simulation results are presented.

7.2 Periodic Output Feedback

POF is a control technique, in which the poles of the controllable and observable discrete-time system could be assigned arbitrarily by the use of periodically time-varying piecewise constant output feedback gains. Here, the value of the input at the particular moment depends on output value at a time prior to this moment, mainly at the beginning of the sampling time [16]. Consider a linear time-invariant controllable and observable continuous-time model

$$\dot{\mathbf{z}} = \mathbf{A}\mathbf{z} + \mathbf{B}\mathbf{u}, \tag{7.1}$$

$$\mathbf{y} = \mathbf{M}\mathbf{z} \tag{7.2}$$

where $\mathbf{z} \in \Re^n$, $\mathbf{u} \in \Re^m$, $\mathbf{y} \in \Re^p$ and $\mathbf{A}$, $\mathbf{B}$ and $\mathbf{M}$ are constant matrices of appropriate dimensions. System (7.1)–(7.2) when sampled at the rate of $1/\tau$ gives discrete-time model as

$$\mathbf{z}_{k+1} = \Phi_\tau \mathbf{z}_k + \Gamma_\tau \mathbf{u}_k, \tag{7.3}$$

$$\mathbf{y}_k = \mathbf{M}\mathbf{z}_k \tag{7.4}$$

where $\Phi_\tau = e^{\mathbf{A}\tau}$ and $\Gamma_\tau = \int_0^\tau e^{\mathbf{A}s}\mathbf{B}ds$. Also, let

$$\mathbf{z}_{k+1} = \Phi_\Delta \mathbf{z}_k + \Gamma_\Delta \mathbf{u}_k \tag{7.5}$$

be the discrete-time system corresponding to the system (7.1) sampled at the rate $1/\Delta$, where $\Delta = \tau/N$, with integer $N \geq \nu$, the controllability index [3] of (Φ_τ, Γ_τ). The output is measured at the time instants $t = k\tau, k = 0, 1, \cdots$ using a sample and hold system. The output sampling interval τ is divided into N subintervals of length $\Delta = \tau/N$. The hold function is assumed to be constant on the subintervals. The graphical representation of the control law is shown in Fig. 7.1 and mathematically control law can be written as

$$\begin{aligned} \mathbf{u}(t) &= \mathbf{K}_l \mathbf{y}_k, \qquad k\tau + l\Delta \leq t < k\tau + (l+1)\Delta, \\ \mathbf{K}_{l+N} &= \mathbf{K}_l, \qquad\qquad l = 0, 1, 2, \cdots, (N-1). \end{aligned} \tag{7.6}$$

A sequence of N gain matrices $\{\mathbf{K}_0, \mathbf{K}_1, \cdots, \mathbf{K}_{N-1}\}$ when substituted in (7.6) generates a time varying, piecewise constant output feedback gain $\mathbf{K}(t)$ for $0 \leq t < \tau$.

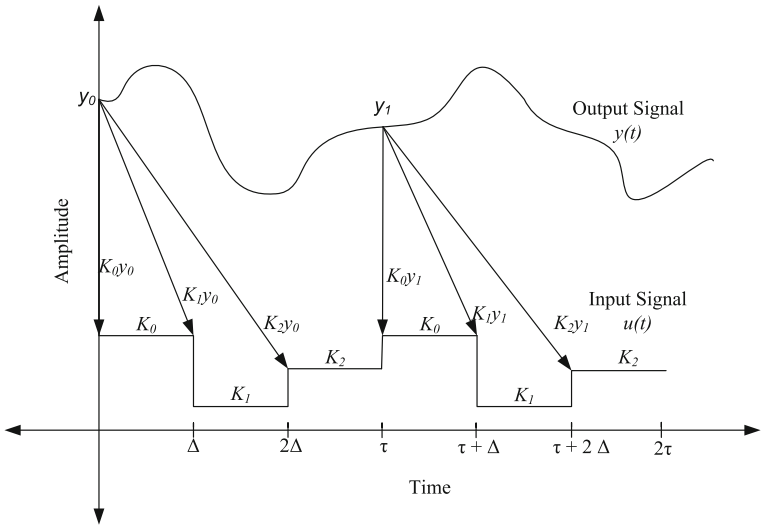

Fig. 7.1 Visualization of periodic output feedback control scheme

Define,

$$\mathbf{K} = \begin{bmatrix} \mathbf{K}_0^T & \mathbf{K}_1^T & \cdots & \mathbf{K}_{N-1}^T \end{bmatrix}^T \tag{7.7}$$

and

$$\mathbf{u}(k\tau) = \mathbf{K}\mathbf{y}(k\tau) = \begin{bmatrix} u(k\tau) \\ u(k\tau + \Delta) \\ \vdots \\ u(k\tau + \tau - \Delta) \end{bmatrix}, \tag{7.8}$$

then a state-space representation for the system (7.3) is obtained as

$$\mathbf{z}_{k+1} = \Phi_\Delta^N \mathbf{z}_k + \Gamma \mathbf{u}_k \tag{7.9}$$

where

$$\Gamma = \begin{bmatrix} \Phi_\Delta^{N-1}\Gamma_\Delta & \Phi_\Delta^{N-2}\Gamma_\Delta & \cdots & \Gamma_\Delta \end{bmatrix} \tag{7.10}$$

and recall that

$$\Phi_\tau = \Phi_\Delta^N.$$

Applying (7.8) to (7.9), the closed-loop system becomes

$$\mathbf{z}_{k+1} = (\Phi_\tau + \Gamma\mathbf{K}\mathbf{M})\mathbf{z}_k. \tag{7.11}$$

Let $\mathbf{G}$ be the output injection gain which stabilizes (7.3), such that absolute eigenvalues lie within the spectral radius $\varphi(.)$, i.e.,

$$\varphi(\Phi_\tau + \mathbf{G}\mathbf{M}) < 1. \tag{7.12}$$

From (7.11) and (7.12), $\mathbf{G}$ is realizable through $\mathbf{K}$, if and only if

$$\Gamma\mathbf{K} = \mathbf{G}. \tag{7.13}$$

Controllability and observability of (7.3) implies controllability and observability of (7.5). Therefore the existence of $\mathbf{K}$ is certain if the number of gain changes is greater than or equal to the controllability index, i.e., if $N \geq \nu$.

7.3 Periodic Output Feedback Control for Three-Time-Scale System

Determining stabilizing output injection gain $\mathbf{G}$ in (7.12) and thereafter periodic output feedback gain $\mathbf{K}$ from (7.13) will be a tedious task for highly ill-conditioned singularly perturbed three-time-scale system. To overcome this difficulty, the original higher order system could be decomposed into individual subsystems and periodic output feedback controller design problem for original system could be addressed in terms of these subsystem controller design problems. Such a formulation of POF controller for two-time-scale system has been reported earlier in [14]. In this section, this approach is extended for the design of POF controller for the system exhibiting three-time-scale property. Assuming that the linear time-invariant discrete-time system given by (7.3), holds three-time-scale structure, it can be written as

$$\begin{bmatrix} \mathbf{z}_{1,k+1} \\ \mathbf{z}_{2,k+1} \\ \mathbf{z}_{3,k+1} \end{bmatrix} = \begin{bmatrix} \Phi_{11} & \Phi_{12} & \Phi_{13} \\ \Phi_{21} & \Phi_{22} & \Phi_{23} \\ \Phi_{31} & \Phi_{32} & \Phi_{33} \end{bmatrix} \begin{bmatrix} \mathbf{z}_{1,k} \\ \mathbf{z}_{2,k} \\ \mathbf{z}_{3,k} \end{bmatrix} + \begin{bmatrix} \Gamma_1 \\ \Gamma_2 \\ \Gamma_3 \end{bmatrix} \mathbf{u}_k, \tag{7.14}$$

$$\mathbf{y}_k = \begin{bmatrix} \mathbf{M}_1 & \mathbf{M}_2 & \mathbf{M}_3 \end{bmatrix} \begin{bmatrix} \mathbf{z}_{1,k}^T & \mathbf{z}_{2,k}^T & \mathbf{z}_{3,k}^T \end{bmatrix}^T \tag{7.15}$$

where $\mathbf{z}_{1,k} \in \Re^{n_1}$, $\mathbf{z}_{2,k} \in \Re^{n_2}$, and $\mathbf{z}_{3,k} \in \Re^{n_3}$ denote states such that $n_1 + n_2 + n_3 = n$ and the matrices Φ_{ij}, Γ_i, and $\mathbf{M}_i$ are of appropriate dimensions. Let $\varphi(\Phi_\tau)$ be the eigenvalues of matrix Φ_τ arranged in the decreasing order of absolute values as

$$\varphi(\Phi_\tau) = \left\{ \varphi_1, ..., \varphi_{n_1}, \varphi_{n_1+1}, ..., \varphi_{n_1+n_2}, \varphi_{n_1+n_2+1}, ..., \varphi_n \right\},$$

where

$$|\varphi_1| > ... > |\varphi_{n_1}| \gg |\varphi_{n_1+1}| > ... > |\varphi_{n_1+n_2}| \gg |\varphi_{n_1+n_2+1}| > ...|\varphi_n| \geq 0.$$

Accordingly the system has three different groups of eigenvalues, out of which n_1 are near the unit circle, n_2 are far, and n_3 are farther from the unit circle close to the origin. Alternatively, the system (7.14) possesses n_1 slow, n_2 fast, and n_3 fastest modes. Using the three-stage decomposition technique [7, 12], given in Appendix B, system (7.14)–(7.15) can be decoupled into three subsystems named slow, fast 1, and fast 2 respectively, and represented in block diagonal form as

$$\begin{bmatrix} \mathbf{z}_{s,k+1} \\ \mathbf{z}_{f1,k+1} \\ \mathbf{z}_{f2,k+1} \end{bmatrix} = \begin{bmatrix} \Phi_{\tau s} & \mathbf{0} & \mathbf{0} \\ \mathbf{0} & \Phi_{\tau f1} & \mathbf{0} \\ \mathbf{0} & \mathbf{0} & \Phi_{\tau f2} \end{bmatrix} \begin{bmatrix} \mathbf{z}_{s,k} \\ \mathbf{z}_{f1,k} \\ \mathbf{z}_{f2,k} \end{bmatrix} + \begin{bmatrix} \Gamma_{\tau s} \\ \Gamma_{\tau f1} \\ \Gamma_{\tau f2} \end{bmatrix} \mathbf{u}_k, \tag{7.16}$$

$$\mathbf{y}_k = \begin{bmatrix} \mathbf{M}_s & \mathbf{M}_{f1} & \mathbf{M}_{f2} \end{bmatrix} \begin{bmatrix} \mathbf{z}_{s,k}^T & \mathbf{z}_{f1,k}^T & \mathbf{z}_{f2,k}^T \end{bmatrix}^T \tag{7.17}$$

where $\mathbf{z}_{s,k} \in \Re^{n_1}$, $\mathbf{z}_{f1,k} \in \Re^{n_2}$, and $\mathbf{z}_{f2,k} \in \Re^{n_3}$ denote respectively slow, fast 1, and fast 2 states such that $n_1 + n_2 + n_3 = n$. The relation between the states of original system (7.14) and the states of decoupled system (7.16) is given by

$$\begin{aligned} \begin{bmatrix} \mathbf{z}_{s,k}^T & \mathbf{z}_{f1,k}^T & \mathbf{z}_{f2,k}^T \end{bmatrix}^T &= \mathbf{T} \begin{bmatrix} \mathbf{z}_{1,k}^T & \mathbf{z}_{2,k}^T & \mathbf{z}_{3,k}^T \end{bmatrix}^T \\ \text{or} \qquad \mathbf{z}_{d,k} &= \mathbf{T}\mathbf{z}_k \end{aligned} \tag{7.18}$$

where $\mathbf{z}_k = \begin{bmatrix} \mathbf{z}_{1,k}^T & \mathbf{z}_{2,k}^T & \mathbf{z}_{3,k}^T \end{bmatrix}^T$, $\mathbf{z}_{d,k} = \begin{bmatrix} \mathbf{z}_{s,k}^T & \mathbf{z}_{f1,k}^T & \mathbf{z}_{f2,k}^T \end{bmatrix}^T$ and transformation matrix $\mathbf{T} \in \Re^{n \times n}$ (refer Appendix B, for more details). System (7.14)–(7.15) is decoupled into three subsystems in (7.16)–(7.17), namely, the slow subsystem $(\Phi_{\tau s}, \Gamma_{\tau s}, \mathbf{M}_s)$, the fast 1 subsystem $(\Phi_{\tau f1}, \Gamma_{\tau f1}, \mathbf{M}_{f1})$, and the fast 2 subsystem $(\Phi_{\tau f2}, \Gamma_{\tau f2}, \mathbf{M}_{f2})$, of orders n_1, n_2, and n_3 respectively. The system formulation (7.16)–(7.17) is related to its original form (7.14)–(7.15) via linear transformation (7.18). Therefore, subsystems $(\Phi_{\tau s}, \Gamma_{\tau s}, \mathbf{M}_s)$, $(\Phi_{\tau f1}, \Gamma_{\tau f1}, \mathbf{M}_{f1})$, and $(\Phi_{\tau f2}, \Gamma_{\tau f2}, \mathbf{M}_{f2})$ are controllable and observable. In the similar manner, the discrete-time system equivalent of (7.5) for the sampling interval Δ can also be decoupled as

$$\begin{bmatrix} \mathbf{z}_{s,k+1} \\ \mathbf{z}_{f1,k+1} \\ \mathbf{z}_{f2,k+1} \end{bmatrix} = \begin{bmatrix} \Phi_{\Delta s} & \mathbf{0} & \mathbf{0} \\ \mathbf{0} & \Phi_{\Delta f1} & \mathbf{0} \\ \mathbf{0} & \mathbf{0} & \Phi_{\Delta f2} \end{bmatrix} \begin{bmatrix} \mathbf{z}_{s,k} \\ \mathbf{z}_{f1,k} \\ \mathbf{z}_{f2,k} \end{bmatrix} + \begin{bmatrix} \Gamma_{\Delta s} \\ \Gamma_{\Delta f1} \\ \Gamma_{\Delta f2} \end{bmatrix} \mathbf{u}_k. \tag{7.19}$$

Design of a stabilizing output injection gain for three-time-scale system (7.16) is described in the Appendix C. It is given by

$$\begin{aligned} \mathbf{G}^T &= \begin{bmatrix} \mathbf{G}_s^T & \mathbf{0} & \mathbf{0} \end{bmatrix} + \begin{bmatrix} \mathbf{0} & \mathbf{G}_{f1}^T & \mathbf{0} \end{bmatrix} \mathbf{T}_{d1} + \begin{bmatrix} \mathbf{0} & \mathbf{0} & \mathbf{G}_{f2}^T \end{bmatrix} \mathbf{T}_{d2}\mathbf{T}_{d1} \\ &= \begin{bmatrix} \mathbf{G}_1^T & \mathbf{G}_2^T & \mathbf{G}_3^T \end{bmatrix} \end{aligned} \tag{7.20}$$

where $\mathbf{G}_s^T$, $\mathbf{G}_{f1}^T$, and $\mathbf{G}_{f2}^T$ are the stabilizing output injection gains for slow, fast 1, and fast 2 subsystems respectively, and $\mathbf{T}_{d1}$ and $\mathbf{T}_{d2}$ are transformation matrices. Now, the following form of Γ in (7.10) for the system (7.16) is assumed

$$\Gamma = \begin{bmatrix} \Gamma_{\mathbf{s_1}} & \Gamma_{\mathbf{s_2}} & \Gamma_{\mathbf{s_3}} \\ \Gamma_{\mathbf{f1_1}} & \Gamma_{\mathbf{f1_2}} & \Gamma_{\mathbf{f1_3}} \\ \Gamma_{\mathbf{f2_1}} & \Gamma_{\mathbf{f2_2}} & \Gamma_{\mathbf{f2_3}} \end{bmatrix} \tag{7.21}$$

where submatrices $\Gamma_{\mathbf{s_1}} \in \Re^{n_1 \times (N-\nu_{f2}-\nu_{f1})m}$, $\Gamma_{\mathbf{s_2}} \in \Re^{n_1 \times \nu_{f1} m}$, $\Gamma_{\mathbf{s_3}} \in \Re^{n_1 \times \nu_{f2} m}$, $\Gamma_{\mathbf{f1_1}} \in \Re^{n_2 \times (N-\nu_{f2}-\nu_{f1})m}$, $\Gamma_{\mathbf{f1_2}} \in \Re^{n_2 \times \nu_{f1} m}$, $\Gamma_{\mathbf{f1_3}} \in \Re^{n_2 \times \nu_{f2} m}$, $\Gamma_{\mathbf{f2_1}} \in \Re^{n_3 \times (N-\nu_{f2}-\nu_{f1})m}$, $\Gamma_{\mathbf{f2_2}} \in \Re^{n_1 \times \nu_{f1} m}$, and $\Gamma_{\mathbf{f2_3}} \in \Re^{n_1 \times \nu_{f2} m}$, are respectively given by

$$\Gamma_{\mathbf{s_1}} = \left[\Phi_{\Delta s}^{N-1} \Gamma_{\Delta s} \cdots \Phi_{\Delta s}^{N-\nu_s} \Gamma_{\Delta s} \right] \tag{7.22}$$

$$\Gamma_{\mathbf{s_2}} = \left[\Phi_{\Delta s}^{N-\nu_s-1} \Gamma_{\Delta s} \cdots \Phi_{\Delta s}^{N-\nu_s-\nu_{f1}} \Gamma_{\Delta s} \right] \tag{7.23}$$

$$\Gamma_{\mathbf{s_3}} = \left[\Phi_{\Delta s}^{N-\nu_s-\nu_{f1}-1} \Gamma_{\Delta s} \cdots \Gamma_{\Delta s} \right] \tag{7.24}$$

$$\Gamma_{\mathbf{f1_1}} = \left[\Phi_{\Delta f1}^{N-1} \Gamma_{\Delta f1} \cdots \Phi_{\Delta f1}^{N-\nu_s} \Gamma_{\Delta f1} \right] \tag{7.25}$$

$$\Gamma_{\mathbf{f1_2}} = \left[\Phi_{\Delta f1}^{N-\nu_s-1} \Gamma_{\Delta f1} \cdots \Phi_{\Delta f1}^{N-\nu_s-\nu_{f1}} \Gamma_{\Delta f1} \right] \tag{7.26}$$

$$\Gamma_{\mathbf{f1_3}} = \left[\Phi_{\Delta f1}^{N-\nu_s-\nu_{f1}-1} \Gamma_{\Delta f1} \cdots \Gamma_{\Delta f1} \right] \tag{7.27}$$

$$\Gamma_{\mathbf{f2_1}} = \left[\Phi_{\Delta f2}^{N-1} \Gamma_{\Delta f2} \cdots \Phi_{\Delta f2}^{N-\nu_s} \Gamma_{\Delta f2} \right] \tag{7.28}$$

$$\Gamma_{\mathbf{f2_2}} = \left[\Phi_{\Delta f2}^{N-\nu_s-1} \Gamma_{\Delta f2} \cdots \Phi_{\Delta f2}^{N-\nu_s-\nu_{f1}} \Gamma_{\Delta f2} \right] \tag{7.29}$$

$$\Gamma_{\mathbf{f2_3}} = \left[\Phi_{\Delta f2}^{N-\nu_s-\nu_{f1}-1} \Gamma_{\Delta f2} \cdots \quad \Gamma_{\Delta f2} \right] \tag{7.30}$$

in which ν_s, ν_{f1}, and ν_{f2} are the controllability indices of respectively slow, fast 1 and fast 2 subsystems. Let us assume $\mathbf{K}$ in (7.13) as

$$\mathbf{K} = \left[\mathbf{K_s}^T \ \mathbf{K_{f1}}^T \ \mathbf{K_{f2}}^T \right] \tag{7.31}$$

where submatrices $\mathbf{K_s}$, $\mathbf{K_{f1}}$ and $\mathbf{K_{f2}}$ are respectively of dimensions $((N - \nu_{f2} - \nu_{f1})m \times p)$, $(\nu_{f1} m \times p)$, and $(\nu_{f2} m \times p)$. Then using (7.13), (7.20), (7.21), and (7.31), expressions for $\mathbf{K_s}$, $\mathbf{K_{f1}}$, and $\mathbf{K_{f2}}$ can be obtained respectively as

$$\begin{aligned} \mathbf{K}_s = & \left[(\Gamma_{\mathbf{s_1}} - \Gamma_{\mathbf{s_3}} \Gamma_{\mathbf{f2_3}}^{-1} \Gamma_{\mathbf{f2_1}}) - (\Gamma_{\mathbf{s_2}} - \Gamma_{\mathbf{s_3}} \Gamma_{\mathbf{f2_3}}^{-1} \Gamma_{\mathbf{f2_2}}) \right. \\ & (\Gamma_{\mathbf{f1_2}} - \Gamma_{\mathbf{f1_3}} \Gamma_{\mathbf{f2_3}}^{-1} \Gamma_{\mathbf{f2_2}})^{-1} (\Gamma_{\mathbf{f1_1}} - \Gamma_{\mathbf{f1_3}} \Gamma_{\mathbf{f2_3}}^{-1} \Gamma_{\mathbf{f2_1}}) \Big]^{-1} \\ & \left[(\mathbf{G}_1^T - \Gamma_{\mathbf{s_3}} \Gamma_{\mathbf{f2_3}}^{-1} \mathbf{G}_3^T) - (\Gamma_{\mathbf{s_2}} - \Gamma_{\mathbf{s_3}} \Gamma_{\mathbf{f2_3}}^{-1} \Gamma_{\mathbf{f2_2}}) \right. \\ & \left. (\Gamma_{\mathbf{f1_2}} - \Gamma_{\mathbf{f1_3}} \Gamma_{\mathbf{f2_3}}^{-1} \Gamma_{\mathbf{f2_2}})^{-1} (\mathbf{G}_2^T - \Gamma_{\mathbf{f1_3}} \Gamma_{\mathbf{f2_3}}^{-1} \mathbf{G}_3^T) \right], \end{aligned} \tag{7.32}$$

$$\begin{aligned} \mathbf{K}_{f1} = & (\Gamma_{\mathbf{f1_2}} - \Gamma_{\mathbf{f1_3}} \Gamma_{\mathbf{f2_3}}^{-1} \Gamma_{\mathbf{f2_2}})^{-1} \left[(\mathbf{G}_2^T - \Gamma_{\mathbf{f1_3}} \Gamma_{\mathbf{f2_3}}^{-1} \mathbf{G}_3^T) \right. \\ & \left. - (\Gamma_{\mathbf{f1_1}} - \Gamma_{\mathbf{f1_3}} \Gamma_{\mathbf{f2_3}}^{-1} \Gamma_{\mathbf{f2_1}}) \mathbf{K_s} \right], \end{aligned} \tag{7.33}$$

$$\mathbf{K}_{f2} = \Gamma_{\mathbf{f2_3}}^{-1} (\mathbf{G}_3^T - \Gamma_{\mathbf{f2_1}} \mathbf{K_s} - \Gamma_{\mathbf{f2_2}} \mathbf{K_{f1}}). \tag{7.34}$$

Since, $\mathbf{G}$ stabilizes $(\Phi_\tau + \mathbf{GM})$ and $\mathbf{K}$ is an exact solution of (7.13), closed-loop system (7.11) will also be stable.

Lemma 7.1 *If fast 1 and fast 2 subsystems are assumed to be stable and an output injection gain* $\mathbf{G}^T = \begin{bmatrix} \mathbf{G}_s^T & \mathbf{0} & \mathbf{0} \end{bmatrix}$ *is applied to (7.16), then closed-loop system* $(\Phi_\tau + \mathbf{GM})$ *is stable.*

Proof Since, systems (7.16) and (7.14) are related through linear transformation (7.18), they have same eigenvalues. Now, if $\mathbf{G}^T = \begin{bmatrix} \mathbf{G}_s^T & \mathbf{0} & \mathbf{0} \end{bmatrix}$ is an output injection gain for (7.16), then closed-loop system becomes

$$\mathbf{z}_{d,k+1} = \begin{bmatrix} \Phi_{\tau s} + \mathbf{G}_s\mathbf{M}_s & \mathbf{0} & \mathbf{0} \\ \mathbf{G}_s\mathbf{M}_{f1} & \Phi_{\tau f1} & \mathbf{0} \\ \mathbf{G}_s\mathbf{M}_{f2} & \mathbf{0} & \Phi_{\tau f2} \end{bmatrix} \mathbf{z}_{d,k}. \tag{7.35}$$

From the above system it is clear that, $(\Phi_{\tau s} + \mathbf{G}_s\mathbf{M}_s)$ is stable by design and both $\Phi_{\tau f1}$ and $\Phi_{\tau f2}$ are assumed to be stable. Therefore, system (7.35) is stable. Using (7.18), system (7.35) can be transformed into original states, which will also be stable. System (7.14) is three-time-scale representation of system (6.1). Hence, closed-loop system $(\Phi_\tau + \mathbf{GM})$ is stable.

Remark 7.1 For systems having stable fast 1 and fast 2 modes, $\mathbf{G}_{f1} = \mathbf{G}_{f2} = \mathbf{0}$ and therefore $\mathbf{G}_1 = \mathbf{G}_s$ which yields reduced three-time-scale approximation to $\mathbf{K}$ as $\hat{\mathbf{K}} = \begin{bmatrix} \hat{\mathbf{K}}_s & \hat{\mathbf{K}}_{f1} & \hat{\mathbf{K}}_{f2} \end{bmatrix}$, where submatrices are approximated as

$$\begin{aligned} \hat{\mathbf{K}}_s = &\big[(\Gamma_{\mathbf{s_1}} - \Gamma_{\mathbf{s_3}}\Gamma_{\mathbf{f2_3}}^{-1}\Gamma_{\mathbf{f2_1}}) - (\Gamma_{\mathbf{s_2}} - \Gamma_{\mathbf{s_3}}\Gamma_{\mathbf{f2_3}}^{-1}\Gamma_{\mathbf{f2_2}}) \\ &(\Gamma_{\mathbf{f1_2}} - \Gamma_{\mathbf{f1_3}}\Gamma_{\mathbf{f2_3}}^{-1}\Gamma_{\mathbf{f2_2}})^{-1}(\Gamma_{\mathbf{f1_1}} - \Gamma_{\mathbf{f1_3}}\Gamma_{\mathbf{f2_3}}^{-1}\Gamma_{\mathbf{f2_1}}) \big]^{-1} \mathbf{G}_s^T, \end{aligned} \tag{7.36}$$

$$\hat{\mathbf{K}}_{f1} = -(\Gamma_{\mathbf{f1_2}} - \Gamma_{\mathbf{f1_3}}\Gamma_{\mathbf{f2_3}}^{-1}\Gamma_{\mathbf{f2_2}})^{-1}(\Gamma_{\mathbf{f1_1}} - \Gamma_{\mathbf{f1_3}}\Gamma_{\mathbf{f2_3}}^{-1}\Gamma_{\mathbf{f2_1}})\mathbf{K_s}, \tag{7.37}$$

$$\mathbf{K}_{f2} = \Gamma_{\mathbf{f2_3}}^{-1}(-\Gamma_{\mathbf{f2_1}}\mathbf{K_s} - \Gamma_{\mathbf{f2_2}}\mathbf{K_{f1}}). \tag{7.38}$$

Remark 7.2 Eigenvalues of $\Phi_{\Delta f2}$ are very small for sampling period Δ. Hence, $\Phi_{\Delta f2}$, $\Phi_{\Delta f2}^2 \cdots$ would be very small. Thus $\Gamma_{\mathbf{f2_1}}$ and $\Gamma_{\mathbf{f2_2}}$ can be neglected in comparison to $\Gamma_{\mathbf{f2_3}}$ in (7.36)–(7.38), which again gives approximation to $\hat{\mathbf{K}}$ as $\bar{\mathbf{K}} = \begin{bmatrix} \bar{\mathbf{K}}_s & \bar{\mathbf{K}}_{f1} & \bar{\mathbf{K}}_{f2} \end{bmatrix}$ where

$$\bar{\mathbf{K}}_s = (\Gamma_{\mathbf{s_1}} - \Gamma_{\mathbf{s_2}}\Gamma_{\mathbf{f1_2}}^{-1}\Gamma_{\mathbf{f1_1}})^{-1}\mathbf{G}_s^T, \tag{7.39}$$

$$\bar{\mathbf{K}}_{f1} = -\Gamma_{\mathbf{f1_2}}^{-1}\Gamma_{\mathbf{f1_1}}\mathbf{K_s}, \tag{7.40}$$

$$\bar{\mathbf{K}}_{f2} = \mathbf{0}. \tag{7.41}$$

Remark 7.3 Further, if $\Gamma_{\mathbf{f1_1}}$ is neglected in comparison to $\Gamma_{\mathbf{f1_2}}$ and $\Gamma_{\mathbf{f1_3}}$, approximation to $\bar{\mathbf{K}}$ as $\tilde{\mathbf{K}} = \begin{bmatrix} \tilde{\mathbf{K}}_s & \tilde{\mathbf{K}}_{f1} & \tilde{\mathbf{K}}_{f2} \end{bmatrix}$ is obtained, where $\tilde{\mathbf{K}}_s = \Gamma_{\mathbf{s_1}}^{-1}\mathbf{G}_s^T$ and $\tilde{\mathbf{K}}_{f1} = \tilde{\mathbf{K}}_{f2} = \mathbf{0}$.

7.4 Application of POF to AHWR System

Linear, controllable, and observable model of AHWR with total power feedback, given by (3.31), is rewritten here for convenience as

$$\dot{\mathbf{z}} = \hat{\mathbf{A}}\mathbf{z} + \mathbf{B}\mathbf{u}_{sp} + \mathbf{B}_{fw}\delta q_{fw}, \tag{7.42}$$

where $\hat{\mathbf{A}} = \mathbf{A} - \mathbf{B}\mathbf{K}_G\mathbf{M}$, has eigenvalues falling in three different clusters. First cluster of 38 eigenvalues is ranging from 6.2899×10^{-3} to $(8.8268 \pm j\,1.8656) \times 10^{-5}$, second cluster of 35 eigenvalues that ranges from -1.8396×10^{-1} to -1.1779×10^{-2}, and the third one of 17 eigenvalues is ranging from -2.7626×10^{2} to -7.2513. For properly chosen sampling time, if the continuous-time system holds three-time-scale structure, its discrete counterpart would also hold three-time-scale structure [14]. For AHWR, sampling time is decided by the time constant representing the dynamics of delayed neutron precursors. The largest unstable eigenvalue of the continuous-time system (7.42) is 6.2899×10^{-3}, which specifies that the sampling time, $\tau < 1/(6.2899 \times 10^{-3})$ or 159 s can be selected. As spatial power of the reactor can experience great variations in small time, it is better to have small sampling time from real-time realization standpoint without losing three-time-scale property required for design simplification. That is why, τ is chosen as 12 s and system (7.42) is discretized to get

$$\mathbf{z}_{k+1} = \Phi\mathbf{z}_k + \Gamma\mathbf{u}_k + \Gamma_{fw}\delta q_{fwk}, \tag{7.43}$$

$$\mathbf{y}_k = \mathbf{M}\mathbf{z}_k \tag{7.44}$$

The system (7.43) is diagonalized to have separate slow, fast 1, and fast 2 subsystems of dimensions 38, 35, and 17 respectively, with the state vector (2.17), divided as

$$\mathbf{z}_{1,k} = \left[\mathbf{z}_H^T\ \mathbf{z}_X^T\ \mathbf{z}_I^T\right]^T, \mathbf{z}_{2,k} = \left[\delta h_d\ \mathbf{z}_C^T\ \mathbf{z}_x^T\right]^T \text{ and } \mathbf{z}_{3,k} = \mathbf{z}_Q. \tag{7.45}$$

Slow, fast 1, and fast 2 subsystem eigenvalues correspond superbly with largest 38, midway 35, and the smallest 17 eigenvalues of the original system for sampling time τ. Eigenvalues of slow and fast 1 subsystems are given respectively in Tables 7.1 and 7.2, whereas eigenvalues of fast 2 subsystem are located at origin. The unstable eigenvalues in slow subsystem have been highlighted in Table 7.1.

It is verified that, all the three subsystems are controllable as well as observable. In addition, it is seen that the eigenvalues of fast 1 and fast 2 subsystems are within unit circle in z-plane. Therefore, design of output injection matrix is carried out for slow subsystem alone, in order to position eigenvalues of slow subsystem from 9.9012×10^{-1} to 9.9992×10^{-1}. Finally, composite output injection matrix is formulated using technique described in Appendix C. Controllability indices of slow, fast 1, and fast 2 subsystems are found to be $\nu_s = 3$, $\nu_{f1} = 2$, and $\nu_{f2} = 1$ respectively. It can be confirmed that the controllability index of original system is 6. This impelled the choice of $N = 6$. Consequently, $\Delta = 2$ s. System (7.42) is discretized with

Table 7.1 Eigenvalues of slow subsystem ($\Phi_{\tau s}$)

Sr. No.	Eigenvalues	Sr. No.	Eigenvalues
1	1.0000	20	9.9947×10^{-1}
2	1.0000	21	9.9943×10^{-1}
3	1.0000	22	9.9941×10^{-1}
4–5	$1.0011 \pm j2.6259 \times 10^{-4}$	23–24	$9.9922 \times 10^{-1} \pm j6.3681 \times 10^{-4}$
6–7	$1.0010 \pm j4.7915 \times 10^{-4}$	25–26	$9.9921 \times 10^{-1} \pm j6.5606 \times 10^{-4}$
8	9.9996	27–28	$9.9912 \times 10^{-1} \pm j4.7141 \times 10^{-4}$
9	9.9982	29–30	$9.9907 \times 10^{-1} \pm j3.5881 \times 10^{-4}$
10	9.9977×10^{-1}	31	9.9831×10^{-1}
11–12	$9.9958 \times 10^{-1} \pm j9.2904 \times 10^{-4}$	32	9.9825×10^{-1}
13	9.9955×10^{-1}	33	9.9812×10^{-1}
14–15	$9.9955 \times 10^{-1} \pm j9.1728 \times 10^{-4}$	34	9.9802×10^{-1}
16	9.9954×10^{-1}	35	9.9800×10^{-1}
17	9.9952×10^{-1}	36	9.9793×10^{-1}
18	9.9950×10^{-1}	37	9.9775×10^{-1}
19	9.9949×10^{-1}	38	9.9774×10^{-1}

Table 7.2 Eigenvalues of fast 1 subsystem ($\Phi_{\tau f1}$)

Sr. No.	Eigenvalues	Sr. No.	Eigenvalues	Sr. No.	Eigenvalues
1	8.7009×10^{-1}	13	4.7554×10^{-1}	25	1.5410×10^{-1}
2	8.2488×10^{-1}	14	4.7305×10^{-1}	26	1.5267×10^{-1}
3	5.4256×10^{-1}	15	4.7261×10^{-1}	27	1.5090×10^{-1}
4	5.4123×10^{-1}	16	4.7176×10^{-1}	28	1.4114×10^{-1}
5	4.9922×10^{-1}	17	4.7030×10^{-1}	29	1.4101×10^{-1}
6	5.0019×10^{-1}	18	4.7014×10^{-1}	30	1.3965×10^{-1}
7	4.8847×10^{-1}	19	2.4520×10^{-1}	31	1.3681×10^{-1}
8	4.8837×10^{-1}	20	1.7112×10^{-1}	32	1.1481×10^{-1}
9	4.8475×10^{-1}	21	1.7108×10^{-1}	33	1.1465×10^{-1}
10	4.8302×10^{-1}	22	1.6914×10^{-1}	34	1.1365×10^{-1}
11	4.7608×10^{-1}	23	1.6832×10^{-1}	35	1.0997×10^{-1}
12	4.7407×10^{-1}	24	1.5419×10^{-1}		

sampling time of Δ and block diagonalized to construct Γ using (7.22)–(7.30). Here, as per Remark 7.2, $\Gamma_{\mathbf{f2_1}}$ and $\Gamma_{\mathbf{f2_2}}$ are ignored in comparison to $\Gamma_{\mathbf{f2_3}}$ and approximated periodic output feedback gain, $\bar{\mathbf{K}}$ is found. Here it is also confirmed that $\bar{\mathbf{K}}_{f2}$ is null matrix of order (4×17), while $\bar{\mathbf{K}}_{f1}$ and $\bar{\mathbf{K}}_s$ are respectively of orders (8×17) and (12×17) given by

$$\bar{\mathbf{K}}_{f1} = \begin{bmatrix} -0.1025 & 0.2941 & -0.1128 & 0.0001 & -0.1202 & 0.0401 & 0.0503 & -0.0026 & 0.0372 \\ -0.0582 & 0.3178 & -0.1710 & 0.2989 & -0.1051 & 0.1927 & 0.1667 & -0.0274 & -0.2082 \\ 0.0153 & 0.0948 & -0.1092 & 0.2239 & -0.0353 & 0.1111 & 0.0681 & -0.0388 & -0.1573 \\ -0.0082 & -0.0579 & -0.0581 & -0.1396 & -0.0337 & -0.0903 & -0.1052 & -0.0095 & 0.1342 \\ -0.2040 & 0.3840 & -0.1964 & -0.0543 & -0.3433 & 0.2840 & 0.0987 & -0.0788 & 0.1799 \\ -0.1054 & 0.7822 & -0.3537 & 0.4893 & -0.1812 & 0.3713 & 0.4253 & 0.0598 & -0.5504 \\ 0.0435 & 0.4325 & -0.3052 & 0.4625 & -0.0230 & 0.0739 & 0.1926 & 0.0098 & -0.4636 \\ -0.0161 & -0.1725 & -0.2117 & -0.1878 & -0.1580 & -0.0950 & -0.2526 & -0.2788 & 0.4088 \end{bmatrix}$$

$$\begin{bmatrix} -0.0696 & -0.1285 & 0.1544 & 0.0755 & -0.1816 & 0.0011 & -0.0488 & -0.1197 \\ -0.2172 & -0.0111 & -0.1664 & -0.0462 & -0.1195 & -0.1946 & -0.0120 & 0.1005 \\ -0.1357 & 0.0474 & -0.1759 & -0.1011 & 0.0015 & -0.1658 & 0.0148 & 0.0948 \\ 0.1193 & -0.0433 & 0.1805 & -0.0208 & 0.0367 & 0.0421 & -0.0306 & -0.1612 \\ -0.0650 & -0.3073 & 0.4307 & 0.1771 & -0.5318 & -0.0252 & -0.1016 & -0.3197 \\ -0.5479 & -0.0490 & -0.3295 & -0.1270 & -0.2925 & -0.4847 & -0.0969 & 0.2432 \\ -0.4043 & 0.0925 & -0.4046 & -0.2704 & 0.0500 & -0.4080 & -0.0110 & 0.2265 \\ 0.3189 & -0.1173 & 0.4169 & -0.0746 & 0.0508 & 0.0827 & 0.0212 & -0.4400 \end{bmatrix} \tag{7.46}$$

$$\bar{\mathbf{K}}_{s} = \begin{bmatrix} 0.1997 & 0.0337 & 0.1460 & 0.1571 & 0.5575 & -0.7050 & -0.0911 & 0.2363 & -0.3959 \\ 0.0820 & -1.0859 & 0.3867 & -0.2677 & 0.1248 & -0.3397 & -0.6068 & -0.2895 & 0.8196 \\ -0.0689 & -0.9399 & 0.4938 & -0.4954 & -0.0701 & 0.2310 & -0.3041 & -0.1840 & 0.7652 \\ 0.0161 & 0.2762 & 0.4204 & -0.0140 & 0.3495 & -0.0867 & 0.3390 & 0.8194 & -0.6939 \\ 0.0979 & 0.1205 & 0.0569 & 0.1052 & 0.3269 & -0.4509 & -0.0439 & 0.1538 & -0.2488 \\ 0.0348 & -0.6095 & 0.1964 & -0.0769 & 0.0467 & -0.1602 & -0.3456 & -0.2009 & 0.4720 \\ -0.0405 & -0.5864 & 0.2873 & -0.2516 & -0.0589 & 0.1892 & -0.1784 & -0.1351 & 0.4528 \\ 0.0078 & 0.1653 & 0.2555 & -0.0532 & 0.2181 & -0.0860 & 0.1887 & 0.5357 & -0.4134 \\ -0.0023 & 0.2068 & -0.0289 & 0.0530 & 0.1022 & -0.2037 & 0.0030 & 0.0745 & -0.1050 \\ -0.0117 & -0.1439 & 0.0114 & 0.1111 & -0.0296 & 0.0164 & -0.0890 & -0.1140 & 0.1310 \\ -0.0126 & -0.2432 & 0.0873 & -0.0130 & -0.0473 & 0.1493 & -0.0549 & -0.0869 & 0.1467 \\ -0.0003 & 0.0543 & 0.0968 & -0.0949 & 0.0910 & -0.0873 & 0.0413 & 0.2607 & -0.1386 \end{bmatrix}$$

$$\begin{bmatrix} -0.0858 & 0.4106 & -0.6761 & -0.2227 & 0.8756 & 0.0858 & 0.1080 & 0.4885 \\ 0.7792 & 0.1073 & 0.3192 & 0.2031 & 0.4016 & 0.6800 & 0.2458 & -0.3198 \\ 0.6772 & -0.0831 & 0.5088 & 0.4137 & -0.1443 & 0.5647 & 0.0942 & -0.2927 \\ -0.4765 & 0.1829 & -0.5257 & 0.1480 & -0.0008 & -0.0740 & -0.1920 & 0.6845 \\ -0.0801 & 0.2279 & -0.3952 & -0.1231 & 0.5171 & 0.0560 & 0.0553 & 0.2815 \\ 0.4416 & 0.0664 & 0.1558 & 0.1176 & 0.2250 & 0.3835 & 0.1581 & -0.1791 \\ 0.4011 & -0.0399 & 0.2777 & 0.2385 & -0.0952 & 0.3170 & 0.0670 & -0.1631 \\ -0.2758 & 0.1056 & -0.2875 & 0.0896 & 0.0109 & -0.0360 & -0.1365 & 0.3970 \\ -0.0747 & 0.0490 & -0.1196 & -0.0242 & 0.1664 & 0.0280 & 0.0032 & 0.0798 \\ 0.1111 & 0.0271 & -0.0053 & 0.0349 & 0.0522 & 0.0934 & 0.0726 & -0.0397 \\ 0.1314 & 0.0034 & 0.0504 & 0.0677 & -0.0467 & 0.0747 & 0.0406 & -0.0345 \\ -0.0781 & 0.0306 & -0.0532 & 0.0336 & 0.0234 & 0.0026 & -0.0830 & 0.1165 \end{bmatrix} \tag{7.47}$$

With this gain, eigenvalues of closed-loop system are observed to be inside the unit circle in z-plane, and these are given in Table 7.3.

Here, effort was taken to employ the two-time-scale POF scheme by taking into account regrouping of states into slow and fast subsystems as

$$\mathbf{z}_{A,k} = \begin{bmatrix} \mathbf{z}_{1,k} \end{bmatrix} \tag{7.48}$$

$$\mathbf{z}_{B,k} = \begin{bmatrix} \mathbf{z}_{2,k} \ \mathbf{z}_{3,k} \end{bmatrix}. \tag{7.49}$$

Table 7.3 Closed-loop Eigenvalues

Sr. No.	Eigenvalues	Sr. No.	Eigenvalues
Slow subsystem		Fast 1 subsystem	
1	9.999×10^{-1}	39	8.707×10^{-1}
2	9.998×10^{-1}	40	8.249×10^{-1}
3	9.993×10^{-1}	41	5.426×10^{-1}
4	9.992×10^{-1}	42	5.412×10^{-1}
5	9.990×10^{-1}	43	5.002×10^{-1}
6	9.989×10^{-1}	44	4.992×10^{-1}
7	9.986×10^{-1}	45	4.885×10^{-1}
8	9.985×10^{-1}	46	4.884×10^{-1}
9	9.985×10^{-1}	47	4.847×10^{-1}
10	9.984×10^{-1}	48	4.830×10^{-1}
11	9.983×10^{-1}	49	4.761×10^{-1}
12	9.982×10^{-1}	50	4.755×10^{-1}
13	9.974×10^{-1}	51	4.741×10^{-1}
14	9.972×10^{-1}	52	4.730×10^{-1}
15	9.972×10^{-1}	53	4.726×10^{-1}
16	9.971×10^{-1}	54	4.718×10^{-1}
17	9.969×10^{-1}	55	4.703×10^{-1}
18	9.968×10^{-1}	56	4.701×10^{-1}
19	9.967×10^{-1}	57	2.452×10^{-1}
20	9.962×10^{-1}	58	1.711×10^{-1}
21	9.957×10^{-1}	59	1.711×10^{-1}
22	9.952×10^{-1}	60	1.691×10^{-1}
23	9.949×10^{-1}	61	1.683×10^{-1}
24	9.948×10^{-1}	62	1.542×10^{-1}
25	9.944×10^{-1}	63	1.541×10^{-1}
26	9.941×10^{-1}	64	1.527×10^{-1}
27	9.940×10^{-1}	65	1.509×10^{-1}
28	9.938×10^{-1}	66	1.411×10^{-1}
29	9.933×10^{-1}	67	1.410×10^{-1}
30	9.932×10^{-1}	68	1.396×10^{-1}
31	9.929×10^{-1}	69	1.368×10^{-1}
32	9.928×10^{-1}	70	1.148×10^{-1}
33	9.924×10^{-1}	71	1.146×10^{-1}
34	9.921×10^{-1}	72	1.137×10^{-1}
35	9.920×10^{-1}	73	1.100×10^{-1}
36	9.918×10^{-1}	Fast 2 subsystem	
37	9.912×10^{-1}	74–90	0
38	9.907×10^{-1}		

It should be noted that the group of fast subsystem states is formed by clubbing states of fast 1 and fast 2 subsystems of three-time-scale system, given by (7.45). Alternatively, fast and very fast modes represented respectively in Fig. 3.1b, c are combined to form fast subsystem of order 52 and slow modes (Fig. 3.1a) are selected as slow subsystem of order 38. Yet, this idea does not work as the various matrices are as ill-conditioned as the matrices of the original system. Afterward the two-time-scale scheme with reorganization of states

$$\mathbf{z}_{a,k} = \left[\, \mathbf{z}_{1,k} \; \mathbf{z}_{2,k} \,\right] \tag{7.50}$$

$$\mathbf{z}_{b,k} = \left[\, \mathbf{z}_{3,k} \,\right] \tag{7.51}$$

was attempted. Herein, slow and fast 1 states of the three-time-scale system (7.45) are combined to get slow subsystem of the two-time-scale system. To be exact, slow and fast modes in Fig. 3.1a, b respectively are clubbed to form slow subsystem of dimension 73 and very fast modes (Fig. 3.1c) are taken as fast subsystem of dimension 17. Considering this type of regrouping, effort reduction in computation is observed to be insignificant. On the other hand, the ill-conditioning could effectively be avoided and the two-time-scale design method [14] could be used to get POF gains. In Sect. 7.4.2, the simulation results generated with three-time-scale based POF scheme are compared with two-time-scale POF and the two-time-scale fast output sampling (FOS) design scheme with the grouping of states given by (7.50) and (7.51) [6].

7.4.1 Controller Implementation

POF controller implementation plan for AHWR spatial control is shown in Fig. 7.2. In this, 17 nodal powers are sensed by the appropriate in-core detectors. These are then sampled periodically with the sampling interval of τ s and compared with their respective equilibrium values to get the normalized deviations. From these deviations the output vector $\mathbf{y}$ is constructed. Then $K_0 y$, $K_1 y$, …, $K_5 y$ are calculated and the spatial component of input $\mathbf{u}_{sp}$ is obtained by choosing the suitable $K_l y$ ($l = 0, 1, \ldots, 5$). Total power deviations from its equilibrium value of 920.48 MW is also calculated and total power-dependent term $\mathbf{u}_{gp}$ is determined on a continuous basis. Afterwards, $\mathbf{u}_{gp}$ and $\mathbf{u}_{sp}$, so generated, are added to obtain v_2, v_4, v_6, and v_8. These control signals are then given to individual regulating rod (RR) drives. This POF-based control method is extremely comparable in structure to straightforward output feedback based method, except the input in POF is changed to different values at the input sampling intervals $l = 0, 1, \ldots, 5$.

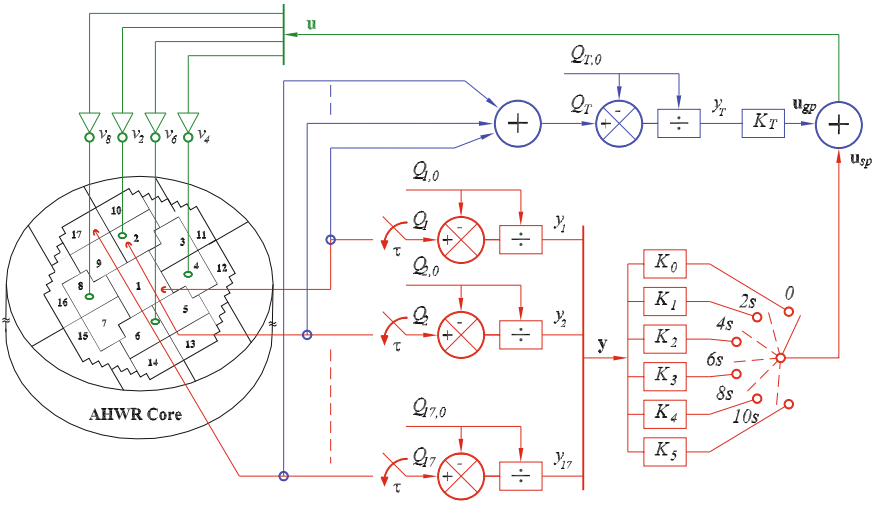

Fig. 7.2 POF control scheme for AHWR

7.4.2 Transient Simulations

Closed-loop performance of the AHWR system under various transient conditions can be assessed by simulating nonlinear model discussed in Chap. 2 with POF controller. As mentioned in Sect. 7.4.1, total power feedback control $\mathbf{u}_{gp}$ is given on continuous basis, i.e., on finer time steps for controlling fast transients in the total power. However, for spatial stabilization, control signal $\mathbf{u}_k$ is generated and given to RRs together with the total power feedback controller, as described in Sect. 7.4.1. For $\mathbf{u}_k$, τ and Δ are respectively taken as 12 and 2 s.

To begin with, transient associated with the spatial power disturbance is considered. In this, the system is observed to be at steady state, with all RRs at their equilibrium positions. Suddenly, RR2, initially under automatic control, is manually taken out by about 1% and thereafter shifted again under automatic control. This created spatial power disturbance. Control signals produced by spatial power controller and respective RR positions are depicted in Figs. 7.3 and 7.4, respectively. During this transient, total power experiences variations from 920.2 and 920.8 MW and reaches steady value of 920.48 MW in about 120 s, as shown in Fig. 7.5. Spatial power variations determined in terms of first and second azimuthal tilts are controlled within 400 s as shown in Fig. 7.6. Throughout prolonged simulation no tilts were observed.

Further to test the performance of system under feed flow disturbance, a situation is simulated wherein the reactor is working at steady state when a 5% positive step was initiated in the feed flow. Here, the controller performance is compared with the fast output sampling (FOS) technique and POF control, both designed using the two-time-scale approach, with the regrouping of states given by (7.50) and (7.51).

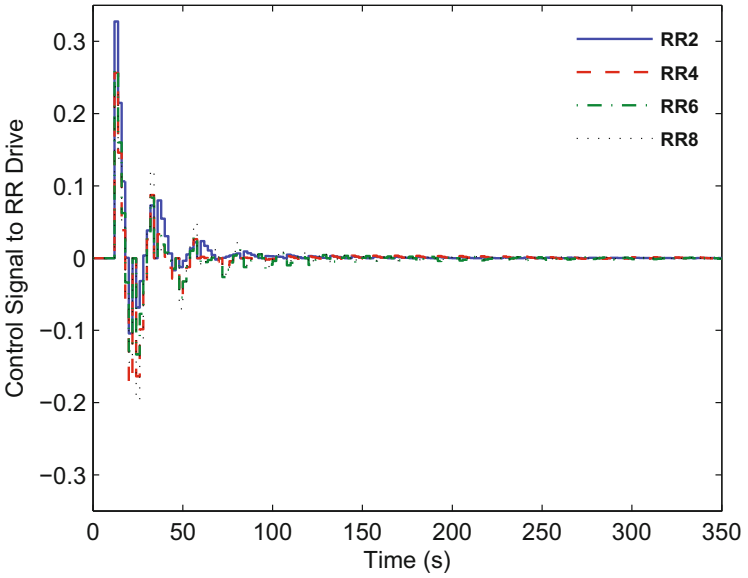

Fig. 7.3 Control signal to RR drives

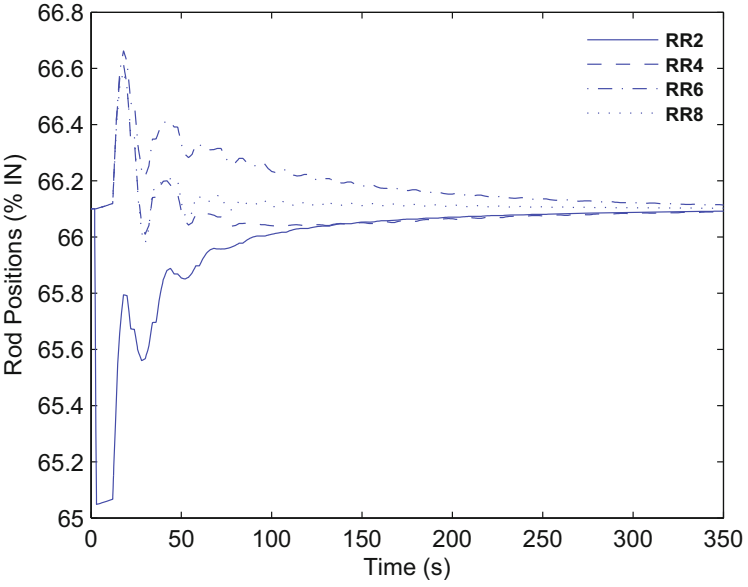

Fig. 7.4 Variations in RR positions

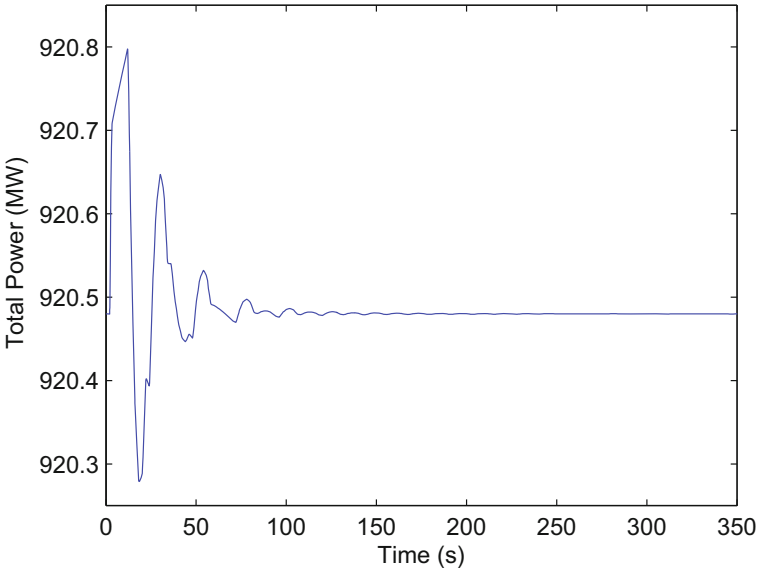

Fig. 7.5 Total power variations following perturbation in RR2

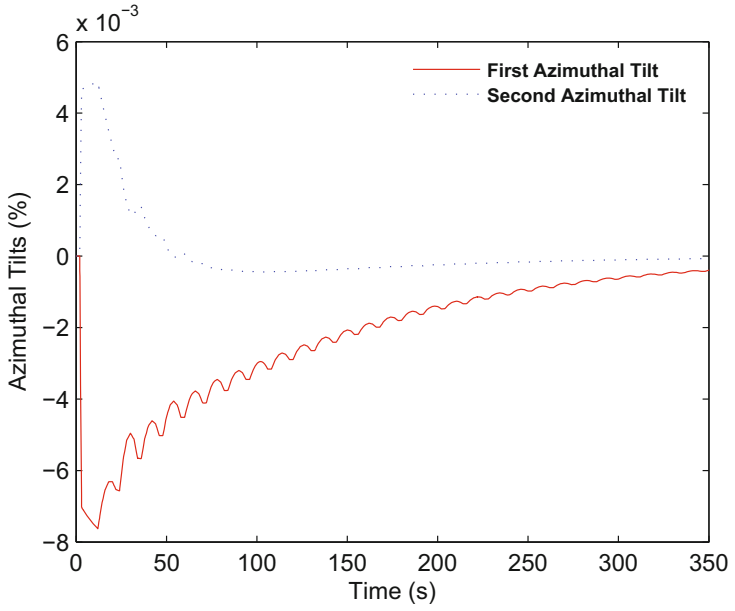

Fig. 7.6 Deviations in azimuthal tilts

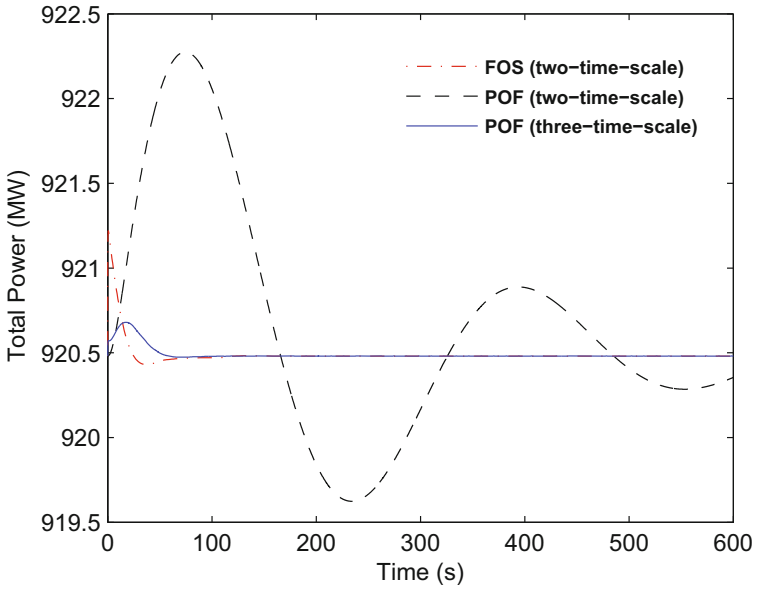

Fig. 7.7 Variations in total power due to feed flow disturbance

As a result of disturbance, the incoming coolant enthalpy decreased by about 0.64% and total power experienced variations as depicted in Fig. 7.7. It is seen that, with all the control techniques the total power is achieving steady state value after the introduction of disturbance. But, time required for stabilization is different. Total power stabilizes in about 100 s in FOS (two-time-scale) and POF (three-time-scale), while in case of POF (two-time-scale) it attains steady state after 650 s. Apart from this, the overshoot is also found to be more in POF (two-time-scale) based controller. For balancing the step change in the feed flow, all RRs are moved in by 1.02, 0.95, and 1% respectively in POF (three-time-scale), FOS and POF (two-time-scale), as depicted in Fig. 7.8. In this case also, the settling time of RR positions is significantly more in POF (two-time-scale) approach.

In one more case of simulation, first, the reactor was observed to be under steady state and working at 920.48 MW with distribution of nodal powers as specified in Table 2.5. Now, the demand in total power is reduced consistently at the rate of 1.5 MW/s to 828.43 MW, in almost 61 s and held steady afterward. Throughout the transient, it is noted that, the total power is tracking the demand power as shown in Fig. 7.9. Once again the results are compared with POF (two-time-scale), and it is found that the performance of presented POF control is better than POF (two-time-scale) control. It is observed that, the xenon concentrations settle to their respective new steady states in about 50 h. Whereas, the nodal powers achieve the steady state within 100 s.

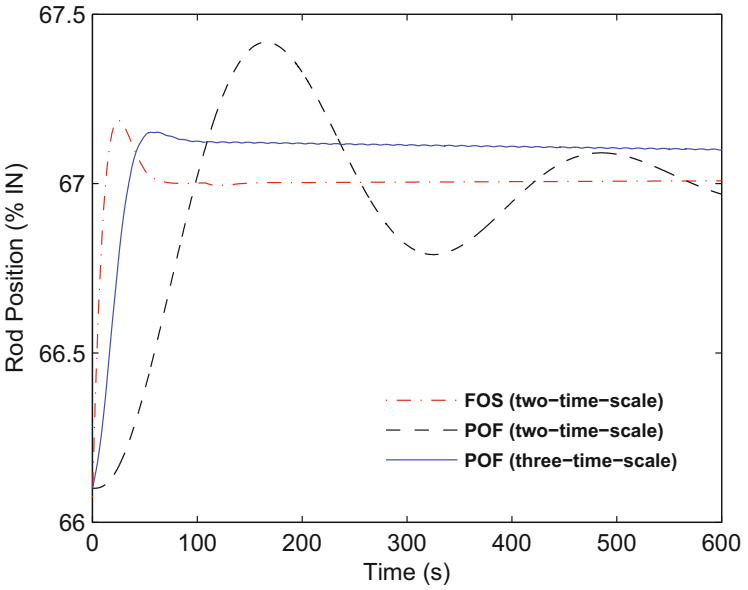

Fig. 7.8 Variations in regulating rod positions due to feed flow disturbance

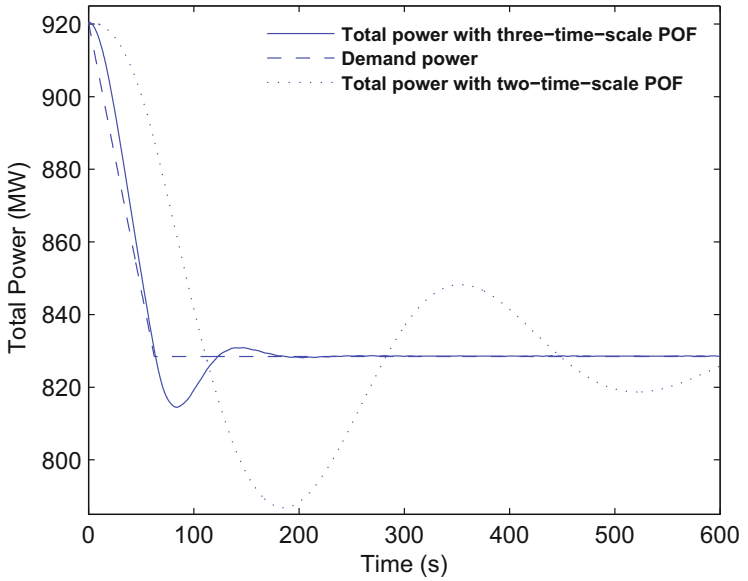

Fig. 7.9 Total power variations during power maneuvering from 920.48 to 828.43 MW

7.5 Conclusion

In this chapter, three-stage design of POF controller for spatial control of AHWR is presented. Three-stage decomposition technique is employed to decouple numerically ill-conditioned model of AHWR into slow, fast 1, and fast 2 subsystems. POF gains of the subsystems are calculated separately and then they are combined to get the POF gains for the original system. Since fast 1 and fast 2 subsystems are observed to be stable, output injection gains for these subsystems are selected as zero. POF gain calculated from the slow subsystem alone is utilized in dynamic simulations, carried out under various transient conditions. Since the controller is utilizing feedback of outputs only, state observer is not required. In addition to this, the controller performance is compared with FOS technique and the performance is observed to be superior. Overall performance of controller is observed to be acceptable.

References

1. Bandyopadhyay, B., Lal Priya, P.S.: Discrete-time sliding mode control using infrequent output measurements. Int. Conf. Adv. Mechatron. Syst., 491–496 (2011)
2. Chammas, A.B., Leondes, C.T.: Pole assignment by piecewise constant output feedback. Int. J. Control **29**(1), 31–38 (1979)
3. Chen, C.-T.: Linear System Theory and Design. Oxford University Press, New York (1999)
4. Hagiwara, T., Araki, M.: On the necessary condition for discrete-time pole assignability by piecewise constant output feedback. Int. J. Control **43**(2), 1905–1909 (1986)
5. Lal Priya, P.S., Bandyopadhyay, B.: Periodic output feedback based discrete-time sliding mode control for multivariable systems. Proc. IEEE Int. Conf. Ind. Technol., 893–898 (2012)
6. Munje, R.K., Patre, B.M., Tiwari, A.P.: Periodic output feedback for spatial control of AHWR: a three-time-scale approach. IEEE Trans. Nucl. Sci. **61**(4), 2373–2382 (2014)
7. Naidu, D.S.: Singular Perturbation Methodology in Control Systems. Peter Peregrinus Ltd., London (1988)
8. Nair, J.M., Lazar, A., Bandyopadhyay, B.: Robust control for uncertain singular perturbed systems using periodic output feedback. Proc. Am. Control Conf., 4326–4331 (2006)
9. Patre, B.M., Bandyopadhyay, B.: Periodic output feedback control for two-time-scale discrete systems. Proc. IEEE Int. Conf. Global Connectivity Energy, Computer, Commun. Control **1**, 174–177 (1998)
10. Patre, B.M., Bandyopadhyay, B., Werner, H.: Control of discrete two-time-scale system by using piecewise constant periodic output feedback. Syst. Sci. **23**, 23–37 (1997)
11. Patre, B.M., Bandyopadhyay, B., Werner, H.: Periodic output feedback control for singularly perturbed discrete model of steam power system. Proc. IEE Control Theory Appl. **146**(3), 247–252 (1999)
12. Shimjith, S.R., Tiwari, A.P., Bandyopadhyay, B.: Design of fast output sampling controller for three-time-scale systems: application to spatial control of advanced heavy water reactor. IEEE Trans. Nucl. Sci. **58**(6), 3305–3316 (2011)
13. Tiwari, A.P., Bandyopadhyay, B., Werner, H.: Spatial control of a large pressurize heavy water reactor by piecewise constant periodic output feedback. IEEE Trans. Nucl. Sci. **47**, 389–402 (2000)
14. Tiwari, A.P., Reddy, G.D., Bandyopadhyay, B.: Design of periodic output feedback and fast output sampling based controllers for systems with slow and fast modes. Asian J. Control **14**(1), 271–277 (2012)

15. Werner, H.: Robust multivariable control of a turbo-generator by periodic output feedback. Proc. Am. Control Conf. **3**, 1979–1983 (1997)
16. Werner, H., Furuta, K.: Simultaneous stabilization based on output measurement. Kybernetica **31**, 395–414 (1995)

Chapter 8
Discrete-Time Sliding Mode Control

8.1 Introduction

The advent of digital computers and samplers in control implementation has broadened the study of discrete-time systems and the design of sliding mode control (SMC) in discrete-time. Discrete sliding mode control (DSMC) theory is being investigated since long. As the control is constant between the sampling intervals, the switching frequency cannot be less than sampling frequency. As a result, the use of discontinuous control in the presence of sample and hold leads to a finite amplitude oscillations [2]. This is known as chattering in DSMC. The system shows a sliding behavior if their motion is confined to a manifold in state space which is reached in finite time [20]. Then, the discrete-time sliding mode may arise in the systems with piecewise constant control. Kotta [9] noticed that unlike in continuous-time SMC, the control in DSMC case must have upper and lower bounds such that trajectory is attracted towards the switching surface. DSMC may generally result in zigzag motion. Conditions for existence of discrete-time sliding mode control, which eliminate zigzag motion are presented in [21]. Further, Gao et al. [6] introduced a new reaching law based approach for DSMC using state feedback.

The analysis and design of controllers of discrete two-timescale system has been studied in [11, 12, 15, 17] using explicitly invertible linear transformation. When certain inequalities relating the norms of subsystem matrices are satisfied, then the original discrete model can be approximately decomposed into two lower order models operating on different time-scales. One is called slow subsystem with absolute large eigenvalues distributed near the unit circle and other is fast subsystem with absolute small eigenvalues centered around the origin in the z-plane. This explicitly invertible transformation, used to decouple slow and fast subsystems is termed as block diagonalization. Block diagonalization of discrete three-time-scale system is also presented in [15, 19], in which the higher order system is decoupled into three subsystems, namely, slow, fast 1, and fast 2 subsystems.

R. Munje et al., *Investigation of Spatial Control Strategies with Application to Advanced Heavy Water Reactor*, Energy Systems in Electrical Engineering, https://doi.org/10.1007/978-981-10-3014-7_8

Regardless of other advantages, the sliding mode controller for any system has a complexity proportional to the number of states in the system. Hence, for a higher order ill-conditioned system, the sliding mode control design is also more complicated. Control of singularly perturbed two-time-scale systems has been attempted by several researches with discrete-time sliding mode control [1, 10, 16, 18]. In [10], higher order system is decomposed into two subsystems, i.e., slow and fast subsystems. Then slow and fast DSMC laws for the subsystems are designed and composite discrete sliding mode controller is obtained. The stability of system is assessed by Lyapunov method. Further in [1], fast subsystem is assumed to be stable and DSMC is designed using only the slow subsystem with constant plus proportional rate reaching law. This is then represented in original states and applied to the full-order system. Since, all the states are not always available for measurement, a chatter-free multirate output feedback based discrete-time sliding mode control for two-time-scale system is proposed in [18]. Output feedback DSMC for singularly perturbed system with disturbance is also addressed in [16].

This chapter describes brief background of discrete-time sliding mode control with both constant plus proportional rate reaching law (CPPRRL) and power rate reaching law (PRRL). The sliding mode controller discussed in Chap. 5 is different from this one in three ways. First the design is in discrete-time, second, in the former, the control was based only on constant rate reaching law and third, SMC implementation in Chap. 5 rests upon two-stage decomposition, whereas in this chapter formulation will be based on three-stage decomposition. In this chapter, a novel algorithm of DSMC for the system with slow, fast, and very fast varying modes with both the reaching laws is presented. These discrete-time sliding mode controls are then examined for spatial control of Advanced Heavy Water Reactor (AHWR). Simulation results, obtained with both the controls under the same transient conditions, are compared.

8.2 Discrete-Time Sliding Mode Control

The term discrete-time sliding mode control was first proposed by Utkin and Drakunov [3]. According to the concept proposed, the system shows a sliding behavior if their motion is confined to a manifold which is reached in finite time. Then, the discrete-time sliding mode may arise with piecewise constant control. For discrete-time sliding mode control, the structures of the control are similar to that of continuous-time control. Gao et al. [6, 8] used a reaching law approach to develop control for discrete variable structure system for robust control, which possesses following attributes:

1. Starting from any initial stage, the trajectory will move monotonically towards the switching plane and cross it in finite time.
2. Once the trajectory has crossed the switching surface the first time, it will keep crossing it resulting in a zigzag motion.
3. The size of each successive zigzagging step is non-increasing and trajectory stays within specified band.

Consider a linear time-invariant, controllable continuous-time system as

$$\dot{\mathbf{z}} = \mathbf{A}\mathbf{z} + \mathbf{B}\mathbf{u}, \tag{8.1}$$

$$\mathbf{y} = \mathbf{M}\mathbf{z} \tag{8.2}$$

where the state $\mathbf{z} \in \Re^n$, input $\mathbf{u} \in \Re^m$, and output $\mathbf{y} \in \Re^p$ with $1 \leq m \leq n$. The matrices $\mathbf{A}$, $\mathbf{B}$, and $\mathbf{M}$ are constants of appropriate dimensions. Sampling the continuous-time system (8.1)–(8.2) with sampling period τ yields discrete-time system as

$$\mathbf{z}_{k+1} = \Phi\mathbf{z}_k + \Gamma\mathbf{u}_k, \tag{8.3}$$

$$\mathbf{y}_k = \mathbf{M}\mathbf{z}_k. \tag{8.4}$$

As the system (8.1) is controllable, the system (8.3) is also generically controllable. Further, it is assumed that input distribution matrix Γ has full rank. Hence, there exits an orthogonal transformation matrix $\mathbf{T}_r \in \Re^{n\times n}$ for system (8.3) such that $\mathbf{T}_r\Gamma = \begin{bmatrix}\mathbf{0} & \bar{\Gamma}_2^T\end{bmatrix}^T$, where $\bar{\Gamma}_2 \in \Re^{m\times m}$ and is nonsingular. This is similar to the continuous-time counterpart of SMC as discussed in Sect. 5.2. Under this transformation, the system (8.3) can be transformed into regular form [4], given as

$$\begin{bmatrix}\bar{\mathbf{z}}_{1,k+1}\\ \bar{\mathbf{z}}_{2,k+1}\end{bmatrix} = \begin{bmatrix}\bar{\Phi}_{11} & \bar{\Phi}_{12}\\ \bar{\Phi}_{21} & \bar{\Phi}_{22}\end{bmatrix}\begin{bmatrix}\bar{\mathbf{z}}_{1,k}\\ \bar{\mathbf{z}}_{2,k}\end{bmatrix} + \begin{bmatrix}\mathbf{0}\\ \bar{\Gamma}_2\end{bmatrix}\mathbf{u}_k \tag{8.5}$$

such that

$$\begin{bmatrix}\bar{\mathbf{z}}_{1,k}\\ \bar{\mathbf{z}}_{2,k}\end{bmatrix} = \bar{\mathbf{z}}_k = \mathbf{T}_r\mathbf{z}_k \tag{8.6}$$

where $\bar{\mathbf{z}}_{1,k} \in \Re^{n-m}$ and $\bar{\mathbf{z}}_{2,k} \in \Re^m$.

8.2.1 Design of Sliding Surface

Let us define a sliding function [4] for the system (8.5) of the form $\mathbf{s}_k = \bar{\mathbf{C}}^T\bar{\mathbf{z}}_k$ with the sliding function parameter be of the form

$$\bar{\mathbf{C}}^T = \begin{bmatrix}\mathbf{K} & \mathbf{E}_m\end{bmatrix}, \tag{8.7}$$

where $\mathbf{K}$ is $(m \times (n-m))$ matrix and $\mathbf{E}_m$ is identity matrix of order m. System dynamics during sliding mode are characterized by the sliding surface. Then, the sliding surface is given by

$$\mathbf{s}_k = \bar{\mathbf{C}}^T\bar{\mathbf{z}}_k = 0. \tag{8.8}$$

Hence, from the sliding function parameter (8.7) and sliding surface expression (8.8), one can easily find the relationship

$$\bar{\mathbf{z}}_{2,k} = -\mathbf{K}\bar{\mathbf{z}}_{1,k} \tag{8.9}$$

where $\bar{\mathbf{z}}_{2,k}$ constitutes the last m states of $\bar{\mathbf{z}}_k$. Then, the sliding mode dynamics of $\bar{\mathbf{z}}_{1,k}$ can be represented as

$$\begin{aligned}\bar{\mathbf{z}}_{1,k+1} &= \bar{\Phi}_{11}\bar{\mathbf{z}}_{1,k} - \bar{\Phi}_{12}\mathbf{K}\bar{\mathbf{z}}_{1,k} \\ &= (\bar{\Phi}_{11} - \bar{\Phi}_{12}\mathbf{K})\bar{\mathbf{z}}_{1,k}.\end{aligned} \tag{8.10}$$

If $\mathbf{K}$, in (8.10), is so designed that the eigenvalues of $(\bar{\Phi}_{11} - \bar{\Phi}_{12}\mathbf{K})$ are assigned within the unit circle, then $\bar{\mathbf{z}}_{1,k}$ is stabilized during sliding phase. Since, the system (8.3) is controllable, pair $(\bar{\Phi}_{11}, \bar{\Phi}_{12})$ is also controllable. Therefore, sliding surface design problem can be considered as the pole placement problem for $(\bar{\Phi}_{11}, \bar{\Phi}_{12})$. Consequently from (8.9), $\bar{\mathbf{z}}_{2,k}$ is also stable confined to the sliding surface. Thus, the stability requirement of the sliding surface is achieved. Now, the sliding surface for original system (8.3) can be expressed in terms of the original state coordinates as

$$\mathbf{s}_k = \bar{\mathbf{C}}^T\bar{\mathbf{z}}_k = \bar{\mathbf{C}}^T\mathbf{T}_r\mathbf{z}_k = \mathbf{C}^T\mathbf{z}_k. \tag{8.11}$$

8.2.2 Design of Discrete-Time Sliding Mode Controller

Once a sliding surface (8.11) is designed, DSMC can be obtained using reaching law approach. The reaching law is a differential equation which specifies the dynamics of a switching function. Following are the two structures of reaching law, which are discussed for design purpose.

8.2.2.1 Constant Plus Proportional Rate Reaching Law

From [6], reaching law is given by

$$\mathbf{s}_{k+1} - \mathbf{s}_k = -q\tau\mathbf{s}_k - \eta\tau sgn(\mathbf{s}_k) \tag{8.12}$$

where $\tau > 0$ is a sampling interval, $\eta > 0$, $q > 0$, $(1 - q\tau) > 0$. Discrete-time controller for system (8.3) using stable sliding surface (8.11) can be obtained from (8.12) as

$$\mathbf{u}_k = \mathbf{F}_1\mathbf{z}_k + p_1 sgn(\mathbf{s}_k) \tag{8.13}$$

where

$$\mathbf{F}_1 = -(\mathbf{C}^T \Gamma)^{-1} \mathbf{C}^T (\Phi - \mathbf{E}_n + q\tau), \tag{8.14}$$

$$p_1 = -(\mathbf{C}^T \Gamma)^{-1} \eta\tau \tag{8.15}$$

where $sgn(\cdot)$ is signum function and $\mathbf{E}_n$ is identity matrix of dimension n. The inequality $(1 - q\tau) > 0$ must hold to guarantee the stability of reaching phase of closed-loop system. This implies that the choice of $\tau > 0$ is restricted. Also, the presence of signum term guarantees that once the trajectory has crossed the switching surface the first time, it will cross the surface again in every successive sampling period. The motion is zigzag and is non-increasing. The trajectory stays within a specified band called the quasi-sliding mode band. The width of quasi-sliding mode band δ [7], within which the system states remain in steady state, can be given by

$$2\delta \leq \frac{2\eta\tau}{2 - q\tau}. \tag{8.16}$$

8.2.2.2 Power Rate Reaching Law

The discrete power rate reaching law can be obtained from the continuous power rate reaching law [5] as

$$\mathbf{s}_{k+1} - \mathbf{s}_k = -q\tau |\mathbf{s}_k|^a sgn(\mathbf{s}_k) \tag{8.17}$$

where $0 < q\tau < 1$ and $0 < a \leq 1$. Thus, DSMC for system (8.3) with sliding surface (8.11), based on reaching law (8.17), can be found as

$$\mathbf{u}_k = \mathbf{F}_2 \mathbf{z}_k + p_2 |\mathbf{s}_k|^a sgn(\mathbf{s}_k) \tag{8.18}$$

where

$$\mathbf{F}_2 = -(\mathbf{C}^T \Gamma)^{-1} \mathbf{C}^T (\Phi - \mathbf{E}_n), \tag{8.19}$$

$$p_2 = -(\mathbf{C}^T \Gamma)^{-1} q\tau. \tag{8.20}$$

The band in which the system remains confined can be obtained as

$$\delta = \left(\frac{q\tau}{2}\right)^{\frac{1}{1-a}}. \tag{8.21}$$

In order to obtain a small band, the condition

$$\left(\frac{q\tau}{2}\right) < 1 \tag{8.22}$$

should be satisfied.

8.3 DSMC for Three-Time-Scale System

Consider that linear time-invariant discrete-time system given by (8.3) possesses three-time-scale property so that it can be represented as

$$\begin{bmatrix} \mathbf{z}_{1,k+1} \\ \mathbf{z}_{2,k+1} \\ \mathbf{z}_{3,k+1} \end{bmatrix} = \begin{bmatrix} \Phi_{11} & \Phi_{12} & \Phi_{13} \\ \Phi_{21} & \Phi_{22} & \Phi_{23} \\ \Phi_{31} & \Phi_{32} & \Phi_{33} \end{bmatrix} \begin{bmatrix} \mathbf{z}_{1,k} \\ \mathbf{z}_{2,k} \\ \mathbf{z}_{3,k} \end{bmatrix} + \begin{bmatrix} \Gamma_1 \\ \Gamma_2 \\ \Gamma_3 \end{bmatrix} \mathbf{u}_k, \tag{8.23}$$

$$\mathbf{y}_k = \begin{bmatrix} \mathbf{M}_1 & \mathbf{M}_2 & \mathbf{M}_3 \end{bmatrix} \begin{bmatrix} \mathbf{z}_{1,k}^T & \mathbf{z}_{2,k}^T & \mathbf{z}_{3,k}^T \end{bmatrix}^T \tag{8.24}$$

where $\mathbf{z}_{1,k} \in \Re^{n_1}$, $\mathbf{z}_{2,k} \in \Re^{n_2}$, $\mathbf{z}_{3,k} \in \Re^{n_3}$ denote states such that $n_1 + n_2 + n_3 = n$ and the matrices Φ_{ij}, Γ_i, and $\mathbf{M}_i$ are of appropriate dimensionality. Using the technique described in Appendix B, system (8.23)–(8.24) can be decoupled into three subsystems, named, slow, fast 1, and fast 2, and can be represented in block diagonal form as

$$\begin{bmatrix} \mathbf{z}_{s,k+1} \\ \mathbf{z}_{f1,k+1} \\ \mathbf{z}_{f2,k+1} \end{bmatrix} = \begin{bmatrix} \Phi_s & \mathbf{0} & \mathbf{0} \\ \mathbf{0} & \Phi_{f1} & \mathbf{0} \\ \mathbf{0} & \mathbf{0} & \Phi_{f2} \end{bmatrix} \begin{bmatrix} \mathbf{z}_{s,k} \\ \mathbf{z}_{f1,k} \\ \mathbf{z}_{f2,k} \end{bmatrix} + \begin{bmatrix} \Gamma_s \\ \Gamma_{f1} \\ \Gamma_{f2} \end{bmatrix} \mathbf{u}_k, \tag{8.25}$$

$$\mathbf{y}_k = \begin{bmatrix} \mathbf{M}_s & \mathbf{M}_{f1} & \mathbf{M}_{f2} \end{bmatrix} \begin{bmatrix} \mathbf{z}_{s,k}^T & \mathbf{z}_{f1,k}^T & \mathbf{z}_{f2,k}^T \end{bmatrix}^T \tag{8.26}$$

where $\mathbf{z}_{s,k} \in \Re^{n_1}$, $\mathbf{z}_{f1,k} \in \Re^{n_2}$ and $\mathbf{z}_{f2,k} \in \Re^{n_3}$ denote respectively slow, fast 1, and fast 2 states. The relation between the states of original system (8.23) and the states of decoupled system (8.25) is given by

$$\mathbf{z}_{d,k} = \mathbf{T}\mathbf{z}_k \tag{8.27}$$

where $\mathbf{z}_{d,k} = \begin{bmatrix} \mathbf{z}_{s,k}^T & \mathbf{z}_{f1,k}^T & \mathbf{z}_{f2,k}^T \end{bmatrix}^T$, $\mathbf{z}_k = \begin{bmatrix} \mathbf{z}_{1,k}^T & \mathbf{z}_{2,k}^T & \mathbf{z}_{3,k}^T \end{bmatrix}^T$ and transformation matrix $\mathbf{T} \in \Re^{n \times n}$. System (8.23) is decoupled into three subsystems in (8.25), namely, the slow subsystem represented by (Φ_s, Γ_s), the fast 1 subsystem given by (Φ_{f1}, Γ_{f1}), and the fast 2 subsystem (Φ_{f2}, Γ_{f2}), of orders n_1, n_2, and n_3 respectively. The system formulation (8.25)–(8.26) is related to its original form (8.23)–(8.24) via linear transformation (8.27). Therefore, pairs (Φ_s, Γ_s), (Φ_{f1}, Γ_{f1}), and (Φ_{f2}, Γ_{f2}) are controllable. Further it is assumed that, the fast 1, and fast 2 subsystems are stable. Hence, discrete-time sliding mode controller is designed, for the system (8.23), using slow subsystem alone. For that, from (8.25), slow subsystem can be written as

$$\mathbf{z}_{s,k+1} = \Phi_s \mathbf{z}_{s,k} + \Gamma_s \mathbf{u}_k. \tag{8.28}$$

The relationship between slow subsystem states (8.28) and states of system (8.25) is given by

$$\mathbf{z}_{s,k} = \begin{bmatrix} \mathbf{E}_{n_1} & \mathbf{0} & \mathbf{0} \end{bmatrix} \mathbf{z}_{d,k} = \mathbf{T}_s \mathbf{z}_{d,k} \tag{8.29}$$

where transformation matrix $\mathbf{T}_s \in \Re^{n_1 \times n}$. If Γ_s has full rank, i.e., $rank(\Gamma_s) = m$, then stable switching surface for system (8.28) can be defined as

$$\mathbf{s}_{s,k} = \mathbf{C}^T \mathbf{z}_{s,k}. \tag{8.30}$$

The design of stable sliding surface is already discussed in Sect. 8.2.1.

Lemma 8.1 *If motion around* $\mathbf{s}_{s,k} = \mathbf{C}^T \mathbf{z}_{s,k}$, *for the system (8.28) is stable then the motion around*

$$\mathbf{s}_k = \mathbf{C}^T \mathbf{T}_s \mathbf{T} \mathbf{z}_k \tag{8.31}$$

for system (8.3) is also stable.

Proof As $\mathbf{s}_{s,k} = \mathbf{C}^T \mathbf{z}_{s,k}$ is a stable sliding surface for (8.28), the motion around $\mathbf{s}_{s,k}$ can be obtained by setting $\mathbf{s}_{s,k+1} = 0$. Therefore, equivalent discrete-time sliding mode control law is

$$\mathbf{u}_k = -(\mathbf{C}^T \Gamma_s)^{-1} \mathbf{C}^T \Phi_s \mathbf{z}_{s,k}. \tag{8.32}$$

Thus, the motion along $\mathbf{z}_{s,k}$ is given by

$$\mathbf{z}_{s,k+1} = (\Phi_s - \Gamma_s (\mathbf{C}^T \Gamma_s)^{-1} \mathbf{C}^T \Phi_s) \mathbf{z}_{s,k}. \tag{8.33}$$

As Eq. (8.33) is stable by design, eigenvalues of $(\Phi_s - \Gamma_s (\mathbf{C}^T \Gamma_s)^{-1} \mathbf{C}^T \Phi_s)$ will be stable. Now let us find motion around $\mathbf{s}_k = \mathbf{C}^T \mathbf{T}_s \mathbf{z}_{d,k}$ for the system (8.25) by setting $\mathbf{s}_{k+1} = 0$ and writing equivalent control as

$$\mathbf{u}_k = -(\mathbf{C}^T \Gamma_s)^{-1} \mathbf{C}^T \begin{bmatrix} \Phi_s & \mathbf{0} & \mathbf{0} \end{bmatrix} \mathbf{z}_{d,k}. \tag{8.34}$$

Thus, the motion around the switching surface $\mathbf{s}_k$ is

$$\begin{aligned} \mathbf{z}_{d,k+1} &= \begin{bmatrix} \Phi_s & \mathbf{0} & \mathbf{0} \\ \mathbf{0} & \Phi_{f1} & \mathbf{0} \\ \mathbf{0} & \mathbf{0} & \Phi_{f2} \end{bmatrix} \mathbf{z}_{d,k} - \begin{bmatrix} \Gamma_s \\ \Gamma_{f1} \\ \Gamma_{f2} \end{bmatrix} (\mathbf{C}^T \Gamma_s)^{-1} \mathbf{C}^T \begin{bmatrix} \Phi_s & \mathbf{0} & \mathbf{0} \end{bmatrix} \mathbf{z}_{d,k} \\ &= \begin{bmatrix} \Phi_s - \Gamma_s (\mathbf{C}^T \Gamma_s)^{-1} \mathbf{C}^T \Phi_s & \mathbf{0} & \mathbf{0} \\ -\Gamma_{f1} (\mathbf{C}^T \Gamma_s)^{-1} \mathbf{C}^T \Phi_s & \Phi_{f1} & \mathbf{0} \\ -\Gamma_{f2} (\mathbf{C}^T \Gamma_s)^{-1} \mathbf{C}^T \Phi_s & \mathbf{0} & \Phi_{f2} \end{bmatrix} \mathbf{z}_{d,k} \end{aligned} \tag{8.35}$$

As $(\Phi_s - \Gamma_s (\mathbf{C}^T \Gamma_s)^{-1} \mathbf{C}^T \Phi_s)$ is stable by design and Φ_{f1} and Φ_{f2} are assumed to be stable, the sliding motion of $\mathbf{s}_k = \mathbf{C}^T \mathbf{T}_s \mathbf{z}_{d,k}$ is stable. Further, systems (8.23)–(8.24) and (8.25)–(8.26) are related through (8.27), therefore (8.31) is stable sliding surface for (8.23) and hence for system (8.3).

Now the discrete-time sliding mode control can be designed for the system (8.28) using two reaching laws as discussed in Sect. 8.2.2.

8.3.1 Constant Plus Proportional Rate Reaching Law

For the slow subsystem (8.28) reaching law (8.12) can be stated as

$$\mathbf{s}_{s,k+1} - \mathbf{s}_{s,k} = -q\tau\mathbf{s}_{s,k} - \eta\tau sgn(\mathbf{s}_{s,k}). \tag{8.36}$$

Then, the control law can be represented as

$$\mathbf{u}_k = \mathbf{F}_1\mathbf{z}_{s,k} + p_1 sgn(\mathbf{s}_{s,k}) \tag{8.37}$$

where

$$\mathbf{F}_1 = -(\mathbf{C}^T\Gamma_s)^{-1}\mathbf{C}^T(\Phi_s - \mathbf{E}_{n_1} + q\tau), \tag{8.38}$$

$$p_1 = -(\mathbf{C}^T\Gamma_s)^{-1}\eta\tau. \tag{8.39}$$

This control will bring quasi-sliding mode motion for system (8.28).

Lemma 8.2 *If the control (8.37) is expressed in terms of the states of the original system (8.23) as*

$$\mathbf{u}_k = \mathbf{F}_1\mathbf{T}_s\mathbf{T}\mathbf{z}_k + p_1 sgn(\mathbf{C}^T\mathbf{T}_s\mathbf{T}\mathbf{z}_k) \tag{8.40}$$

and applied to the same, it results in a quasi-sliding mode motion of the same.

Proof From (8.30), reaching law (8.36) can be expressed as

$$\mathbf{C}^T\mathbf{z}_{s,k+1} - \mathbf{C}^T\mathbf{z}_{s,k} = -q\tau(\mathbf{C}^T\mathbf{z}_{s,k}) - \eta\tau\text{sgn}(\mathbf{C}^T\mathbf{z}_{s,k}). \tag{8.41}$$

Using relations (8.27) and (8.29), reaching law (8.41) can be rewritten as

$$\mathbf{C}^T\mathbf{T}_s\mathbf{T}\mathbf{z}_{k+1} - \mathbf{C}^T\mathbf{T}_s\mathbf{T}\mathbf{z}_k = -q\tau(\mathbf{C}^T\mathbf{T}_s\mathbf{T}\mathbf{z}_k) - \eta\tau\text{sgn}(\mathbf{C}^T\mathbf{T}_s\mathbf{T}\mathbf{z}_k). \tag{8.42}$$

Further using (8.31), system (8.42) can be modified to get

$$\mathbf{s}_{k+1} - \mathbf{s}_k = -q\tau\mathbf{s}_k - \eta\tau\text{sgn}(\mathbf{s}_k). \tag{8.43}$$

Thus, the reaching law (8.36) is equivalent to reaching law (8.43). Therefore, it can be concluded that, any control that satisfies the reaching law (8.41), would automatically satisfy the original system reaching law (8.43).

8.3.2 The Power Rate Reaching Law

For the slow subsystem (8.28) reaching law (8.17) can be defined as

$$\mathbf{s}_{s,k+1} - \mathbf{s}_{s,k} = -q\tau|\mathbf{s}_{s,k}|^a sgn(\mathbf{s}_{s,k}). \tag{8.44}$$

Then the control law can be given as

$$\mathbf{u}_k = \mathbf{F}_2\mathbf{z}_{s,k} + p_2|\mathbf{s}_{s,k}|^a sgn(\mathbf{s}_{s,k}) \tag{8.45}$$

where

$$\mathbf{F}_2 = -(\mathbf{C}^T\Gamma_s)^{-1}\mathbf{C}^T(\Phi_s - \mathbf{E}_{n_1}), \tag{8.46}$$

$$p_2 = -(\mathbf{C}^T\Gamma_s)^{-1}q\tau. \tag{8.47}$$

This control will bring quasi-sliding mode motion for system (8.28). Again, if the control in (8.45) is expressed in terms of the states of the original system as

$$\mathbf{u}_k = \mathbf{F}_2\mathbf{T}_s\mathbf{T}\mathbf{z}_k + p_2|\mathbf{C}^T\mathbf{T}_s\mathbf{T}\mathbf{z}_k|^a sgn(\mathbf{C}^T\mathbf{T}_s\mathbf{T}\mathbf{z}_k) \tag{8.48}$$

and applied to (8.23), it will result in a quasi-sliding mode motion of the same. Proof for this can be derived in the same way as that of Lemma 8.2.

8.4 Application of DSMC to AHWR Model

Three-time-scale nature of AHWR is discussed in Sect. 7.4. For properly selected sampling time, discrete version of the continuous-time system, exhibiting three-time-scale property, also exhibits three-time-scale property. In the case of AHWR, selection of sampling interval is based on time constant of delayed neutron precursor, which is of the order of 159 s [13]. For the several values of sampling period above 2 s, the proposed controller gives stable response but gain magnitude increases. However, below 2 s, time-scale property is not preserved. Hence, τ is selected as 2 s and system (7.42) is discretized to obtain

$$\mathbf{z}_{k+1} = \Phi\mathbf{z}_k + \Gamma\mathbf{u}_k + \Gamma_{fw}\delta q_{fwk} \tag{8.49}$$

where $\Phi = e^{\hat{\mathbf{A}}\tau}$, $\Gamma = \int_0^\tau e^{\hat{\mathbf{A}}s}\mathbf{B}ds$, and $\Gamma_{fw} = \int_0^\tau e^{\hat{\mathbf{A}}s}\mathbf{B}_{fw}ds$. Now, the discrete-time model (8.49) is block diagonalized, resulting into a slow subsystem of order 38, fast 1 subsystem of order 35, and fast 2 subsystem of order 17, with the state vector (2.17), partitioned as

$$\mathbf{z}_{1,k} = \left[\, \mathbf{z}_H^T \; \mathbf{z}_X^T \; \mathbf{z}_I^T \,\right]^T,$$
$$\mathbf{z}_{2,k} = \left[\, \delta h_d \; \mathbf{z}_C^T \; \mathbf{z}_x^T \,\right]^T,$$
$$\mathbf{z}_{3,k} = \mathbf{z}_Q.$$

The matrices Φ, Γ, and $\mathbf{M}$ are partitioned accordingly. The eigenvalues of the slow, fast 1, and fast 2 subsystems agree very well respectively with the largest 38, intermediate 35, and the smallest 17 eigenvalues of the original system for sampling rate $1/\tau$. It is verified that the slow, fast 1, and fast 2 subsystems are controllable and $rank(\Gamma_s) = m$. Also, it is observed that the eigenvalues of fast 1 and fast 2 subsystems are stable i.e. within unit circle in z-plane. Hence, discrete-time sliding mode controller is designed simply for the slow subsystem.

The stable sliding surface for slow subsystem, given by (8.30), is determined using the procedure discussed in Sect. 8.2.1. This is a common sliding surface for both CPPRRL and PRRL. With the hyperplane matrix $\mathbf{C}^T$ of order (4×38) sliding surface for original system of AHWR is formulated as per (8.31) satisfying Lemma 8.1. All the 90 eigenvalues of AHWR system are found to be stable, defined by (8.35). After that DSMC laws are constructed using both the reaching conditions.

First of all, DSMC is designed using CPPRRL. Sampling time τ is 2 s, therefore q is selected as 0.05, so that the condition $(1 - q\tau) > 0$ is satisfied. Further, η is taken as 0.005. Thus, the width of quasi-sliding mode band is found to be $\delta \leq 0.0026$. Using all these parameters, $\mathbf{F}_1$ of order (4×38) is calculated with maximum value of 43.1863 and minimum value of 39.8434 as

$$\mathbf{F}_1 = \begin{bmatrix}
39.8512 & 39.8513 & 39.8506 & 39.8513 & 40.4230 & 40.1480 & 40.1710 & 40.1664 \\
42.5716 & 42.5723 & 42.5715 & 42.5717 & 43.1863 & 42.8842 & 42.9152 & 42.9173 \\
39.8506 & 39.8513 & 39.8512 & 39.8513 & 40.4230 & 40.1351 & 40.1612 & 40.1658 \\
42.5715 & 42.5717 & 42.5715 & 42.5723 & 43.1863 & 42.8835 & 42.9054 & 42.9033
\end{bmatrix}$$

$$\begin{matrix}
40.1375 & 40.1351 & 40.1612 & 40.1658 & 40.1456 & 40.0689 & 40.1229 & 40.1168 \\
42.8890 & 42.8836 & 42.9054 & 42.9033 & 42.8788 & 42.7981 & 42.8625 & 42.8652 \\
40.1456 & 40.1480 & 40.1710 & 40.1664 & 40.1375 & 40.0560 & 40.1114 & 40.1174 \\
42.8788 & 42.8842 & 42.9152 & 42.9173 & 42.8890 & 42.7997 & 42.8529 & 42.8502
\end{matrix}$$

$$\begin{matrix}
40.0575 & 40.0560 & 40.1114 & 40.1174 & 40.0673 & 39.8592 & 39.8583 & 39.8580 \\
42.8032 & 42.7997 & 42.8529 & 42.8502 & 42.7946 & 42.5803 & 42.5726 & 42.5785 \\
40.0673 & 40.0689 & 40.1229 & 40.1168 & 40.0575 & 39.8592 & 39.8453 & 39.8477 \\
42.7946 & 42.7981 & 42.8624 & 42.8652 & 42.8032 & 42.5803 & 42.5723 & 42.5687
\end{matrix}$$

$$\begin{matrix}
39.8530 & 39.8475 & 39.8453 & 39.8477 & 39.8527 & 39.8561 & 39.8558 & 39.8562 \\
42.5807 & 42.5775 & 42.5723 & 42.5688 & 42.5665 & 42.5675 & 42.5692 & 42.5757 \\
39.8527 & 39.8561 & 39.8583 & 39.8580 & 39.8530 & 39.8475 & 39.8434 & 39.8455 \\
42.5665 & 42.5675 & 42.5726 & 42.5785 & 42.5807 & 42.5775 & 42.5711 & 42.5673
\end{matrix}$$

$$\begin{bmatrix}
39.8504 & 39.8448 & 39.8434 & 39.8455 & 39.8514 & 39.8544 \\
42.5783 & 42.5742 & 42.5711 & 42.5673 & 42.5647 & 42.5661 \\
39.8514 & 39.8544 & 39.8558 & 39.8562 & 39.8504 & 39.8448 \\
42.5647 & 42.5661 & 42.5692 & 42.5756 & 42.5783 & 42.5742
\end{bmatrix} \tag{8.50}$$

and p_1 is evaluated as

$$p_1 = \begin{bmatrix} -0.0088 & 0.0002 & 0.0002 & 0.0002 \\ 0 & -0.0088 & 0.0002 & 0.0002 \\ 0 & 0 & -0.0088 & 0.0002 \\ 0 & 0 & 0 & -0.0088 \end{bmatrix}. \tag{8.51}$$

While designing DSMC with PRRL, the width of quasi-sliding mode band is taken same as that of CPPRRL with the same value of q [14]. Therefore a is selected as 0.5. Using these parameters $\mathbf{F}_2$ of order (4×38) is computed, with maximum and minimum values of 0.6218 and -0.0011 respectively, as given by

$$\mathbf{F}_2 = \begin{bmatrix} 0.0066 & 0.0067 & 0.0060 & 0.0067 & 0.5784 & 0.3034 & 0.3264 & 0.3219 \\ 0.0068 & 0.0075 & 0.0067 & 0.0069 & 0.6216 & 0.3195 & 0.3504 & 0.3525 \\ 0.0060 & 0.0067 & 0.0066 & 0.0067 & 0.5784 & 0.2905 & 0.3166 & 0.3212 \\ 0.0067 & 0.0069 & 0.0068 & 0.0075 & 0.6216 & 0.3188 & 0.3406 & 0.3385 \end{bmatrix}$$

$$\begin{matrix} 0.2929 & 0.2905 & 0.3166 & 0.3212 & 0.3010 & 0.2243 & 0.2783 & 0.2723 \\ 0.3242 & 0.3188 & 0.3406 & 0.3385 & 0.3140 & 0.2333 & 0.2977 & 0.3004 \\ 0.3010 & 0.3034 & 0.3264 & 0.3219 & 0.2929 & 0.2114 & 0.2668 & 0.2729 \\ 0.3140 & 0.3195 & 0.3504 & 0.3525 & 0.3242 & 0.2349 & 0.2881 & 0.2854 \end{matrix}$$

$$\begin{matrix} 0.2129 & 0.2114 & 0.2668 & 0.2729 & 0.2228 & 0.0146 & 0.0137 & 0.0134 \\ 0.2384 & 0.2349 & 0.2881 & 0.2854 & 0.2298 & 0.0155 & 0.0078 & 0.0137 \\ 0.2228 & 0.2243 & 0.2783 & 0.2723 & 0.2129 & 0.0146 & 0.0007 & 0.0031 \\ 0.2298 & 0.2333 & 0.2977 & 0.3004 & 0.2384 & 0.0155 & 0.0075 & 0.0040 \end{matrix}$$

$$\begin{matrix} 0.0084 & 0.0030 & 0.0007 & 0.0031 & 0.0081 & 0.0115 & 0.0112 & 0.0116 \\ 0.0159 & 0.0127 & 0.0075 & 0.0040 & 0.0017 & 0.0027 & 0.0045 & 0.0109 \\ 0.0081 & 0.0115 & 0.0137 & 0.0134 & 0.0084 & 0.0030 & -0.0011 & 0.0010 \\ 0.0017 & 0.0027 & 0.0078 & 0.0137 & 0.0159 & 0.0127 & 0.0063 & 0.0026 \end{matrix}$$

$$\begin{bmatrix} 0.0058 & 0.0002 & -0.0011 & 0.0010 & 0.0068 & 0.0098 \\ 0.0135 & 0.0094 & 0.0063 & 0.0026 & -0.0001 & 0.0013 \\ 0.0068 & 0.0098 & 0.0112 & 0.0116 & 0.0058 & 0.0002 \\ -0.0001 & 0.0013 & 0.0045 & 0.0109 & 0.0135 & 0.0094 \end{bmatrix} \tag{8.52}$$

and p_2 is estimated as

$$p_2 = \begin{bmatrix} -0.0881 & 0.0024 & 0.0023 & 0.0023 \\ 0 & -0.0881 & 0.0023 & 0.0024 \\ 0 & 0 & -0.0881 & 0.0023 \\ 0 & 0 & 0 & -0.0881 \end{bmatrix}. \tag{8.53}$$

8.4.1 Transient Simulations

Performances of the DSMC laws presented here, are evaluated using vectorized nonlinear model of AHWR. Consider the transient involving a spatial power disturbance in which the system was initially assumed to be at full-power steady-state conditions, with all regulating rods (RRs) at their equilibrium positions. Shortly, RR2, originally under auto control was driven out by almost 1% manually, by giving proper control signal and left under the effect of automatic control thereafter. This resulted in the perturbations in total and spatial power distribution, which were suppressed by both the controllers, as illustrated in Figs. 8.1, 8.2, and 8.3. Spatial oscillations are measured in terms of first and second azimuthal tilts, as shown in Figs. 8.1 and 8.2. Total power variations are shown in Fig. 8.3. From Fig. 8.3 it can be noted that total power with PRRL attains steady state value of 920.48 MW exactly after 4.5 s, whereas with CPPRRL it reaches steady-state after 140 s. When RR2 is driven out by 1%, all other RRs are driven in by 0.33%, as shown in Figs. 8.4 and 8.5. As a result of action of controllers, all the RRs come back to their equilibrium positions of 66.1%. However, the settling time is different. Though the settling time for CPPRRL is less that that of PRRL, total power settles much earlier in PRRL than in CPPRRL. It was also observed that the chattering is effectively reduced in case of PRRL than CPPRRL.

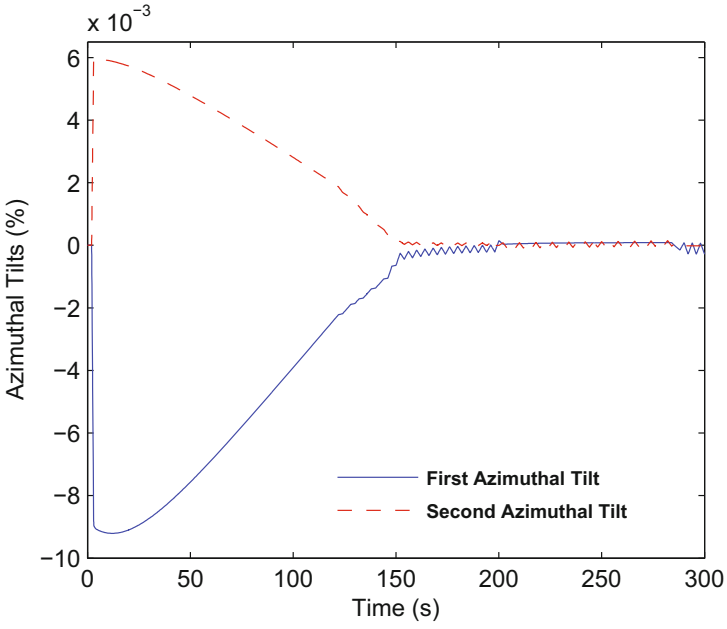

Fig. 8.1 Variations in azimuthal tilts with constant plus proportional rate reaching law

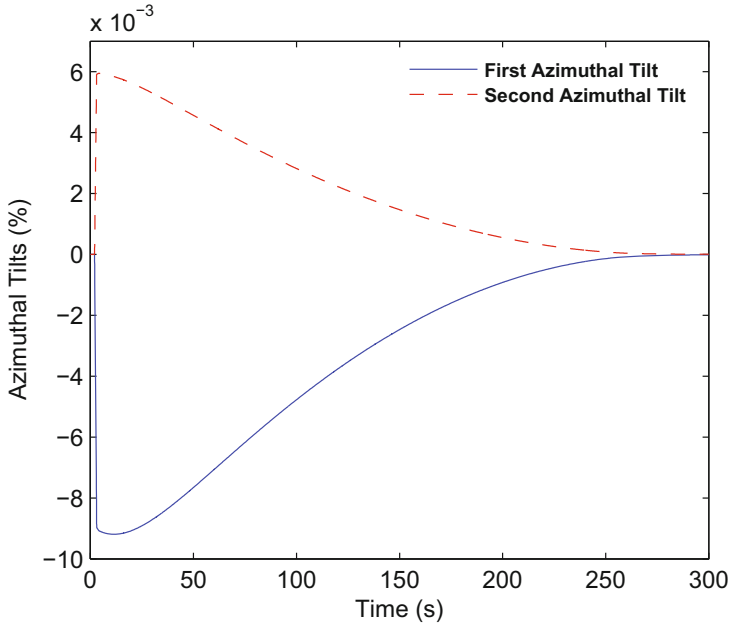

Fig. 8.2 Variations in azimuthal tilts with power rate reaching law

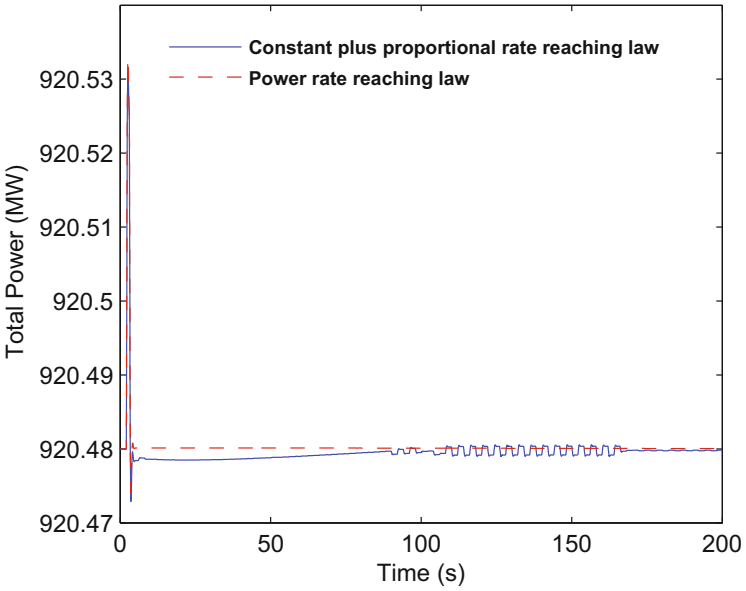

Fig. 8.3 Total power variations for RR2 disturbance

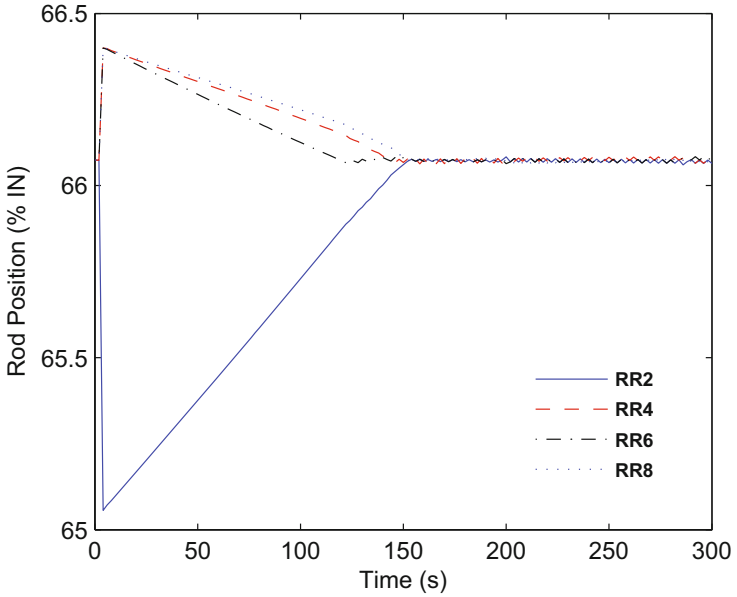

Fig. 8.4 Variations in RR positions with constant plus proportional rate reaching law

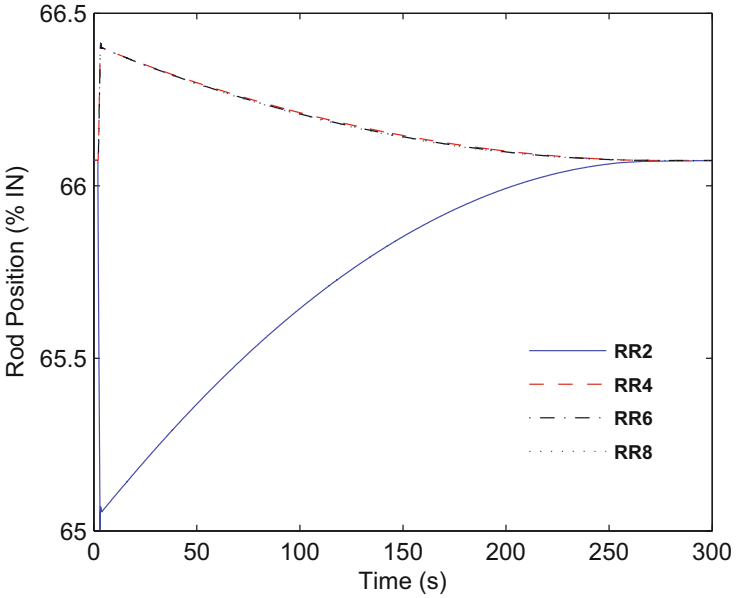

Fig. 8.5 Variations in RR positions with power rate reaching law

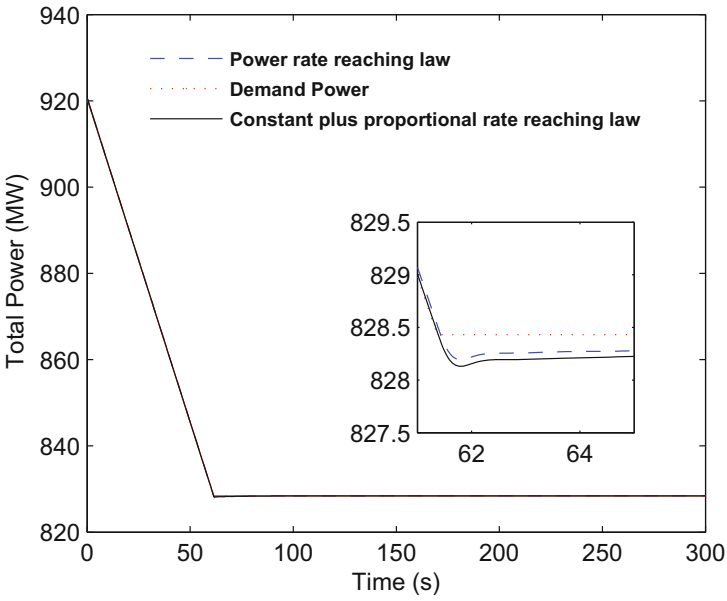

Fig. 8.6 Total power variations during power maneuvering

In another transient, again the reactor is under steady state and is assumed to be operating at 920.48 MW with nodal power distributions at steady state. Now, the demand is reduced uniformly at the rate of 1.5 MW/s to 828.43 MW, in approximately 61 s and held constant thereafter. During the transient, variations in total power obtained with different DSMCs are shown in Fig. 8.6. It can be observed that, the total power is following the demand power exactly, in both the cases. However, from the magnified part of Fig. 8.6, it is revealed that DSMC with PRRL is doing well.

In order to assess robustness response of the system to disturbances in feed flow, a situation was simulated in which the reactor was operating at steady full power when a 5% positive step change was introduced in the feed flow. As a result of this, total power underwent variations as given in Fig. 8.7. Due to the controller action, total as well as nodal powers are regulated at their respective steady-state values with the error of $\pm 2 \times 10^{-4}$%. This is compensated by changing the position of RRs. Variations in RR2 positions with both the reaching laws are shown in Fig. 8.8. Here also the performance of DSMC with PRRL is found to be better.

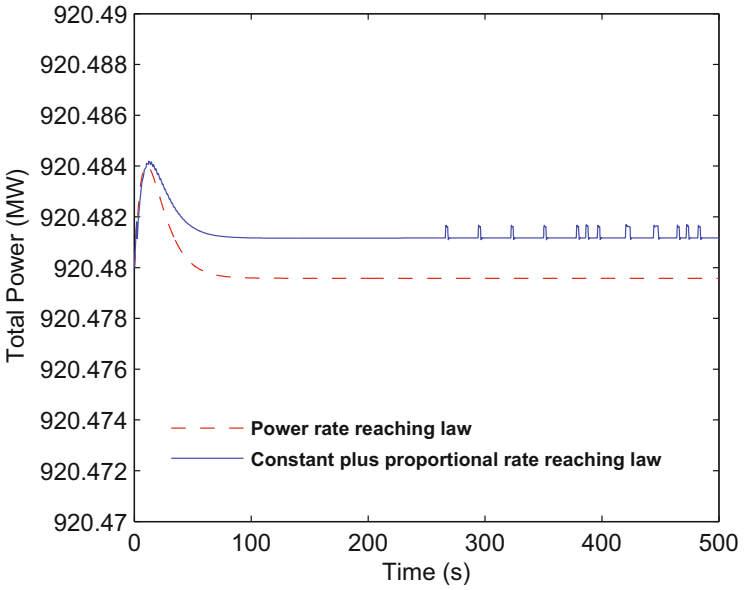

Fig. 8.7 Total power variations during feed flow disturbance

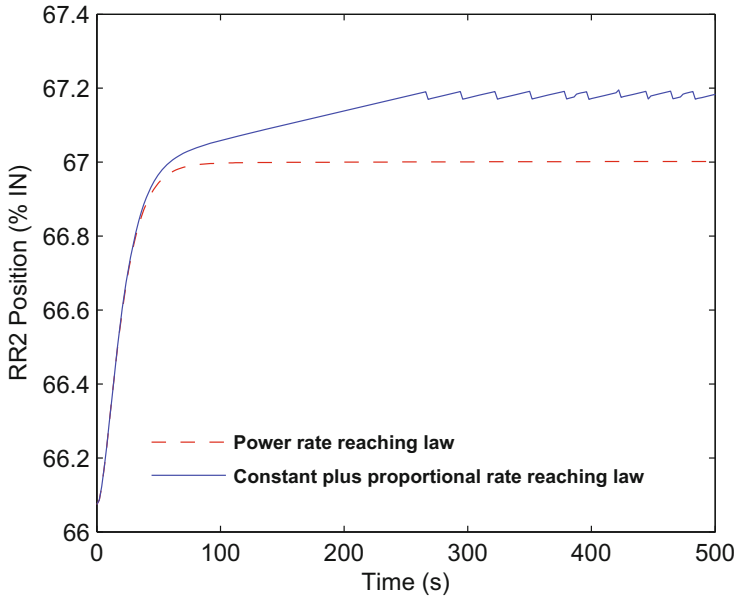

Fig. 8.8 RR2 positions during feed flow disturbance

8.5 Conclusion

In this chapter, DSMC laws are formulated for spatial stabilization of AHWR. The original numerically ill-condition system is decomposed into three subsystems by direct block diagonalization. DSMC laws are then designed using slow subsystem. Subsequently, DSMC laws for full order system are obtained using linear transformation matrices. Performances of the presented controllers are judged via simulations carried out under the same transient conditions. It is observed that the controllers are stabilizing the spatial oscillations and total power variations. However, the performance of DSMC with power rate reaching law is comparatively better than DSMC with constant plus proportional rate reaching law. These control strategies for AHWR utilize the feedback of nodal powers, regulating rods' positions and xenon and iodine concentrations. For the latter two variables, it would be necessary to employ an observer or estimator.

References

1. Bandyopadhyay, B., G'Egziabher, A., Janardhanan, S.: Sliding mode control design via reduced order model approach. Proc. IEEE Int. Conf. Ind. Technol., 1538–1541 (2006)
2. Bartolini, G., Ferrara, A., Utkin, A.: Adaptive sliding mode control in discrete-time systems. Automatica **31**(5), 769–773 (1995)
3. Drakunov, S.V., Utkin, V.I.: On discrete-time sliding mode control. Proc. IFAC Conf. Nonlin. Control **22**(3), 273–278 (1989)
4. Edwards, C., Spurgeon, S.K.: Sliding Mode Control: Theory and Applications. Taylor & Francis, London (1998)
5. Gao, W., Hung, J.C.: Variable structure control of nonlinear systems: a new approach. IEEE Trans. Ind. Electron. **40**(1), 45–55 (1993)
6. Gao, W., Wang, Y., Homaifa, A.: Discrete-time variable structure control systems. IEEE Trans. Ind. Electron. **42**(2), 117–122 (1995)
7. Gao, W., Wang, Y., Homaifa, A.: Remarks on discrete-time variable structure control systems. IEEE Trans. Ind. Electron. **43**(1), 235–238 (1996)
8. Hung, J.Y., Gao, W., Hung, J.C.: Variable structure control: a survey. IEEE Trans. Ind. Electron. **40**, 2–22 (1993)
9. Kotta, U.: Comments on "on the stability of discrete-time sliding mode control system". IEEE Trans. Autom. Control **34**(9), 1021–1022 (1989)
10. Li, T.-H.S., Lin, J.-L., Kung, F.-C.: Design of sliding mode controller for discrete singular perturbation systems. Proc. Int. Conf. Ind. Electron. Control Instrum. **2**, 736–741 (1995)
11. Mahmoud, M.S.: Order reduction and control of discrete systems. Proc. IEE Control Theory Appl. **129**(4), 129–135 (1982)
12. Mahmoud, M.S.: Discrete Systems with Multiple Time Scales. Control and Dynamic Systems. Academic, New York (1988)
13. Munje, R.K., Patre, B.M., Tiwari, A.P.: Periodic output feedback for spatial control of AHWR: a three-time-scale approach. IEEE Trans. Nucl. Sci. **61**(4), 2373–2382 (2014)
14. Munje, R.K., Patre, B.M., Tiwari, A.P.: Discrete time sliding mode control of advanced heavy water reactor. IEEE Trans. Control Syst. Technol. **24**, 357–364 (2016)
15. Naidu, D.S.: Singular Perturbation Methodology in Control Systems. Peter Peregrinus Ltd., London (1988)

16. Nguyen, T., Su, W.-C., Gajic, Z.: Singular perturbation analysis of output feedback discrete-time sliding mode control. Proc. Am. Control Conf., 757–762 (2009)
17. Phillips, R.G.: Reduced order modeling and control of two-time-scale discrete systems. Int. J. Control **31**, 765–780 (1980)
18. Reddy, G.D., Bandyopadhyay, B., Tiwari, A.P.: Discrete-time sliding mode control for two-time-scale systems. Proc. IEEE Int. Conf. Ind. Electron., 170–175 (2008)
19. Shimjith, S.R., Tiwari, A.P., Bandyopadhyay, B.: Design of fast output sampling controller for three-time-scale systems: application to spatial control of advanced heavy water reactor. IEEE Trans. Nucl. Sci. **58**(6), 3305–3316 (2011)
20. Utkin, V.I.: Variable structure systems with sliding modes. IEEE Trans. Autom. Control **22**, 212–222 (1977)
21. Yu, X.H.: Conditions for existence of discrete-time sliding mode. Proc. IFAC World Congr. **26**(2), 215–218 (1993)

Chapter 9
Comparison of Spatial Control Techniques

9.1 Introduction

In the preceding chapters, Advanced Heavy Water Reactor (AHWR) spatial control problem is investigated by eight different control approaches. Initially static output feedback control (SOFC) [6] is examined for 90th order nonlinear model of AHWR. Remaining seven control techniques are state feedback control using pole placement (SFC-PP) [5], state feedback control using LQR (SFC-LQR) [4], sliding mode control (SMC) [7], fast output sampling (FOS) [8], periodic output feedback (POF) [9], and discrete-time SMC (DSMC) [10] using constant plus proportional rate reaching law (CPPRRL) and power rate reaching law (PRRL). These are applied to the reduced model of AHWR, which is obtained by decomposing higher order system of AHWR into lower order subsystems either by two-time-scale decomposition or three-time-scale decomposition. Again this decomposition is achieved by either quasi-steady-state method or direct block diagonalization method. Complete formulation of design methods and simulation results are already discussed separately in earlier chapters. This chapter compares results obtained under the same transient conditions and tries to make a comprehensive viewpoint on all the methods to rank them in respect of their suitability to AHWR control. Moreover, the comparison of results helps to appreciate the consequence of diverse spatial control strategies. Brief comparative summary of design of spatial control techniques is given in Table 9.1 [11].

9.2 Performance Comparison

Three different transient conditions have been considered for performance comparison of spatial controllers. All the transients are simulated using vectorized nonlinear model of AHWR, developed in Chap. 2. For each transient, time domain specifications [1–3] and error performance indices [3, 13] are calculated. These

R. Munje et al., *Investigation of Spatial Control Strategies with Application to Advanced Heavy Water Reactor*, Energy Systems in Electrical Engineering, https://doi.org/10.1007/978-981-10-3014-7_9

Table 9.1 Design comparison of controllers

Controller	Type of design	System decomposition	Subsystems and their orders	Type of feedback	Remark
SOFC	Continuous-time	Not required	Not applicable	Output	Feedback of nodal powers in which RRs are placed
SFC(LQR)	Continuous-time	Two-time-scale (Quasi-steady-state)	Slow (73), Fast (17)	Reduced state	Feedback of 73 states
SFC(PP) and SMC	Continuous-time	Two-time-scale (Block Diagonalization)	Slow (73), Fast (17)	Full state	Feedback of all the states
FOS	Discrete-time	Two-time-scale (Block diagonalization)	Slow (73), Fast (17)	Output	Feedback of all the nodal powers ($\tau = 54$ s, $\Delta = 9$ s)
POF	Discrete-time	Three-time-scale (Block diagonalization)	Slow (38), Fast 1 (35), Fast 2 (17)	Output	Feedback of all the nodal powers ($\tau = 12$ s, $\Delta = 2$ s)
DSMC	Discrete-time	Three-time-scale (Block diagonalization)	Slow (38), Fast 1 (35), Fast 2 (17)	Full state	Feedback of all the states ($\tau = 2$ s)

are well explained in control literature. Nevertheless, for brevity these are defined in Appendix D.

9.2.1 State Regulation

Disturbance in the regulating rod (RR) position can be treated as the case of state regulation. The system is originally assumed to be at full power steady-state conditions, with all RRs at their equilibrium positions. Shortly, RR2, first under auto control was moved out by almost 1.05% manually, by giving suitable control signal and left under the effect of automatic control later on. This resulted in the perturbations in total and spatial power distribution, which were suppressed by all the controllers, as demonstrated in Figs. 9.1, 9.2 and 9.3. Oscillations in spatial power are measured in terms of first and second azimuthal tilts [12], as shown in Figs. 9.2 and 9.3 respectively. Performance indices (see Appendix D, for more details), i.e., integral square error (ISE), integral absolute error (IAE), integral time square error (ITSE), and integral time absolute error (ITAE), determined for total power (Fig. 9.1)

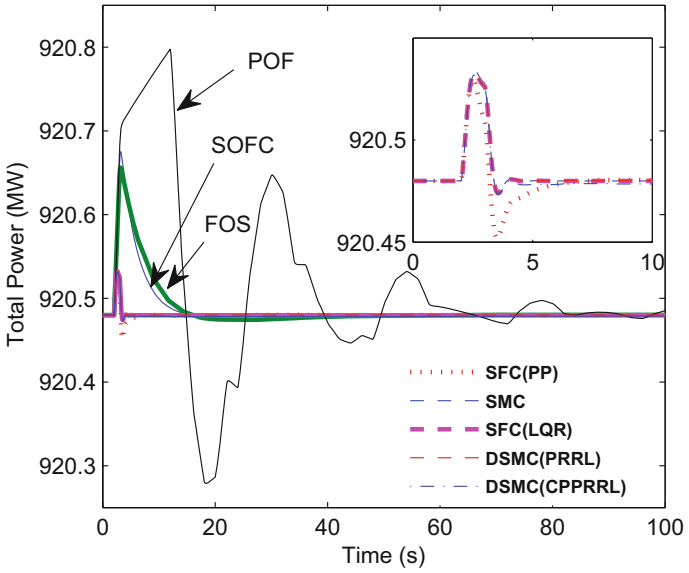

Fig. 9.1 Effect of withdrawal of RR2 on total power

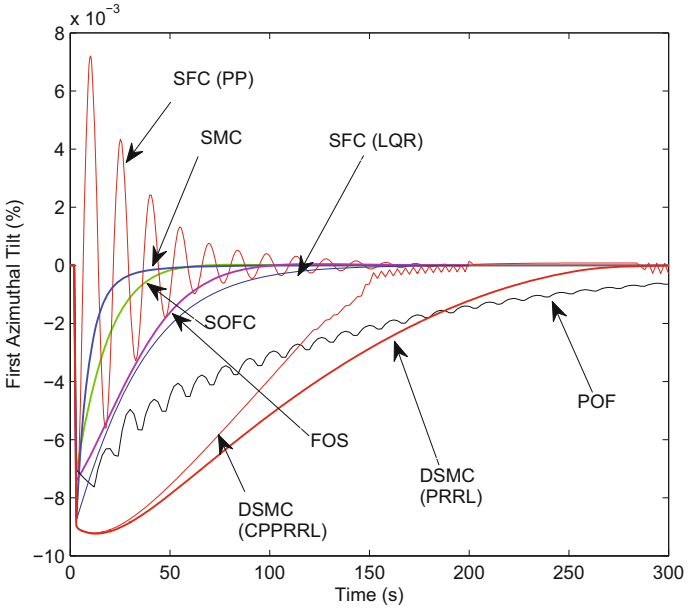

Fig. 9.2 Effect of withdrawal of RR2 on first azimuthal tilt

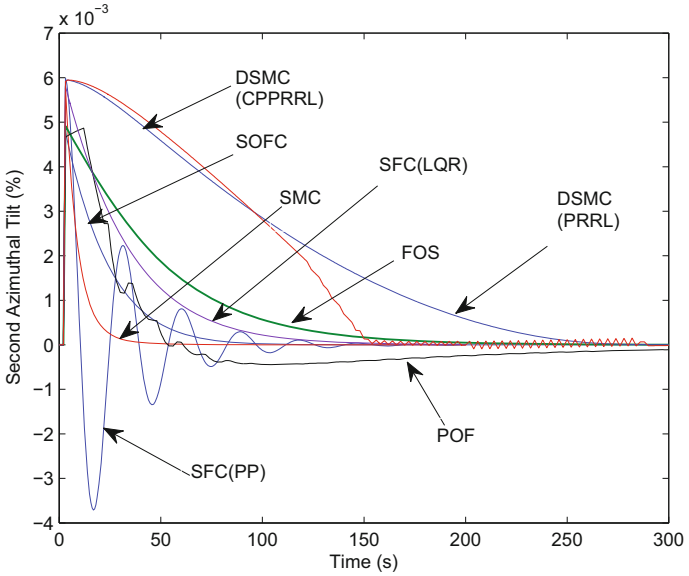

Fig. 9.3 Effect of withdrawal of RR2 on second azimuthal tilt

are given in Table 9.2. Equivalent deviations in RR2 position and control signals to RR2 drive are given in Figs. 9.4 and 9.5 respectively. When RR2 is driven out by 1.05%, all other RRs are driven in. Their respective percentage values are mentioned in Table 9.3. As a result of controller action, all the RRs return to their equilibrium positions, i.e., 66.1%. But, the settling time (t_s) is different for all the controllers. Settling time and performance indices are also calculated for position of RR2 and are stated in Table 9.3.

In Fig. 9.1, even if the maximum variation in total power is observed in POF, it is only ±0.034%. However, it takes somewhat longer time, i.e., 100 s to settle down to steady-state value of 920.48 MW. Total power variations with SOFC and FOS are approximately 0.021% and achieve steady state in 18 s. In rest of the controllers, total power variations are insignificant (about 0.005%), as shown in zoomed part of Fig. 9.1, and rather similar excluding SFC(PP). Performance indices for total power, mentioned in Table 9.2, are calculated by taking an error signal as $e(t) = Q_T - Q_{T,0}$, where Q_T and $Q_{T,0}$ are, respectively, instantaneous and steady-state values of total power in MW. From Table 9.2 it can be concluded that SFC (LQR), SFC (PP), SMC, and DSMCs have less error performance indices, which means improved, than other controllers and in remaining methods, SOFC is having lesser values and then FOS and POF controls.

First azimuthal and second azimuthal tilts, represented in Figs. 9.2 and 9.3 respectively, show overdamped responses for SMC, SOFC, SFC (LQR), FOS, DSMC (CPPRRL), DSMC (PRRL), and POF with increasing damping ratio. As a result, settling time also increases from SMC to POF. Response with SFC (PP) is

Table 9.2 Total power results following to withdrawal of RR2

Controller	SOFC	SFC (LQR)	SFC (PP)	SMC	FOS	POF	DSMC (CPPRRL)	DSMC (PRRL)
ISE ($\times 10^{-3}$)	79.8	2.06	1.89	2.27	110	1650	2.23	2.13
IAE	0.76	0.05	0.09	0.05	1.05	9.18	0.24	0.07
ITSE ($\times 10^{-2}$)	34.3	0.55	0.56	0.61	53.4	3020	2.03	0.59
ITAE	6.31	0.43	1.62	0.45	10.72	353	14.46	2.71

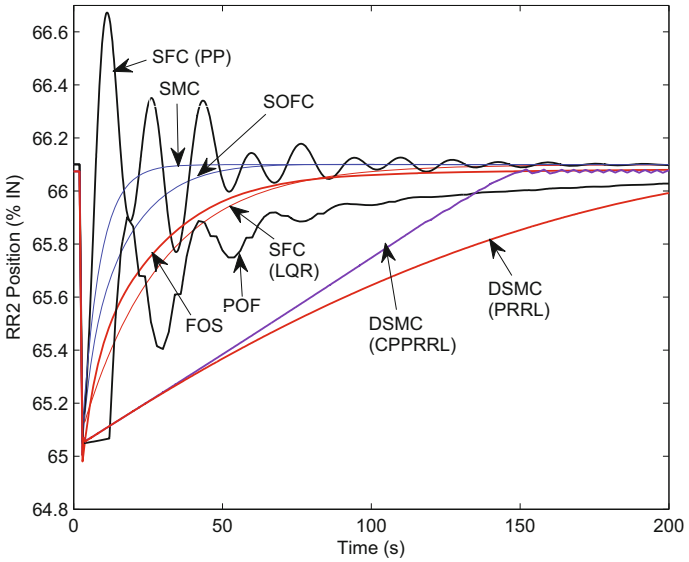

Fig. 9.4 Variations in RR2 position

oscillatory with decreasing magnitude and it attains equilibrium value after nine and six cycles of oscillations, respectively, in first and second azimuthal tilts. Whereas with POF controller, the overdamped response undergoes little oscillations, which are more prominent in first azimuthal (Fig. 9.2). As the disturbance is of extremely small period, variations in first and second azimuthal tilts are, respectively, $\pm 9 \times 10^{-3}\%$ and $\pm 6 \times 10^{-3}\%$. Although variations in total power (zoomed part of Fig. 9.1) with DSMCs are negligible, spatial power variations (Figs. 9.2 and 9.3) are next largest after POF. They are suppressed after about 300 s and in POF, after 350 s. However, in rest of the controllers first and second azimuthal tilts are controlled in 150 and 200 s, respectively.

Variations in RR2 positions are somewhat similar to that of first azimuthal tilt. Error performance indices for RR2 are calculated by using error signal as $e(t) = H_2 - H_{2,0}$, where H_2 and $H_{2,0}$ are, respectively, instantaneous and equilibrium values of RR2 position. Settling time calculations are done for $\pm 2\%$ tolerance. From Table 9.3,

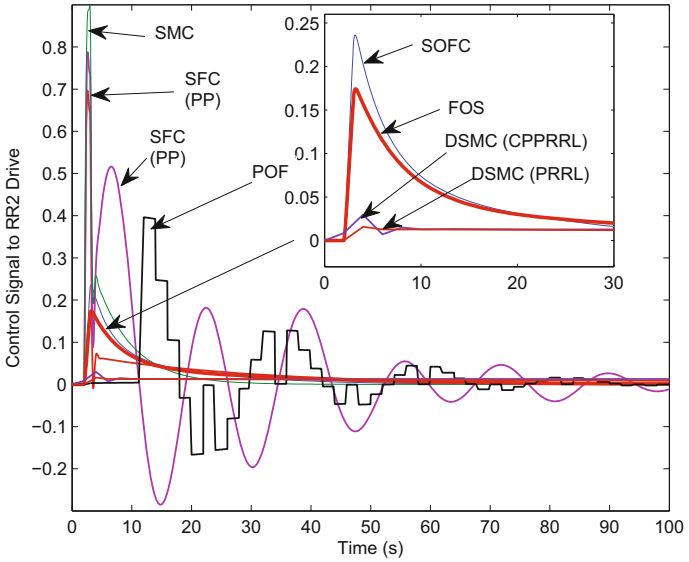

Fig. 9.5 Control signal efforts following to withdrawal of RR2

Table 9.3 RR position results following to withdrawal of RR2

Controller	SOFC	SFC (LQR)	SFC (PP)	SMC	FOS	POF	DSMC (CPPRRL)	DSMC (PRRL)
RR4 (% in)	0.20	0.33	0.37	0.31	0.18	0.50	0.33	0.33
RR6 (% in)	0.15	0.33	0.33	0.31	0.13	0.55	0.33	0.33
RR8 (% in)	0.18	0.33	0.36	0.31	0.26	0.50	0.33	0.33
t_s (s)	50	97	112	24	123	398	150	240
ISE ($\times 10^{-3}$)	1.4	3.1	1.2	0.8	2.3	4.3	11.9	13.5
IAE ($\times 10^{-1}$)	1.9	4	2.2	1.0	3.2	6	11.5	14.5
ITSE ($\times 10^{-2}$)	1.2	5	1.6	0.4	3.0	8	46	66
ITAE	3	7	1.2	12.5	8.3	27	60.75	104.60

it can be observed that performance of SMC is better compared to other controllers. Thereafter, the performances of SOFC, SFC (PP), SFC (LQR), and FOS can be ranked. Performance indices of RR2 obtained with POF controller are less compared to DSMC controllers, however, the settling time is more. In case of DSMC controllers, CPPRRL is performing well compared to PRRL. Control signal, in Fig. 9.5, to RR2 drive varies from 0.9 to −0.3 V. Maximum variations are noted with SFC (LQR), SFC (PP), SMC and then with POF controllers. Control signal with SFC (PP) and POF shows oscillatory behavior with decreasing amplitude. However, negligible variations are observed in control signal of DSMCs.

9.2.2 Trajectory Tracking

In a further transient, yet again the reactor is under steady state and is assumed to be in use at 920.48 MW with nodal power distributions as given in Table 2.5. Iodine, xenon, and delayed neutron precursor concentrations are in equilibrium with the respective nodal power levels. Now, the demand is reduced uniformly at the rate of 1.5 MW/s to 828.43 MW, in about 61 s and held constant afterward. This transient can be useful to study the trajectory tracking performance of the system. Throughout the transient, variations in total power obtained with different controllers are depicted in Fig. 9.6. Maximum undershoot (M_u) and error performance indices computed for total power are listed in Table 9.4. The error signal is taken as $e(t) = Q_T - Q_D$, where Q_D is demand power (MW). From Fig. 9.6, it can be observed that in all the controllers response is underdamped and M_u is observed in case of POF and then in FOS based controllers, thereafter, in case of SOFC, SFC(LQR), and SFC(PP). Undershoots in SMC and DSMCs (both CPPRRL and PRRL) are observed to be very minor. Moreover in DSMC (PRRL), the total power is tracking the demand power exactly. This is also obvious from error performance indices given in Table 9.4. In all the controllers, after attaining demand power, no variations were observed further as seen from a long simulation.

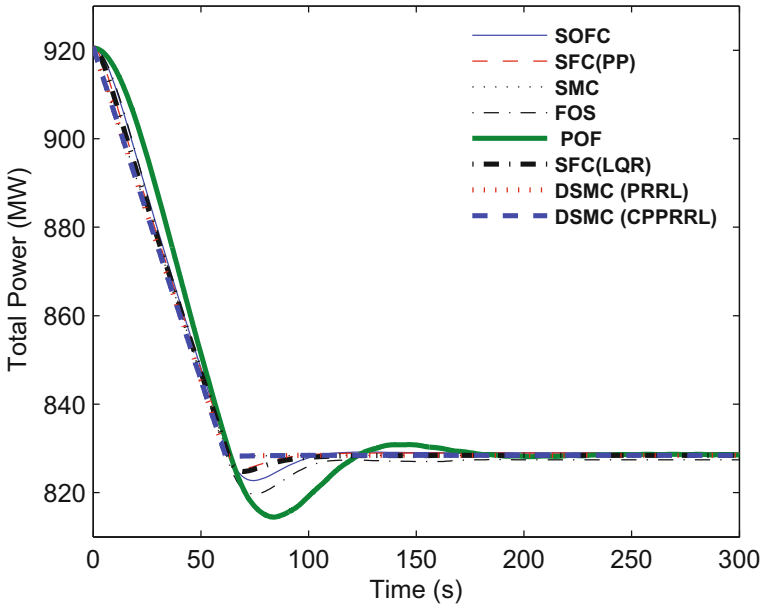

Fig. 9.6 Effect of power maneuvering on total power

Table 9.4 Total power results for the period of power maneuvering

Controller	SOFC	SFC (LQR)	SFC (PP)	SMC	FOS	POF	DSMC (CPPRRL)	DSMC (PRRL)
M_u (%)	0.72	0.43	0.35	0.04	1.05	1.74	0.04	0.02
ISE ($\times 10^2$)	13.83	3.78	3.94	0.011	26.24	102.35	0.014	0.011
IAE	421	169	261	9.09	623	1094	11.25	9.22
ITSE ($\times 10^3$)	70.71	16.30	22.93	0.043	181.18	596.89	0.042	0.043
ITAE ($\times 10^3$)	37.37	8.69	27.38	0.45	64.74	74.38	0.56	0.46

9.2.3 Disturbance Rejection

So as to evaluate the performance of the system to disturbance in feed flow, nonlinear model of AHWR is again simulated, in which the reactor was working at steady full power, when a 5% positive step change was initiated in the feed flow. Consequently, the total power underwent variations as given in Fig. 9.7. Due to the controller action, total as well as nodal powers are regulated at their respective steady-state values. This is compensated by changing the positions of RRs as shown in Fig. 9.8. Delay time (t_d), rise time (t_r), peak time (t_p), settling time (t_s), maximum overshoot (M_p), and percentage change in RR positions are given in Table 9.5.

From Fig. 9.7 it is noticed that total power varies in the range of $\pm 0.13\%$. Maximum total power variations are noted in SFC (both LQR and PP). After two cycles of oscillations, they reach steady-state value of 920.48 MW. Comparable kind of response with relatively less amplitude is observed in SMC. In case of FOS, total power shows rapid variation and settles down in just 65 s. Same amount of time is taken by SOFC and POF controllers, however, overshoot is seen to be less in comparison to FOS. Performances of DSMCs are shown in the zoomed part of Fig. 9.7. These variations are certainly insignificant.

Deviations in RR2 position, shown in Fig. 9.8, are equivalent with related variations in total power. Settling time of RR2 position with SFC (LQR) and SFC (PP) is almost one and the same. Settling time is calculated for $\pm 2\%$ tolerance. Delay time, rise time, peak time, and percent overshoot are also large for these two controllers. Afterwards, the performance of SMC can be analyzed with moderately lesser values of overshoot, settling time, rise time, and peak time. Even though the overshoot in case of FOS is observed to be more in remaining controllers, settling time, peak time, and rise time are less. For the overdamped response of DSMCs, t_r is considered from 10 to 90%. All these values are given in Table 9.5.

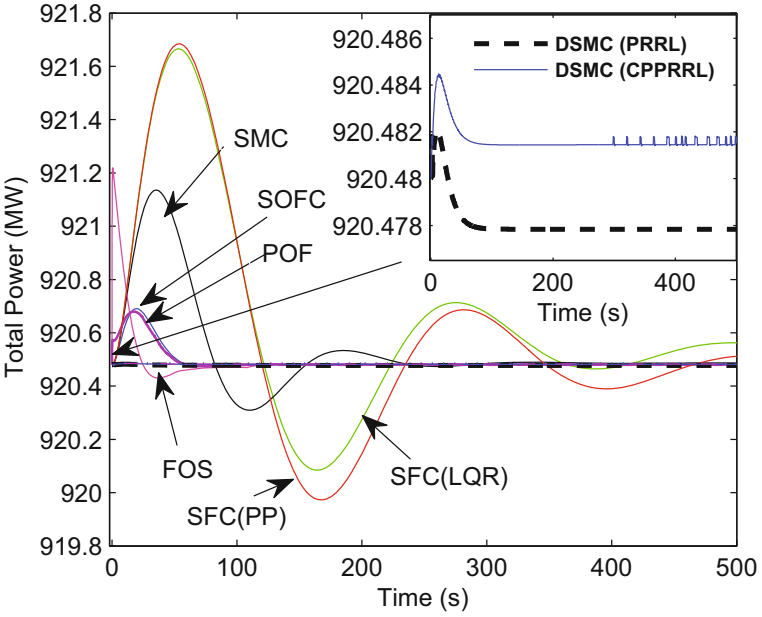

Fig. 9.7 Effect of step change in feed flow on total power

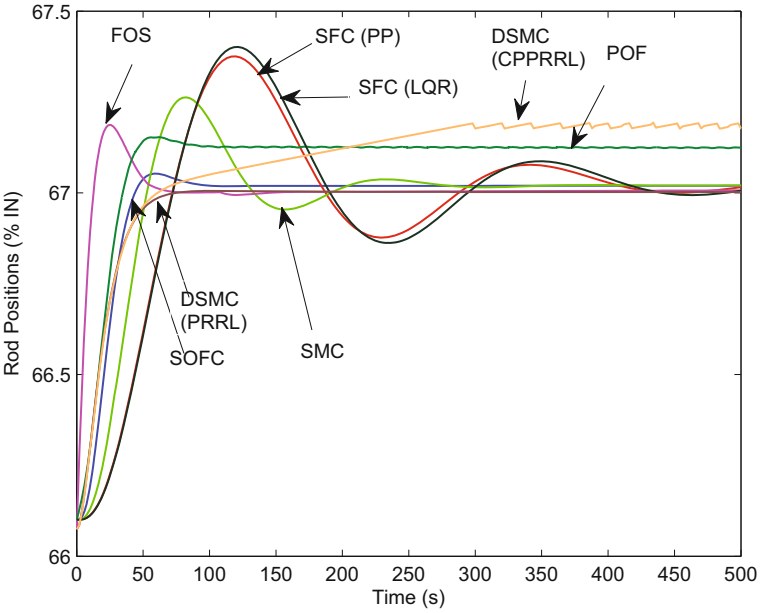

Fig. 9.8 Effect of step change in feed flow on RR positions

Table 9.5 RR position results for the period of feed flow disturbance

Controller	SOFC	SFC (LQR)	SFC (PP)	SMC	FOS	POF	DSMC (CPPRRL)	DSMC (PRRL)
t_d (s)	22	45	46	34	5	19	24	19
t_r (s)	46.5	73.8	74.0	53.9	13.5	46.0	200	50
t_p (s)	59.5	121	119.0	82.0	24.8	60.0	210	55
t_s (s)	100	490	488	256	50	76	220	60
M_p (%)	4.4	40	36.6	25.7	16.2	2.9	0	0
% Change	0.90	0.92	0.93	0.92	0.95	1.02	1.11	0.93

9.3 Conclusion

In this chapter, various spatial controllers are studied for AHWR. All are examined under the identical transient settings and graphical simulation results are compared. In addition to this, time domain specifications and error performance indices are also calculated for each transient and compared. From these results and observation tables, it is noticed that the performance of state feedback-based controllers (i.e., SFC (LQR), SFC (PP), SMC, DSMC) is better, in terms of total power variations for state regulation and trajectory tracking. While for disturbance rejection, performances of output feedback controllers (i.e., SOFC, FOS, POF) along with DSMC is good. However, for all the transients, DSMC is doing better than other controllers. In remaining controllers, SMC, SOFC, and FOS reasonably show good performance and then state feedback controls and POF.

References

1. American National Standard, ANSI/ISA-S51.1-1979, Process Instrumentation Terminology
2. American National Standard, C85.11963, Terminology for Automatic Control
3. Dorf, R., Bishop, R.H.: Modern Control Systems. Prentice Hall Inc., Englewood Cliffs (2000)
4. Munje, R.K., Patre, B.M.: Spatial power control of singularly perturbed nuclear reactor. J. Control Eng. Appl. Inform. **18**(3), 22–29 (2016)
5. Munje, R.K., Parkhe, J.G., Patre, B.M.: Spatial control of advanced heavy water reactor via two stage decomposition. Ann. Nucl. Energy **77**, 326–334 (2015)
6. Munje, R.K., Patre, B.M., Tiwari, A.P.: Nonlinear simulation and control of xenon induced oscillations in advanced heavy water reactor. Ann. Nucl. Energy **64**, 191–200 (2014)
7. Munje, R.K., Patre, B.M., Shimjith, S.R., Tiwari, A.P.: Sliding mode control for spatial stabilization of advanced heavy water reactor. IEEE Trans. Nucl. Sci. **60**, 3040–3050 (2013)
8. Munje, R.K., Londhe, P.S., Parkhe, J.G., Patre, B.M., Tiwari, A.P.: Spatial control of advanced heavy water reactor by fast output sampling technique. Proc. IEEE Int. Conf. Control Appl., 1212–1217 (2013)
9. Munje, R.K., Patre, B.M., Tiwari, A.P.: Periodic output feedback for spatial control of AHWR: a three-time-scale approach. IEEE Trans. Nucl. Sci. **61**(4), 2373–2382 (2014)
10. Munje, R.K., Patre, B.M., Tiwari, A.P.: Discrete time sliding mode control of advanced heavy water reactor. IEEE Trans. Control Syst. Technol. **24**, 357–364 (2016)

11. Munje, R.K., Patre, B.M., Londhe, P.S., Tiwari, A.P., Shimjith, S.R.: Investigation of spatial control strategies for AHWR: a comparative study. IEEE Trans. Nucl. Sci. **63**, 1236–1246 (2016)
12. Shimjith, S.R., Tiwari, A.P., Bandyopadhyay, B., Patil, R.K.: Spatial stabilization of advanced heavy water reactor. Ann. Nucl. Energy **38**(7), 1545–1558 (2011)
13. Shinners, S.M.: Modern Control System Theory and Design. Wiley, New York (1998)

Appendix A
Two-Stage Design

Systems (6.8) and (6.10) are related through (6.12). Therefore, controllability of (3.1), and hence (6.8), implies the controllability of subsystems, i.e., pairs $(\Phi_{\tau s}, \Gamma_{\tau s})$ and $(\Phi_{\tau f}, \Gamma_{\tau f})$ are controllable. Now, in order to design the state feedback for (6.10), consider two-stage pole placement problem with the input $\mathbf{u}_k = \mathbf{u}_{s,k} + \mathbf{u}_{f,k}$. In the first stage $(m \times n_1)$ feedback matrix $\mathbf{F}_s$ is designed to place eigenvalues of $(\Phi_{\tau s} + \Gamma_{\tau s}\mathbf{F}_s)$ at desired n_1 locations. The input $\mathbf{u}_{s,k}$ is computed as

$$\mathbf{u}_{s,k} = \begin{bmatrix} \mathbf{F}_s & \mathbf{0} \end{bmatrix} \begin{bmatrix} \mathbf{z}_{s,k}^T & \mathbf{z}_{f,k}^T \end{bmatrix}^T . \tag{A.1}$$

Substituting the value of $\mathbf{u}_{s,k}$ from (A.1) in (6.10) yields

$$\begin{bmatrix} \mathbf{z}_{s,k+1} \\ \mathbf{z}_{f,k+1} \end{bmatrix} = \begin{bmatrix} \Phi_{\tau s} + \Gamma_{\tau s}\mathbf{F}_s & \mathbf{0} \\ \Gamma_{\tau f}\mathbf{F}_s & \Phi_{\tau f} \end{bmatrix} \begin{bmatrix} \mathbf{z}_{s,k} \\ \mathbf{z}_{f,k} \end{bmatrix} + \begin{bmatrix} \Gamma_{\tau s} \\ \Gamma_{\tau f} \end{bmatrix} \mathbf{u}_{f,k}. \tag{A.2}$$

Now using a transformation

$$\begin{bmatrix} \mathbf{z}_{s,k} \\ \mathbf{g}_{f,k} \end{bmatrix} = \begin{bmatrix} \mathbf{E}_{n_1} & \mathbf{0} \\ \mathbf{U} & \mathbf{E}_{n_2} \end{bmatrix} \begin{bmatrix} \mathbf{z}_{s,k} \\ \mathbf{z}_{f,k} \end{bmatrix} = \mathbf{T}_3 \begin{bmatrix} \mathbf{z}_{s,k} \\ \mathbf{z}_{f,k} \end{bmatrix} \tag{A.3}$$

where $(n_2 \times n_1)$ matrix $\mathbf{U}$ satisfies $\mathbf{U}(\Phi_{\tau s} + \Gamma_{\tau s}\mathbf{F}_s) - \Phi_{\tau f}\mathbf{U} + \Gamma_{\tau f}\mathbf{F}_s = \mathbf{0}$, the system (A.2) can be transformed into

$$\begin{bmatrix} \mathbf{z}_{s,k+1} \\ \mathbf{g}_{f,k+1} \end{bmatrix} = \begin{bmatrix} \Phi_{\tau s} + \Gamma_{\tau s}\mathbf{F}_s & \mathbf{0} \\ \mathbf{0} & \Phi_{\tau f} \end{bmatrix} \begin{bmatrix} \mathbf{z}_{s,k} \\ \mathbf{g}_{f,k} \end{bmatrix} + \begin{bmatrix} \Gamma_{\tau s} \\ \bar{\Gamma}_{\tau f} \end{bmatrix} \mathbf{u}_{f,k}, \tag{A.4}$$

where $\bar{\Gamma}_{\tau f} = \Gamma_{\tau f} + \mathbf{U}\Gamma_{\tau s}$. In second stage, taking $\mathbf{u}_{f,k}$ as

$$\mathbf{u}_{f,k} = \begin{bmatrix} \mathbf{0} & \mathbf{F}_f \end{bmatrix} \begin{bmatrix} \mathbf{z}_{s,k}^T & \mathbf{g}_{f,k}^T \end{bmatrix}^T , \tag{A.5}$$

R. Munje et al., *Investigation of Spatial Control Strategies with Application to Advanced Heavy Water Reactor*, Energy Systems in Electrical Engineering, https://doi.org/10.1007/978-981-10-3014-7

where $\mathbf{F}_f$ is $(m \times n_2)$ feedback gain matrix to place eigenvalues of $(\Phi_{\tau f} + \bar{\Gamma}_{\tau f}\mathbf{F}_f)$ at n_2 desired locations. After applying $\mathbf{u}_{f,k}$, the closed-loop system (A.4) is of the form

$$\begin{bmatrix} \mathbf{z}_{s,k} \\ \mathbf{g}_{f,k} \end{bmatrix} = \begin{bmatrix} \Phi_{\tau s} + \Gamma_{\tau s}\mathbf{F}_s & \Gamma_{\tau s}\mathbf{F}_f \\ \mathbf{0} & \Phi_{\tau f} + \bar{\Gamma}_{\tau f}\mathbf{F}_f \end{bmatrix} \begin{bmatrix} \mathbf{z}_{s,k} \\ \mathbf{g}_{f,k} \end{bmatrix}. \tag{A.6}$$

The control input $\mathbf{u}_k = \mathbf{u}_{s,k} + \mathbf{u}_{f,k}$ can be expressed as

$$\mathbf{u}_k = \begin{bmatrix} \mathbf{F}_1 & \mathbf{F}_2 \end{bmatrix} \begin{bmatrix} \mathbf{z}_{s,k}^T & \mathbf{z}_{f,k}^T, \end{bmatrix}^T \tag{A.7}$$

where $\mathbf{F}_1 = \mathbf{F}_s + \mathbf{F}_f\mathbf{U}$ and $\mathbf{F}_2 = \mathbf{F}_f$.

Appendix B
Three-Stage Decomposition

The system (7.14) can be decomposed into three subsystems, namely, slow, fast 1, and fast 2 by three-stage linear transformation. The first stage is to apply the change of variables

$$\begin{bmatrix} \mathbf{z}_{1,k} \\ \mathbf{z}_{2,k} \\ \mathbf{z}_{f2,k} \end{bmatrix} = \begin{bmatrix} \mathbf{E}_{n_1} & \mathbf{0} & \mathbf{0} \\ \mathbf{0} & \mathbf{E}_{n_2} & \mathbf{0} \\ \mathbf{L}_{31} & \mathbf{L}_{32} & \mathbf{E}_{n_3} \end{bmatrix} \begin{bmatrix} \mathbf{z}_{1,k} \\ \mathbf{z}_{2,k} \\ \mathbf{z}_{3,k} \end{bmatrix} = \mathbf{T}_1 \begin{bmatrix} \mathbf{z}_{1,k} \\ \mathbf{z}_{2,k} \\ \mathbf{z}_{3,k} \end{bmatrix} \tag{B.1}$$

to system (7.14). Here $\mathbf{E}_{n_1}$, $\mathbf{E}_{n_2}$, and $\mathbf{E}_{n_3}$ are respectively n_1, n_2, and n_3 identity matrices and $(n_3 \times n_1)$ matrix $\mathbf{L}_{31}$ and $(n_3 \times n_2)$ matrix $\mathbf{L}_{32}$ satisfy the nonsymmetric algebraic Riccati equations:

$$\begin{aligned} &\mathbf{L}_{31}\Phi_{11} - \mathbf{L}_{31}\Phi_{13}\mathbf{L}_{31} + \mathbf{L}_{32}\Phi_{21} - \mathbf{L}_{32}\Phi_{23}\mathbf{L}_{31} - \Phi_{33}\mathbf{L}_{31} + \Phi_{31} = \mathbf{0}, \\ &\mathbf{L}_{31}\Phi_{12} - \mathbf{L}_{31}\Phi_{13}\mathbf{L}_{32} + \mathbf{L}_{32}\Phi_{22} - \mathbf{L}_{32}\Phi_{23}\mathbf{L}_{32} - \Phi_{33}\mathbf{L}_{32} + \Phi_{32} = \mathbf{0}. \end{aligned}$$

Then the system (7.14) reduces to

$$\begin{bmatrix} \mathbf{z}_{1,k+1} \\ \mathbf{z}_{2,k+1} \\ \mathbf{z}_{f2,k+1} \end{bmatrix} = \begin{bmatrix} \bar{\Phi}_{11} & \bar{\Phi}_{12} & \bar{\Phi}_{13} \\ \bar{\Phi}_{21} & \bar{\Phi}_{22} & \bar{\Phi}_{23} \\ \mathbf{0} & \mathbf{0} & \Phi_{\tau f2} \end{bmatrix} \begin{bmatrix} \mathbf{z}_{1,k} \\ \mathbf{z}_{2,k} \\ \mathbf{z}_{f2,k} \end{bmatrix} + \begin{bmatrix} \Gamma_1 \\ \Gamma_2 \\ \Gamma_{\tau f2} \end{bmatrix} \mathbf{u}_k, \tag{B.2}$$

where

$$\begin{aligned} &\bar{\Phi}_{11} = \Phi_{11} - \Phi_{13}\mathbf{L}_{31}, \bar{\Phi}_{12} = \Phi_{12} - \Phi_{13}\mathbf{L}_{32}, \bar{\Phi}_{13} = \Phi_{13}, \\ &\bar{\Phi}_{21} = \Phi_{21} - \Phi_{23}\mathbf{L}_{31}, \bar{\Phi}_{22} = \Phi_{22} - \Phi_{23}\mathbf{L}_{32}, \bar{\Phi}_{23} = \Phi_{23}, \\ &\Phi_{\tau f2} = \Phi_{33} + \mathbf{L}_{31}\Phi_{13} + \mathbf{L}_{32}\Phi_{23}, \\ &\Gamma_{\tau f2} = \Gamma_3 + \mathbf{L}_{32}\Gamma_2 + \mathbf{L}_{31}\Gamma_1. \end{aligned}$$

The second linear transformation is applied as

R. Munje et al., *Investigation of Spatial Control Strategies with Application to Advanced Heavy Water Reactor*, Energy Systems in Electrical Engineering, https://doi.org/10.1007/978-981-10-3014-7

$$\begin{bmatrix} \mathbf{z}_{1,k} \\ \mathbf{z}_{f1,k} \\ \mathbf{z}_{f2,k} \end{bmatrix} = \begin{bmatrix} \mathbf{E}_{n_1} & \mathbf{0} & \mathbf{0} \\ \mathbf{L}_{21} & \mathbf{E}_{n_2} & \mathbf{L}_{23} \\ \mathbf{0} & \mathbf{0} & \mathbf{E}_{n_3} \end{bmatrix} \begin{bmatrix} \mathbf{z}_{1,k} \\ \mathbf{z}_{2,k} \\ \mathbf{z}_{f2,k} \end{bmatrix} = \mathbf{T}_2 \begin{bmatrix} \mathbf{z}_{1,k} \\ \mathbf{z}_{2,k} \\ \mathbf{z}_{f2,k} \end{bmatrix} \tag{B.3}$$

to the system (B.2) and choose $(n_2 \times n_1)$ matrix $\mathbf{L}_{21}$ and $(n_2 \times n_3)$ matrix $\mathbf{L}_{23}$ such that

$$\begin{aligned} \mathbf{L}_{21}\bar{\Phi}_{11} - \bar{\Phi}_{22}\mathbf{L}_{21} - \mathbf{L}_{21}\bar{\Phi}_{12}\mathbf{L}_{21} + \bar{\Phi}_{21} &= \mathbf{0}, \\ \mathbf{L}_{21}\bar{\Phi}_{13} - \mathbf{L}_{21}\bar{\Phi}_{12}\mathbf{L}_{23} - \bar{\Phi}_{22}\mathbf{L}_{23} + \bar{\Phi}_{23} + \mathbf{L}_{23}\Phi_{\tau f2} &= \mathbf{0}. \end{aligned}$$

Therefore, the system (B.2) gets transformed to

$$\begin{bmatrix} \mathbf{z}_{1,k+1} \\ \mathbf{z}_{f1,k+1} \\ \mathbf{z}_{f2,k+1} \end{bmatrix} = \begin{bmatrix} \Phi_{\tau s} & \tilde{\Phi}_{12} & \tilde{\Phi}_{13} \\ \mathbf{0} & \Phi_{\tau f1} & \mathbf{0} \\ \mathbf{0} & \mathbf{0} & \Phi_{\tau f2} \end{bmatrix} \begin{bmatrix} \mathbf{z}_{1,k} \\ \mathbf{z}_{f1,k} \\ \mathbf{z}_{f2,k} \end{bmatrix} + \begin{bmatrix} \Gamma_1 \\ \Gamma_{\tau f1} \\ \Gamma_{\tau f2} \end{bmatrix} \mathbf{u}_k, \tag{B.4}$$

where

$$\begin{aligned} \Phi_{\tau s} &= \bar{\Phi}_{11} - \bar{\Phi}_{12}\mathbf{L}_{21}, \\ \tilde{\Phi}_{12} &= \bar{\Phi}_{12}, \tilde{\Phi}_{13} = \bar{\Phi}_{13} - \bar{\Phi}_{12}\mathbf{L}_{23}, \\ \Phi_{\tau f1} &= \bar{\Phi}_{22} + \mathbf{L}_{21}\bar{\Phi}_{12}, \\ \Gamma_{\tau f1} &= \Gamma_2 + \mathbf{L}_{21}\Gamma_1 + \mathbf{L}_{23}\Gamma_{\tau f2}. \end{aligned}$$

Finally in the third stage, linear transformation

$$\begin{bmatrix} \mathbf{z}_{s,k} \\ \mathbf{z}_{f1,k} \\ \mathbf{z}_{f2,k} \end{bmatrix} = \begin{bmatrix} \mathbf{E}_{n_1} & \mathbf{L}_{12} & \mathbf{L}_{13} \\ \mathbf{0} & \mathbf{E}_{n_2} & \mathbf{0} \\ \mathbf{0} & \mathbf{0} & \mathbf{E}_{n_3} \end{bmatrix} \begin{bmatrix} \mathbf{z}_{1,k} \\ \mathbf{z}_{f1,k} \\ \mathbf{z}_{f2,k} \end{bmatrix} = \mathbf{T}_3 \begin{bmatrix} \mathbf{z}_{1,k} \\ \mathbf{z}_{f1,k} \\ \mathbf{z}_{f2,k} \end{bmatrix} \tag{B.5}$$

is applied to system (B.4) and matrices $\mathbf{L}_{12}$ and $\mathbf{L}_{13}$ of dimensions respectively $(n_1 \times n_2)$ and $(n_1 \times n_3)$ are selected such that

$$\begin{aligned} \mathbf{L}_{12}\Phi_{\tau f1} + \Phi_{\tau s}\mathbf{L}_{12} + \tilde{\Phi}_{12} &= 0, \\ \mathbf{L}_{13}\Phi_{\tau f2} + \Phi_{\tau s}\mathbf{L}_{13} + \tilde{\Phi}_{13} &= 0. \end{aligned}$$

As a result system (B.4) is transformed into block diagonal form as

$$\begin{bmatrix} \mathbf{z}_{s,k+1} \\ \mathbf{z}_{f1,k+1} \\ \mathbf{z}_{f2,k+1} \end{bmatrix} = \begin{bmatrix} \Phi_{\tau s} & \mathbf{0} & \mathbf{0} \\ \mathbf{0} & \Phi_{\tau f1} & \mathbf{0} \\ \mathbf{0} & \mathbf{0} & \Phi_{\tau f2} \end{bmatrix} \begin{bmatrix} \mathbf{z}_{s,k} \\ \mathbf{z}_{f1,k} \\ \mathbf{z}_{f2,k} \end{bmatrix} + \begin{bmatrix} \Gamma_{\tau s} \\ \Gamma_{\tau f1} \\ \Gamma_{\tau f2} \end{bmatrix} \mathbf{u}_k, \tag{B.6}$$

where

$$\Gamma_{\tau s} = \Gamma_1 + \mathbf{L}_{12}\Gamma_{\tau f1} + \mathbf{L}_{13}\Gamma_{\tau f2}.$$

The submatrices $\mathbf{L}_{ij}$ in transformations (B.1), (B.3), and (B.5) are computed using an iterative procedure. From (B.1), (B.3), and (B.5), one can get

$$\left[\mathbf{z}_{s,k}^T\ \mathbf{z}_{f1,k}^T\ \mathbf{z}_{f2,k}^T\right]^T = \mathbf{T}\left[\mathbf{z}_{1,k}^T\ \mathbf{z}_{2,k}^T\ \mathbf{z}_{3,k}^T\right]^T$$

where $\mathbf{T} = \mathbf{T}_3\mathbf{T}_2\mathbf{T}_1$. Note that the original system (7.14) is now decoupled into three subsystems given by (B.6).

Appendix C
Design of Output Injection Gain

Design of output injection gain for system (7.16)–(7.17) is equivalent to design of a state feedback for its adjoint system, given by

$$\begin{bmatrix} \hat{\mathbf{z}}_{s,k+1} \\ \hat{\mathbf{z}}_{f1,k+1} \\ \hat{\mathbf{z}}_{f2,k+1} \end{bmatrix} = \begin{bmatrix} \Phi_{\tau s}^T & \mathbf{0} & \mathbf{0} \\ \mathbf{0} & \Phi_{\tau f1}^T & \mathbf{0} \\ \mathbf{0} & \mathbf{0} & \Phi_{\tau f2}^T \end{bmatrix} \begin{bmatrix} \hat{\mathbf{z}}_{s,k} \\ \hat{\mathbf{z}}_{f1,k} \\ \hat{\mathbf{z}}_{f2,k} \end{bmatrix} + \begin{bmatrix} \mathbf{M}_s^T \\ \mathbf{M}_{f1}^T \\ \mathbf{M}_{f2}^T \end{bmatrix} \mathbf{u}_k \tag{C.1}$$

$$\mathbf{y}_k = \begin{bmatrix} \Gamma_{\tau s}^T & \Gamma_{\tau f1}^T & \Gamma_{\tau f2}^T \end{bmatrix} \begin{bmatrix} \hat{\mathbf{z}}_{s,k}^T & \hat{\mathbf{z}}_{f1,k}^T & \hat{\mathbf{z}}_{f2,k}^T \end{bmatrix}^T. \tag{C.2}$$

In order to design a state feedback based controller for (C.1), consider three-stage pole placement problem with input $\mathbf{u}_k = \mathbf{u}_{s,k} + \mathbf{u}_{f1,k} + \mathbf{u}_{f2,k}$. In the first stage, $(p \times n_1)$ matrix $\mathbf{G}_s^T$ is designed to place eigenvalues of $(\Phi_{\tau s}^T + \mathbf{M}_s^T \mathbf{G}_s^T)$ at desired locations. The input $\mathbf{u}_{s,k}$ is computed as

$$\mathbf{u}_{s,k} = \begin{bmatrix} \mathbf{G}_s^T & \mathbf{0} & \mathbf{0} \end{bmatrix} \hat{\mathbf{z}}_{d,k} \tag{C.3}$$

where $\hat{\mathbf{z}}_{d,k} = \begin{bmatrix} \hat{\mathbf{z}}_{s,k}^T & \hat{\mathbf{z}}_{f1,k}^T & \hat{\mathbf{z}}_{f2,k}^T \end{bmatrix}^T$. Substituting the value of $\mathbf{u}_{s,k}$ from (C.3) into (C.1) yields

$$\hat{\mathbf{z}}_{d,k+1} = \begin{bmatrix} \Phi_{\tau s}^T + \mathbf{M}_s^T \mathbf{G}_s^T & \mathbf{0} & \mathbf{0} \\ \mathbf{M}_{f1}^T \mathbf{G}_s^T & \Phi_{\tau f1}^T & \mathbf{0} \\ \mathbf{M}_{f2}^T \mathbf{G}_s^T & \mathbf{0} & \Phi_{\tau f2}^T \end{bmatrix} \hat{\mathbf{z}}_{d,k} + \begin{bmatrix} \mathbf{M}_s^T \\ \mathbf{M}_{f1}^T \\ \mathbf{M}_{f2}^T \end{bmatrix} \mathbf{u}_{d1,k} \tag{C.4}$$

where $\mathbf{u}_{d1,k} = \mathbf{u}_{f1,k} + \mathbf{u}_{f2,k}$. Now, for decoupling fast 1 subsystem, let us take $\hat{\mathbf{z}}_{d1,k} = \begin{bmatrix} \hat{\mathbf{z}}_{s,k}^T & \bar{\mathbf{z}}_{f1,k}^T & \bar{\mathbf{z}}_{f2,k}^T \end{bmatrix}^T = \mathbf{T}_{d1} \hat{\mathbf{z}}_{d,k}$, where transformation matrix $\mathbf{T}_{d1} \in \Re^{n \times n}$ is given by

$$\mathbf{T}_{d1} = \begin{bmatrix} \mathbf{E}_{n_1} & \mathbf{0} & \mathbf{0} \\ \mathbf{N}_{21} & \mathbf{E}_{n_2} & \mathbf{0} \\ \mathbf{N}_{31} & \mathbf{0} & \mathbf{E}_{n_3} \end{bmatrix} \tag{C.5}$$

R. Munje et al., *Investigation of Spatial Control Strategies with Application to Advanced Heavy Water Reactor*, Energy Systems in Electrical Engineering, https://doi.org/10.1007/978-981-10-3014-7

and $(n_2 \times n_1)$ matrix $(\mathbf{N}_{21})$ and $(n_3 \times n_1)$ matrix $\mathbf{N}_{31}$ satisfy

$$\mathbf{N}_{21}(\Phi_{\tau s}^T + \mathbf{M}_s^T \mathbf{G}_s^T) + \mathbf{M}_{f1}^T \mathbf{G}_s^T - \Phi_{\tau f1}^T \mathbf{N}_{21} = \mathbf{0},$$
$$\mathbf{N}_{31}(\Phi_{\tau s}^T + \mathbf{M}_s^T \mathbf{G}_s^T) + \mathbf{M}_{f2}^T \mathbf{G}_s^T - \Phi_{\tau f2}^T \mathbf{N}_{31} = \mathbf{0}.$$

Then, the equivalent system is obtained as follows:

$$\hat{\mathbf{z}}_{d1,k+1} = \begin{bmatrix} \Phi_{\tau s}^T + \mathbf{M}_s^T \mathbf{G}_s^T & \mathbf{0} & \mathbf{0} \\ \mathbf{0} & \Phi_{\tau f1}^T & \mathbf{0} \\ \mathbf{0} & \mathbf{0} & \Phi_{\tau f2}^T \end{bmatrix} \hat{\mathbf{z}}_{d1_k} + \begin{bmatrix} \mathbf{M}_s^T \\ \bar{\mathbf{M}}_{f1}^T \\ \bar{\mathbf{M}}_{f2}^T \end{bmatrix} \mathbf{u}_{d1,k}, \tag{C.6}$$

where $\bar{\mathbf{M}}_{f1}^T = \mathbf{N}_{21}\mathbf{M}_s^T + \mathbf{M}_{f1}^T$ and $\bar{\mathbf{M}}_{f2}^T = \mathbf{N}_{31}\mathbf{M}_s^T + \mathbf{M}_{f2}^T$. Systems (C.6) and (C.4) are related through transformation matrix (C.5). As a result, when pair $(\Phi_{\tau f1}^T, \mathbf{M}_{f1}^T)$ is controllable, pair $(\Phi_{\tau f1}^T, \bar{\mathbf{M}}_{f1}^T)$ is also controllable. Therefore, in the second stage, $(p \times n_2)$ matrix $\mathbf{G}_{f1}^T$ is designed to place eigenvalues of $(\Phi_{\tau f1}^T + \bar{\mathbf{M}}_{f1}^T \mathbf{G}_{f1}^T)$ at desired locations. For that, input $\mathbf{u}_{f1,k}$ is taken as

$$\mathbf{u}_{f1,k} = \begin{bmatrix} \mathbf{0} & \mathbf{G}_{f1}^T & \mathbf{0} \end{bmatrix} \hat{\mathbf{z}}_{d1,k}. \tag{C.7}$$

Substituting this value of $\mathbf{u}_{f1,k}$ into (C.6) gives

$$\hat{\mathbf{z}}_{d1,k+1} = \begin{bmatrix} \Phi_{\tau s}^T + \mathbf{M}_s^T \mathbf{G}_s^T & \mathbf{M}_s^T \mathbf{G}_{f1}^T & \mathbf{0} \\ \mathbf{0} & \Phi_{\tau f1}^T + \bar{\mathbf{M}}_{f1}^T \mathbf{G}_{f1}^T & \mathbf{0} \\ \mathbf{0} & \bar{\mathbf{M}}_{f2}^T \mathbf{G}_{f1}^T & \Phi_{\tau f2}^T \end{bmatrix} \hat{\mathbf{z}}_{d1,k} + \begin{bmatrix} \mathbf{M}_s^T \\ \bar{\mathbf{M}}_{f1}^T \\ \bar{\mathbf{M}}_{f2}^T \end{bmatrix} \mathbf{u}_{f2,k}. \tag{C.8}$$

Now, fast 2 subsystem is decoupled using $\hat{\mathbf{z}}_{d2,k} = \begin{bmatrix} \bar{\mathbf{z}}_{s,k}^T & \bar{\mathbf{z}}_{f1,k}^T & \tilde{\mathbf{z}}_{f2,k}^T \end{bmatrix}^T = \mathbf{T}_{d2} \hat{\mathbf{z}}_{d1,k}$, where $\mathbf{T}_{d2} \in \Re^{n \times n}$ is

$$\mathbf{T}_{d2} = \begin{bmatrix} \mathbf{E}_{n_1} & \mathbf{N}_{12} & \mathbf{0} \\ \mathbf{0} & \mathbf{E}_{n_2} & \mathbf{0} \\ \mathbf{0} & \mathbf{N}_{32} & \mathbf{E}_{n_3} \end{bmatrix} \tag{C.9}$$

and $(n_1 \times n_2)$ matrix $\mathbf{N}_{12}$ and $(n_3 \times n_2)$ matrix $\mathbf{N}_{32}$ satisfy

$$\mathbf{M}_s^T \mathbf{G}_{f1}^T + \mathbf{N}_{12}(\Phi_{\tau f1}^T + \bar{\mathbf{M}}_{f1}^T \mathbf{G}_{f1}^T) - (\Phi_{\tau s}^T + \mathbf{M}_s^T \mathbf{G}_s^T)\mathbf{N}_{12} = \mathbf{0},$$
$$\bar{\mathbf{M}}_{f2}^T \mathbf{G}_{f1}^T + \mathbf{N}_{32}(\Phi_{\tau f1}^T + \bar{\mathbf{M}}_{f1}^T \mathbf{G}_{f1}^T) - \Phi_{\tau f2} \mathbf{N}_{32} = \mathbf{0}.$$

Then the following equivalent system is obtained:

$$\hat{\mathbf{z}}_{d2,k+1} = \begin{bmatrix} \Phi_{\tau s}^T + \mathbf{M}_s^T \mathbf{G}_s^T & \mathbf{0} & \mathbf{0} \\ \mathbf{0} & \Phi_{\tau f1}^T + \bar{\mathbf{M}}_{f1}^T \mathbf{G}_{f1}^T & \mathbf{0} \\ \mathbf{0} & \mathbf{0} & \Phi_{\tau f2}^T \end{bmatrix} \hat{\mathbf{z}}_{d2,k} + \begin{bmatrix} \tilde{\mathbf{M}}_s^T \\ \bar{\mathbf{M}}_{f1}^T \\ \tilde{\mathbf{M}}_{f2}^T \end{bmatrix} \mathbf{u}_{f2,k}, \tag{C.10}$$

where $\tilde{\mathbf{M}}_s^T = \mathbf{M}_s^T + \mathbf{N}_{12}\bar{\mathbf{M}}_{f1}^T$ and $\tilde{\mathbf{M}}_{f2}^T = \mathbf{N}_{32}\bar{\mathbf{M}}_{f1}^T + \bar{\mathbf{M}}_{f2}^T$. Finally, input $\mathbf{u}_{f2,k}$ is computed as

$$\mathbf{u}_{f2,k} = \begin{bmatrix} \mathbf{0} & \mathbf{0} & \mathbf{G}_{f2}^T \end{bmatrix} \hat{\mathbf{z}}_{d2,k}. \tag{C.11}$$

where $\mathbf{G}_{f2}^T$ is designed to place eigenvalues of $(\Phi_{f2}^T + \tilde{\mathbf{M}}_{f2}^T \mathbf{G}_{f2}^T)$ at desired locations. Now from (C.3), (C.7), and (C.11), the composite control $\mathbf{u}_k = \mathbf{u}_{s,k} + \mathbf{u}_{f1,k} + \mathbf{u}_{f2,k}$ is given by

$$\begin{aligned} \mathbf{u}_k &= \left(\begin{bmatrix} \mathbf{G}_s^T & \mathbf{0} & \mathbf{0} \end{bmatrix} + \begin{bmatrix} \mathbf{0} & \mathbf{G}_{f1}^T & \mathbf{0} \end{bmatrix} \mathbf{T}_{d1} + \begin{bmatrix} \mathbf{0} & \mathbf{0} & \mathbf{G}_{f2}^T \end{bmatrix} \mathbf{T}_{d2} \mathbf{T}_{d1} \right) \hat{\mathbf{z}}_{d,k} \\ &= \begin{bmatrix} \mathbf{G}_1^T & \mathbf{G}_2^T & \mathbf{G}_3^T \end{bmatrix}, \end{aligned} \tag{C.12}$$

where $\mathbf{G}_1^T = \mathbf{G}_s^T + \mathbf{G}_{f1}^T \mathbf{N}_{21} + \mathbf{G}_{f2}^T \mathbf{N}_{32} \mathbf{N}_{21} + \mathbf{G}_{f2}^T \mathbf{N}_{31}$, $\mathbf{G}_2^T = \mathbf{G}_{f1}^T + \mathbf{G}_{f2}^T \mathbf{N}_{32}$, $\mathbf{G}_3^T = \mathbf{G}_{f2}^T$.

Appendix D
Specifications and Error Indices

In specifying the transient response specifications, it is common to specify the following quantities.

- **Delay Time** (t_d): It is the time required for the response to reach half the final value the very first time.
- **Rise Time** (t_r): It is the time required for the response to rise from $x\%$–$y\%$ of its final value. For overdamped system, the 10–90% rise time is normally used and for underdamped system, 0–100% rise time is commonly used.
- **Peak Time** (t_p): It is the time required for the response to reach the first (or maximum) peak.
- **Settling Time** (t_s): It is the time required for the response to settle within a certain percent of its final value. Typical values used are ± 2 and $\pm 5\%$.
- **Maximum (Percent) Overshoot/Undershoot** (M_p/M_u): The maximum (percent) overshoot/undershoot represents the value of the response overshoots/ undershoots from its steady-state (or final) value, expressed as percentage of the steady-state value.

An error performance index is a quantitative measure of the behavior of a system and is chosen so that emphasis is given to the important system characteristics. Error performance indices used in this monograph are given below.

- **Integral Square Error** (ISE) is given by

$$\text{ISE} = \int_0^T e^2(t)dt, \tag{D.1}$$

where $e(t)$ is an error signal and T is the finite time, chosen arbitrarily, so that the integral approaches a steady-state value.

R. Munje et al., *Investigation of Spatial Control Strategies with Application to Advanced Heavy Water Reactor*, Energy Systems in Electrical Engineering, https://doi.org/10.1007/978-981-10-3014-7

- **Integral Absolute Error** (IAE) is written as

$$\text{IAE} = \int_0^T |e(t)|dt. \tag{D.2}$$

- **Integral Time Square Error** (ITSE) is calculated using

$$\text{ITSE} = \int_0^T te^2(t)dt. \tag{D.3}$$

- **Integral Time Absolute Error** (ITAE) is represented by

$$\text{ITAE} = \int_0^T t|e(t)|dt. \tag{D.4}$$